Dissertation

Master in Civil Engineering – Building Construction

Analysis of reinforced concrete elements exposed to fire after earthquake

Hugo Manuel Mendes Vitorino

Leiria, September of 2018

This page was intetionally left blank

Dissertation

Master in Civil Engineering – Building Construction

Analysis of reinforced concrete elements exposed to fire after earthquake

Hugo Manuel Mendes Vitorino

Dissertation developed under the supervision of Doctor Hugo Filipe Pinheiro Rodrigues, professor at the School of Technology and Management of the Polytechnic Institute of Leiria and co-supervision of Doctor Carlos André Soares Couto, Post-doctoral Researcher at Aveiro University.

Leiria, September of 2018

This page was intetionally left blank

Dedication

To my parents and brother

This page was intetionally left blank

Acknowledgements

I want to express my deepest gratitude and appreciation to the Doctor Hugo Rodrigues for all the advice, help and teachings that made the development of this dissertation possible.

I will also want to express my gratitude and appreciation to Doctor Carlos Couto for all the explanations and clarifications regarding the numerical analysis and for the availability to help run the numerical simulations.

I am also grateful to Doctor Paulo Vila Real, for providing the access to the software SAFIR at the Aveiro University.

Lastly, I would like to thank my family, specially my grandfather, parents and brother for all the support throughout my life; without them it was not possible to develop this work.

This page was intetionally left blank

Resumo

Os Sismos podem provocar uma cadeia de eventos, sendo que um deles pode ser a ocorrência de um incêndio. Os efeitos do incêndio após um sismo em áreas urbanas podem ser mais severos que os efeitos diretos do próprio sismo. Os edifícios podem não estar adequadamente dimensionados para a ação de incêndio após um sismo visto que a maioria dos regulamentos ignora essa possibilidade. O objetivo deste trabalho é perceber as consequências que o dano introduzido pela ação sísmica pode causar na resistência ao fogo em vários elementos de betão armado. Foram desenvolvidas várias análises numéricas com o programa SAFIR, considerando a análise térmica e mecânica da estrutura, tanto ao nível da secção como em elementos isolados (pilares, vigas e pórticos). As principais variáveis nas análises foram o tipo de dano nos elementos. As análises numéricas foram realizadas usando a curva de incêndio padrão ISO 834. Os resultados mostram que o dano nos elementos de betão armado reduz a resistência ao fogo, especialmente quando as armaduras ficam expostas ao fogo. Após um sismo, e dado o elevado número de ocorrências, as equipas de socorro vão ser muito solicitadas, pelo que os tempos de resposta serão consequente mais elevados. Esta situação associada a uma redução na resistência ao fogo dos elementos de betão armado pode originar a perda de vidas e o colapso de estruturas. Assim, é importante uma melhor compreensão sobre o comportamento em incêndio após um sismo, em particular em estruturas de maior importância, para que seja possível implementar algumas medidas prescritivas que possam garantir melhor desempenho das estruturas nestas circunstâncias.

Palavras-chave: Fogo após um sismo, Segurança Contra Incêndio, Resistência ao Fogo, Estruturas de Betão Armado, Métodos Avançados de Cálculo, Elementos Finitos.

This page was intetionally left blank

Abstract

Large earthquakes can cause a chain of catastrophic events, one of which can be fire after earthquake. The effects of fire after earthquake on urban areas can be even worse than the effects of the earthquake itself. Buildings are not adequately designed for fire after an earthquake since most standards ignore that possibility. The aim of the work is to better understand the consequences of the damage introduced by the seismic action on the fire resistance of several reinforced concrete elements. Several numerical analyses were performed using the SAFIR program, considering the thermal and mechanical analysis of the structure, both at section level and in structural elements (columns, beams and frames). The main variables in the analysis were the type of damage in the elements. The numerical analysis was performed using the standard fire curve ISO 834. The results show that damage to reinforced concrete structures reduces the fire resistance, especially if the cover of the elements is removed and the reinforcement is exposed to fire. After an earthquake, and given the high number of occurrences, the rescue teams will very solicitated, so the response times will consequently be higher. This situation together with the reduced fire resistance of the damaged reinforced concrete elements can lead to the loss of lives and structures. Thus, a better understanding of fire behaviour following an earthquake, particularly in major structures, is important so that it is possible to implement some prescriptive measures that can ensure better performance of structures in the circumstances.

Keywords: Fire after earthquake, Fire Safety, Fire Resistance, Reinforced Concrete Structure, Advanced Calculation Method, Finite Element.

This page was intetionally left blank

List of figures

Chapter 2

Chapter 3

Chapter 6

Chapter 7

Chapter 8

Chapter 9

Appendix A

Appendix B

List of tables

Chapter 2

Chapter 3

Chapter 5

Chapter 6

Chapter 7

Chapter 8

Chapter 9

List of acronyms

PEF – Post-earthquake fire

RC – Reinforced concrete

CFRP – Carbon Fibre Reinforcement Polymer

FF – Fire Frontiers

This page was intetionally left blank

Table of Contents

1. Introduction

1.1. Initial considerations

The requirements that structures must fulfil have become increasingly demanding and it is necessary to verify the performance of these increasingly complex requests. Only this way it is possible to guarantee a safe structure with good behaviour to different types of actions. The fire safety is a fundamental requirement in buildings. The reinforced concrete buildings have an overall good behaviour against fire because concrete is a material that has a good resistance against high temperatures, low conductivity and does not produce smoke or toxic vapours. The elevated temperatures change the mechanical properties of the concrete and can change the forces diagrams of the structures. It is important to understand the behaviour of reinforced concrete structures under fire. There are several investigations and research developed regarding this, but not so much regarding the behaviour of a concrete structure to a fire after an earthquake. A fire that occurs after an earthquake can be very different from a fire that occurs at any other time. The damage caused by the earthquake can change the fire resistance of the structure. It is important to understand the behaviour of reinforced concrete structure against the seismic action, fire action but it is also important to understand the combined effect of these actions.

1.2. Dissertation objectives

The objective of this dissertation is to evaluate the effect that a post-earthquake fire has on reinforced concrete buildings. To be able to access this effect there were developed several numerical simulations on reinforced concrete columns, beams

and frames. There are different typologies of damage considered in the reinforced concrete elements. The aim is to compare the results of the reinforced concrete elements with different typologies of damage to be able to see the impact that the damage has on the fire resistance of the reinforced concrete elements. Other objectives are related with the analysis of the forces in the beams and frames. The aim the comparison of the axial force, shear force, moments and displacements of different reinforced concrete elements with different typologies of damage.

1.3. Outline of the dissertation chapters

Chapter 2

Post-earthquake fire

In this Chapter it is presented some concepts regarding the phenomenon of earthquakes, fire and post-earthquake fire on buildings. The Chapter is divided into three parts, one related with earthquakes, other with fires and finally one related with the combined effect of earthquakes and fires, the post-earthquake fire.

Chapter 3

Materials thermal and mechanical properties at elevated temperatures

This Chapter introduces the thermal and mechanical properties at elevated temperatures of the concrete and steel. This Chapter is divided into four parts. Two parts for the thermal and mechanical properties of the concrete and two parts for the thermal and mechanical properties of the steel.

Chapter 4

SAFIR: A thermal/structural program for modelling structures under fire

A brief introduction of the program used in this dissertation is presented in this Chapter. There are introduced some capabilities and limitations of the software and some information related with the concrete and steel properties.

Chapter 5

Regulatory requirements

This Chapter shows some information regarding the Portuguese technical regulation of fire safety in buildings.

Chapter 6

Study of the concrete section

In this Chapter it is presented a brief parametric study to evaluate the impact of different meshes on the temperatures of a concrete section. It is also analysed a small example regarding the influence of damage in the temperature of a certain point of the section.

Chapter 7

Post-earthquake fire on RC columns under axial load

In this Chapter there were developed several numerical models to evaluate the influence that different types of damage, fire frontiers and loads have on the time until collapse of a column. The evolution of the thermal profiles in the section of the reinforced concrete column is also analysed considering different loads and types of damage.

Chapter 8

Post-earthquake fire on RC beams

This Chapter presents three different beams with different types of damage in each beam. It is analysed the influence of the damage on the time until collapse, axial force, moments and displacements of the beams.

Chapter 9

Post-earthquake fire on RC frames

In this Chapter there were developed fifteen numerical models. Each model represents a frame with different characteristics regarding the damage and fire frontiers. It is analysed the influence the of the damage and fire frontiers on the time

until collapse, axial forces, shear forces, bending moments and displacements of the frames.

Chapter 10

Conclusions and further works

This Chapter summarizes the main conclusions obtained during the development of this dissertation and indicates further works than can be developed regarding the phenomenon of post-earthquake fire in reinforced concrete buildings.

2. Post-earthquake fire – Brief Overview

2.1. Earthquake action

2.1.1. General overview

Most earthquakes originate inside the Earth in faults that break due to accumulation of tensions around it. This accumulation of tensions is a natural phenomenon that happens due to the internal dynamics of the land that has been perpetuated over the decades, centuries and millennia. When the accumulated tension is excessive for the resistance in the plane of the fault, it breaks off given rise to earthquakes. This rupture phenomenon has periodicity characteristics, but until now is not possible to predict with accuracy the next earthquake in terms of days, weeks or months. The main consequence of earthquakes is the effect of the propagation of the elastic waves that originate from the rupture of the fault. More than 80% of the worldwide damages in buildings in the past are related with this natural hazard [1].

2.1.2. Types of earthquake effects

The impact of earthquakes can be diverse. The earthquake consequences can be divided into three groups, direct, indirect and immaterial losses. The direct losses are the effects on the population, for example, fatalities, seriously injured, minor injured, homeless and psychological trauma. The damage in the urban environment, infrastructures, supply networks and historical heritage built is also a direct effect. The indirect losses are related with the socio-economic impact due to

difficulty in restoring the daily life. The immaterial losses are related with aspects that are difficult to quantify, those can be cultural values, patrimonial, aesthetics, religious, etc, that can be lost with the occurrence of earthquakes [1].

2.1.3. Earthquake damages on buildings

The earthquake can cause different types of structural and non-structural damage in buildings. The masonry walls normally are not considered as structural elements. The masonry bricks usually have a brittle behaviour and can modify the structure response of the building by changing the structural stiffness, attracting forces to structural elements not designed to resist such forces [2]. In Figures 2.1 and 2.2 are examples of the damage caused by an earthquake in the masonry walls of a building. This situation can be avoided with more ductile masonry walls.

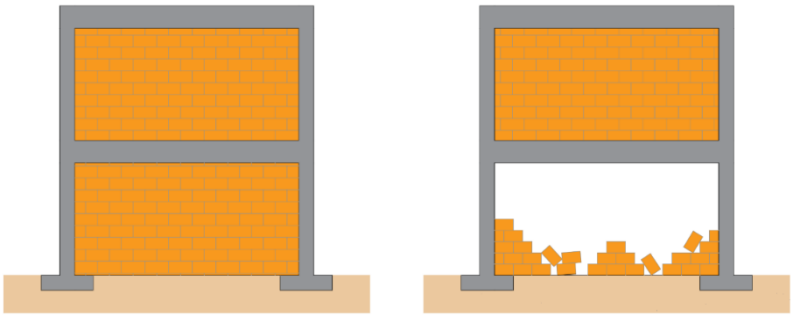

a) b)

Figure 2.1 – Involuntary creation of a leaked floor. a) Situation at the beginning of the earthquake. b) Situation after the collapse of the masonry walls in the ground floor.

Figure 2.2 – Damage to reinforced concrete buildings with masonry walls [3].

There is also the structural damage in the structural elements like beams and columns, walls, slabs or even foundations. To assure a proper structural behaviour under an earthquake action it is important to have structural elements with proper strength, stiffness and ductility but it is also important that the beam-column joints are well connected and with a proper ductile behaviour [2]. Figure 2.3 show damage at the beam-column joints caused by an earthquake.

Figure 2.3 – Damage at the beam-column joints. [2][4]

The poor detailing of the reinforcing steel is a common deficit in the existing structures, especially on old reinforced concrete structures, designed without seismic concerns. There are several cases reported related with the poor detail, namely related with the confinement reinforcement not correctly constituted at the beam-column joints, deficiency of transverse reinforcement in the columns with wide spacing of the ties and poor confinement of the concrete core. The short lap splices and incorrect end hook angle are also examples of poor detailing of the reinforcing steel. The use of smooth reinforcing bar that creates a weaker bond between concrete and steel can also be observed in some cases [4]. In Figure 2.4 is an example of poor detailing of the reinforcing steel.

There are other cases that lead to a poor behaviour of the structures to the seismic action, such as, poor concrete quality, damage related with strong beam-weak column, soft stories at the first-floor level, and defects in the workmanship [5] [6].

Figure 2.4 – Poor detailing of the reinforcing steel [2].

2.2. Fire action

2.2.1. General overview

Fire is a combustion characterized by the appearance, conservation and propagation of the flame, heat release, gas emission and smoke production. Given that a fire is a combustion this means that only happens if in the same place is present a fuel and an oxidizer. The fuel material can be any material that is susceptible to burn (wood, paper, plastics). The oxidizer is the oxygen. The presence of the fuel and oxidizer is not enough to produce the fire, it is also necessary a third factor, the activation energy. The activation energy can be a heat source that will cause a change in the thermal level of the fuel. The pyrolysis of a certain solid combustible material occurs when that material temperature reaches a certain value. Due to heat action, the material starts to emit decomposition gases that are fuels. Once this temperature is reached, the reaction develops into a chain with the continuity of the combustion, appearing this way a fourth factor, the chain reaction. So, in this way is possible to organize these four factors in a tetrahedron like is shown in Figure 2.5 [7].

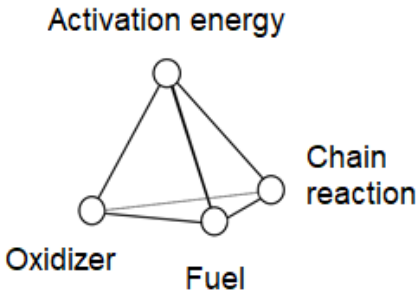

Figure 2.5 – Fire tetrahedron.

During the natural development of a fire, from the beginning until the extinction, there are several important stages, namely: ignition, growth, flashover, burning and decay. In the Figure 2.6 is represented the relation between the previous mentioned stages and the temperature evolution with time [7].

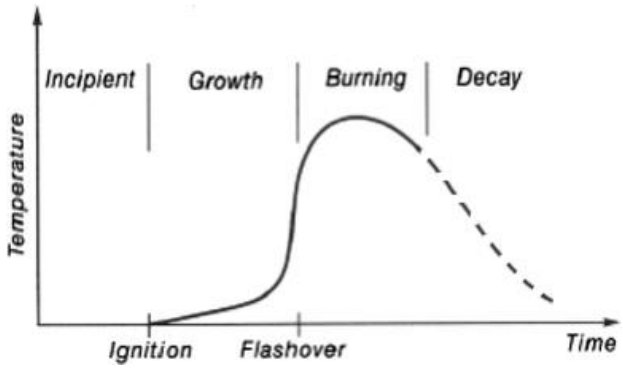

Figure 2.6 – Temperature-time curve for fully developed fire [6].

The fire evolution from the ignition until the flashover depends from several factors, some related with the fuel and oxidizer, others related with the local characteristics of the place where the fire develops. The main factors are the following:

- Type and quantity of available fuel;
- Quantity of oxidizer (oxygen) available, that depends on the compartment ventilation conditions and the dimensions of the openings;
- Compartment geometry;
- Type of pavements, walls and coatings;
- Atmospheric conditions (temperature, wind direction, etc.)

After the ignition, the fire starts to develop according to the fuel available in the place, releasing heat that causes the temperature increase. In this phase, the fire can conclude due to the lack of fuel material (fire controlled by the fuel), or by oxidizer deficit (fire controlled by ventilation). If there is sufficient fuel and oxidizer and no outside intervention, the temperature in the compartment continuous to increase. This situation leads to the ignition of materials that until that moment had not initiated the combustion process yet. The flashover establishes the transition to the burning phase. The burning phase takes place when all the fuel in the compartment is involved in the fire. Usually the flashover occurs when the temperature of the released gases reaches close to 600 ºC. It is in the burning phase where the higher temperature can be observed, it can reach values higher than 1000 ºC [7]. However, the temperature inside a compartment where a fire is developing is not uniform, near the ceiling the temperature is higher when compared with the flooring and lower places of the walls. The hot gases produced during the fire go to the higher part of the compartment and the flames elongate towards the ceiling [10]. Not all the fires have a complete development, due to direct intervention (firefighters action or automatic extinguishing systems, for example), or due to the compartment characteristics (lack of oxidizer, for example), the fire can be extinguished before reaching the burning phase [7].

2.2.2. Fire curves

In a fire scenario, for a given compartment it is possible to obtain temperature evolution curves. The effect of these curves, with reasonable approximation shouldn’t be exceed during the life time of the building. The determination of these curves is obtained by solving the energy balance equation for that compartment, obeying to some frontier conditions. Comparing several curves that had been proposed, frequently, is possible to see that for a continuous combustion and controlled ventilation the curve values are similar. In the part 1.2 of Eurocode 1 are defined the thermal actions that should be considered for the design of elements

with support function. In the Figure 2.7 is possible to see the time temperature curves [4].

Standard temperature-time curve is given by [9]:

$\theta_g = 20 + 345 \log_{10}(8t + 1)$ [ºC]

where

θ_g is the gas temperature in the fire compartment [ºC]

t is the time [min]

External fire curve is given by [9]:

$\theta_g = 660 (1 - 0{,}687\, e^{-0{,}32t} - 0{,}313\, e^{-3{,}8t}) + 20$ [ºC]

where

θ_g is the gas temperature in the fire compartment [ºC]

t is the time [min]

Hydrocarbon curve is given by [9]:

$\theta_g = 1080 (1 - 0{,}325\, e^{-0{,}167t} - 0{,}675\, e^{-2{,}5t}) + 20$ [ºC]

where

θ_g is the gas temperature in the fire compartment [ºC]

t is the time [min]

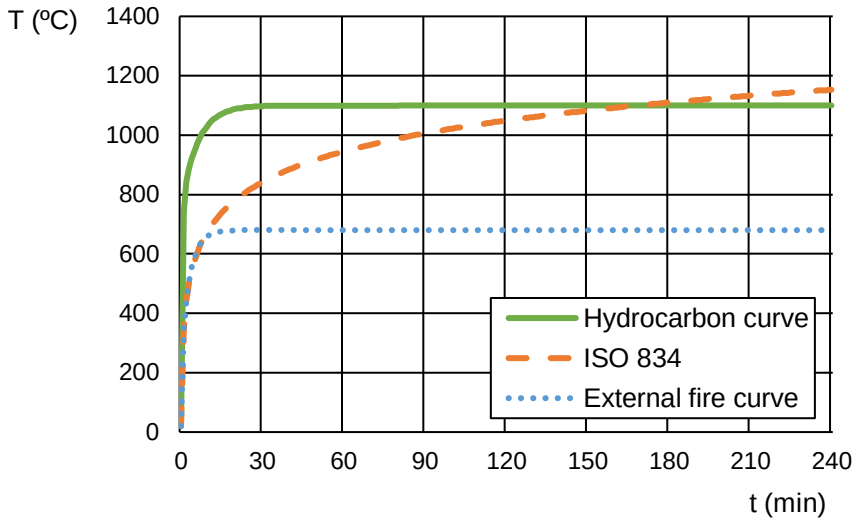

Figure 2.7 – Time temperature curves for post-flashover fires.

2.2.3. Fire resistance according to European legislation

In terms of requirements regarding the fire performance in construction materials it was publish by CE and CEN several documents, highlighting the *"Decisão nº 2000/367/CE"*. This document defines the classification to adopt at community level. The fundamental criteria used to characterize the fire resistance are:

- Load bearing capacity (represented by R);
- Integrity against flames and hot gases (represented by E);
- Thermal insulation (represented by I).

These criteria can be associated with each other as shown in Table 2.1.

Table 2.1 – Fire resistance classification [7].

<table>
<tr><td rowspan="2">Element functions</td><td colspan="3">Requirements</td></tr>
<tr><td>Stability</td><td>Integrity</td><td>Insulation</td></tr>
<tr><td>Support</td><td>R</td><td>-</td><td>-</td></tr>
<tr><td rowspan="2">Compartmentalization</td><td rowspan="2">-</td><td>E</td><td>-</td></tr>
<tr><td colspan="2">EI</td></tr>
<tr><td rowspan="2">Support and compartmentalization</td><td colspan="2">RE</td><td>-</td></tr>
<tr><td colspan="3">REI</td></tr>
</table>

The classification applicable to walls, pavements, beams, columns, balconies and stairs is presented in Table 2.2. The numbers associated to the classification specifies the number of minutes that an element can withstand while performing their function [7].

Table 2.2 – Requirements for load-bearing elements and without compartmentalization function [7].

Classification	Time steps (min)									
R	15	20	30	45	60	90	120	180	240	360

2.2.4. Passive and active fire protection systems in buildings

Fire safety in a building is usually achieved with a combination of active and passive fire protection systems [10]. Passive fire protection systems are those elements in a building that may contribute to increased fire safety and are characterized by the following:

- Do not require activation by fire effects or products to carry out their intended purpose;
- Are self-contained or independent in action;
- Are not intentionally acting upon the inherent fire process.

In pre-flashover fires, passive fire protection includes a selection of materials for building construction and interior linings that do not support rapid flame spread or smoke production in the growth period. In post-flashover fires, passive fire protection is provided by structures and assemblies with sufficient fire resistance to prevent both spread of fire and structural collapse [10].

Active fire protection systems are those which require activation by fire effects or products to carry out their intended purpose. These protection systems are characterized by time dependent performance. They need performance testing and maintenance throughout their service life to ensure their response in their “through life” state. The following examples are different types of active fire protection systems [10]:

- Detection and alarm equipment;
- Suppression systems;
- Exit and emergency lighting;
- Automatic doors, and fire dampers;
- Smoke management systems;
- Supporting services, for example, power and water supplies.

One of the best forms of active fire protection is an automatic sprinkler system. The sprinkler system discharges water over a local area under one sprinkler head when is activated by local high temperatures. As the local temperatures increase more sprinkler heads will be activated. Sprinkler systems can prevent small fires from growing larger and may even extinguish some fires. A sprinkler system must operate early in a fire because the water supply system is designed to tackle a small or moderate fire, well before flashover occurs [10].

2.2.5. Fire effects on RC elements

Nowadays, the behavior of the reinforced concrete exposed to fire is not well characterized and future investigation is needed in almost all the aspects. Most of the research is focused on isolated reinforced concrete elements. There is a need to develop models that consider the fire effects in a complete structure [11]. In this Chapter it is presented some of the fire effects on RC elements.

a) Chemical changes of concrete subjected to high temperatures

When subjected to heating, the concrete has physical and chemical changes. The chemical changes are especially complex due to the non-uniformity of the concrete constituted by cement and aggregates. Initially, the water in the concrete vaporizes between 100-140 ºC, causing an increase in pressure in water vapour. Close to 400 ºC the calcium hydroxide in the cement begins to dehydrate generating more water vapour that leads to a reduction in the physical strength of the material. The physical and chemical changes of the concrete reduce the compressive

strength, which remains constant until a certain temperature. After that temperature the compressive strength dramatically reduces [11].

b) Spalling

Spalling is one of the less understood processes in the concrete. There are several prerequisites for the spalling to occur. Normally it is necessary at least 2% volume of water and a thermal gradient of at least 5 ºC/mm. The spalling is practically certain if the thermal gradient is 7-8 ºC/mm. On the other hand, the effect of spalling can be reduced with the use of polypropylene fibres. These when heated change from solid to gas and this can create a passage for the water vapour to go from the inside of the concrete to the outside. This situation reduces the vapour pressure in the concrete. It is important to mention that the polypropylene fibres can lead to cracks in the deeper layers of the concrete that can lead to adverse structural consequences [11].

Figure 2.8 – Fire spalling of the external wall [12].

Figure 2.9 – Fire spalling in the roof [12].

c) Cracking

It is believed that the process that originates the cracks is the same that originates the spalling that is the thermal expansion and the concrete dehydration. In a study performed on the cracks in a building exposed to fire was associated the depth of the cracks with the temperature of the fire and mainly with the origin of the fire [11] [13].

2.3. Post-Earthquake Fire

2.3.1. General overview

The ordinary fires in the urban environment will generally follow several steps, ignition, growth, detection, report, response, suppression activities and extinguishment (by suppression activities, or due to exhaustion of the fuel). The process of post-earthquake fires will be like ordinary fires, but the fire protection response interactions are likely to be disrupted during and following a major earthquake. The disruption can be because of several factors, for example, the likelihood of multiple simultaneous ignitions, detection delays, reporting delays,

response of fire brigades, water supplies reduced or exhausted. The multiple simultaneous ignitions arise from the widespread effects of earthquakes. The fires would be easily extinguished in normal situations but due to insufficient fire service resources they could have the opportunity to grow and spread over large areas. The detection delays can happen due to damaged detectors or distracted observers but usually the time until the discovery of post-earthquake fire is not different from that at other times. The reporting delays can be caused by failure of communications systems due to damage and overload from high usage levels [10] [14].

There are historical evidences that confirm the appearance of fire after an earthquake in the built urban environment. The consequences of these events lead to losses of lives and property. There are three main combined aspects that under normal circumstances allow a response to fires in buildings, both active and passive fire protection systems and manual fire-fighting by a fire brigade. Adequate water supplies need to be available because of the difficulty of stopping fire spread without water. However, urban underground water distribution systems are vulnerable to earthquake shaking and failures are to be expected after an earthquake. The structural and non-structural damage caused to buildings by earthquakes can lead to the failure of passive protection systems. The passive protection can be damaged by cracking, buckling or breaking, and the openings can lead to increase ventilation of compartment fires. The openings also allow the migration of smoke and hot gases to other areas of the building. Sometimes, after an earthquake, active fire protection systems (detection, alarm and suppression systems) can also be unreliable. This situation leads to undetected ignitions which can result in large fires that are more difficult to extinguish. Following a major earthquake, it is likely that the response of fire brigades be impaired. Can be impaired by several reasons, reporting delays caused by the failure of communications systems, impassable access routes or traffic jams, loss of operational availability of vehicles and equipment caused by earthquake damage. The possibility of multiple simultaneous ignitions and insufficient fire brigade resources will delay fire brigade attendance [10].

2.3.2. Post-Earthquake fire ignition sources

Post-earthquake ignition sources are mainly electrical or gas related, but can also include open flame, hot surfaces, exothermic chemical reactions from spilled chemicals and fires intentionally lit [14]. Structural damage caused by earthquake shaking can stress electrical wiring causing short-circuits that can lead to ignitions. Earthquake damage to gas appliances, gas supply lines or gas storage facilities can liberate gas which can be ignited by electrical sources or flames in the appliances themselves. Electrical appliances, for example, cookers, gas-fuelled water heaters and solid fuel burners that are insufficiently restrained can topple or shift sideways, and their residual heat may initiate fires in combustible materials brought in contact with the hot surfaces. The restoration of electrical and gas supplies to damaged appliances and wiring can lead to ignition of combustibles in contact and ignition of leaking gas. It is not possible to eliminate all initial fire outbreaks following a major earthquake but the risk of these could be reduced if some fire preventive practices and installation procedures are performed. The main actions to reduce the post-earthquake fire sources are the education of the population to minimize the risk of fire and the adequate design of the gas networks including an automatic valve that reduces the gas quantities in case of damage in the network. These automatic valves are placed in the pipe after the gas meter, with these after an earthquake the amount of gas inside the house is reduced. In the Figures 2.10 and 2.11 are represented the cutaway view of horizontal valves that can be used to reduce the quantity of gas to the building. The electric power networks usually have a security device that shuts off the network during several seconds after the beginning of a big earthquake [10].

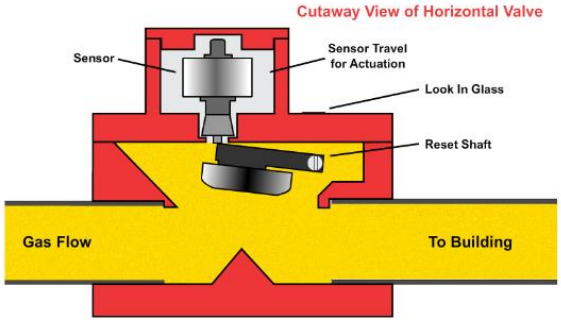

Figure 2.10 – Cutaway view of horizontal valve in normal operation [15].

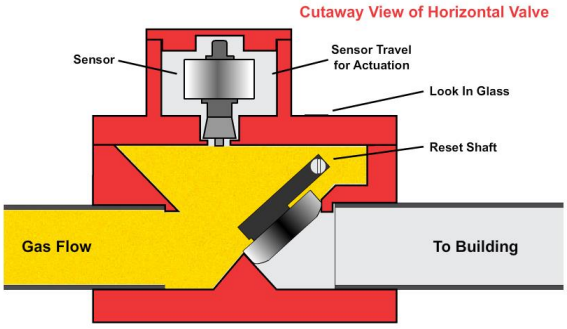

Figure 2.11 – Cutaway view of horizontal valve after an earthquake [15].

2.3.3. Review of historical data

Throughout the history is possible to find several examples of post-earthquake fires. In Portugal the most know case of post-earthquake fire was in Lisbon in the November first in 1755. About 2/3 of the constructions were destroyed by the vibrations and fire. The total values of victims are between 5000 and 40 000 dead [1]. There are also more recent examples, like the Hokkaido Nansei-oki earthquake, Northern Japan in 1993. In this earthquake 246 people were dead or missing, 190 houses and buildings were consumed by fire over an 11-hour period [10]. The town of Aonae was destroyed by conflagration following earthquake and tsunami. Building-to-building fire spread was accelerated by externally stored propane and kerosene tanks used for cooking and heating. Another example is the 1994 earthquake in Northridge, San Fernando Valley in Southern California. This earthquake had 58 fatalities (none from fire) and 1500 serious injuries. There were 30 to 50 significant fires initially following the earthquake, and after less than 8 hours the total number of fires was about 110. Principal cause was gas leaks from natural gas pipelines and appliances. The restoration of gas and power after a few days caused significant number of fires [10]. There is also a different perspective for the post-earthquake fire when the fire does not start immediately after the earthquake. The Great East Japan Earthquake, which occurred on 11 March 2011 was one of the largest earthquake in recent Japanese history and resulted in the generation of

large amounts of disaster waste. It was necessary the creation of outdoor storage areas to be able to deposit the disaster waste. In these areas, in the Tohoku region, more than 40 fires occurred. One probable cause of the fires is thought to have been the heat generated by fermentation of microorganisms. The microorganisms can thrive easy in those conditions, and the heat created can lead to spontaneous ignition. The materials deposited in the outdoor storage areas have a huge influence on this process, it is expected that the presence of wood will most likely lead to more ignitions than the presence of concrete, for instance. A study performed in this topic revealed that the heat generated during fermentation of wood chips and rotten tatami was most likely the trigger of the spontaneous ignition. This situation only serves as an example that the post-earthquake fires can appear from different causes and maybe in places where were not initially expected [16] [17].

2.3.4. Previous works developed

The effects of fire after an earthquake on the RC buildings are not very well known. In the past years there were developed several numerical and experimental studies regarding the post-earthquake fire to be able to better understand the phenomenon.

Beyond the research of post-earthquake fire on RC buildings there are also works developed regarding the post-earthquake fire on steel structures. In some works, the focus is the analysis of the behavior of steel frames to post-earthquake fire [18]. There are studies were the aim is to analyse the impact that the earthquake has on the passive fire protection of the steel structures. Some materials that are used as passive fire protection have a brittle behavior and suffer damage due to the seismic action, leading to a lower fire resistance of the steel structures [19] [20]. There is also research regarding the behavior of the joints and connections of the steel frames. The results show that severe damage on the connections lead to reduced fire resistance capacities [21] [22].

Some experimental studies developed in frames showed that using standard fire curve may not be very accurate since different elements can have different temperature profiles [23] [24]. It was observed that the brick infill walls provide insulation to the RC structural elements and slow the transmission of heat to these elements. This shows the beneficial effect that the masonry walls have on the columns and beams integrated in the masonry walls, and this beneficial effect should be considered while designing the columns and beams [23]. The position of the openings in the compartments and the resulting movement of fire plume and hot gases have also an influence in terms of the evolution of temperatures in the structural sections. This situation may or may not lead to an overlap between the locations of the damage caused by the earthquake and the damage caused by the fire [24]. Some numerical and experimental studies were also developed regarding the fire resistance of CFRP-strengthened reinforced concrete elements [25] [26]. The results show that the fire resistances of the specimens subjected to life safety (LS) and collapse prevention (CP) damage levels are about 32 and 15 min and for the CFRP-strengthened specimen is about 43 and 23 min, respectively. This solution represents a 25% increase at LS level and 35% increase at CP level [25]. Also, regarding the use of CFRP, using this solution to relocate plastic hinges of the beams away from the columns improve the post-earthquake fire resistance of the frames [27].

It was also observed that buildings designed for stronger earthquakes have more resistance against fire, even in the case of fire alone. This shows that the stiffness of structures has an important role in the fire resistance [28]. Other study showed that a structure that have significantly suffered damaged from an earthquake have lower fire resistance when compared with undamaged structures and that the fire resistance of the frames is mostly dependent of the resistance of the frames [29].

Although using the standard fire curve may not be very accurate, in this dissertation it is used the fire curve ISO 834 for the numerical analysis. Using the ISO 834 simplifies the models because there are not considered different temperature evolutions in different elements in the reinforced concrete structures. This consideration will also lead to an overlap between the damage caused by the seismic action and the fire. The numerical simulations developed in this dissertation

maybe do not completely correspond to a real situation but can serve as a preliminary study to see the impact of different typologies of damage in reinforced concrete structures.

3. Materials thermal and mechanical properties at elevated temperatures

3.1. Concrete thermal properties

The concrete properties change with the temperature. In this Chapter there will be presented the concrete thermal properties such as the thermal elongation, specific heat, density and thermal conductivity.

3.1.1. Thermal elongation

The following equations 3.1 and 3.2 can be used to obtain the thermal strain $\varepsilon_c(\theta)$ of concrete with reference to the length at 20 ºC [30]:

Siliceous aggregates:

$$\varepsilon_c(\theta) = -1{,}8 \times 10^{-4} + 9 \times 10^{-6}\,\theta + 2{,}3 \times 10^{-11}\,\theta^3 \quad \text{for } 20\,^{\circ}\text{C} \le \theta \le 700\,^{\circ}\text{C}$$

$$\varepsilon_c(\theta) = 14 \times 10^{-3} \quad \text{for } 700\,^{\circ}\text{C} < \theta \le 1200\,^{\circ}\text{C} \qquad (3.1)$$

Calcareous aggregates:

$$\varepsilon_c(\theta) = -1{,}2 \times 10^{-4} + 6 \times 10^{-6}\,\theta + 1{,}4 \times 10^{-11}\,\theta^3 \quad \text{for } 20\,^{\circ}\text{C} \le \theta \le 805\,^{\circ}\text{C}$$

$$\varepsilon_c(\theta) = 12 \times 10^{-3} \quad \text{for } 805\,^{\circ}\text{C} < \theta \le 1200\,^{\circ}\text{C} \qquad (3.2)$$

Where θ is the concrete temperature (ºC).

In the Figure 3.1 is represented the variation of the thermal elongation with temperatures for siliceous and calcareous aggregate concrete.

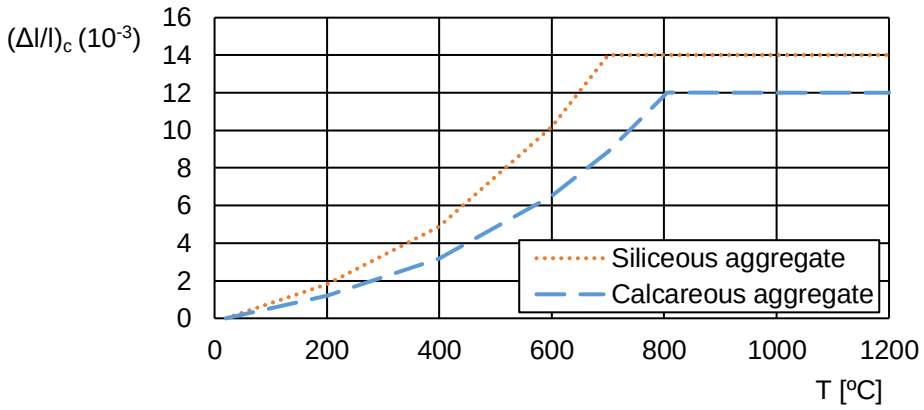

Figure 3.1 – Total thermal elongation of concrete [30].

3.1.2. Specific heat

The specific heat $c_p(\theta)$ of siliceous and calcareous dry concrete (u = 0%) can be obtained by equation 3.3 [30]:

$C_p(\theta) = 900$ (J/kg.K) for 20 ºC ≤ θ ≤ 100 ºC

$C_p(\theta) = 900 + (\theta - 100)$ (J/kg.K) for 100 ºC < θ ≤ 200 ºC

$C_p(\theta) = 1000 + (\theta - 200)/2$ (J/kg.K) for 200 ºC < θ ≤ 400 ºC

$C_p(\theta) = 1100$ (J/kg.K) for 400 ºC < θ ≤ 1200 ºC

(3.3)

The specific heat and the peaks of specific heat are represented in Figure 3.2. For other moisture contents is acceptable to use a linear interpolation [30].

$C_{p,peak}$ = 900 J/kg.K for moisture content of 0 % of concrete weight

$C_{p,peak}$ = 1470 J/kg.K for moisture content of 1,5 % of concrete weight

$C_{p,peak}$ = 2020 J/kg.K for moisture content of 3,0 % of concrete weight

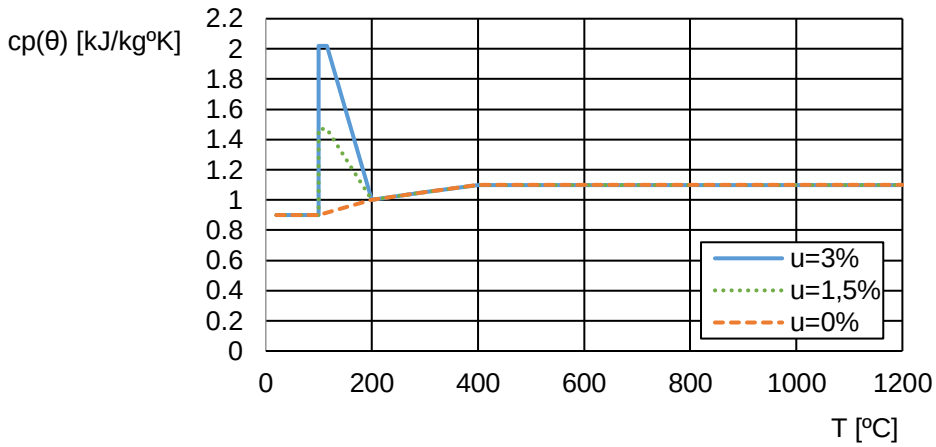

Figure 3.2 – Specific heat, as function of temperature at 3 different moisture contents [30].

3.1.3. Density

The variation of density with temperature is influenced by water loss and is defined by the equation 3.4 [30].

$\rho(\theta) = \rho(20ºC)$ for $20ºC \leq \theta \leq 115ºC$

$\rho(\theta) = \rho(20ºC).(1 - 0{,}02(\theta - 115)/85)$ for $115ºC < \theta \leq 200ºC$

$\rho(\theta) = \rho(20ºC).(0{,}98 - 0{,}03(\theta - 200)/200)$ for $200ºC < \theta \leq 400ºC$

$\rho(\theta) = \rho(20ºC).(0{,}95 - 0{,}07(\theta - 400)/800)$ for $400ºC < \theta \leq 1200ºC$ (3.4)

3.1.4. Thermal conductivity

The thermal conductivity λ_c of concrete is defined between two different values, upper limit value and lower limit value.

The upper limit of thermal conductivity λ_c of normal weight concrete can be obtained with the equation 3.5 [30]:

$$\lambda_c = 2 - 0{,}2451\,(\theta/100) + 0{,}0107\,(\theta/100)^2 \text{ W/m K} \qquad \text{for } 20^{o}C \leq \theta \leq 1200^{o}C$$

(3.5)

Where θ is the concrete temperature.

The lower limit of thermal conductivity λ_c of normal weight concrete can be obtained with the equation 3.6 [30]:

$$\lambda_c = 1{,}36 - 0{,}136\,(\theta/100) + 0{,}0057\,(\theta/100)^2 \text{ W/m K} \qquad \text{for } 20^{o}C \leq \theta \leq 1200^{o}C$$

(3.6)

Where θ is the concrete temperature.

In the Figure 3.3 is represented the variation of the upper limit and lower limit of thermal conductivity with temperature [30].

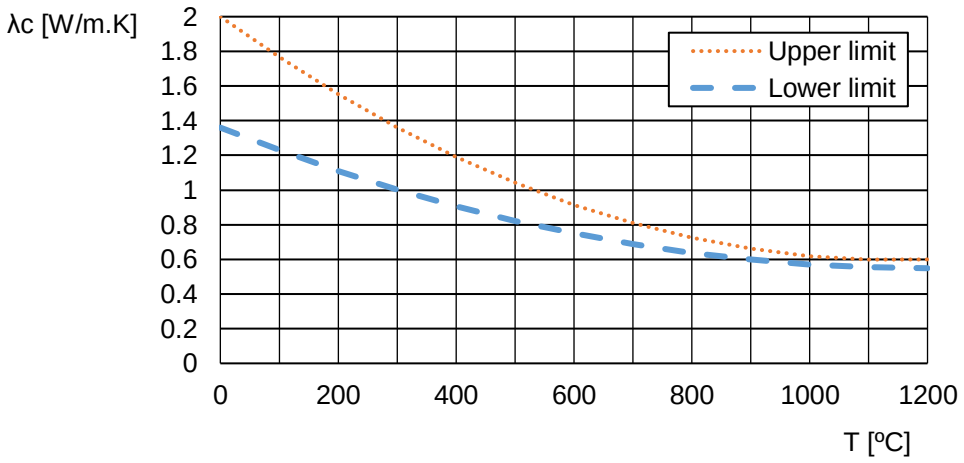

Figure 3.3 – Thermal conductivity of concrete, (1) upper limit, (2) lower limit [30].

3.2. Steel thermal properties

The steel properties change with the temperature. In this Chapter there will be presented the steel thermal properties such as the thermal elongation, specific heat and thermal conductivity.

3.2.1. Thermal elongation

The thermal elongation of steel Δl/l is defined from the following equations. The variation of the thermal elongation with temperature is represented in Figure 3.4 [30] [31].

For $20^{o}C \leq \theta_a < 750^{o}C$:

$$\Delta l/l = 1{,}2 \times 10^{-5}\, \theta_a + 0{,}4 \times 10^{-8}\, \theta_a^2 - 2{,}416 \times 10^{-4} \quad (3.7)$$

For $750^{o}C \leq \theta_a \leq 860^{o}C$:

$$\Delta l/l = 1{,}1 \times 10^{-2} \quad (3.8)$$

For $860^{o}C < \theta_a \leq 1200^{o}C$:

$$\Delta l/l = 2 \times 10^{-5}\, \theta_a - 6{,}2 \times 10^{-3} \quad (3.9)$$

Where:

l is the length at 20ºC;

Δl is the temperature induced elongation;

θ_a is the steel temperature [ºC].

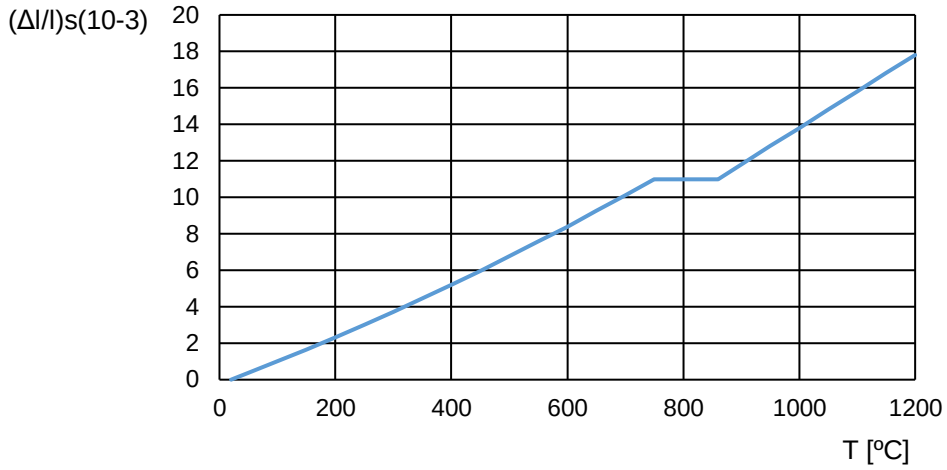

Figure 3.4 – Thermal elongation of carbon steel as function of the temperature [30] [31].

3.2.2. Specific heat

The specific heat of steel c_a is defined from the following equations. The variation of the specific heat with temperature is represented in Figure 3.5 [31].

For 20ºC ≤ θ_a < 600ºC:

$$C_a = 425 + 7{,}73 \times 10^{-1}\,\theta_a - 1{,}69 \times 10^{-3}\,\theta_a^2 + 2{,}22 \times 10^{-6}\,\theta_a^3 \text{ J/kgK} \quad (3.10)$$

For 600ºC ≤ θ_a < 735ºC:

$$C_a = 666 + 13002/(738 - \theta_a) \text{ J/kgK} \quad (3.11)$$

For 735ºC ≤ θ_a < 900ºC:

$$C_a = 545 + 17820/(\theta_a - 731) \text{ J/kgK} \quad (3.12)$$

For 900ºC ≤ θ_a ≤ 1200ºC:

$$C_a = 650 \text{ J/kgK} \quad (3.13)$$

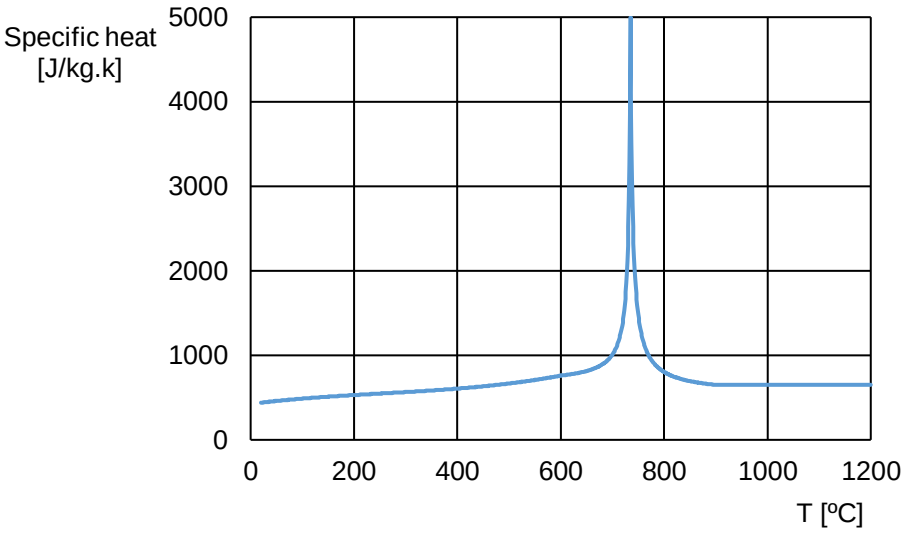

Figure 3.5 – Specific heat of carbon steel as a function of the temperature [31].

3.2.3. Unit mass

The unit mass of steel ρ_a can be independent of the steel temperature. The value that can be used is the following [31]:

$\rho_a = 7850 \text{ kg/m}^3$

3.2.4. Thermal conductivity

The thermal conductivity of steel λ_a is defined from the following equations and is represented in Figure 3.6 [31].

$\lambda_a = 54 - 3{,}33 \times 10^{-2} \times \theta_a$ W/mK for $20^oC \leq \theta_a < 800^oC$ (3.14)

$\lambda_a = 27{,}3$ W/mK for $800^oC \leq \theta_a \leq 1200^oC$ (3.15)

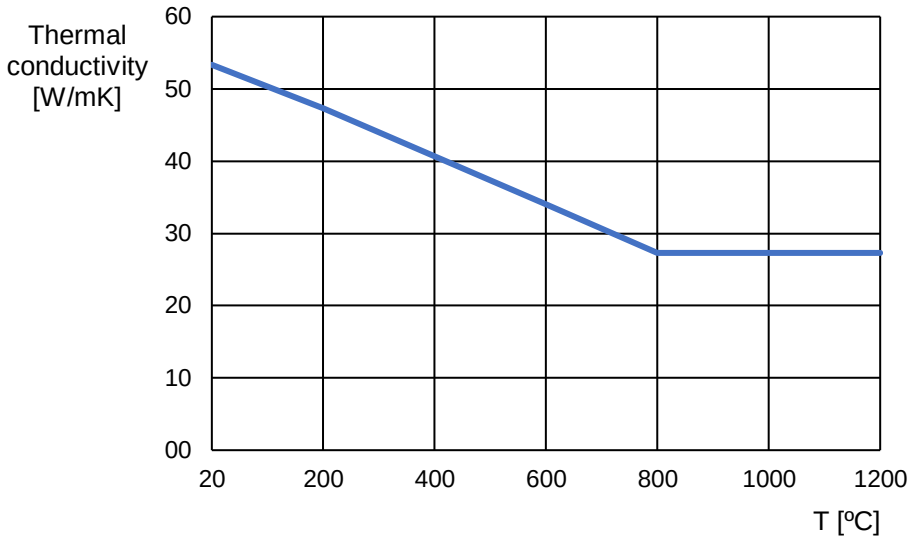

Figure 3.6 – Thermal conductivity of carbon steel as a function of the temperature [31].

3.3. Concrete mechanical properties

Numerical values of strength and deformation properties presented in this section are based on a steady and transient state tests and sometimes a combination of both. The materials models presented are only applicable for heating rates between 2 and 50 K/min because the creep effects are not explicitly considered [30].

For uniaxial stressed concrete at elevated temperatures, the strength and deformation properties shall be obtained from the stress-strain relationships presented in Figure 3.7. The stress-strain relationships are defined by two parameters [30]:

- The compressive strength $f_{c,\theta}$
- The strain $\varepsilon_{c1,\theta}$ corresponding to $f_{c,\theta}$

The values for the two mentioned parameters are presented in Table 3.1 as a function of concrete temperatures. A linear interpolation can be used for intermediate values of temperature [30].

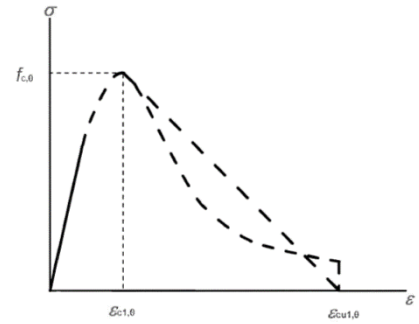

Range	Stress $\sigma(\theta)$
$\varepsilon \leq \varepsilon_{c1,\theta}$	$\frac{3\varepsilon f_{c,\theta}}{\varepsilon_{c1,\theta}\left(2+\left(\frac{\varepsilon}{\varepsilon_{c1,\theta}}\right)^3\right)}$
$\varepsilon_{c1(\theta)} < \varepsilon \leq \varepsilon_{cu1,\theta}$	For numerical purposes a descending branch should be adopted. Linear or non-linear models are permitted.

Figure 3.7 – Mathematical model for stress-strain relationships of concrete under compression at elevated temperatures [30].

Table 3.1 – Values for the main parameters of the stress-strain relationships of normal weight concrete with siliceous or calcareous aggregates concrete at elevated temperatures [30].

Concrete temperature θ	Siliceous aggregates			Calcareous aggregates		
	$f_{c,\theta} / f_{ck}$	$\varepsilon_{c1,\theta}$	$\varepsilon_{cu1,\theta}$	$f_{c,\theta} / f_{ck}$	$\varepsilon_{c1,\theta}$	$\varepsilon_{cu1,\theta}$
[ºC]	[-]	[-]	[-]	[-]	[-]	[-]
1	2	3	4	5	6	7
20	1,00	0,0025	0,0200	1,00	0,0025	0,0200
100	1,00	0,0040	0,0225	1,00	0,0040	0,0225
200	0,95	0,0055	0,0250	0,97	0,0055	0,0250
300	0,85	0,0070	0,0275	0,91	0,0070	0,0275
400	0,75	0,0100	0,0300	0,85	0,0100	0,0300
500	0,60	0,0150	0,0325	0,74	0,0150	0,0325
600	0,45	0,0250	0,0350	0,60	0,0250	0,0350
700	0,30	0,0250	0,0375	0,43	0,0250	0,0375
800	0,15	0,0250	0,0400	0,27	0,0250	0,0400
900	0,08	0,0250	0,0425	0,15	0,0250	0,0425
1000	0,04	0,0250	0,0450	0,06	0,0250	0,0450
1100	0,01	0,0250	0,0475	0,02	0,0250	0,0475
1200	0,00	-	-	0,00	-	-

The tensile strength of the concrete should normally be ignored (conservative approach). In the case of the necessity of considering the tensile strength the following expression can be used [30]:

$$f_{ck,t}(\theta) = k_{c,t}(\theta)\, f_{ck,t} \qquad (3.16)$$

In the absence of more accurate information, the following $k_{c,t}$ (θ) should be used (Figure 3.8) [30].

$k_{c,t}$ (θ) = 1,0 for 20ºC ≤ θ ≤ 100ºC (3.17)

$k_{c,t}$ (θ) = 1,0 – 1,0 (θ – 100)/500 for 100ºC < θ ≤ 600ºC (3.18)

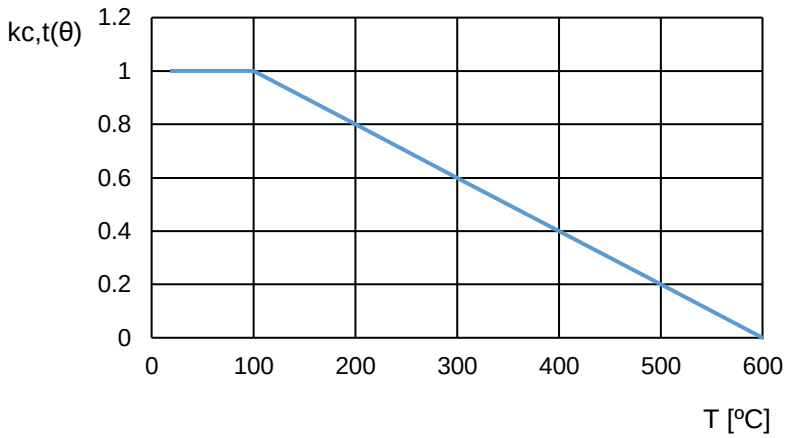

Figure 3.8 – Coefficient kc,t(θ) allowing for decrease of tensile strength (fck,t) of concrete at elevated temperatures [30].

3.4. Steel mechanical properties

The strength and deformation properties of steel at elevated temperatures should be obtained from the stress-strain relationship presented in Figure 3.9. The stress-strain relationship are defined by three parameters: slope of the linear elastic range $E_{s,\theta}$, the proportional limit $f_{sp,\theta}$ and the maximum stress level $f_{sy,\theta}$. The variation of these parameters with temperature is represented in Table 3.2, where intermediate values can be obtained by linear interpolation [30] [31].

Strain range	Stress σ	Tangent modulus
$\varepsilon \le \varepsilon_{p,\theta}$	$\varepsilon E_{a,\theta}$	$E_{a,\theta}$
$\varepsilon_{p,\theta} < \varepsilon < \varepsilon_{y,\theta}$	$f_{p,\theta} - c + (b/a)\left[a^2 - (\varepsilon_{y,\theta} - \varepsilon)^2\right]^{0,5}$	$\frac{b(\varepsilon_{y,\theta} - \varepsilon)}{a\left[a^2 - (\varepsilon_{y,\theta} - \varepsilon)^2\right]^{0,5}}$
$\varepsilon_{y,\theta} \le \varepsilon \le \varepsilon_{t,\theta}$	$f_{y,\theta}$	0
$\varepsilon_{t,\theta} < \varepsilon < \varepsilon_{u,\theta}$	$f_{y,\theta}\left[1 - (\varepsilon - \varepsilon_{t,\theta})/(\varepsilon_{u,\theta} - \varepsilon_{t,\theta})\right]$	-
$\varepsilon = \varepsilon_{u,\theta}$	0,00	-
Parameters	$\varepsilon_{p,\theta} = f_{p,\theta}/E_{a,\theta}$ $\varepsilon_{y,\theta} = 0,02$	$\varepsilon_{t,\theta} = 0,15$ $\varepsilon_{u,\theta} = 0,20$
Functions	$a^2 = (\varepsilon_{y,\theta} - \varepsilon_{p,\theta})(\varepsilon_{y,\theta} - \varepsilon_{p,\theta} + c/E_{a,\theta})$ $b^2 = c(\varepsilon_{y,\theta} - \varepsilon_{p,\theta})E_{a,\theta} + c^2$ $c = \frac{(f_{y,\theta} - f_{p,\theta})^2}{(\varepsilon_{y,\theta} - \varepsilon_{p,\theta})E_{a,\theta} - 2(f_{y,\theta} - f_{p,\theta})}$	

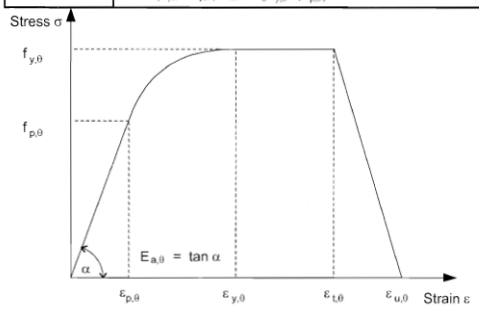

Figure 3.9 – Stress-strain relationship for carbon steel at elevated temperatures [30] [31].

Table 3.2 – Reduction factors for stress-strain relationship of carbon steel at elevated temperatures [30] [31].

Steel temperature θ_a	Reduction factors at temperature θ_a relative to the value of f_y or E_a at 20ºC		
	Reduction factor (relative to f_y) for effective yield strength	Reduction factor (relative to f_y) for proportional limit	Reduction factor (relative to E_a) for the slope of the linear elastic range
	$k_{y,\theta} = f_{y,\theta}/f_y$	$k_{y,\theta} = f_{y,\theta}/f_y$	$k_{E,\theta} = E_{a,\theta}/E_a$
20 ºC	1,000	1,000	1,000
100 ºC	1,000	1,000	1,000
200 ºC	1,000	0,807	0,900
300 ºC	1,000	0,613	0,800
400 ºC	1,000	0,420	0,700
500 ºC	0,780	0,360	0,600
600 ºC	0,470	0,180	0,310
700 ºC	0,230	0,075	0,130
800 ºC	0,110	0,050	0,090
900 ºC	0,060	0,0375	0,0675
1000 ºC	0,040	0,0250	0,0450
1100 ºC	0,020	0,0125	0,0225
1200 ºC	0,000	0,0000	0,0000
NOTE: For intermediate values of the steel temperature, linear interpolation may be used.			

4. SAFIR: A thermal/structural program for modelling structures under fire

4.1. General overview

SAFIR is a computer program for the analysis of structures under ambient temperature and elevated temperature conditions. The program is based on the Finite Element Method (FEM) and can be used to study the behaviour of one, two and three-dimensional structures [32]. SAFIR can perform thermal and mechanical analysis. They are performed separately and subsequently. The temperature distribution will deeply influence the mechanical response, but the opposite is not currently handled by the software. There is no influence of the cracking of concrete determined in the mechanical analysis on the thermal conductivity that is used in the thermal analysis [33]. If a 2D or 3D beam finite element is used in the mechanical analysis, a 2D thermal analysis is performed to determine the temperature distribution on the cross section of the beam. This means that the heat flux is not considered along the longitudinal axis of the beam finite element during the structural analysis [32].

4.2. Capabilities and limitations of SAFIR

It is important to know the capabilities and limitations of SAFIR to understand the results and achieve consistent conclusions. The contact between two adjacent materials is assumed to be perfect, there is no resistance to heat transfer by conduction at the interface between two adjacent elements with different properties. The stress distribution does not influence the thermal analysis. Cracking in concrete will not create anisotropy in the thermal properties. SAFIR cannot predict spalling in

the concrete. The beam finite element cannot detect failure by local buckling, by slip between concrete and the rebars or shear failure because SAFIR is based on the Bernoulli hypothesis [32].

4.3. Concrete and steel thermal properties

The input parameters to be introduced in SAFIR are the type of aggregate (siliceous or calcareous), the specific mass of dry concrete (kg/m^3), free water content (kg/m^3), and a last parameter that allows tuning the thermal conductivity between the lower and upper limit (clause 3.3.3 of EN 1992-1-2) [15] [34]. The specific heat of the dry material and variation of specific mass are according to clause 3.3.2 o EN 1992-1-2 [15] [34]. The evaporation of moisture is considered in the enthalpy formulation (the energy dissipated by the evaporation is released at constant rate from 100 to 115 ºC, and then the energy release rate is linearly decreasing from 115 to 200 ºC). The subsequent movements and participation in the heat balance of vapor are neglected. There is no re-condensation of the water during cooling and the thermal conductivity is considered at the value of the maximum reached temperature and not reversible. The steel used for reinforcement bars follows the equations of Eurocode EN 1992-1-2 [30]. In SAFIR the thermal properties are considered reversible during cooling [34].

4.3.1. Concrete structural properties

In SAFIR the concrete models are based on the laws of EN 1992-1-2 [30] [34]. The input parameters to be introduced in SAFIR are the aggregate type (siliceous or calcareous), the Poisson's ratio, the compressive strength and the tensile strength. In addition, in the model, the user can select if the transient creep

is treated implicitly or explicitly. The user can also select between normal strength concrete (NSC) and high strength concrete (HSC) [34].

4.3.2. Steel mechanical properties

In SAFIR the steel models are based on the corresponding Eurocodes. The input parameters to be introduced in SAFIR are Young modulus, the Poisson's ratio and the yield strength. There are two additional parameters to be defined by the user to specify the behaviour during cooling. The parameters are the maximum temperature beyond which the behaviour is not reversible during cooling (threshold) and the rate of decrease of the residual yield strength when the maximum temperature has exceeded the threshold (in MPa/ºC). For reinforcing carbon steel, the models for ductility class A, B and C (Figure 3.3 of EN 1992-1-2) with class N values for hot rolled and for cold worked steel (Table 3.2a of EN 1992-1-2) are available [30] [34].

5. Regulatory requirements

5.1. SCIE

5.1.1. Introduction

In the present Chapter will be presented some concepts of regulatory requirements in Portugal regarding the fire safety in buildings. The technical regulation of fire safety in buildings (SCIE) establishes 12 different types of buildings according to its occupancy. It also divides the buildings into 6 risk areas and 4 risk categories. The risk areas can be from A to F and the risk categories from 1st to 4th.

5.1.2. Building type occupancy

The 12 different building types are presented below:

- Building type I – Housing
- Building type II – Parking
- Building type III – Administrative
- Building type IV – Schools
- Building type V – Hospitals and nursing homes
- Building type VI – Shows and public meetings
- Building type VII – Hotel and catering
- Building type VIII – Shops and transport hubs
- Building type IX – Sports and leisure activities
- Building type X – Museums and art galleries

- Building type XI – Library and archives
- Building type XII – Industrial, workshops and warehouses

5.1.3. Risk areas

All the areas in a building are classified according to the nature of the risk. There are 6 defined risk areas, from A to F, where the risk areas A is the area with the lowest degree of risk. Below are presented the risk areas and the information needed to categorize each one of them [35] [36].

a) Risk area “A”
   - Area where there is no particular risk in which the following conditions are met:
     i) The effective does not exceed 100 people;
     ii) The effective number of the public does not exceed 50 people;
     iii) More than 90% of occupants are not limited in mobility or in the ability to perceive and react to an alarm;
     iv) The activities carried out therein or the products, materials and equipment it contains do not involve aggravated fire hazards [35] [36];

b) Risk area “B”
   - Area accessible to the public or to staff assigned to the establishment with the effective higher than 100 people or a public effective of more than 50 persons in which the following conditions are met:
     i) More than 90% of occupants are not limited in mobility or in the ability to perceive and react to an alarm;

ii) The activities carried out therein or the products, materials and equipment it contains do not involve aggravated fire hazards [35] [36];

c) Risk area “C”
   - Area which presents exacerbated risks of outbreak and fire developing due to the activities carried out therein or the characteristics of the products, materials or equipment contained therein, namely the fire load, quantity of inflammable liquids and compartment volumes [35] [36];

d) Risk area “D”
   - Area of building with bed rest or intended to receive children with age inferior to 6 years or persons with limited mobility or ability to perceive and respond to an alarm [35] [36];

e) Risk area “E”
   - Area of a building for sleeping, in which persons do not present the limitations indicated in places of risk D [35] [36];

f) Risk area “F”
   - Area which has the means and systems essential to the continuity of relevant social activities, namely the centres of communication, command and control [35] [36];

5.1.4. Risk categories

Each one of the 12 building types is classified, regarding the risk, in one of four categories (from 1st, less burdensome, to 4th, more burdensome). The following factors allow to define the risk category of a certain building [36]:

- Height of the building;

- Effective (maximum number o people present);
- Gross area;
- Indoor or outdoor space;
- Number of floors below reference plane;
- Independent exit (direct to the outside and at the level of the reference plane) of places type D and E;
- Fire load and density of fire load.

Each utilization type can have different factors influencing the risk category. Table 5.1 shows which factor should be considered for each utilization type.

Table 5.1 – Risk factors for each utilization type [37].

Utilization type	I	II	III	IV	V	VI	VII	VIII	IX	X	XI	XII
Height	x	x	x	x	x	x	x	x	x	x	x	
Gross area		x										
Direct exit to the exterior - place D, E				x	x		x					
Indoor/Outdoor		x				x			x			x
Total effective			x	x	x	x	x	x	x	x	x	
Effective in place D, E				x	x		x					
Number of floors below reference plane	x	x				x		x	x		x	x
Fire load											x	
Density of fire load												x

By analysing the information in the Table is possible to see that the height and the total effective are the most influential risk factors. The Tables 5.2 to 5.4 are some examples of how to classify the risk categories for some utilization types. In each case the category chosen is the lowest one that respects all the indicated criteria.

Table 5.2 – Risk categories in utilization type II – Parking [36].

Categories	Maximum values for utilization type II when integrated in a building			Outdoor
	Height	Gross area	Number of floors below reference plane	
1st	-			Yes
	≤ 9 m	≤ 3200 m^2	≤ 1	No
2nd	≤ 28 m	≤ 9600 m^2	≤ 3	No
3rd	≤ 28 m	≤ 32000 m^2	≤ 5	No
4th	> 28 m	> 32000 m^2	> 5	No

Table 5.3 – Risk categories in utilization type XI – Library and archives [36].

Categories	Maximum values for utilization type XI			
	Height	Number of floors below reference plane	Effective	Modified density of fire load
1st	≤ 9 m	0	≤ 100	≤ 1000 MJ/m^2
2nd	≤ 28 m	≤ 1	≤ 500	≤ 10000 MJ/m^2
3rd	≤ 28 m	≤ 2	≤ 1500	≤ 30000 MJ/m^2
4th	> 28 m	> 2	> 1500	> 30000 MJ/m^2

Table 5.4 – Risk categories in utilization type XII – Industrial, workshops and warehouses [36].

Categories	Maximum values for utilization type XII		
	Integrated in building		Outdoor
	Modified density of fire load	Number of floors below reference plane	Modified density of fire load
1st	≤ 500 MJ/m^2	0	≤ 1000 MJ/m^2
2nd	≤ 5000 MJ/m2	≤ 1	≤ 10000 MJ/m^2
3rd	≤ 15000 MJ/m2	≤ 1	≤ 30000 MJ/m^2
4th	> 15000 MJ/m2	> 1	> 30000 MJ/m^2

5.1.5. Fire resistance

With the utilization type and risk category defined, it is possible to determine the minimum fire resistance for the structural elements of buildings, as it is possible to see in Table 5.5. The occupancy type II (parking), XI (library and archives) and XII (industrial, workshops and warehouses) have higher minimum fire resistance when compared with the other utilization types. Those buildings have higher fire loads due to the presence of cars, books and industrial equipment, that leads to higher fire risk and consequently higher requirements. The classification of the risk categories for utilization type II, XI and XII were presented previously in Tables 5.2, 5.3 and 5.4 [35].

Table 5.5 – Minimum fire resistance of structural elements of buildings [35].

Utilization type	Risk categories				Element functions
	1st	2nd	3rd	4th	
I, III, IV, V, VI, VII, VIII, IX and X	R 30	R 60	R 90	R 120	Load bearing only
	REI 30	REI 60	REI 90	REI 120	Load bearing and fire separating function
II, XI and XII	R 60	R 90	R 120	R 180	Load bearing only
	REI 60	REI 90	REI 120	REI 180	Load bearing and fire separating function

6. Study at reinforced concrete section level

6.1. Introduction

The developing of numerical models based on finite element method (FEM) will always lead to errors in the results. The user must be aware of those errors and model limitations, evaluate mesh options, time-steps, type of materials and analysis, among other options that may lead to an accurate model. Although a time-step analysis is helpful to evaluate the errors, in the present work it will not be performed once it is considered that a time step of 5 seconds leads to acceptable results. In this Chapter it will be analysed the influence of the mesh and later it is also analysed the influence of damage in the section and the influence of the location of the fire frontiers. Due to symmetry, the sections observed in Figure 6.1 lead to the same results, considering that both have the same properties. This could be helpful to simplify big or complex sections. The section used in the mesh analysis is represented in Figure 6.1b and the characteristics used are in Table 6.1.

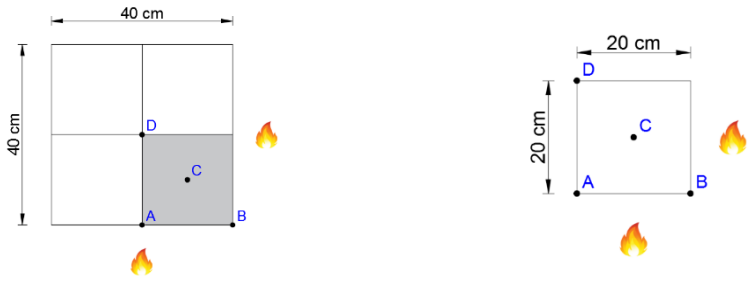

a) b)

Figure 6.1 – Simplification of the section. a) Entire section. b) One fourth of the section.

Table 6.1 – Section geometry, thermal concrete properties and fire curve.

Section geometry	A	0,2 x 0,2 m

Concrete properties [30]		
Concrete model		Siliceous aggregate
Specific mass of concrete	rho	2300 kg/m^3
Water content	w	46 kg/m^3
Coefficient of convection on heated surfaces	h_h	25 W/m^{2}K
Coefficient of convection on unheated surfaces	h_c	4 W/m^{2}K
Emissivity	ε	0,7

Fire curve		ISO 834

6.2. Influence of the mesh

For the sake of simplicity in the mesh analysis, the only material in the section is concrete and the section is quadrangular with the fire frontiers in perpendicular sides. The section configuration is possible to see in Figure 6.2. In the mesh analysis there will be four points analysed (A, B, C, D).

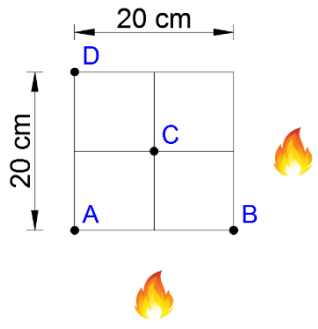

Figure 6.2 – Mesh 1, location of the points being analysed and fire frontiers.

In total there were developed six different meshes with different number of elements, which are presented below and can also be seen in Figure 6.3.

- Mesh 1: 2×2 (4 Elements), 10 cm width in each element;
- Mesh 2: 4×4 (16 Elements), 5 cm width in each element;
- Mesh 3: 8×8 (64 Elements), 2,5 cm width in each element;
- Mesh 4: 10×10 (100 Elements), 2 cm width in each element;
- Mesh 5: 16×16 (256 Elements), 1,25 cm width in each element;
- Mesh 6: 20×20 (400 Elements), 1 cm width in each element.

In Table 6.2 is represented the temperatures in points A, B, C and D in each mesh for different times. The mesh 1, with 4 elements leads to bigger errors when compared with the others meshes. It is possible to see negative values of temperature and that it is not plausible. With more elements the values of the temperature tend to approximate a certain value, and that value should be more accurate.

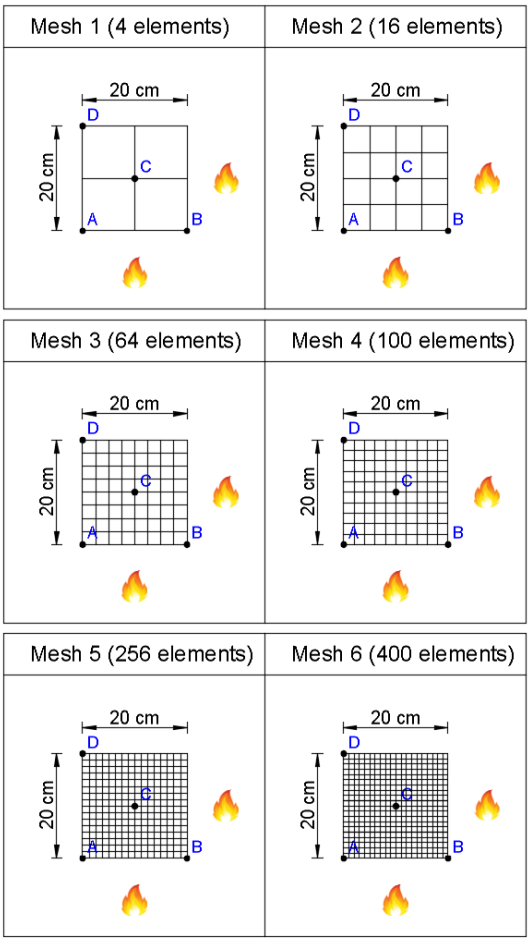

Figure 6.3 – Mesh 1 to 6.

Table 6.2 – Temperatures in nodes A, B, C and D for mesh 1 to 6.

		Mesh 1	Mesh 2	Mesh 3	Mesh 4	Mesh 5	Mesh 6
		4 Elements	16 Elements	64 Elements	100 Elements	256 Elements	400 Elements
Time (min)	Node	Temp. (ºC)	Temp. (ºC)	Temp. (ºC)	Temp. (ºC)	Temp. (ºC)	Temp. (ºC)
15	A	426,77	528,61	544,93	548,59	552,97	553,88
	B	615,05	702,24	708,76	709,11	708,76	708,61
	C	-153,29	6,56	19,67	20,58	21,64	21,9
	D	76,4	20,12	20	20	20	20
30	A	721,94	744,24	744,18	744,54	744,73	744,81
	B	831,16	835,21	834,13	833,82	833,51	833,46
	C	-187,18	20,99	34,69	37,92	41,31	42,08
	D	36,39	19,98	19,98	20,02	20,09	20,11
45	A	834,54	834,48	835,01	834,98	834,94	834,93
	B	898,64	899,1	898,29	898,18	898,14	898,15
	C	-103,64	68,06	67,49	70,87	74,32	75,15
	D	-35,26	17,18	20,51	20,96	21,48	21,6
60	A	892,54	893,07	892,78	892,77	892,68	892,66
	B	943,6	943,07	942,67	942,66	942,69	942,72
	C	-13,5	119,56	99,96	103,2	106,57	107,4
	D	-77,27	23,23	24,22	25,3	26,44	26,71
75	A	933,77	935,27	935,15	935,08	935	934,99
	B	977,7	976,96	976,76	976,78	976,84	976,87
	C	61,67	176,47	140,06	142,9	145,96	146,72
	D	-88,77	38,06	32,66	34,24	35,87	36,26
90	A	966,91	968,51	968,49	968,45	968,39	968,38
	B	1005,19	1004,56	1004,48	1004,51	1004,57	1004,6
	C	123,36	230,01	185,42	187,68	190,13	190,74
	D	-79,44	57,51	45,26	47,1	49,02	49,48

With the results presented on Table 6.2 is possible to perform an error analysis. Using the root of sum of squares, expression (6.1), it was possible to develop the graphs in Figures 6.4 and 6.5. The graphs show that time and number of elements affects the error. At 15 minutes is where the error variation between sections with different number of elements is higher. In the Figures 6.4 and 6.5 is observed the small differences between meshes 4, 5 and 6 when compared with meshes 1, 2 and 3. These differences are especially visible for 15 minutes time. It is also possible to see that more elements lead to more accurate results. For future section analysis it is considered that a section with elements with width of approximate 2,0 cm or less will lead to acceptable results.

$$||T|| = \sqrt{T_A^2 + T_B^2 + T_C^2 + T_D^2} \qquad (6.1)$$

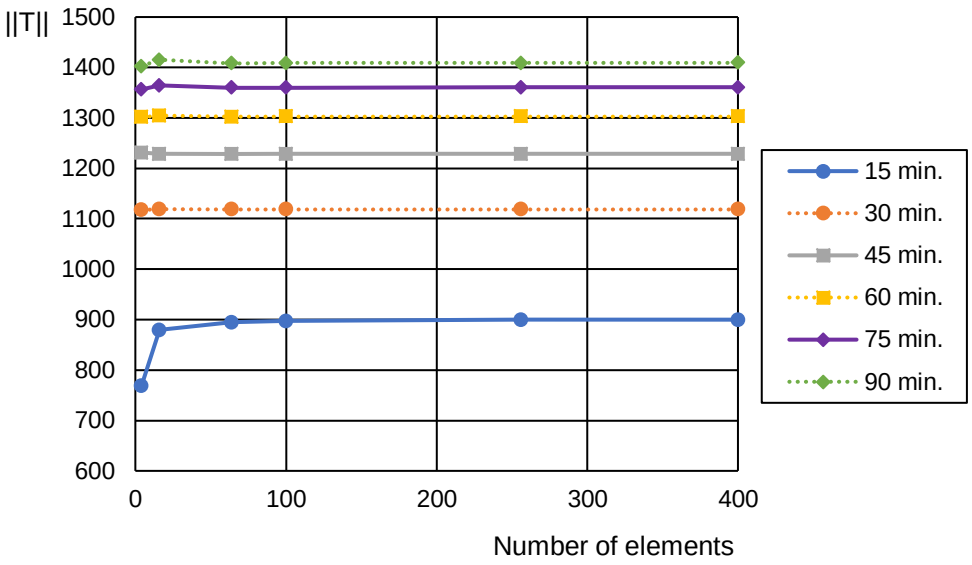

Figure 6.4 – Root sum of squares of the temperatures in the different meshes for different times.

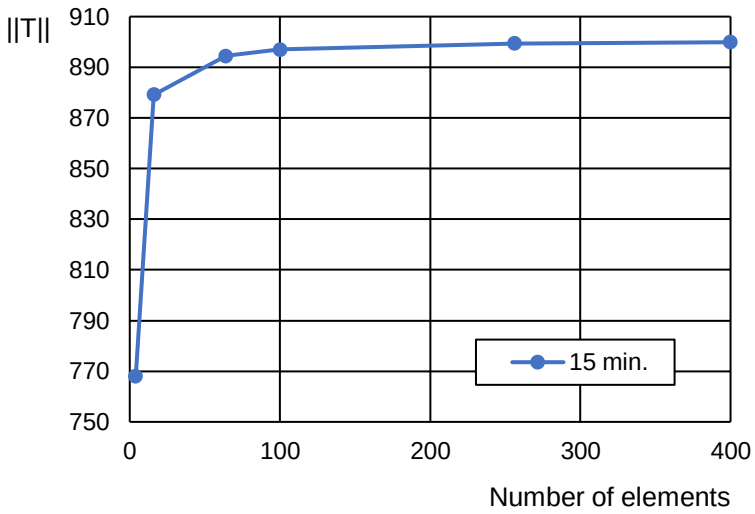

Figure 6.5 – Root sum of squares of the temperatures in the different meshes at 15 minutes.

6.3. Study of the damage

After an earthquake is possible to find several types of damage in the reinforced concrete structure. In this section is showed the influence of the damage in a reinforced concrete section to the temperature in a certain point of the section. It is also studied the influence of the fire frontiers to the temperature of that point. It was considered four different situations corresponding the damage of the section. The four situations are presented below:

- Situation D0: no damage in the section (original);
- Situation D1: section with minor cracks;
- Situation D2: 2 cm of the cover removed (concrete spalling due to earthquake damage);
- Situation D3: 4 cm of the cover removed (large concrete spalling and crushing due to earthquake damage).

The minor cracks do not affect significantly the thermal diffusivity of concrete, this means that the effects of tensile cracking on thermal diffusivity are negligible and do not need to be accounted for in analysis or design [33] [38]. Considering this, to simplify, the model for situation D0 and D1 will be the same. So, no damage or tensile cracking in the section will leads to the same results. In the Figures 6.7, 6.9 and 6.11 is possible to see the sections analysed considering the different damage and fire frontiers. The point being analysed, node A, it is also represented. In situation D0/D1 the distance of point A to the face of the concrete is 4 cm, in situation D2 the distance of point A to the face is 2 cm and in situation D3 point A is in the surface of the concrete section. Figure 6.6 shows a plan with some columns (in grey) and walls. It serves as an example to see several different configurations of the fire frontiers (FF) positions in the columns. The brick infill walls can provide insulation to the RC structural elements and can slow the transmission of heat to those elements [23]. The degree of the insulation is not analysed in this work. To simplify it is considered that the walls completely remove the effects of the fire to the sides that are covered by the walls. This situation may not be case and depends also in the materials used to build the walls. Different fire frontier configurations in the columns are also possible considering different compartment fire scenarios.

A side of a column can be protected because there is no fire in the compartment where that side of the column is located.

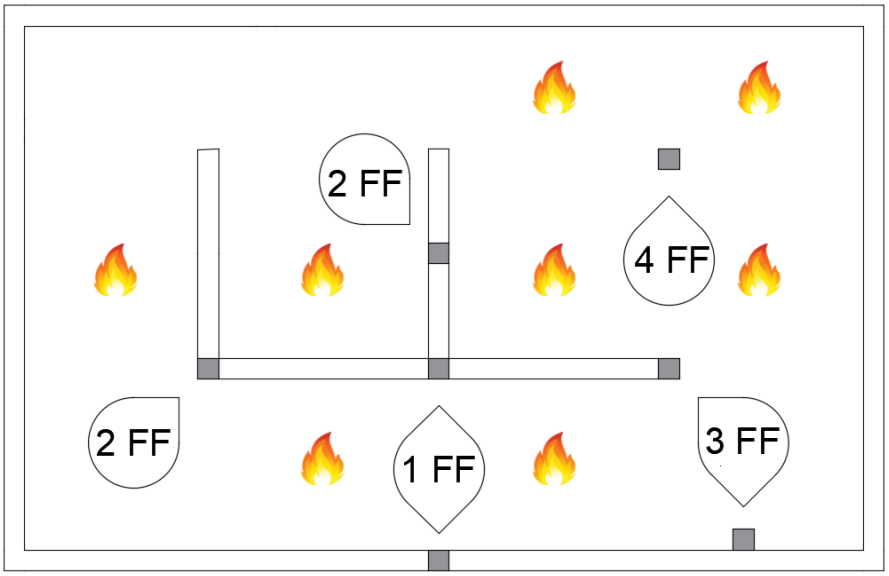

Figure 6.6 – Fire frontiers configuration in columns.

Tables 6.3, 6.4 and 6.5 show the temperatures in node A for different types of damage and different fire frontiers. The temperature is then related with the values obtained from the previous Table 3.1 ($f_{c,\theta} / f_{ck}$) for a better understanding of the impact of the fire and damage in the node A. The results show that for each type of damage the number of the fire frontiers do not have a significant influence in the temperature of point A. The type of damage has a huge impact on the temperatures of node A. For example, at 90 minutes, the temperature at node A for the section with 4 fire frontiers with damage D0/D1 is 406,41 ºC, 624,18 ºC for damage D2 and 968,26 ºC for damage D3. For other fire frontiers, the temperatures are similar. The temperature in node A in section with damage D2 is more than 50% higher than the temperature in the section with damage D0/D1 and the temperature in node A in the section with damage D3 is also more than 50% higher that the temperature in the section with damage D2. The same comparison can also be made regarding the relation $f_{c,\theta} / f_{ck}$, the result is 0,74 for damage D0/D1, 0,414 for damage D2 and 0,052 for damage D3. These results clearly show the huge impact that the different types of damage have in the temperature of node A and consequently on the compressive strength of the concrete.

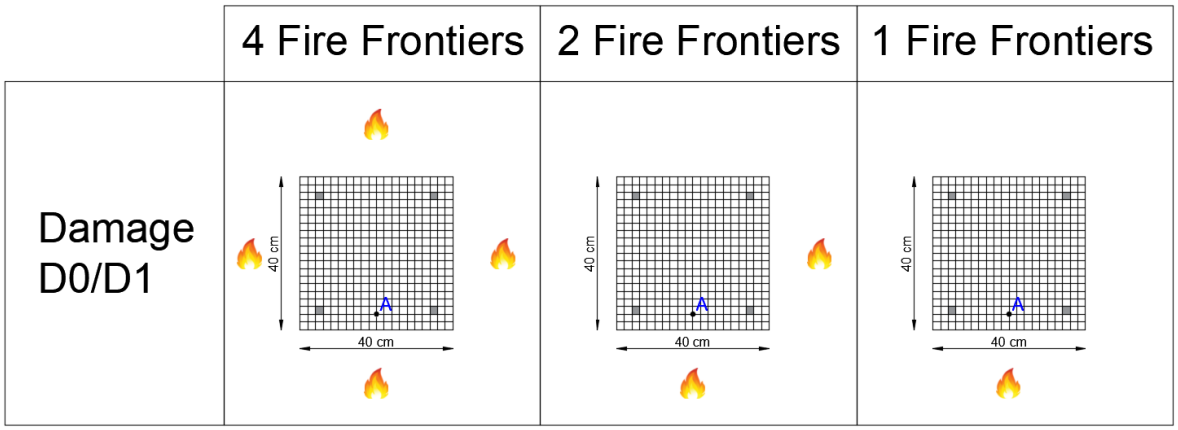

Figure 6.7 – Numerical models with damage D0/D1 for 4, 2 and 1 fire frontiers.

Table 6.3 – Temperatures in node A, for damage D0/D1 for the different fire frontiers.

	Damage D0/D1					
	4 Fire Frontiers		2 Fire Frontiers		1 Fire Frontiers	
t (min)	T (ºC)	$f_{c,\theta} / f_{ck}$	T (ºC)	$f_{c,\theta} / f_{ck}$	T (ºC)	$f_{c,\theta} / f_{ck}$
15	65,68	1	65,68	1	65,68	1
30	158,79	0,971	158,78	0,971	158,78	0,971
45	243,45	0,907	243,41	0,907	243,37	0,907
60	307,79	0,842	307,55	0,842	307,31	0,843
75	360,97	0,789	360,21	0,79	359,46	0,791
90	406,41	0,74	404,78	0,743	403,15	0,745

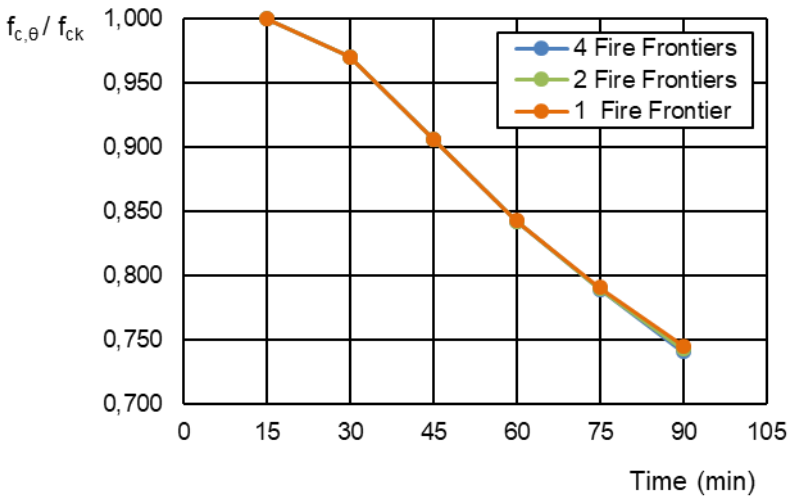

Figure 6.8 – Reduction factors evolution for a section with damage D0/D1 with 4, 2 and 1 fire frontiers

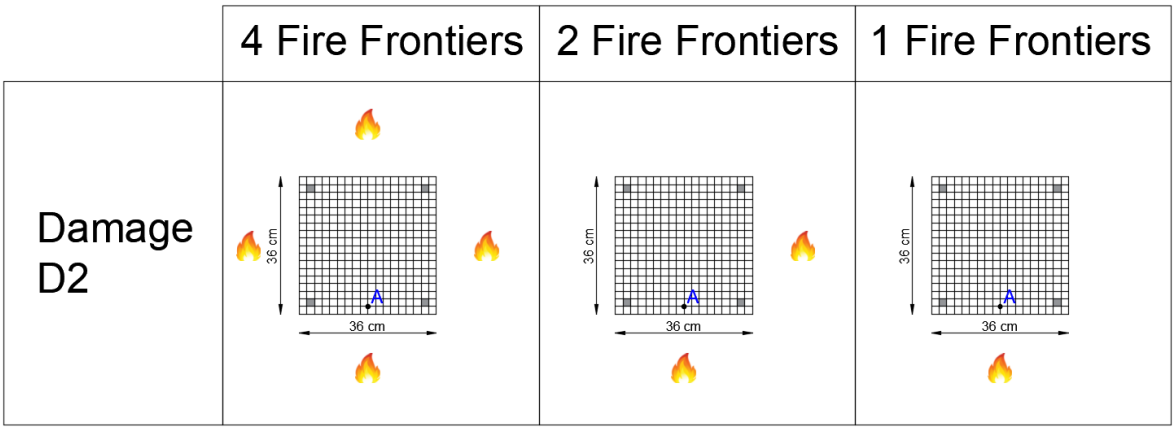

Figure 6.9 – Numerical models with damage D2 for 4, 2 and 1 fire frontiers.

Table 6.4 – Temperatures in node A, for damage D2 for the different fire frontiers.

	Damage D2					
	4 Fire Frontiers		2 Fire Frontiers		1 Fire Frontiers	
t (min)	T (ºC)	$f_{c,\theta} / f_{ck}$	T (ºC)	$f_{c,\theta} / f_{ck}$	T (ºC)	$f_{c,\theta} / f_{ck}$
15	176,42	0,962	176,42	0,962	176,42	0,962
30	343,91	0,806	343,91	0,806	343,91	0,806
45	446,62	0,68	446,54	0,68	446,47	0,68
60	519,43	0,571	519,06	0,571	518,68	0,572
75	576,61	0,485	575,67	0,486	574,52	0,488
90	624,18	0,414	622,11	0,417	620,04	0,42

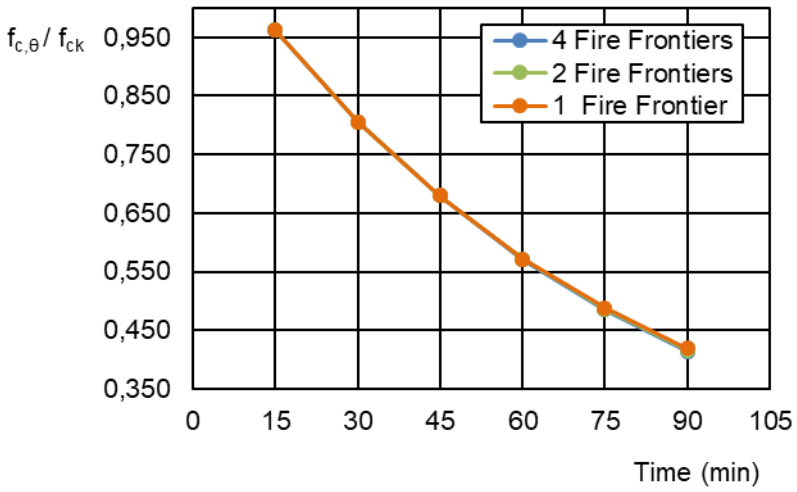

Figure 6.10 – Reduction factors evolution for a section with damage D2 with 4, 2 and 1 fire frontiers

	4 Fire Frontiers	2 Fire Frontiers	1 Fire Frontiers
Damage D3	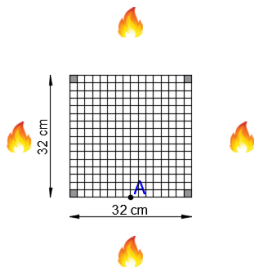	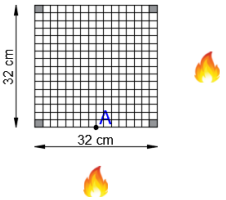	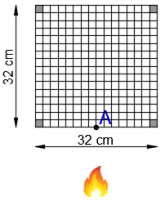

Figure 6.11 – Numerical models with damage D3 for 4, 2 and 1 fire frontiers.

Table 6.5 – Temperatures in node A, for damage D3 for the different fire frontiers.

	Damage D3					
	4 Fire Frontiers		2 Fire Frontiers		1 Fire Frontiers	
t (min)	T (ºC)	$f_{c,\theta} / f_{ck}$	T (ºC)	$f_{c,\theta} / f_{ck}$	T (ºC)	$f_{c,\theta} / f_{ck}$
15	548,59	0,527	548,59	0,527	548,59	0,527
30	744,55	0,233	744,54	0,233	744,54	0,233
45	835,07	0,125	835,03	0,125	834,99	0,126
60	893,04	0,085	892,9	0,085	892,77	0,085
75	935,61	0,066	935,33	0,066	935,05	0,066
90	969,26	0,052	968,81	0,052	968,36	0,053

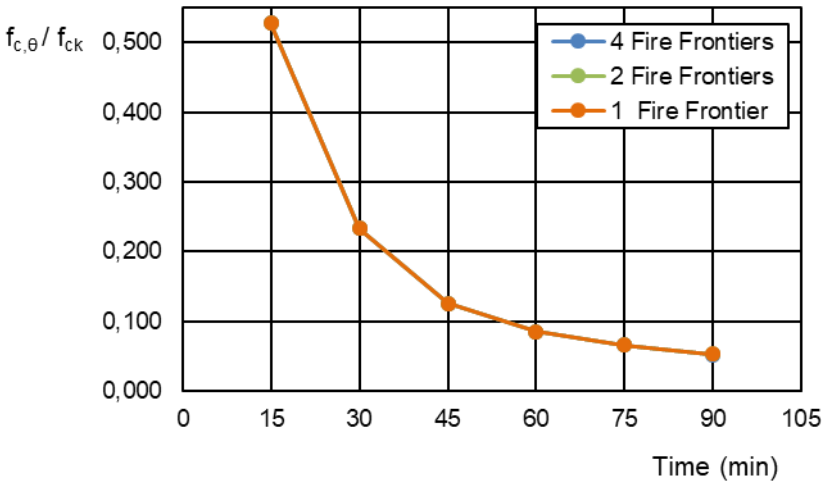

Figure 6.12 – Reduction factors evolution for a section with damage D2 with 4, 2 and 1 fire frontiers

7. Post-earthquake fire on RC columns under axial load

7.1. Introduction

In the present Chapter is described the numerical analysis of RC columns exposed to fire after an earthquake, or by other words the behaviour of RC columns under fire with earthquake damage. The fire curve used in this analysis is the ISO 834. Figure 7.1 represents the schematic of the column being analysed in this Chapter. The column has one fixed support and a point load is applied. It is also represented the characterization of the finite element mesh used in SAFIR. All the numerical analysis of the columns analysed in this Chapter will be regarding the column in Figure 7.1. The main differences will be related with the load and the sections of the column. The sections considered in the numerical analysis are presented in Chapter 7.2.

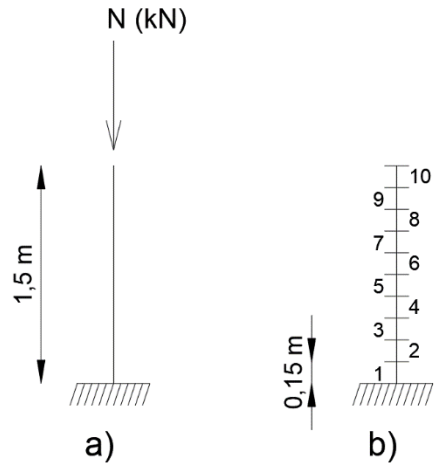

Figure 7.1 – Column with fixed support: a) Column length and load applied; b) Characterization of the finite element mesh.

7.2. Column section analysis

7.2.1. Geometric configuration

In Figure 7.2 is represented the section of the column without damage, it also shows the location of the reinforcement (8Φ25). The damage D0/D1 corresponds to an intact section or a section with small cracks, the damage D2 corresponds to the slight damage with some concrete spalling, traduced in the removal of the exterior fibers and damage D3 corresponds the complete unconfined concrete spalling, related with a major damage and traduced in the removal of the entire cover, leaving the reinforcement steel exposed. These types of damage follow the same principle already explored in the Chapter 6.The different types of damage can be seen in Figure 7.3. Although the fire frontiers can be different, the damage is apllied in all the surfaces of the concrete section.

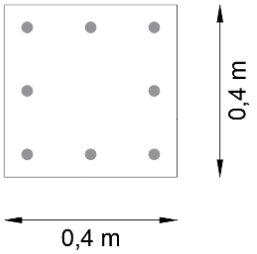

Figure 7.2 – Column section.

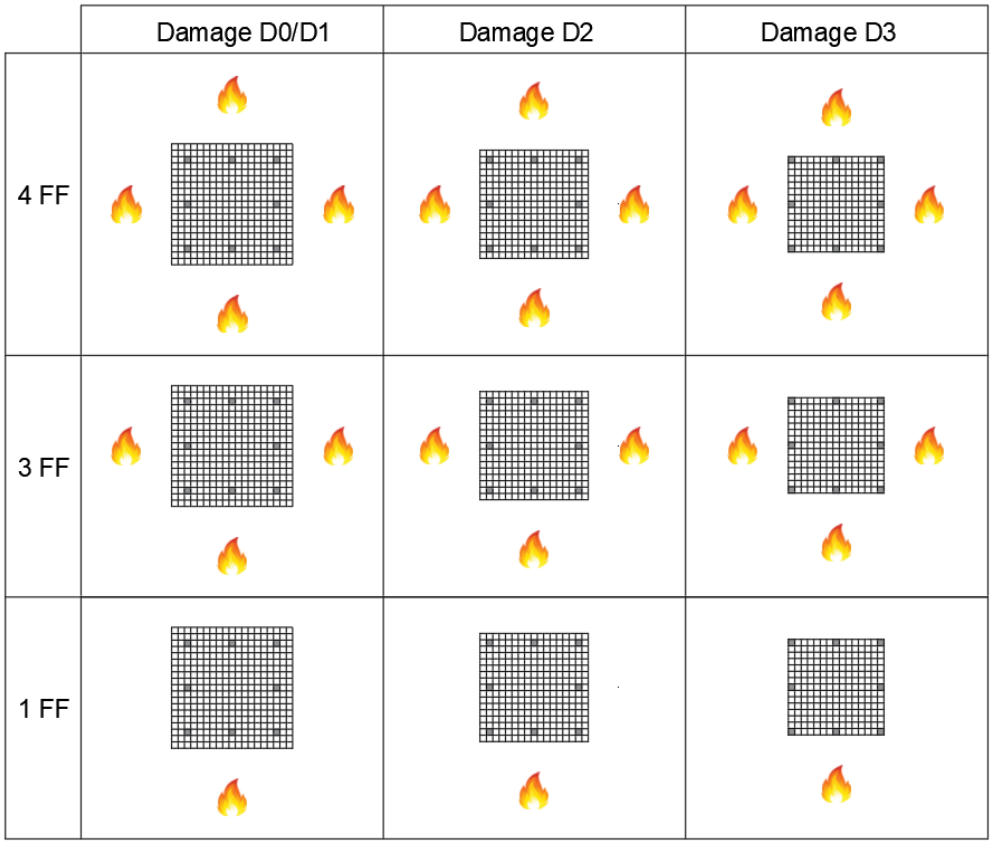

Figure 7.3 – Numerical models for damage D0/D1, D2 and D3 with four, three and one fire frontiers.

Several columns will be analysed in this Chapter, with different types of damage, fire frontiers and level of initial load. All of the sections are represented in Figure 7.3. In Figure 7.1 b) the column is divided in 10 elements. Element 1 and 2 are the elements where different types of damage will be considered. The other elements (3 to 10) will have always sections with damage D0/D1, once is assumed that the earthquake damage in typical columns and beams is concentrated in the extermities of RC elements, as observed in Chapter 2.1.3. Later, when the damage of a column is mentioned is always the damage in elements 1 and 2 because the damage in elements 3 to 10 will always be damage D0/D1.

7.2.2. Material properties

In Table 7.1 are all the columns geometry characteritics, the material properties, loads and fire curve used in the numerical models.

Table 7.1 – Geometric and material characterization of the columns.

Columns geometry		
Length	L	1,5 m
Height	h	40 cm
Width	b	40 cm

Concrete properties [30]		
Concrete model		Siliceous aggregate
Specific mass of concrete	rho	2300 kg/m^3
Water content	w	46 kg/m^3
Coefficient of convection on heated surfaces	h_h	25 W/m^{2}K
Coefficient of convection on unheated surfaces	h_c	4 W/m^{2}K
Emissivity	ε	0,7
Compression strength	f_{cd}	30 MPa
Tensile strength	f_{ct}	Zero
Poisson's ratio	v	0,2

Reinforcing Steel properties [30] [31]		
Steel model		Hot rolled, class B
Modulus of elasticity	E_s	210 GPa
Yield strength	f_y	500 MPa
Poisson's ratio	v	0,3
Coefficient of convection on heated surfaces	h_h	25 W/m^{2}K
Coefficient of convection on unheated surfaces	h_c	4 W/m^{2}K
Emissivity	ε	0,7
Reinforcing Steel diameter	Φ_s	25 mm

Loads	N	500 to 3000 kN with increments of 250 kN

Fire curve		ISO 834

7.2.3. Thermal analysis

In the Figures 7.4 and 7.5 it is represented the temperature evolution of the reinforcing steel bars. Figure 7.4 represents the reinforcing steel bars in the corners of the section and Figure 7.5 represents the reinforcing steel bars in the middle. As is possible to see in Figures 7.6, 7.7 and 7.8 each reinforcing steel bar (represented with ticker lines) is constituted by only one element. Each element has four different nodes and each node has different temperatures. The temperature considered to develop the graphs in Figures 7.4 and 7.5 was the higher one of those four nodes. The difference between the temperatures in those four nodes is almost negligible and it was considered sufficient to analyse only the higher value. By analysing the graphs in Figures 7.4 and 7.5 is possible to see that the temperature in the corner reinforcing steel bars is higher when compared with the reinforcing steel bars in the middle, and this is true for all types of damage. The fire curve ISO 834 is represented in the graphs to serve as a comparison between the results. For the reinforcing steel bars in the corner, for section with damage D3, the evolution of the temperature is very similar with the fire curve ISO 834, especially about 90 minutes after the beginning of the fire curve. In each graph is also showed three different temperature lines that are associated with the reducing factors in Table 3.2. These values are helpful because allow the comparison between the effective yield strength in each steel bar for different types of damage. For damage D0/D1 it takes about 120 minutes for the steel bars to reach a temperature of 600 ºC, it takes about 60 minutes for the section with damage D2 and about 20 minutes for the section with damage D3. For the steel bars in the middle it takes about 240 minutes for the steel bars in the section with damage D0/D1 to reach a temperature of 600 ºC, it takes about 120 minutes for the section with damage D2 and about 30 minutes for the section with damage D3. These examples allow a better understanding regarding the impact that the damage has on the effective yield strength of the steel bars. The difference in time between section with damage D0/D1 and D3 for the reinforcing steel bars to reach 600 ºC is about 100 minutes for the reinforcing steel bars in the corner and 200 minutes for the reinforcing steel bars in the middle. These results show how

much sooner the steel bars in the damaged sections reach less than half of their yield strength.

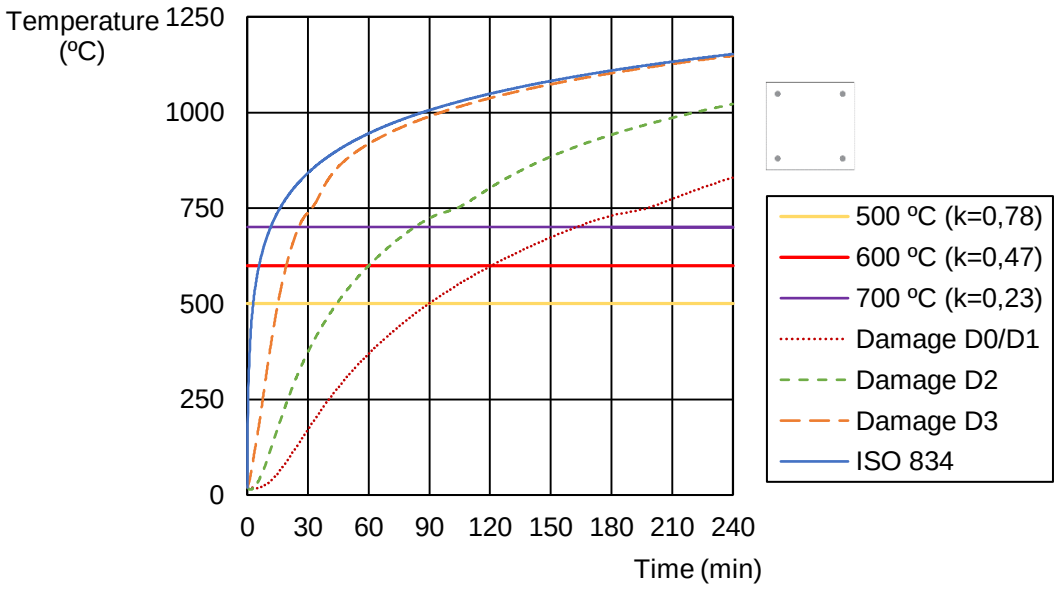

Figure 7.4 – Temperature evolution in the columns corner reinforcing steel bars.

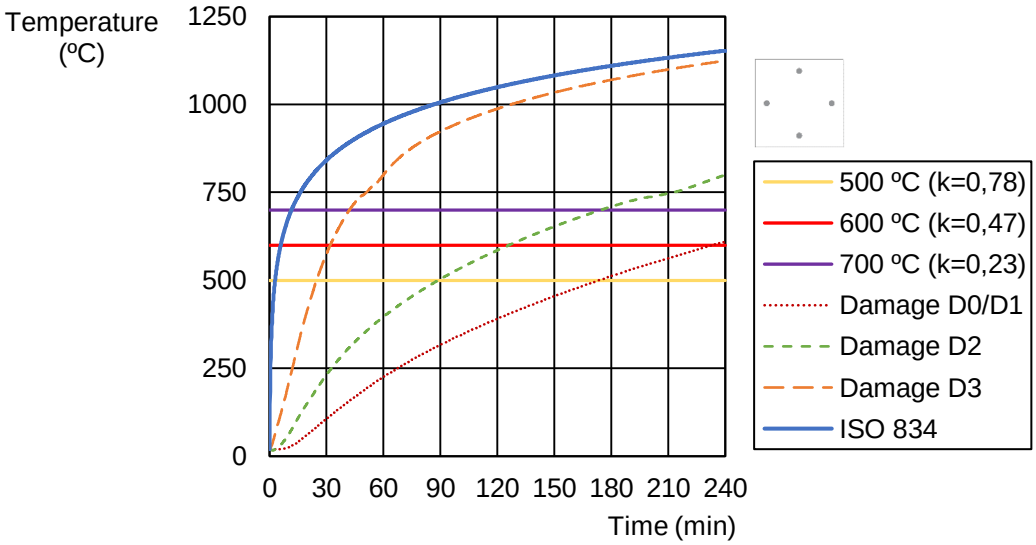

Figure 7.5 – Temperature evolution in the columns middle reinforcing steel bars.

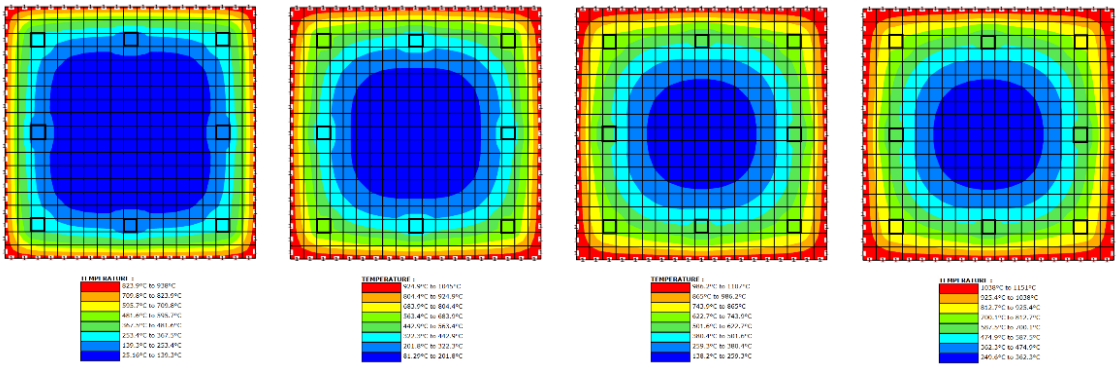

Figure 7.6 – Temperature profiles of beam with damage D0/D1 at 60, 120, 180 and 240 minutes (left to right).

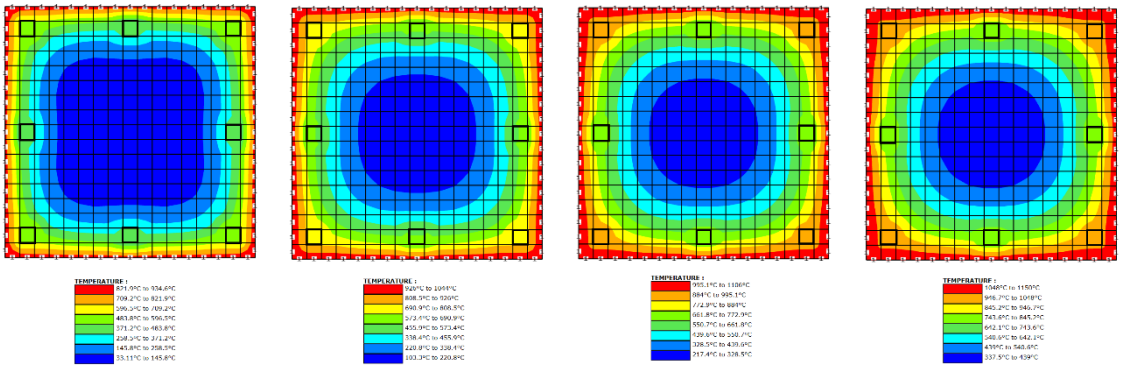

Figure 7.7 – Temperature profiles of beam with damage D2 at 60, 120, 180 and 240 minutes (left to right).

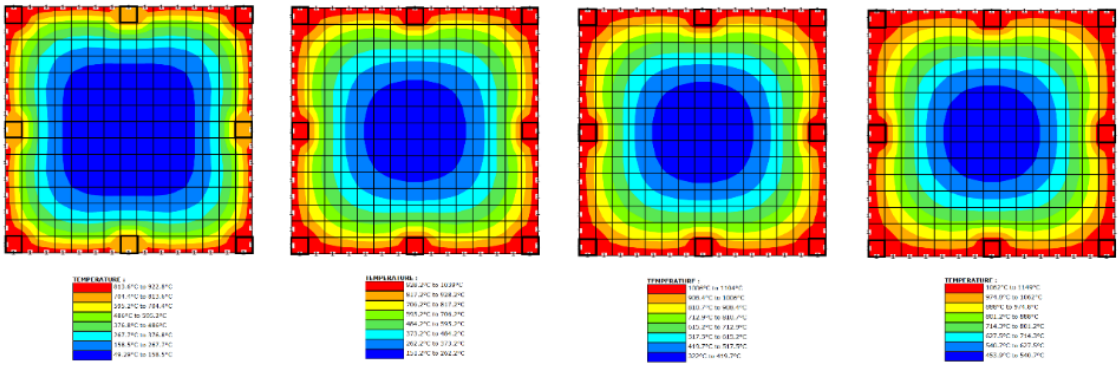

Figure 7.8 – Temperature profiles of beam with damage D3 at 60, 120, 180 and 240 minutes (left to right).

In the Figures 7.9, 7.10 and 7.11 are represented the temperature profiles of the sections of the columns with one fire frontier for damage D0/D1, D2 and D3 at 60, 120, 180 and 240 minutes. The graphs that show the evolution of the temperature in the reinforcing steel bars of those sections are represented in Figures 7.12 and 7.13. The three reinforcing steel bars near the fire frontier are the ones more susceptible to the temperature. The temperatures obtained in Figure 7.12 are very similar with the temperatures obtained in Figure 7.5. The Figure 7.13 shows that the temperature does not affect the effective yield strength of the reinforcing steel bars analysed in that Figure.

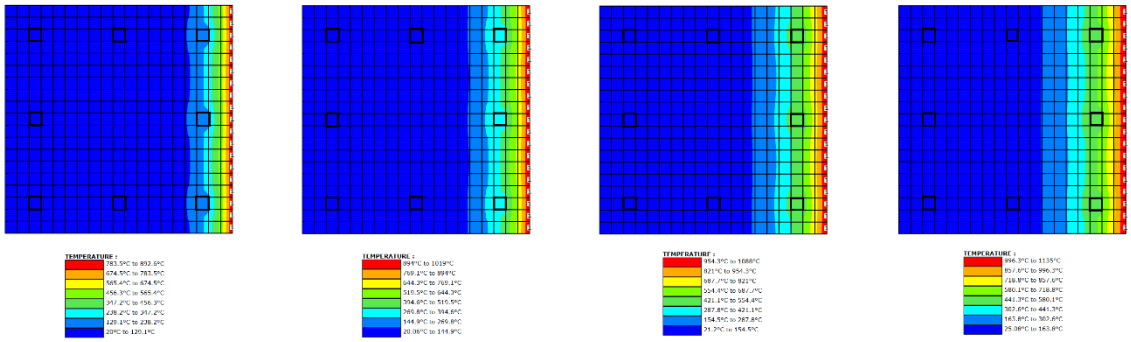

Figure 7.9 – Temperature profiles of column with damage D0/D1 at 60, 120, 180 and 240 minutes (left to right).

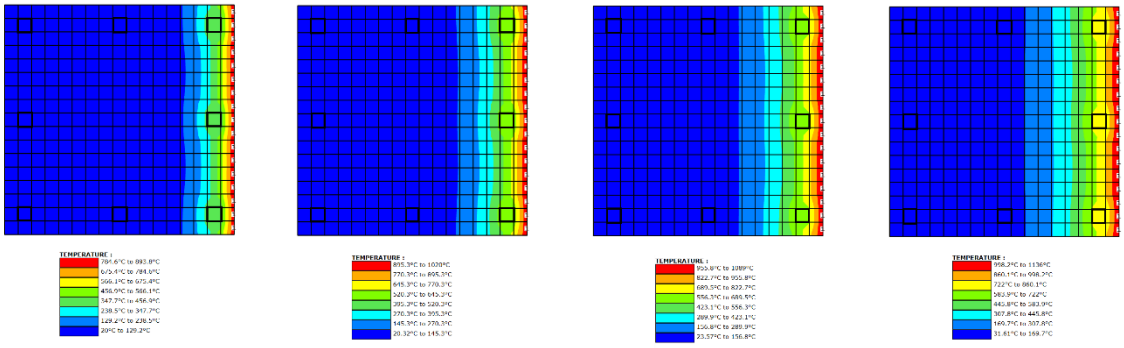

Figure 7.10 – Temperature profiles of column with damage D2 at 60, 120, 180 and 240 minutes (left to right).

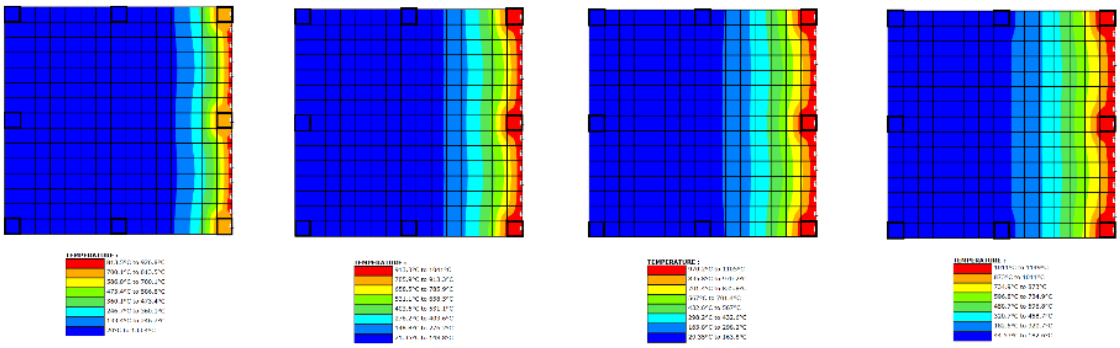

Figure 7.11 – Temperature profiles of column with damage D3 at 60, 120, 180 and 240 minutes (left to right).

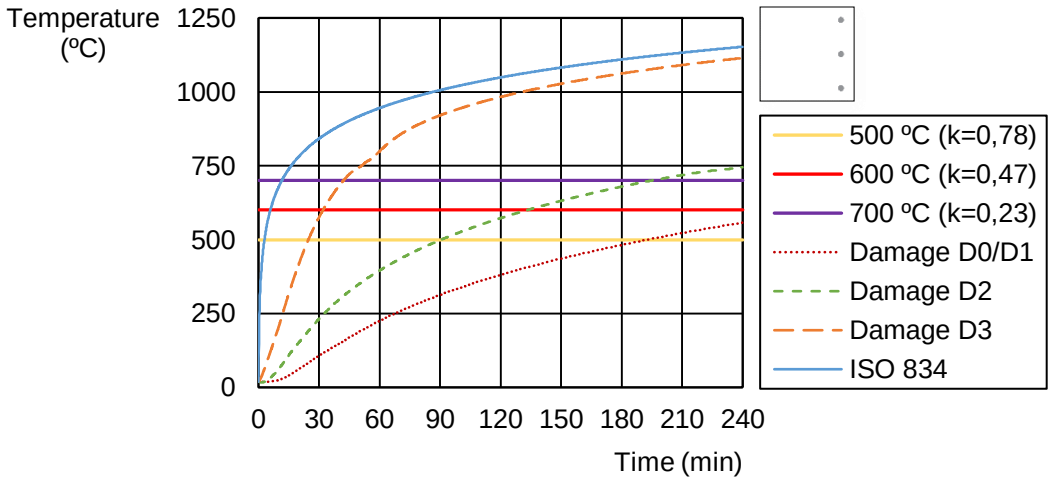

Figure 7.12 – Temperature evolution in the columns reinforcing steel bars.

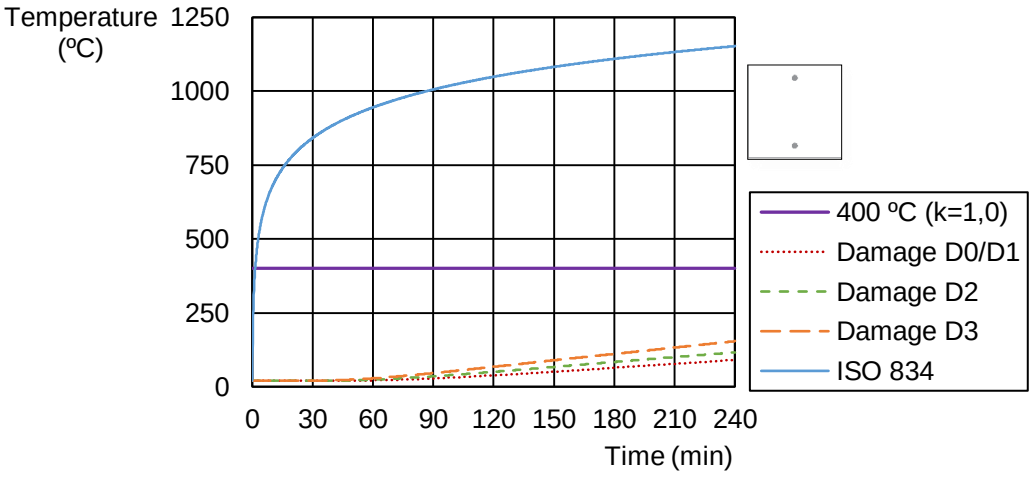

Figure 7.13 – Temperature evolution in the columns reinforcing steel bars.

In the Figures 7.14, 7.15 and 7.16 are represented the temperature profiles of the sections of the columns with three fire frontiers for damage D0/D1, D2 and D3 at 60, 120, 180 and 240 minutes. The graphs that show the evolution of the temperature in the reinforcing steel bars of those sections are represented in Figures 7.17 and 7.18. Not all the reinforcing steel bars are represented because most of them have the same temperatures of the ones in the sections with four fire frontiers. The reinforcing steel bars analysed are on the left side of the section, that is the side without the fire frontier. The results obtained in Figure 7.17 are the same obtained in Figure 7.12. Comparing the section with four fire frontiers with the section with three fire frontiers it is observed that the temperatures of the reinforcing steel bars in Figure 7.5 are very similar with the temperatures of the reinforcing steel bars in the Figure 7.17. The main difference in the reinforcing steel bars temperature between the section with three fire frontiers and four fire frontiers is in the reinforcing steel bar analysed in Figure 7.18 where the temperature does not affect the effective yield strength of the steel bar.

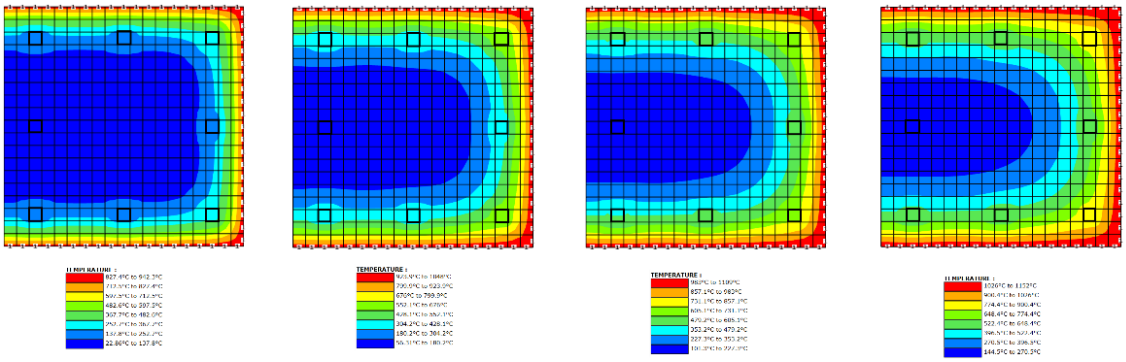

Figure 7.14 – Temperature profiles of column with damage D0/D1 at 60, 120, 180 and 240 minutes (left to right).

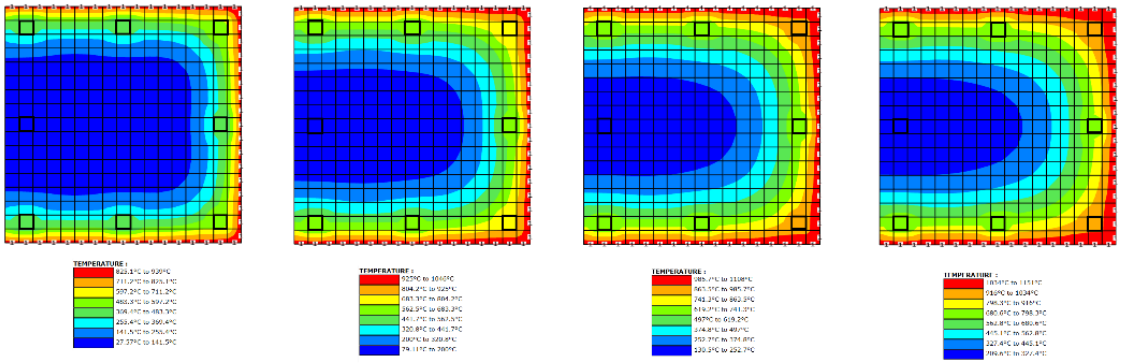

Figure 7.15 – Temperature profiles of column with damage D2 at 60, 120, 180 and 240 minutes (left to right).

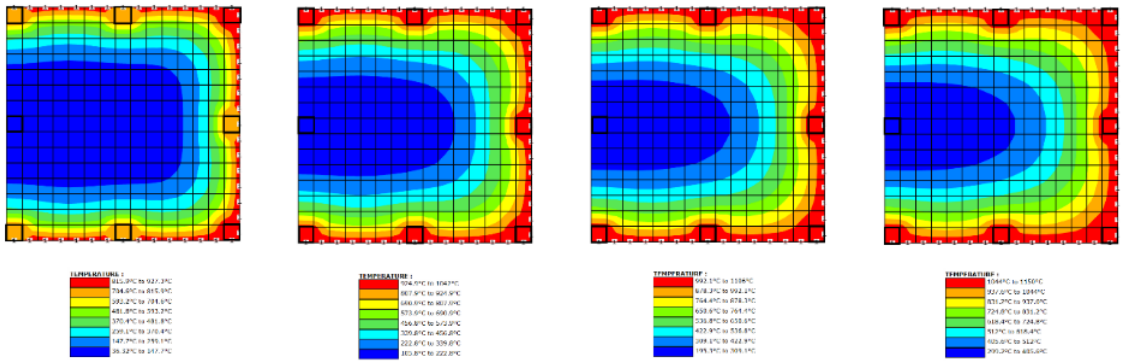

Figure 7.16 – Temperature profiles of column with damage D3 at 60, 120, 180 and 240 minutes (left to right).

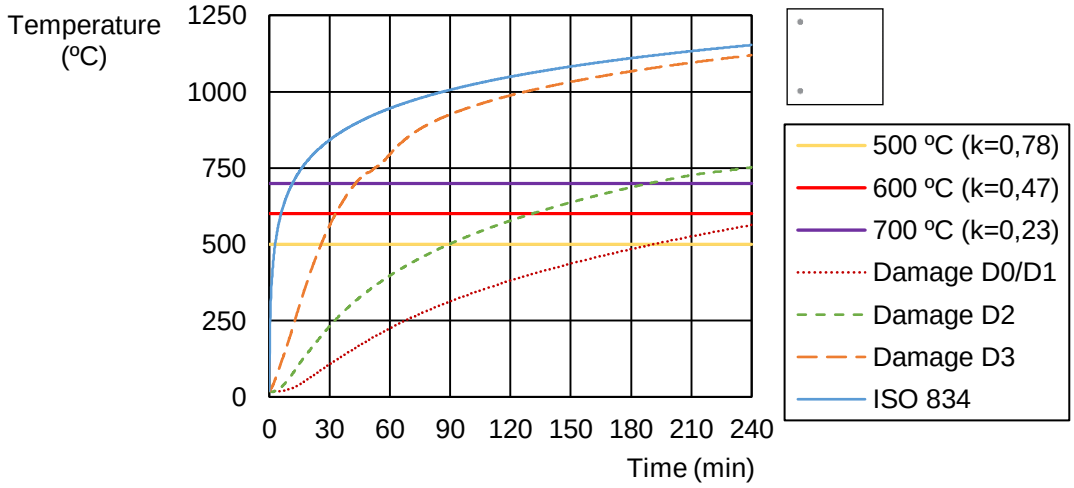

Figure 7.17 – Temperature evolution in the columns reinforcing steel bars.

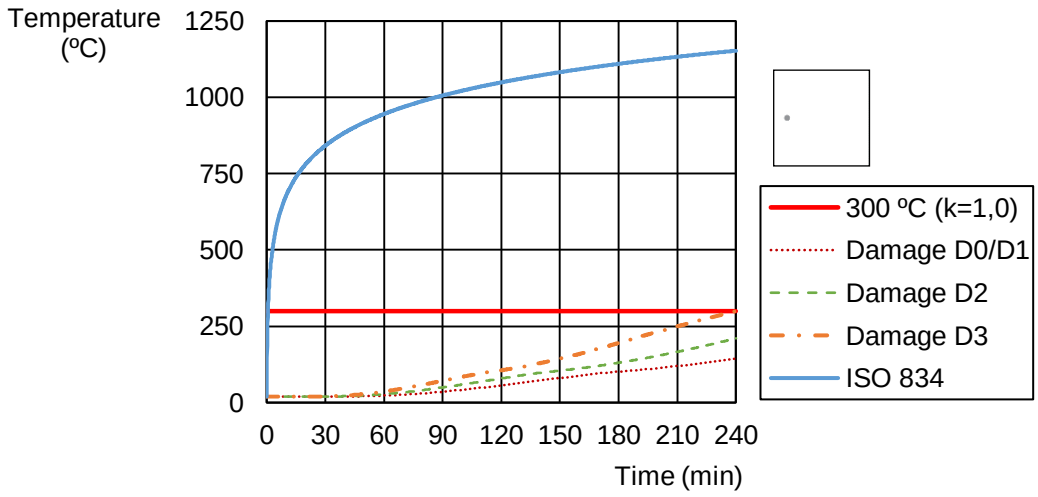

Figure 7.18 – Temperature evolution in the columns reinforcing steel bars.

7.3. Column analysis

7.3.1. Time until conventional collapse

The times until collapse of the columns with four, three and one fire frontiers for different types of damage and loads are presented in Table 7.2. Each load is related with the relative axial force, which can be obtained with expression 7.1. The program SAFIR runs until reaches 240 minutes or until the collapse of the structure.

$$n = \frac{N_{Ed}}{A_c f_{cd}} \qquad (7.1)$$

As expected the results in the columns with four fire frontiers are lower than the results in the columns with three fire frontiers. For the columns with only one fire frontier there is no collapse of the column in less than 240 minutes for the loads and types of damage considered. In Figures 7.19 and 7.20 is represented the evolution of the times until collapse of the columns with four and three fire frontiers, respectively, for different loads and types of damage. In the Figure 7.20 there is an interesting similarity in the results between columns with different loads and type of damage. For instance, the time until collapse of the column with damage D0/D1 with a relative axial force of 0,859 is very similar with the column with damage D2 with relative axial force of 0,625 and very similar with the column with damage D3 with relative axial force of 0,469. Other example is between the column with damage D0/D1 with relative axial force of 0,938 and column with damage D2 with relative axial force of 0,703 and the column with damage D3 with relative axial force of 0,547. These examples follow the same trend in terms of variation of loads or relative axial force. There are also other similarities between other columns with damage D2 and D3. As for the columns with four fire frontiers there are also similar results, but these are not as similar as the ones in the columns with three fire frontiers. By comparing the results where there is collapse of the columns (times lower than 240 minutes) with damage D2 and D3 is possible to observe that the time until collapse of the columns with damage D3 is always more than half of the time until collapse of the columns with damage D2. Also, by comparing the results where there is collapse of

the columns with damage D0/D1 and D2 the same conclusion is applicable to almost all the columns. The exceptions are the columns with relative axial force of 0,938 and the columns with relative axial force of 0,859 for three fire frontiers. In all the other columns the time until collapse of columns with damage D2 is more than half of the time until collapse of the columns with damage D0/D1.

Table 7.2 – Time until collapse of the columns with 4, 3 and 1 fire frontiers.

			4 FF	3 FF	1 FF
Load	**n**	**Damage**	**Time (min)**	**Time (min)**	**Time (min)**
500 kN	0,156	D0D1	240,00	240,00	240,00
		D2	240,00	240,00	240,00
		D3	240,00	240,00	240,00
750 kN	0,234	D0D1	240,00	240,00	240,00
		D2	240,00	240,00	240,00
		D3	204,44	240,00	240,00
1000 kN	0,313	D0D1	240,00	240,00	240,00
		D2	240,00	240,00	240,00
		D3	164,29	240,00	240,00
1250 kN	0,391	D0D1	240,00	240,00	240,00
		D2	215,02	240,00	240,00
		D3	132,85	217,69	240,00
1500 kN	0,469	D0D1	240,00	240,00	240,00
		D2	178,27	240,00	240,00
		D3	105,10	179,02	240,00
1750 kN	0,547	D0D1	228,40	240,00	240,00
		D2	148,60	223,19	240,00
		D3	80,23	140,65	240,00
2000 kN	0,625	D0D1	197,60	240,00	240,00
		D2	120,56	180,23	240,00
		D3	63,40	108,10	240,00
2250 kN	0,703	D0D1	169,88	240,00	240,00
		D2	97,52	143,94	240,00
		D3	51,60	78,77	240,00
2500 kN	0,781	D0D1	143,27	216,94	240,00
		D2	76,48	109,77	240,00
		D3	41,23	60,69	240,00
2750 kN	0,859	D0D1	117,81	181,19	240,00
		D2	59,04	82,65	240,00
		D3	34,44	46,77	240,00
3000 kN	0,938	D0D1	96,29	147,65	240,00
		D2	40,19	60,44	240,00
		D3	29,65	38,27	240,00

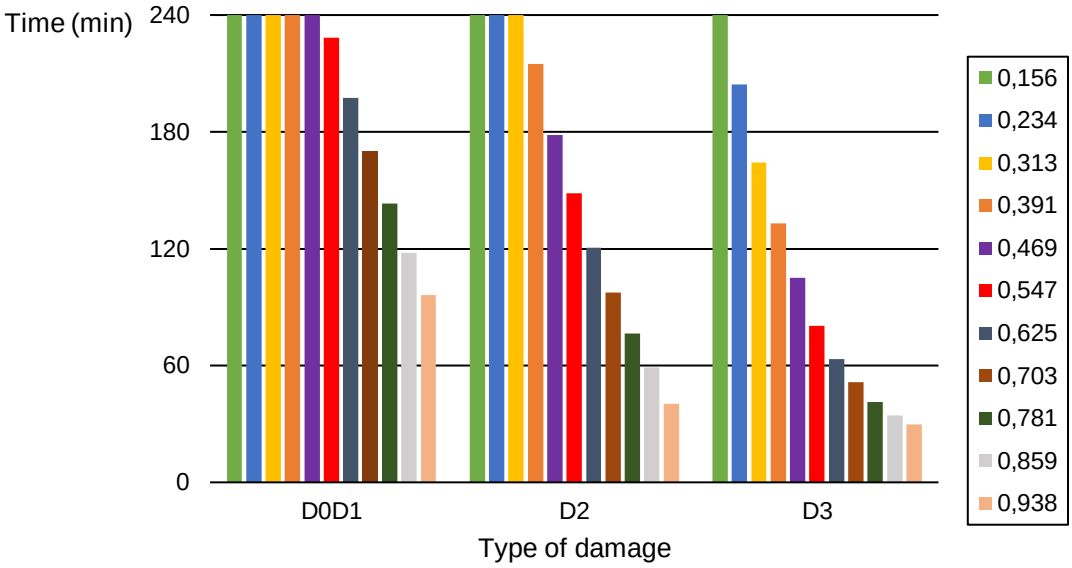

Figure 7.19 – Time until collapse of the columns with 4 fire frontiers.

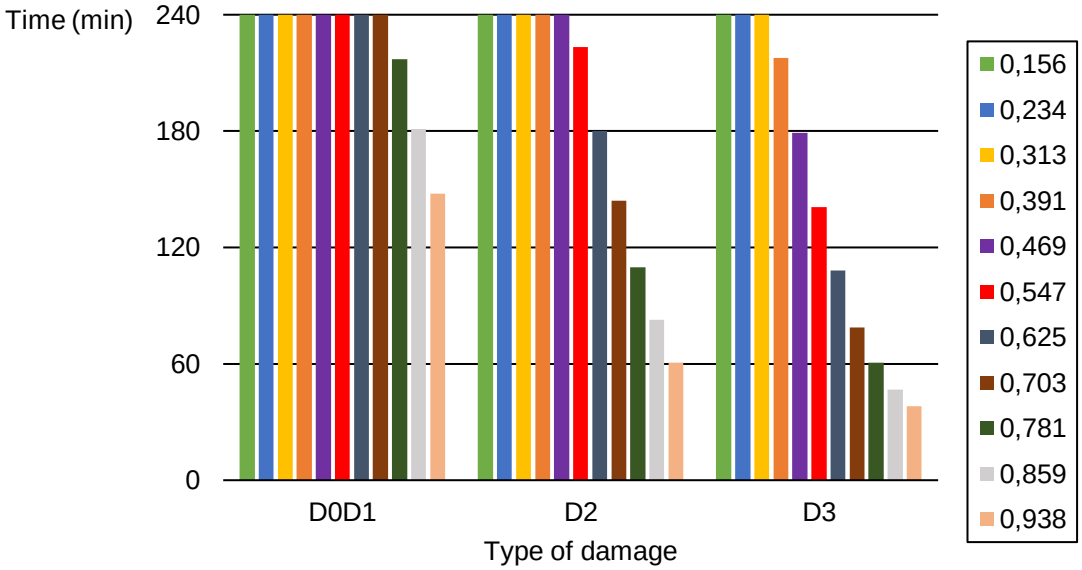

Figure 7.20 – Time until collapse of the columns with 3 fire frontiers.

In the Figures 7.19, 7.20 the factor that remained constant was the number of fire frontiers. In the Figures 7.21, 7.22 and 7.23 the factor that is constant is the load. This allows an analysis regarding the impact of the damage and fire frontiers

on the columns. As said earlier, columns with one fire frontier do not collapse until 240 minutes. The Figures show that there is a big difference between the results of columns with one fire frontier with the columns with three or four fire frontiers, especially for damage D3. This aspect is more evident in Figure 7.23, for a load of 2750 kN (n=0,859), with damage D3, the column with one fire frontier do not collapses until 240 minutes and the columns with three or four fire frontiers collapse in less than 60 minutes.

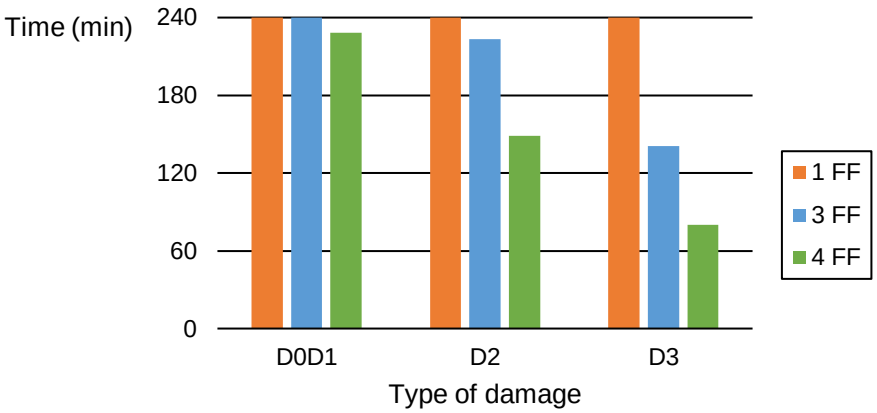

Figure 7.21 – Time until collapse of the columns with a load of 1750 kN (n=0,547).

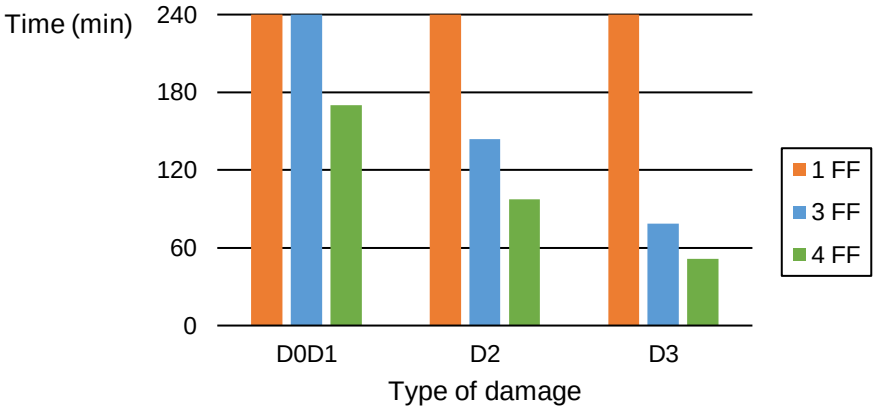

Figure 7.22 – Time until collapse of the columns with a load of 2250 kN (n=0,703).

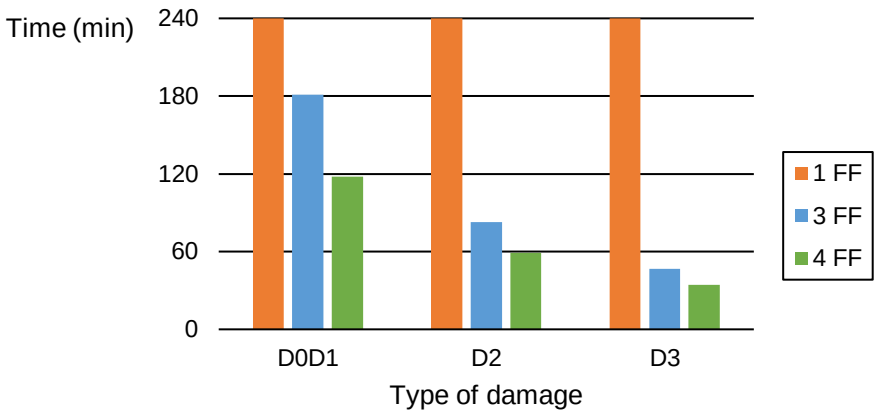

Figure 7.23 – Time until collapse of the columns with a load of 2750 kN (n=0,859).

In the Table 7.3 is represented the intersection between the results in Table 7.2 with the minimum fire resistance of structural elements of buildings that are in the Table 5.5. Table 7.3 shows the higher risk category that is respected by each column. The utilization types II, XI and XII have higher requirements regarding the minimum fire resistance of structural elements compared to utilization types I, III, IV, V, VI, VII, VIII, IX and X. This situation leads to overall lower risk category in the utilization types II, XI and XII when compared with the other utilization types. For lower values of the relative axial force the risk category of the columns do not change for different types of damage. For all the columns considered with one fire frontier the risk category is the 4th. This situation changes when is considered three or four fire frontiers. For instance, with a relative axial force of 0,703 there is huge different in the risk categories of the columns when there is considered different types of damage. For utilization types II, XI and XII, for the column with four fire frontiers the risk category is the 3rd for damage D0/D1, and for damage D3 there is no risk category that is verified. For the same utilization types, for the column with three fire frontiers the risk category is the 4th for damage D0/D1 and the 1st for damage D3. These examples show the impact that the damage can have in the columns. As expected, the damage in the column lowers the times until collapse and these examples show the impact that those differences in times can have on the risk categories of the column.

Table 7.3 – Risk category respected by each column.

			Utilization type					
			II, XI and XII			I, III, IV, V, VI, VII, VIII, IX and X		
Load	**n**	**Damage**	**4 FF**	**3 FF**	**1 FF**	**4 FF**	**3 FF**	**1 FF**
500 kN	0,156	D0D1	4th	4th	4th	4th	4th	4th
		D2	4th	4th	4th	4th	4th	4th
		D3	4th	4th	4th	4th	4th	4th
750 kN	0,234	D0D1	4th	4th	4th	4th	4th	4th
		D2	4th	4th	4th	4th	4th	4th
		D3	4th	4th	4th	4th	4th	4th
1000 kN	0,313	D0D1	4th	4th	4th	4th	4th	4th
		D2	4th	4th	4th	4th	4th	4th
		D3	3rd	4th	4th	4th	4th	4th
1250 kN	0,391	D0D1	4th	4th	4th	4th	4th	4th
		D2	4th	4th	4th	4th	4th	4th
		D3	3rd	4th	4th	4th	4th	4th
1500 kN	0,469	D0D1	4th	4th	4th	4th	4th	4th
		D2	3rd	4th	4th	4th	4th	4th
		D3	2nd	3rd	4th	3rd	4th	4th
1750 kN	0,547	D0D1	4th	4th	4th	4th	4th	4th
		D2	3rd	4th	4th	4th	4th	4th
		D3	1st	3rd	4th	2nd	4th	4th
2000 kN	0,625	D0D1	4th	4th	4th	4th	4th	4th
		D2	3rd	4th	4th	4th	4th	4th
		D3	1st	2nd	4th	2nd	3rd	4th
2250 kN	0,703	D0D1	3rd	4th	4th	4th	4th	4th
		D2	2nd	3rd	4th	3rd	4th	4th
		D3	-	1st	4th	1st	2nd	4th
2500 kN	0,781	D0D1	3rd	4th	4th	4th	4th	4th
		D2	1st	2nd	4th	2nd	3rd	4th
		D3	-	1st	4th	1st	2nd	4th
2750 kN	0,859	D0D1	2nd	4th	4th	3rd	4th	4th
		D2	-	1st	4th	1st	2nd	4th
		D3	-	-	4th	1st	1st	4th
3000 kN	0,938	D0D1	2nd	3th	4th	3rd	4th	4th
		D2	-	1st	4th	1st	2nd	4th
		D3	-	-	4th	-	1st	4th

(-) Do not verify any risk category

8. Post-earthquake fire on RC beams

8.1. Introduction

In this Chapter is presented a numerical analysis of reinforced concrete beams exposed to fire after an earthquake. The fire curve used in this analysis is the ISO 834. In Figure 8.1 is represented the schematic of the beam being analysed in this Chapter. The beam has fixed supports and a continuous load is applied. It is also represented the characterization of the finite element mesh used in SAFIR. The beam was divided into 60 elements, each element with 10 cm.

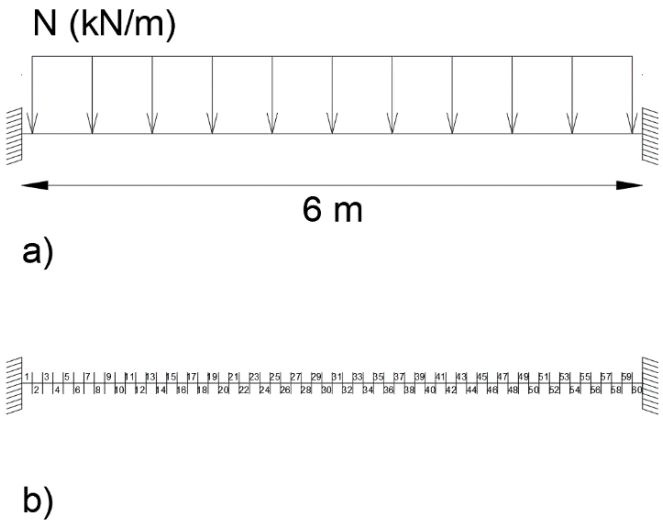

Figure 8.1 – Beam with fixed supports: a) Beam length and load applied; b) Characterization of the finite element mesh.

8.2. Beam section analysis

8.2.1. Geometric configuration

In Figure 8.2 is represented the section of the beam without damage and the location of the reinforcement (4Φ25). The methodology regarding the damage applied in the beam is similar to the one used in the columns. The damage D0/D1 corresponds to an intact section or a section with small cracks, the damage D2 corresponds to the removal of the exterior fibers and damage D3 corresponds to the removal of the entire cover, leaving the reinforcement visible. The different types of damage can be seen in Figure 8.3. In the columns the fibers were removed in all sides, in the case of the beams, the fibers in the top side are not removed. It was considered that the earthquake does not damage the top side of the beam and there is no detachement of concrete there. There is also no fire frontier on the top side of the beam, it was considered that the fire develops below the beam.

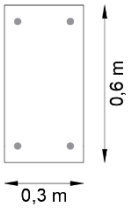

Figure 8.2 – Beam section.

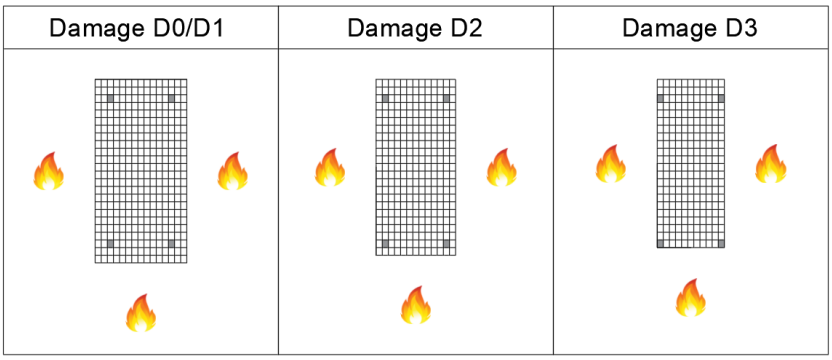

Figure 8.3 – Different sections of the beam according to the type of damage. The fire frontiers are also represented.

8.2.2. Material properties

In Table 8.1 are all the beam geometry characteritics, the material properties, loads and fire curve used in the numerical models.

Table 8.1 – Geometric and material characterization of the beams.

Beam geometry		
Length	L	6 m
Height	h	60 cm
Width	b	30 cm

Concrete properties [30]		
Concrete model		Siliceous aggregate
Specific mass of concrete	rho	2300 kg/m^3
Water content	w	46 kg/m^3
Coefficient of convection on heated surfaces	h_h	25 W/m^{2}K
Coefficient of convection on unheated surfaces	h_c	4 W/m^{2}K
Emissivity	ε	0,7
Compression strength	f_{cd}	30 MPa
Tensile strength	f_{ct}	Zero
Poisson's ratio	v	0,2

Reinforcing Steel properties [30] [31]		
Steel model		Hot rolled, class B
Modulus of elasticity	E_s	210 GPa
Yield strength	f_y	500 MPa
Poisson's ratio	v	0,3
Coefficient of convection on heated surfaces	h_h	25 W/m^{2}K
Coefficient of convection on unheated surfaces	h_c	4 W/m^{2}K
Emissivity	ε	0,7
Reinforcing Steel diameter	Φ_s	25 mm

Load	N	45 kN/m

Fire curve		ISO 834

8.2.3. Thermal analysis

In Figure 8.4 and 8.5 is represented the evolution of the temperature in the beam reinforcing steel bars. The evolution of the temperature in the steel bars is compared with the fire curve ISO 834. For the damage D0/D1 and D2 the bottom steel bars are the ones with higher temperature. In damage D3, with the steel bars directly exposed to the fire, the temperature of the bottom and top steel bars is the same. In damage D3 the temperature of the steel bars is similar with the temperature of the fire curve ISO 834. The analysis regarding the effective yield strength performed earlier in the section of the column can also be applied here and the methodology used earlier is the same used here. In the Figures 8.6, 8.7 and 8.8 it is represented the temperature profiles of the beams with damage D0/D1, D2 and D3 at 60, 120, 180 and 240 minutes. In the temperatures profiles of the beam the top side does not have any type of damage, so there are no elements removed at the top side of the section.

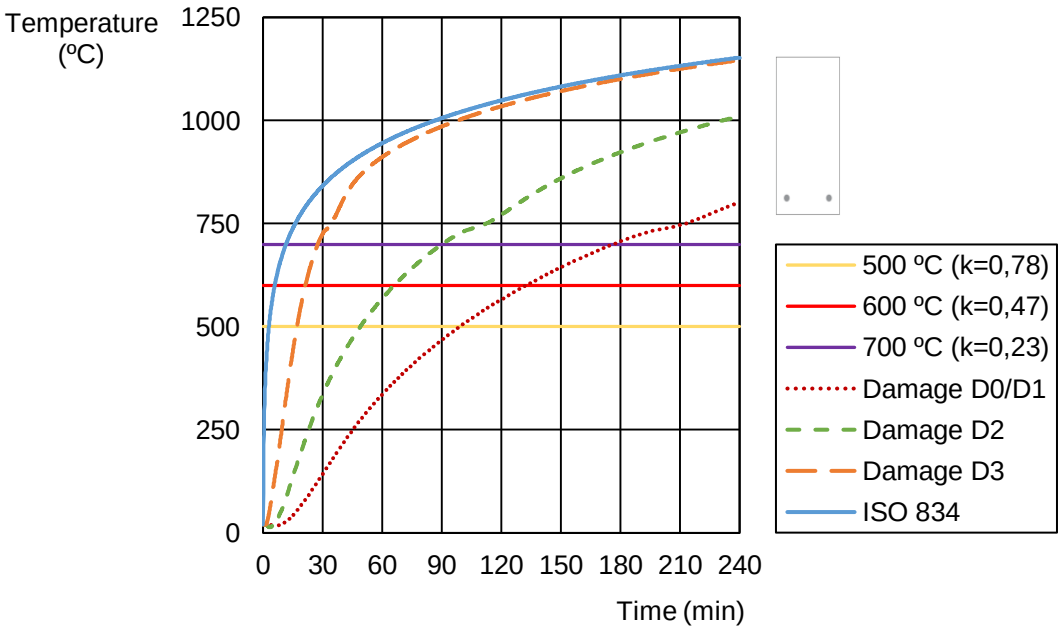

Figure 8.4 – Temperature evolution in the beams bottom reinforcing steel bars.

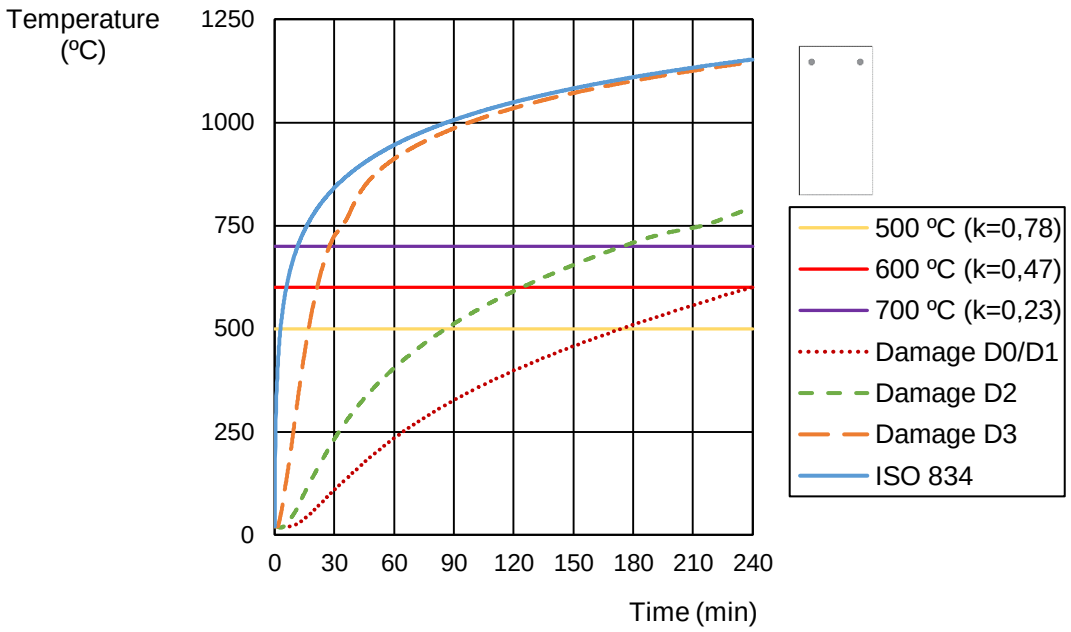

Figure 8.5 – Temperature evolution in the beams top reinforcing steel bars.

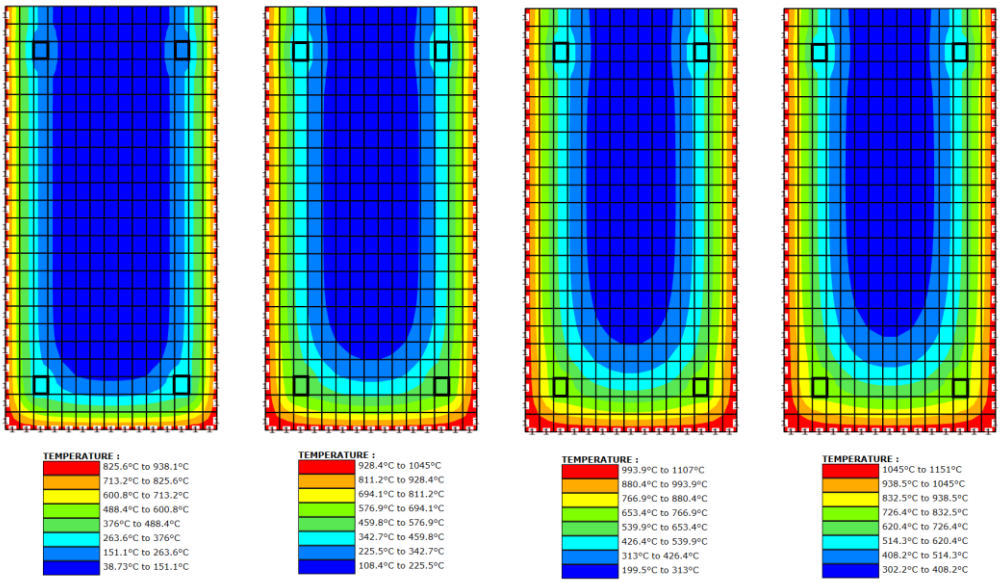

Figure 8.6 – Temperature profiles of beam with damage D0/D1 at 60, 120, 180 and 240 minutes (left to right).

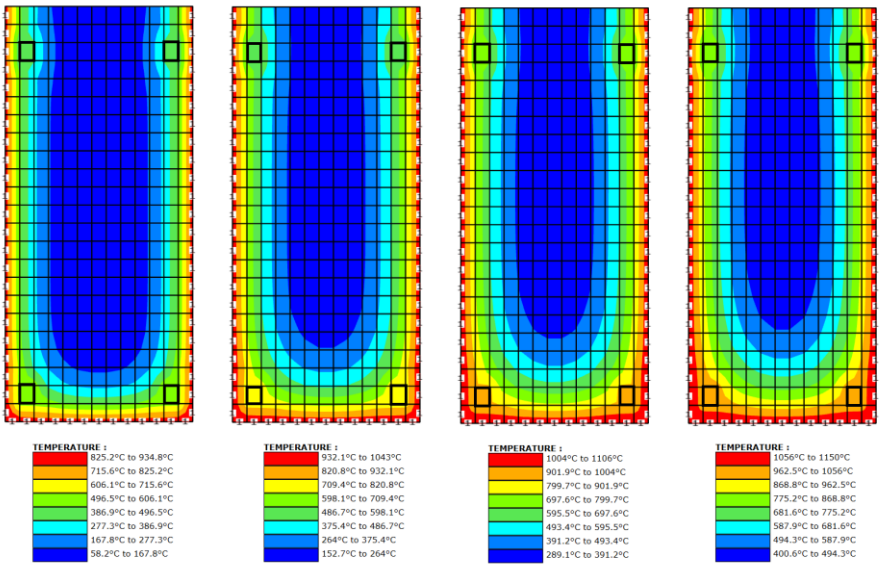

Figure 8.7 – Temperature profiles of beam with damage D2 at 60, 120, 180 and 240 minutes (left to right).

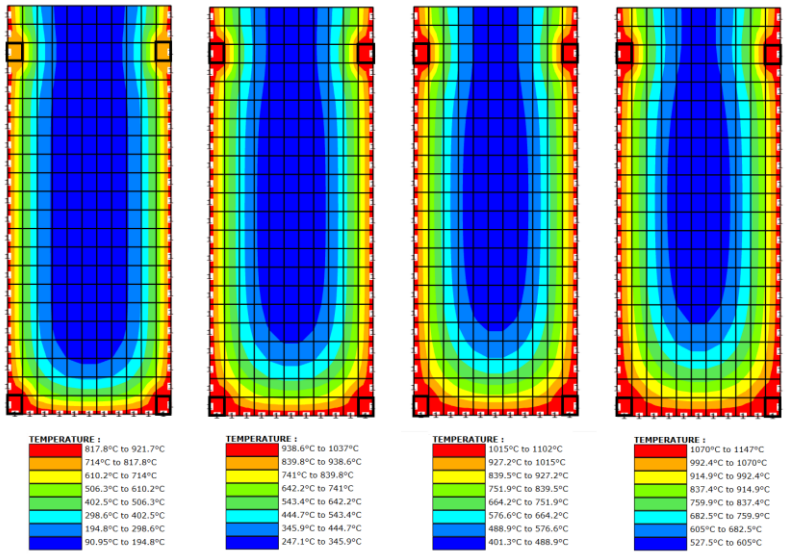

Figure 8.8 – Temperature profiles of beam with damage D3 at 60, 120, 180 and 240 minutes (left to right).

8.3. Beam analysis

8.3.1. Beam characteristics

In this Chapter there will be analysed three different beams. The Table 8.2 shows the description and the location of the damage in each beam. In beam A1 all the 60 elements have the section with damage D0/D1, and in beams A2 and A3 the damage is in the 6 elements closer to the fixed supports.

Table 8.2 – Location of the damage in the beam.

Beam	Damage	Elements	Distance
A1	D0/D1	All	6 m
A2	D2	1 to 6 and 55 to 60	0,6 m
A3	D3	1 to 6 and 55 to 60	0,6 m

8.3.2. Time until conventional collapse

In the Table 8.3 are represented the time until collapse of the beams. As expected, the results show that the damage reduce the time until collapse of the beam. For beam A1 there is not collapse until 240 minutes. The differences between the beams regarding the time until collapse are not small. The difference between beam A2 and A3 is almost 60 minutes. The time until collapse of beam A2 is more than the double of the time until collapse of the beam A3.

Table 8.3 – Time until collapse of the beam.

Beam	Damage	Time (min)
A1	D0/D1	240,0
A2	D2	106,8
A3	D3	49,2

The same methodology used in Table 7.3 for the columns is also used in Table 8.4 for the beams. Once again is possible to see the influence of the damage in the risk category of the beams. A beam that is in the 4th risk category with damage D0/D1 goes to the 1st or to not even verifying any risk category with damage D3.

Table 8.4 – Risk category respected by each beam.

Beam	Damage	Location	Utilization type	
			II, XI and XII	I, III, IV, V, VI, VII, VIII, IX and X
A1	D0/D1	All Elem.	4th	4th
A2	D2	0,6 m	2nd	3rd
A3	D3	0,6 m	-	1st

(-) Do not verify any risk category

8.3.3. Axial force

In the Figure 8.9 is represented the evolution of the axial forces in the beams. The evolution of the axial forces in the beams is similar until about 30 minutes. However, there is a slightly difference, the beam with damage D3 reaches higher axial forces sooner than the beam with damage D2 and the beam with damage D2 reach higher axial forces sooner than the beam with damage D0/D1. One possible explanation for this is related with the thermal elongation of the steel bars. The effect of the temperature happens earlier in the beam with damage D3 because the steel bars are exposed. For the other beams the idea is the same, the steel bars in the beam A1 are more protected than the steel bars in the beam A2 and that leads that the thermal elongation of the steel bars happens a bit later. Since the beams have fixed supports there is no horizontal displacement in the beam. This type of supports lead to the higher axial forces because of the total horizontal restraint. It is expected that these beams inserted in a structure with more flexible supports will have lower

axial forces compared to the ones obtained here. For the beam A3 the axial forces increase until the collapse of the beam. For the beams A1 and A2 the axial force increases until around 60 minutes and then starts to decrease. The decrease of the axial force happens due to the deterioration of the materials. In the appendices are the schematics of the axial force of the beams.

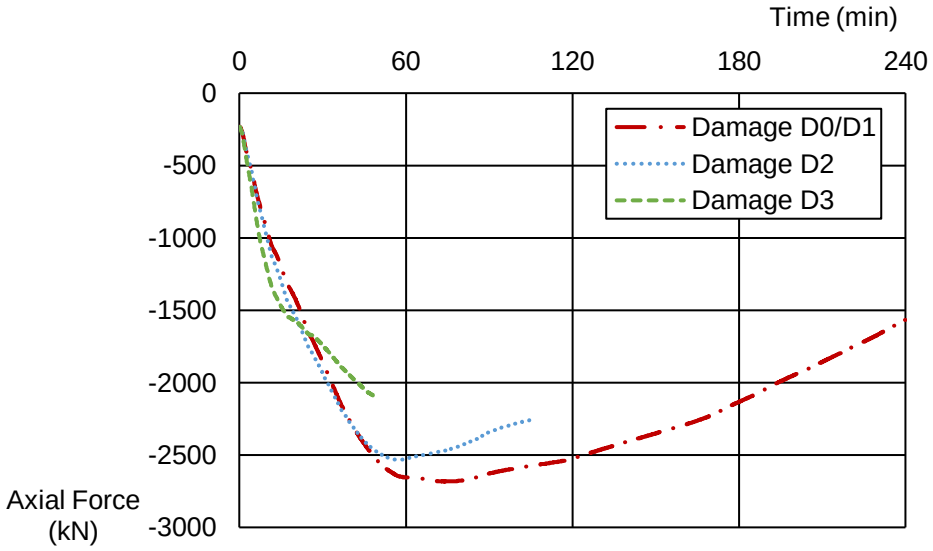

Figure 8.9 – Evolution of the axial force in the beams.

8.3.4. Mid-span moments

In the Figure 8.10 is represented the evolution of the mid-span moments in the beams. In the first minutes there is a flexural restraint to the rotation created by the thermal gradient in the section of the beam. After that there is a deterioration of the materials and the moments start to re-distribute towards the mid-span of the beam. The moments in the mid-span of the beam start to increase and the moments in the supports decrease. The deterioration that leads to the redistribution of the moments happens first in the beam with damage D3, followed by the beam with damage D2 and followed by the beam with damage D0/D1. In the appendices are the schematics of the bending moments of the beams.

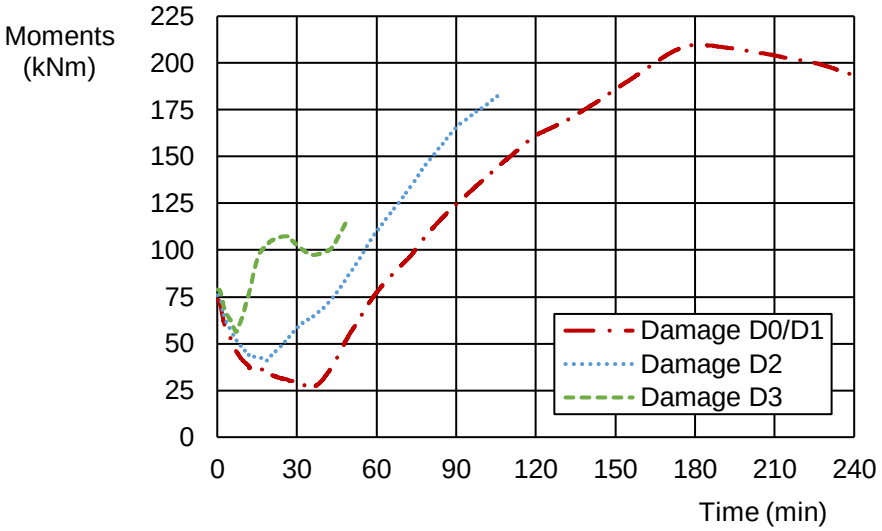

Figure 8.10 – Evolution of the mid-span moments in the beams.

8.3.5. Moments in supports

In the Figure 8.11 is represented the evolution of the moments in the supports of the beams. The evolution of the moments in the supports follow the same trend of the moments in the mid-span of the beam. In the first minutes the moments increase due to thermal gradient in the section of the beam and then due to the materials deterioration the moments decrease.

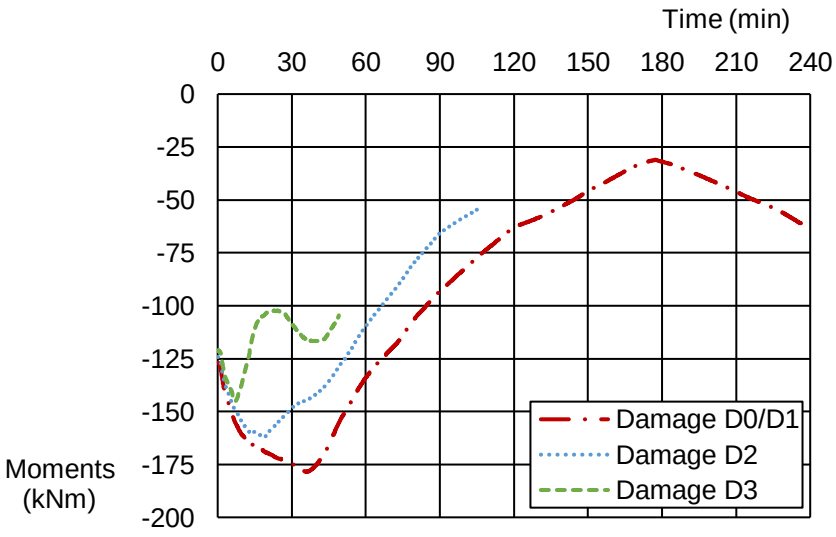

Figure 8.11 – Evolution of the moments in the supports in the beams.

8.3.6. Displacement mid-span

In the Figure 8.12 is represented the evolution of the displacements in the mid-span of the beams. The higher vertical displacement observed is in the beam A1, -36,55 mm at 240 minutes. The highest displacement observed in beams A2 and A3 is at the time of collapse of the beams. The displacement in beam A2 is -16,5 mm and the displacement in beam A3 is -10,49 mm. In the appendices are the schematics of the deformed shape of the beams.

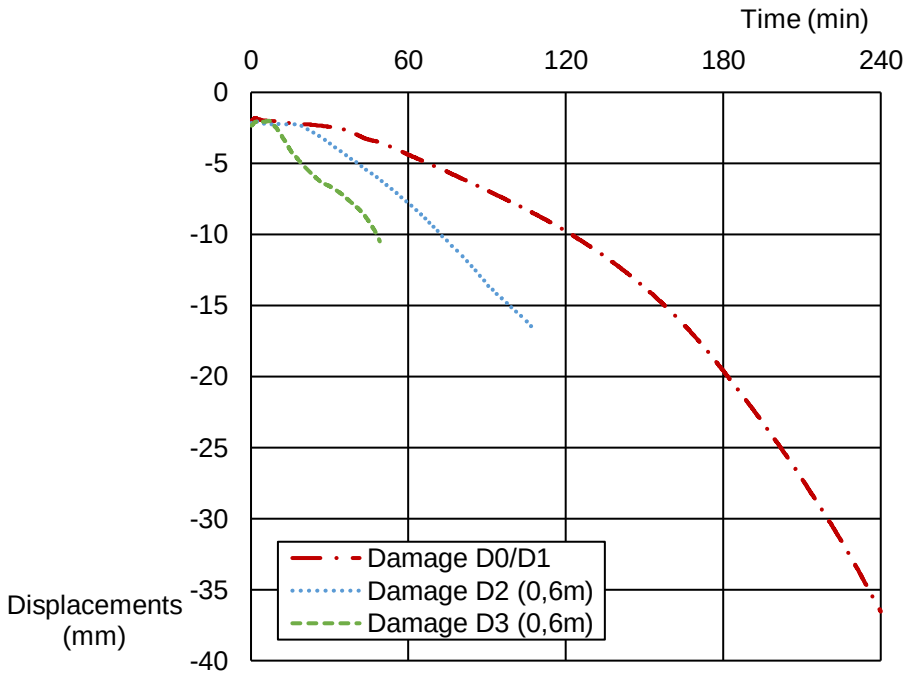

Figure 8.12 – Evolution of displacement in the mid-span of the beam.

9. Post-earthquake fire on RC frames

9.1. Introduction

In this Chapter it is presented a numerical analysis of a reinforced concrete frame exposed to fire after an earthquake. The fire curve used in this analysis is the ISO 834. In Figure 9.1 it is represented a schematic of the frame. The developing of the fire happens only in the bottom compartment of the frame. The frame has a continuous load in the beams and point loads in the top of the columns. In Figure 9.2 is represented the finite element mesh developed in SAFIR and in Figure 9.3 is represented the location and numbering of the nodes of the frame. The numbering of the finite element mesh is used in the moments and shear force analysis and the numbering of the nodes is used in the displacement analysis.

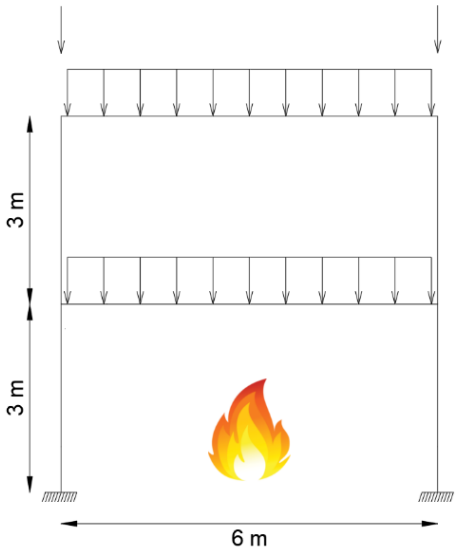

Figure 9.1 – Frame model.

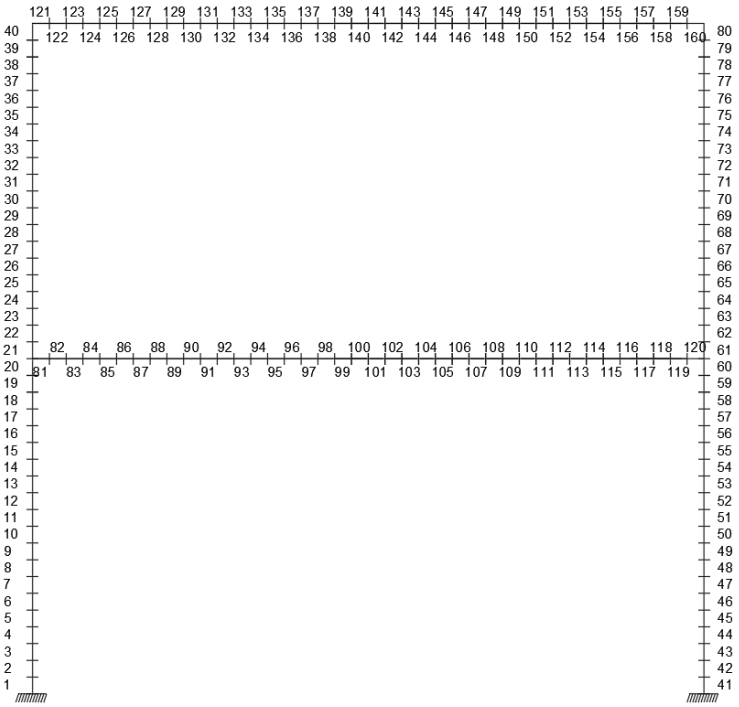

Figure 9.2 – Finite element mesh for structural analysis with SAFIR.

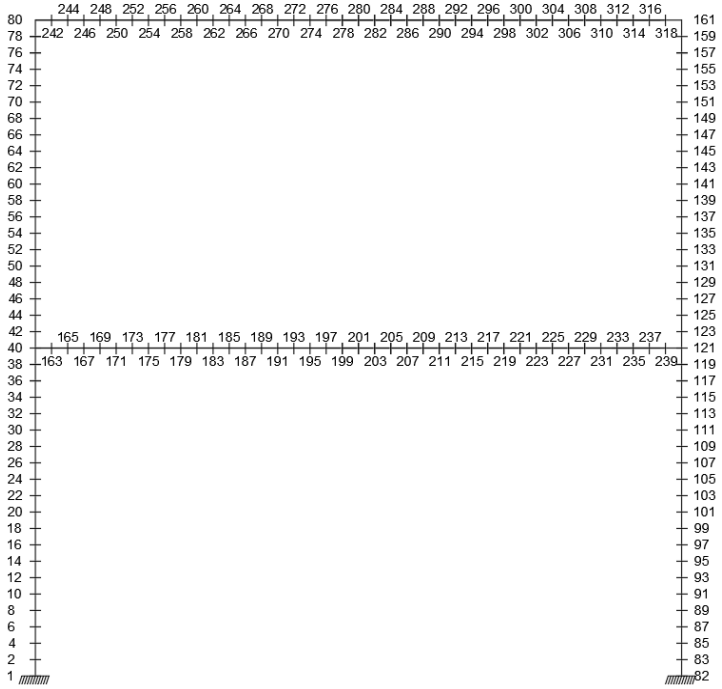

Figure 9.3 – Location of nodes in the finite element mesh.

9.2. Frames section analysis

9.2.1. Material properties

In Table 9.1 are all the material properties, loads and fire curve used in the frame numerical models.

Table 9.1 – Concrete properties, reinforcing steel properties, loads and fire curve in the frames.

Concrete properties [30]		
Concrete model		Siliceous aggregate
Specific mass of concrete	rho	2300 kg/m^3
Water content	w	46 kg/m^3
Coefficient of convection on heated surfaces	h_h	25 W/m^{2}K
Coefficient of convection on unheated surfaces	h_c	4 W/m^{2}K
Emissivity	ε	0,7
Compression strength	f_{cd}	30 MPa
Tensile strength	f_{ct}	Zero
Poisson's ratio	v	0,2

Reinforcing Steel properties [30] [31]		
Steel model		Hot rolled, class B
Modulus of elasticity	E_s	210 GPa
Yield strength	f_y	500 MPa
Poisson's ratio	v	0,3
Coefficient of convection on heated surfaces	h_h	25 W/m^{2}K
Coefficient of convection on unheated surfaces	h_c	4 W/m^{2}K
Emissivity	ε	0,7
Reinforcing Steel diameter	Φ_s	25 mm

Loads		
Point load		370 kN
Distributed load		45 kN/m

Fire curve		ISO 834

9.3. Frames analysis

9.3.1. Frame characteristics

In SAFIR where developed fifteen different frames. The differences between them are related with the type of damage and the fire frontiers applied. The beam and columns sections used in the frames are the same used in the Chapter 7 and 8. It is only in the bottom compartment that the fire develops. It was considered that the earthquake damage is only in the bottom beam and columns. In Figure 9.4 is represented the location of the damage. Three different zones where considered, zone 1, 2 and 3. In Table 9.2 is it presented the fifteen different frames as well as the type of damage in each zone and the fire frontiers in the columns. Basically, it is possible to divide the fifteen frames into three groups of five frames. In a group A it is considered one fire frontier in the columns, in group B it is considered three fire frontiers in the columns and in group C it is considered four fire frontiers in the columns. In each group there are five different frames analysed. In three frames it is considered the three types of damage (D0/D1, D2 and D3) in all the zones, one type of damage for each frame. The two remaining frames of each group are to analyse the influence of the damage D2 and D3 in the columns and beam.

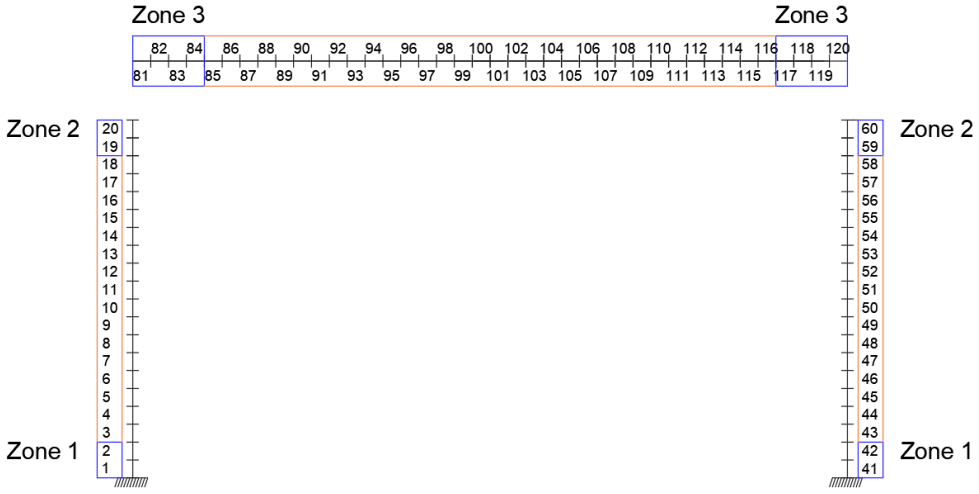

Figure 9.4 – Representation of the three zones where different types of damage are applied.

Table 9.2 – Characteristics of the different analysed frames.

Frame	Zone 1	Zone 2	Zone 3	Fire Frontiers (in columns)
Frame A1	Damage D0/D1			1 FF
Frame A2	Damage D2			1 FF
Frame A3	Damage D3			1 FF
Frame A4	Damage D3	Damage D2	Damage D3	1 FF
Frame A5	Damage D3	Damage D3	Damage D2	1 FF
Frame B1	Damage D0/D1			3 FF
Frame B2	Damage D2			3 FF
Frame B3	Damage D3			3 FF
Frame B4	Damage D3	Damage D2	Damage D3	3 FF
Frame B5	Damage D3	Damage D3	Damage D2	3 FF
Frame C1	Damage D0/D1			4 FF
Frame C2	Damage D2			4 FF
Frame C3	Damage D3			4 FF
Frame C4	Damage D3	Damage D2	Damage D3	4 FF
Frame C5	Damage D3	Damage D3	Damage D2	4 FF

9.3.2. Time until conventional collapse

In the Table 9.3 and Figure 9.5 are the times until collapse of each frame. Figure 9.5 shows that each frame type A have higher time until collapse when compared with each correspondent frame type B and C. For example, frame A1 have higher time until collapse when compared to frame B1 and C1. This shows that the different numbers of fire frontiers in the columns have can lead to different times until collapse of the structure. Comparing frames B and C it is possible to observe that the results of frames with the same number are very similar. For example, in frame B2 and C2 the time until collapse is practically the same. This shows that, regarding time until collapse, in the analysed frame having three or four fire frontiers in the bottom columns is practically equal. The frame with higher time until collapse is the frame A1. Frame A1 is the frame without damage and with one fire frontier in the bottom columns. On the other hand, the frame that collapses earlier is frame C3 which is a frame with damage D3 in all zones and with four fire frontiers in the bottom columns. The difference in time until collapse between frame

A1 and C1 is 54 minutes. This shows the difference in having one or four fire frontiers in the bottom columns in an undamaged frame. Maybe after an earthquake the structural elements are not damaged but the non-structural can walls suffer damage, this situation can change between a situation where the columns have one fire frontier and where the columns have four fire frontiers. The difference in time until collapse between frame A3 and C3 is 62 minutes. This shows that even in a heavily damage structure the fire frontiers have a high influence in the time until collapse of the structure. The difference in time until collapse between frame C1 and C3 is 126 minutes. This situation are two frames with the same fire frontier conditions but with different types of damage. Frame C1 is without damage and C3 is with damage D3 in all zones. With this example the impact of the damage is easily observed. The frame C3 collapses more than two hours earlier than the frame C1. The results obtained in frames A2 and A5, B2 and B5 and C2 and C5 are very similar. Frames A5, B5 and C5 have damage D3 in the columns and damage D2 in the beam. Frames A2, B2 and C2 have damage D2 in all zones. Even if the type of damage is different the results are practically the same. This shows that in the analysed frame the bottom beam has a higher influence on the time until collapse of the structure. For the frames B3 and B4 the situation is similar but instead of damage D2 in the beam the damage is D3. As for frames B3 and B4, C3 and C4 the situation is different. In this case it appears that fire frontiers on the columns have a higher impact on the collapse of the structure than the bottom beam. The difference between the frames is in zone 2, frames B3 and C3 have damage D3 in zone 1 and 2 while frame B4 and C4 have damage D3 in zone 1 and damage D2 in zone 2. So, the damage in the columns of frames B3 and C3 is higher than in the columns of frames C4 and D4. More damage signifies more susceptibility to the fire and consequently a reduced time until collapse.

Table 9.3 – Time until collapse of the frames.

Damage	Frame	Fire Frontiers (in columns)	Time (min)
D0/D1	Frame A1	1 FF	227,19
D2	Frame A2	1 FF	144,46
D3	Frame A3	1 FF	109,53
D3D2D3	Frame A4	1 FF	109,50
D3D3D2	Frame A5	1 FF	143,25
D0/D1	Frame B1	3 FF	180,06
D2	Frame B2	3 FF	131,93
D3	Frame B3	3 FF	54,45
D3D2D3	Frame B4	3 FF	78,79
D3D3D2	Frame B5	3 FF	127,00
D0/D1	Frame C1	4 FF	173,16
D2	Frame C2	4 FF	132,47
D3	Frame C3	4 FF	47,08
D3D2D3	Frame C4	4 FF	69,08
D3D3D2	Frame C5	4 FF	125,00

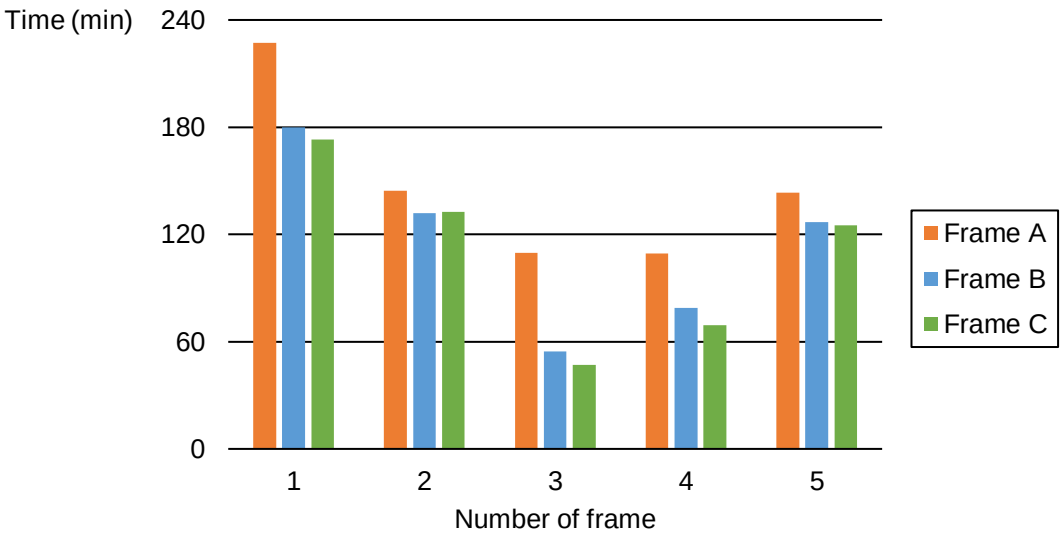

Figure 9.5 – Time until collapse of the frames

By comparing the values in Table 5.5 with the results in Table 9.3 it is possible to observe if a given frame has the minimum fire resistance of structural elements for a given building. Table 9.4 shows the maximum risk category respected by each frame. Given the similarity of the results between the frames with 3 and 4 fire

frontiers, the risk categories respected are also very similar. The only difference regarding the risk category is between frame B1 and C1, for utilization types II, XI and XII. The risk category in frame B1 is the 4th and in frame C1 is the 3rd. As observed earlier, the frames with lower times until collapse are frames B3 and C3. These frames do not respect any risk category of utilization types II, XI and XII. For the other utilization types these frames are in the 1st risk category. The higher difference between risk categories is observed in frames B1 and B3 for utilization types II, XI, and XII. Frame B1 respects the 4th risk category and frame B3 does not respect any risk category. This shows once again the huge impact of the damage on the frames.

Table 9.4 – Risk category of each frame.

			Utilization type	
Damage	Frame	Fire Frontiers	II, XI and XII	I, III, IV, V, VI, VII, VIII, IX and X
D0/D1	A1	1 FF	4th	4th
D2	A2	1 FF	3rd	4th
D3	A3	1 FF	2nd	3rd
D3D2D3	A4	1 FF	2nd	3rd
D3D3D2	A5	1 FF	3rd	4th
D0/D1	B1	3 FF	4th	4th
D2	B2	3 FF	3rd	4th
D3	B3	3 FF	-	1st
D3D2D3	B4	3 FF	1st	2nd
D3D3D2	B5	3 FF	3rd	4th
D0/D1	C1	4 FF	3rd	4th
D2	C2	4 FF	3rd	4th
D3	C3	4 FF	-	1st
D3D2D3	C4	4 FF	1st	2nd
D3D3D2	C5	4 FF	3rd	4th

(-) Do not verify any risk category

9.3.3. Axial force in beam

In Figures 9.6 to 9.10 are represented the axial force in the bottom beam in the different frames. The frames are grouped in a way that each Figure shows the axial force for a certain typology of damage and for frames A, B and C.

The frames with one fire frontier in the columns (A1, A2, A3, A4 and A5) have the highest values of the axial force in the beam. The columns with one fire frontier create a higher horizontal restraint when compared with the columns with three or four fire frontiers. This situation leads to higher axial forces in the beam. The frame with the highest axial force is frame A1, this frame has the lowest damage and one fire frontier in the columns. The damage in the columns lowers the flexural stiffness of the columns and this lowers the horizontal restraint to the beams thermal elongation. This situation is observed by comparing, for example, frame B1 with frame B2 or C1 with C2. The frame B1 and C1 have damage D0/D1 in the columns and frames B2 and C2 has damage D2 in the columns. The results show higher axial forces in frames B1 and C1 when compared with frames B2 and C2.

The beam characteristics considered in the frames are the same of the previous Chapter 8. The axial forces are considerable lower in the frames compared with the beam in Chapter 8 due to the supports. In Chapter 8 the beam with fixed supports creates a total horizontal restraint to the thermal elongation of the beam, leading to high axial forces. In the frames the beams are connected to the columns where the horizontal restraint is not total, leading this way to lower axial forces.

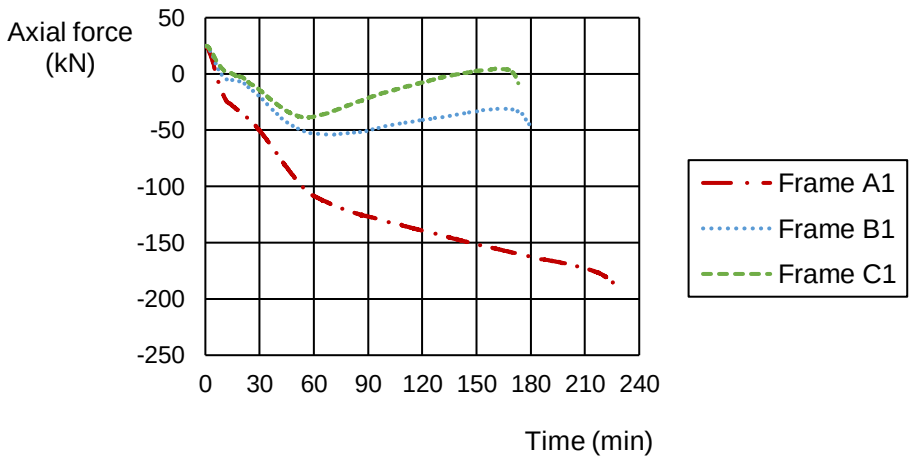

Figure 9.6 – Axial force in the bottom beam in frames A1, B1 and C1.

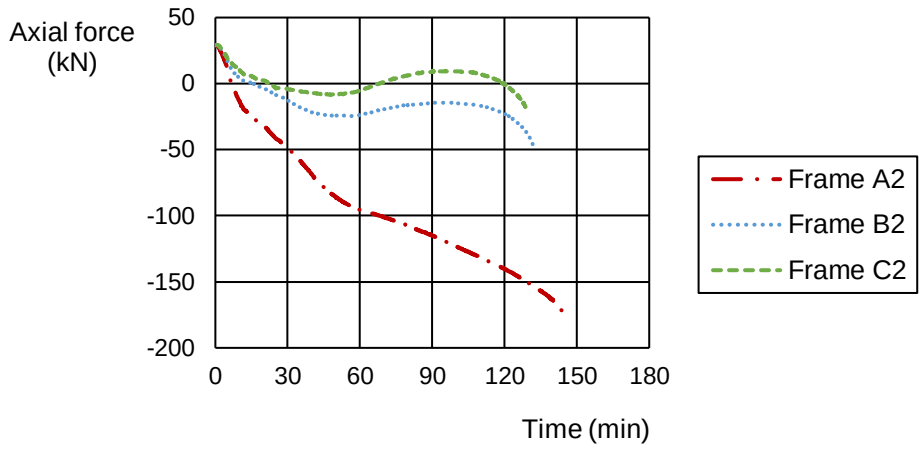

Figure 9.7 – Axial force in the bottom beam in frames A2, B2 and C2.

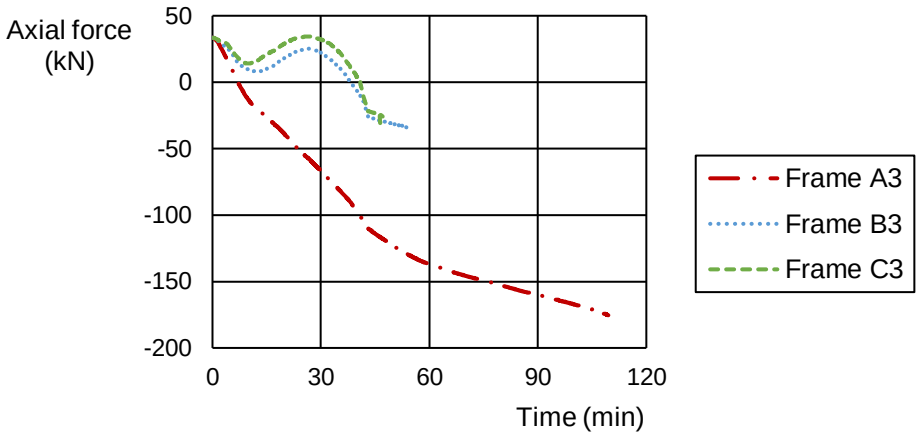

Figure 9.8 – Axial force in the bottom beam in frames A3, B3 and C3.

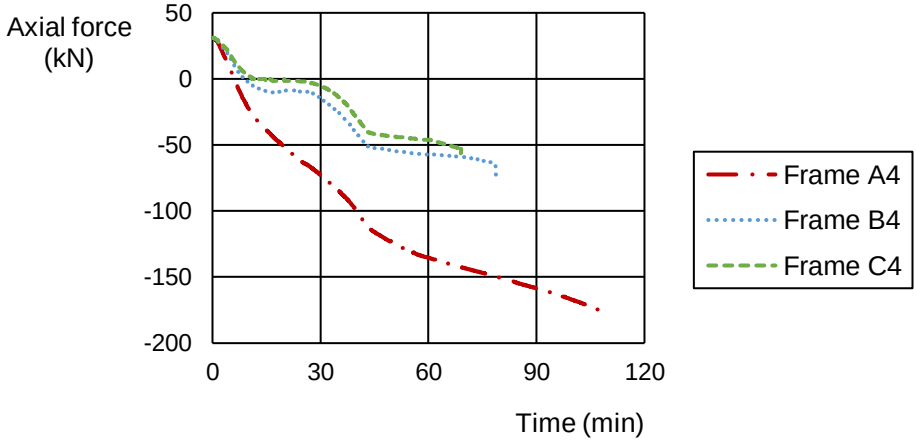

Figure 9.9 – Axial force in the bottom beam in frames A4, B4 and C4.

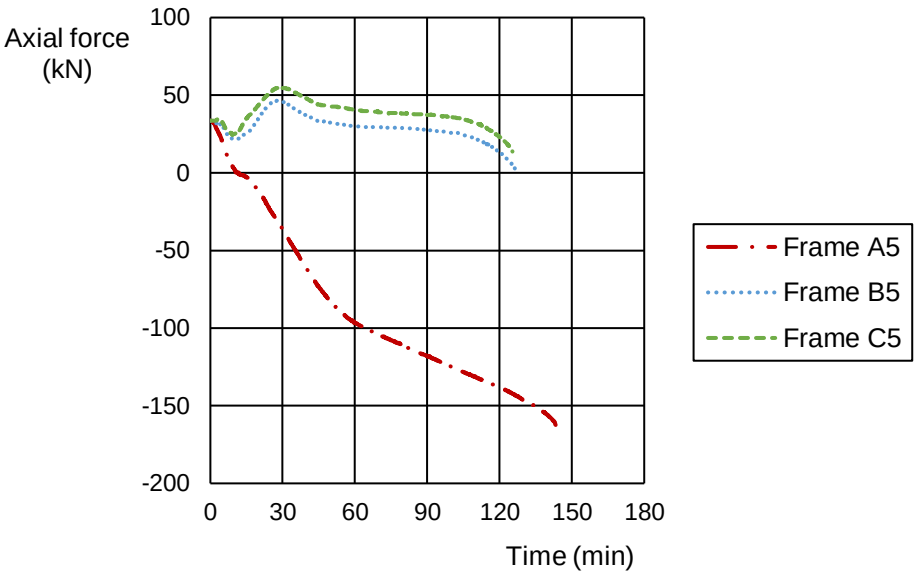

Figure 9.10 – Axial force in the bottom beam in frames A5, B5 and C5.

9.3.4. Moments in beam

In Figures 9.11, 9.12 and 9.13 are represented the moments in element 81 (left end of the beam) in the different frames. In each Figure the fire frontiers are the same, the difference lies in the typology of damage in the frames. In the appendices are the schematics of the bending diagrams of the frames.

The bending moment diagram in element 81 in frame A1, B1 and C1 goes upwards until around minute 75 and then downwards until the collapse of the structure. The bending moments in element 81 in frame A1 is higher than in frame B1 and the bending moments in frame B1 is higher than in frame C1. This may be explained by the fact that frame A1 is stiffer than frame B1 and C1 because possesses only one fire frontiers in the columns while frames B and C possess three and four fire frontiers in the columns. The differences are not very high, especially between frames B1 and C1 where the results are practically the same. This situation also applies for the other numbers of frames B and C. The bending moment diagram in element 81 in frames A1, B1 and C1 goes upwards until minute 75 due to the flexural restraint to the rotation induced by the thermal gradient along the section of the beam. The higher bending moments in element 81 are at 75 minutes in the

frames without damage. Frame A1 has a moment of -180,3 kN/m, frame B1 has a moment of -173,9 kN/m and frame C1 has a moment of -171,6 kN/m. After the 75 minutes, due to the materials deterioration the bending moment diagram goes downwards until the collapse of the structure. For the frames with damage D2 in the beam (frames A2, A5, B2, B5, C2 and C5) the bending moment diagram in element 81 goes upwards until about minute 50 and then downwards until the collapse. In these frames the damage D2 in the beam serves as an already deteriorated material and will lead to a faster deterioration of the reinforcing steel. This situation leads to lower bending moments and a lower time at when the bending moments diagrams changes from going upward to going downward. For the frames with damage D3 in the beam (frames A3, A4, B3, B4, C3 and C4) the bending moment diagram in element 81 goes upwards until about minute 10 and then downwards until the collapse. The sections with damage D3 are smaller and lead to a faster deterioration of the reinforcing steel when compared with sections with damage D2.

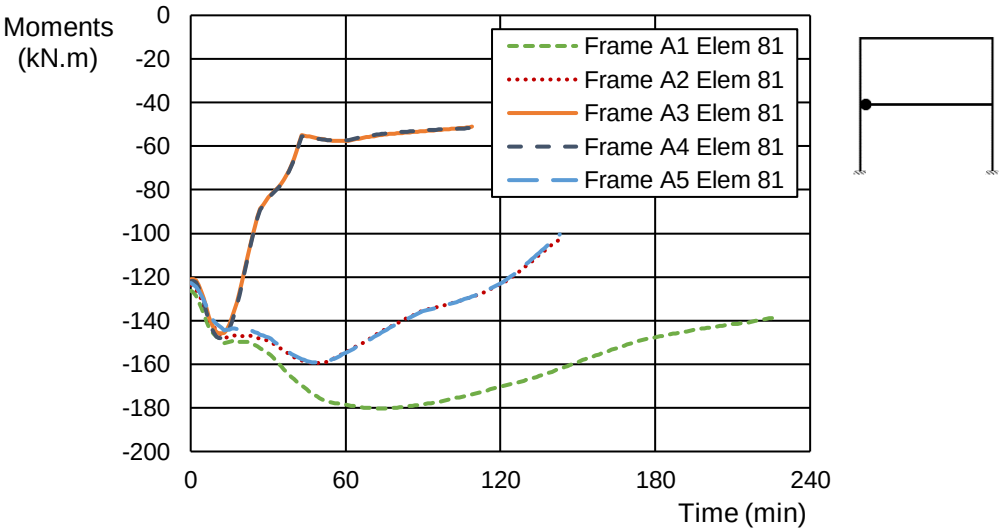

Figure 9.11 – Moments in element 81 in frames A1, A2, A3, A4 and A5.

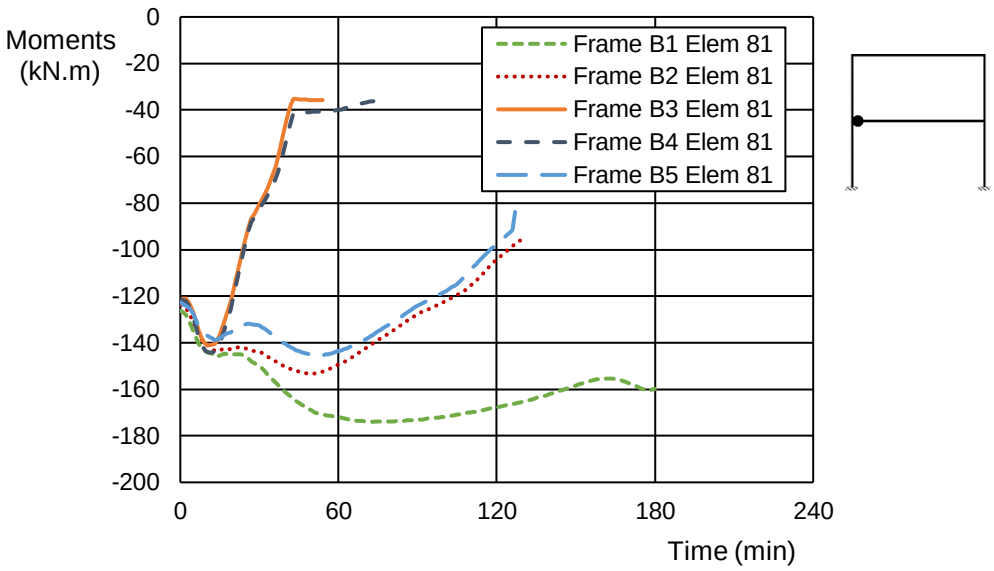

Figure 9.12 – Moments in element 81 in frames B1, B2, B3, B4 and B5.

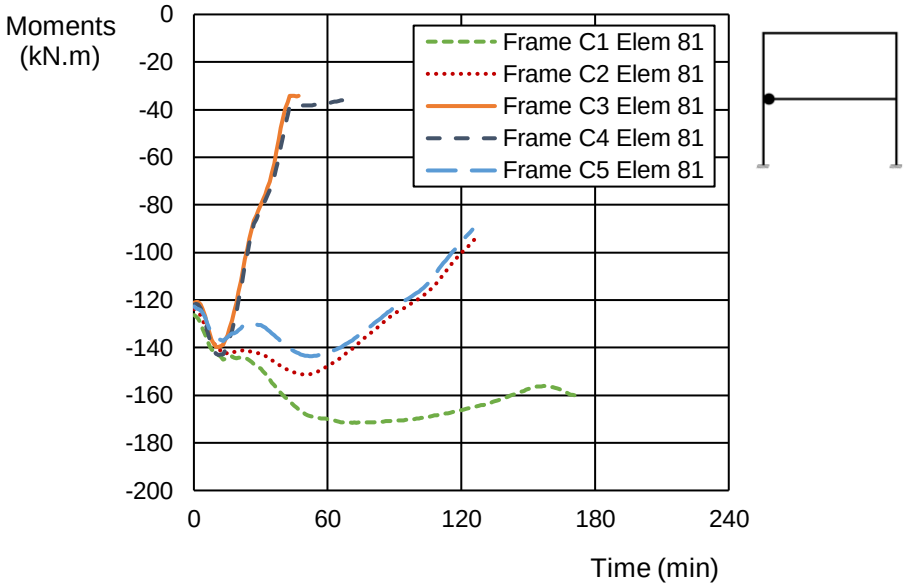

Figure 9.13 – Moments in element 81 in frames C1, C2, C3, C4 and C5.

In Figures 9.14, 9.15 and 9.16 are represented the moments in element 101 (beam mid-span) in the different frames. In each Figure the fire frontiers are the same, the difference lies in the typology of damage in the frames. The moments in the mid-span of the beam follow the same trend of the moments in element 81.

The materials deterioration leads to redistributing of the bending moments to the mid-span. This situation leads to higher bending moments in the mid-span and the beams with higher damage is where the higher moments are observed. The frames A3, A4, B3, B4, C3 and C4 are the frames with damage D3 in the beam. The higher bending moment in element 101 in frame A3 is 159,9 kN/m, in frame B3 is 164,2 kN/m and in frame C3 is 165 kN/m. These bending moments show the influence of the fire frontiers in the columns. Having three or four fire frontiers leads to practically the same bending moment in the mid-span of the beam and to higher results when compared with the frames with one fire frontier in the column.

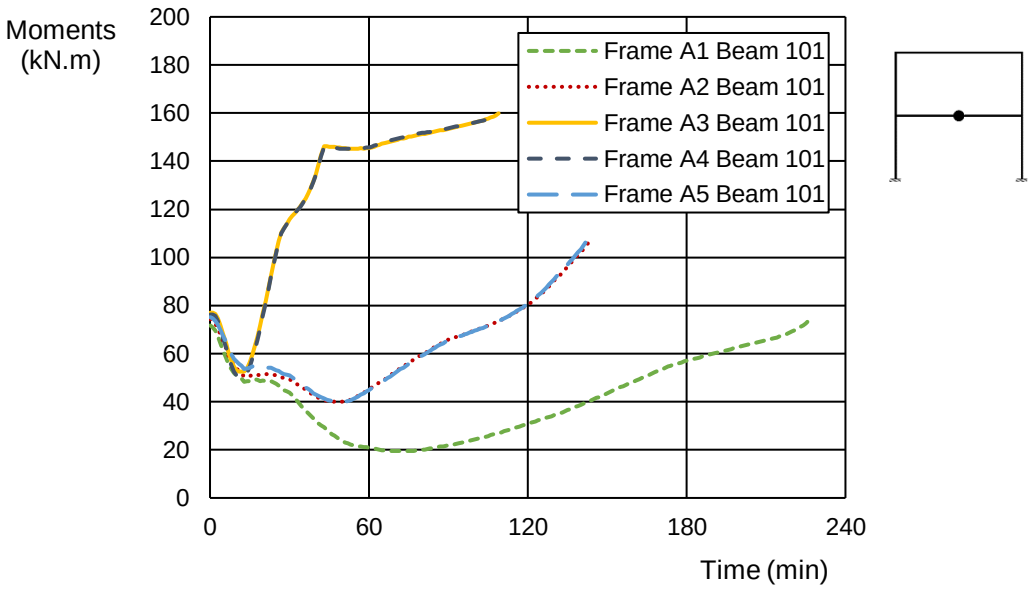

Figure 9.14 – Moments in element 101 in frames A1, A2, A3, A4 and A5.

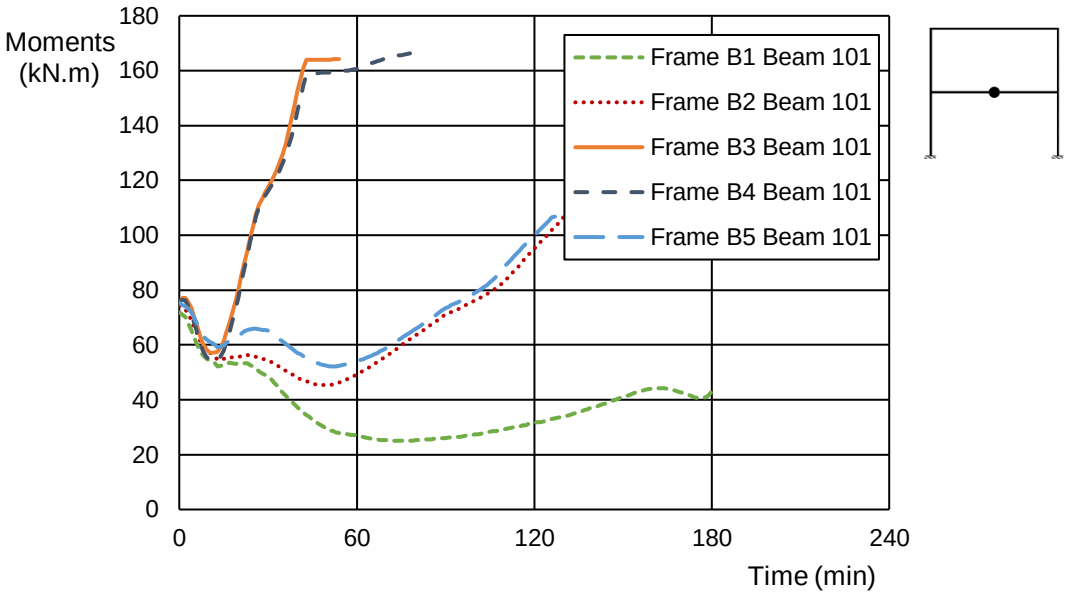

Figure 9.15 – Moments in element 101 in frames B1, B2, B3, B4 and B5.

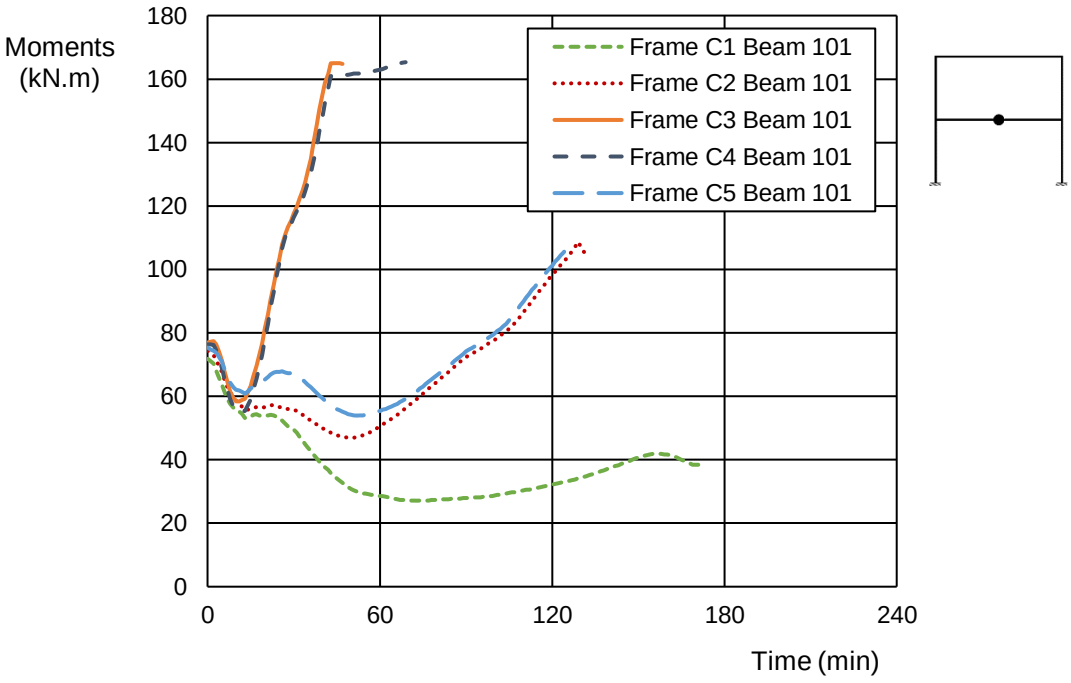

Figure 9.16 – Moments in element 101 in frames C1, C2, C3, C4 and C5.

9.3.5. Moments in column

In Figures 9.17, to 9.21 are represented the moments in elements 1 and 20 in the different frames. The frames are grouped in a way that each Figure shows the moments in elements 1 and 20 for a certain typology of damage and for frames A, B and C.

As it was expected, the bending moments in elements 1 and 20 in frames A, B and C follow a symmetrical path. The frames with less damage are the ones with higher moments in the columns. In Figures 9.17 to 9.21 is possible to see that the number of fire frontiers in the columns has a huge impact on the moments. The difference between having three or four fire frontiers in the columns is more noticeable in the moments of columns. The sections of the columns with four fire frontiers have a double symmetry in the temperature profiles, this situation leads to a lower effect caused by the temperature in the columns forces. In the section with one and three fire frontiers there is not double symmetry in the temperature profiles, this situation leads to a higher effect of the temperature in the forces of the column when compared with the section with four fire frontiers. This can be observed in Figures 9.17 to 9.21. The higher moment observed in element 1 is 227,9 kN/m in frame A1 and the higher moment observed in element 20 is -254,6 kN/m also in frame A1. The maximum moments at frame B1 in element 1 and 20 are achieved at 67 minutes and the maximum values at frame C1 in element 1 and 20 are achieved at 55 minutes. After that, the moments reduce until the collapse of the structure.

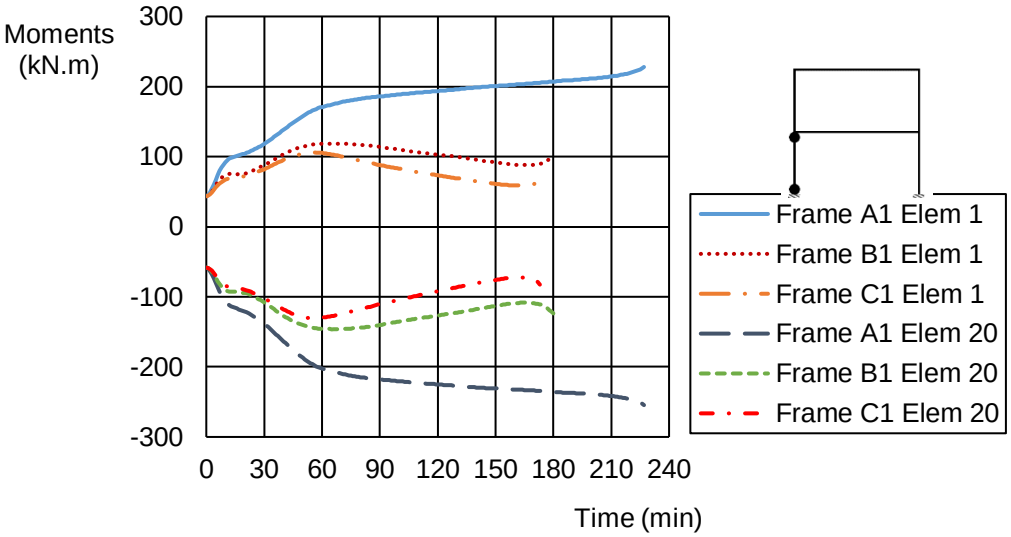

Figure 9.17 – Moments in elements 1 and 20 in frames A1, B1 and C1.

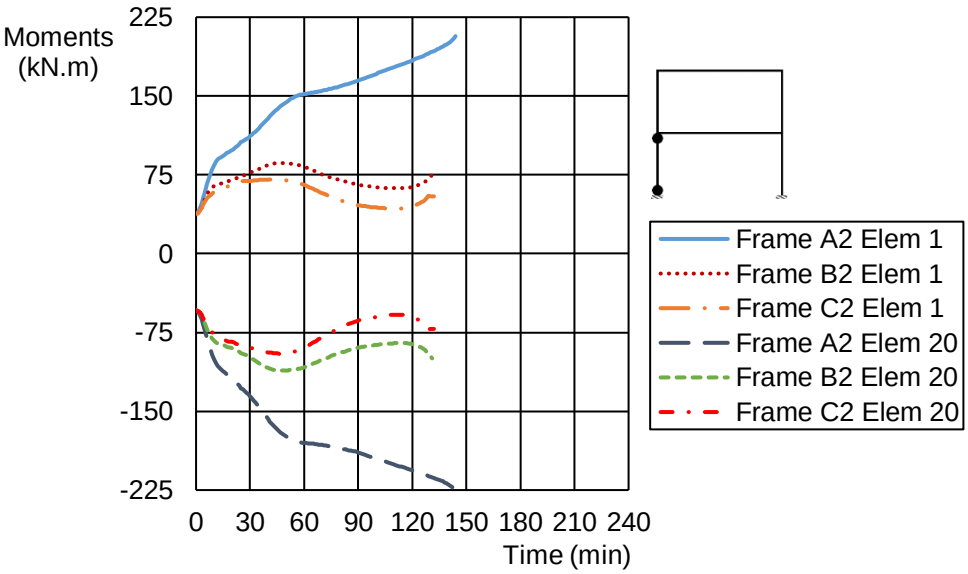

Figure 9.18 – Moments in elements 1 and 20 in frames A2, B2 and C2.

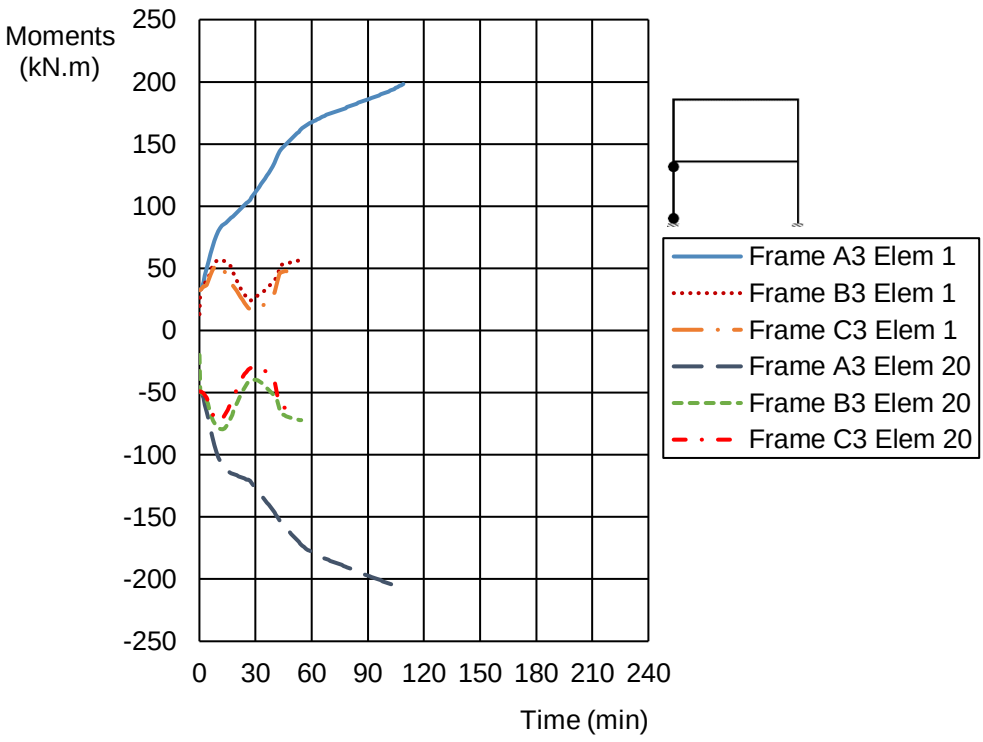

Figure 9.19 – Moments in elements 1 and 20 in frames A3, B3 and C3.

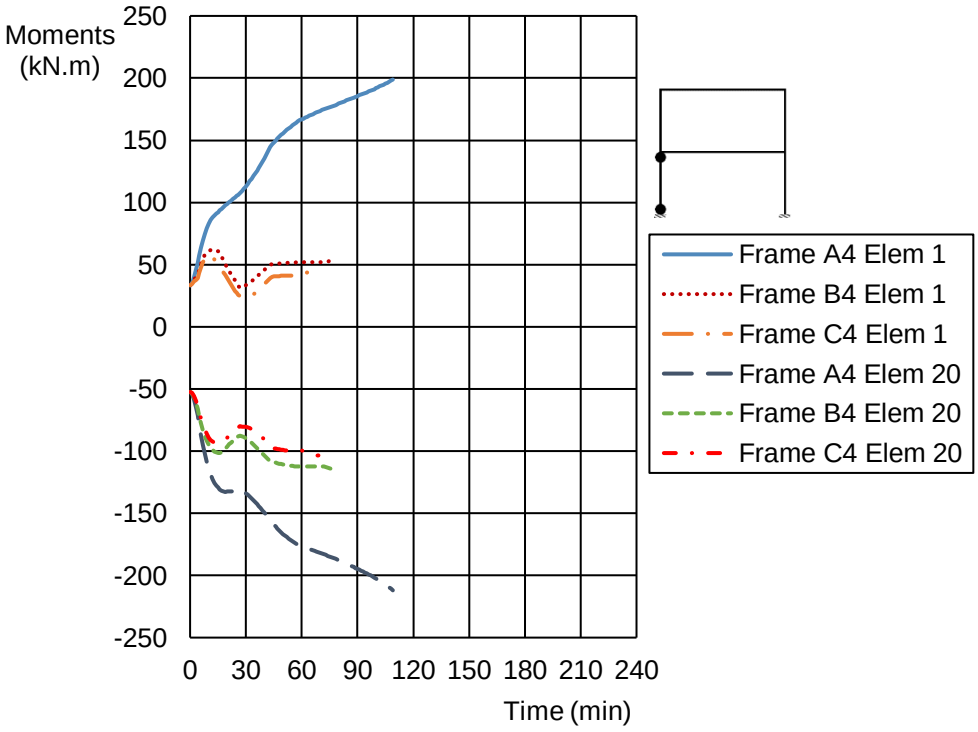

Figure 9.20 – Moments in elements 1 and 20 in frames A4, B4 and C4.

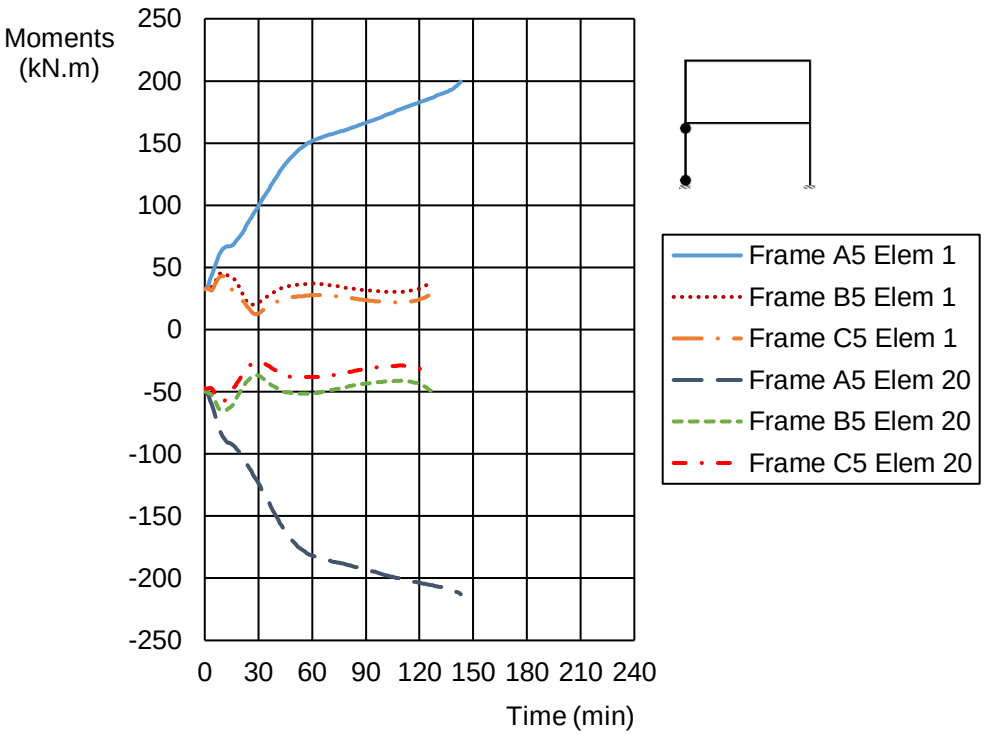

Figure 9.21 – Moments in elements 1 and 20 in frames A5, B5 and C5.

9.3.6. Shear force in column

In Figures 9.22, to 9.26 are represented the shear force in elements 1 and 20 in the different frames. The frames are grouped in a way that each Figure shows the shear force in elements 1 and 20 for a certain typology of damage and for frames A, B and C. In the appendices are the schematics of the shear force diagrams of the frames.

The shear force in frames A have a steeper increase when compared to frames B and C which is in accordance with the evolution of the bending moments in the column. The highest shear force is observed in frame A1 in the moment of collapse. The shear forces in frames B and C are similar, especially when there is damage D3 in the columns (Figures 9.24, 9.25, 9.26). The frames with damage D0/D1 and D2 (Figures 9.22 and 9.23) follow the same pattern regarding the evolution of the shear forces but with different values. The frames with damage D2

have lower shear forces than the frames with damage D0/D1. This shows that the damage has an impact on the shear forces of the columns. The columns with more damage will have lower shear forces. The frames with columns with damage D3 are frames 3 and 5, in Figures 7.24 and 7.26.

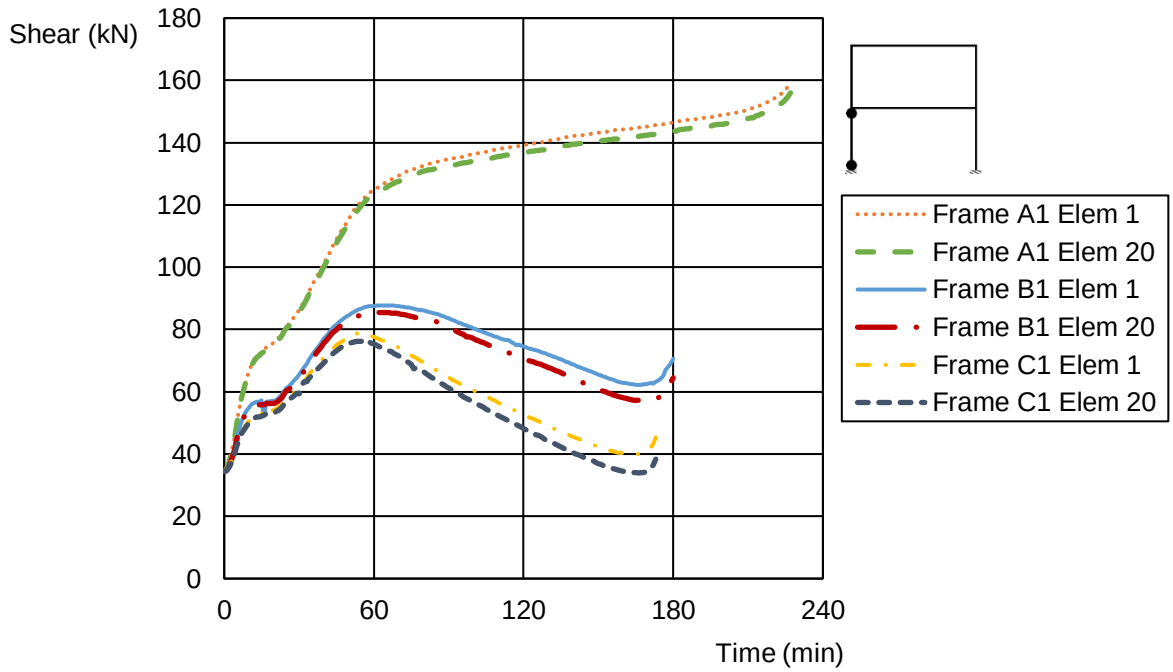

Figure 9.22 – Shear force in elements 1 and 20 in frames A1, B1 and C1.

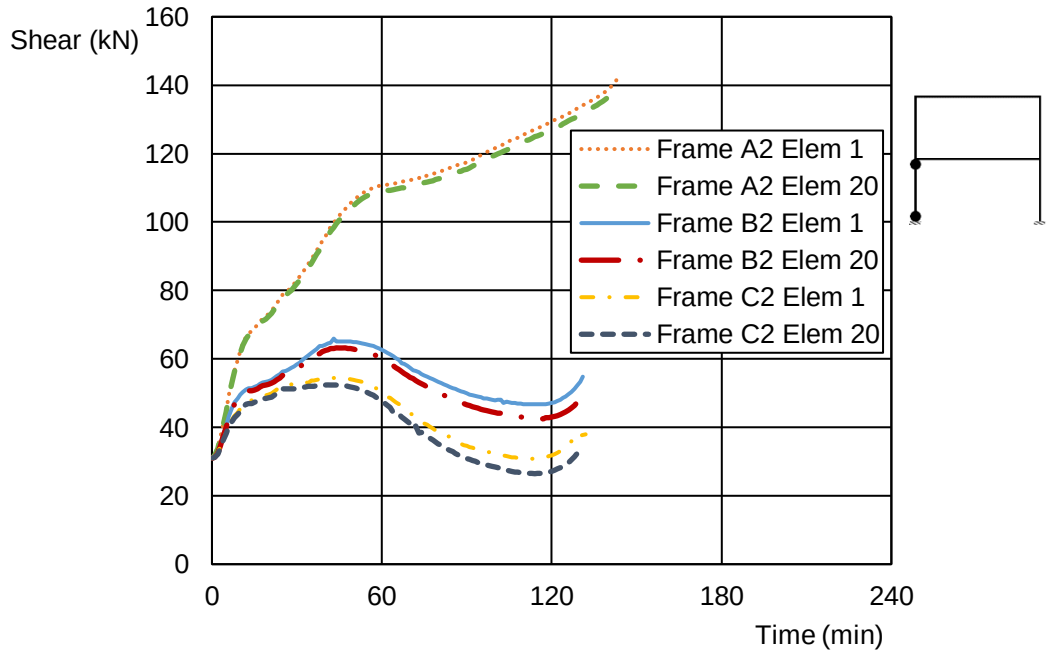

Figure 9.23 – Shear force in elements 1 and 20 in frames A2, B2 and C3.

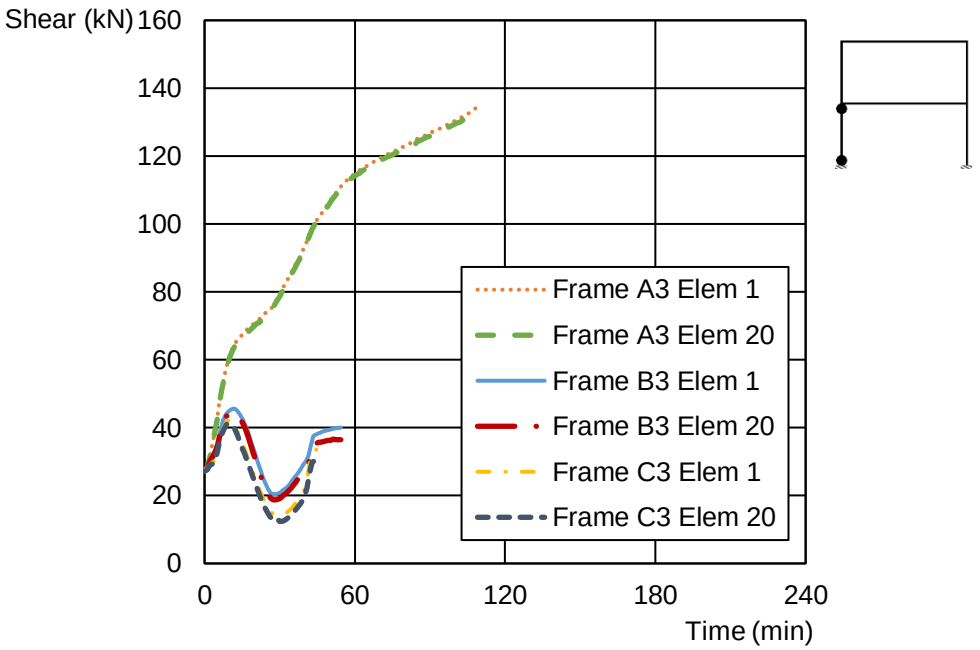

Figure 9.24 – Shear force in elements 1 and 20 in frames A3, B3 and C3.

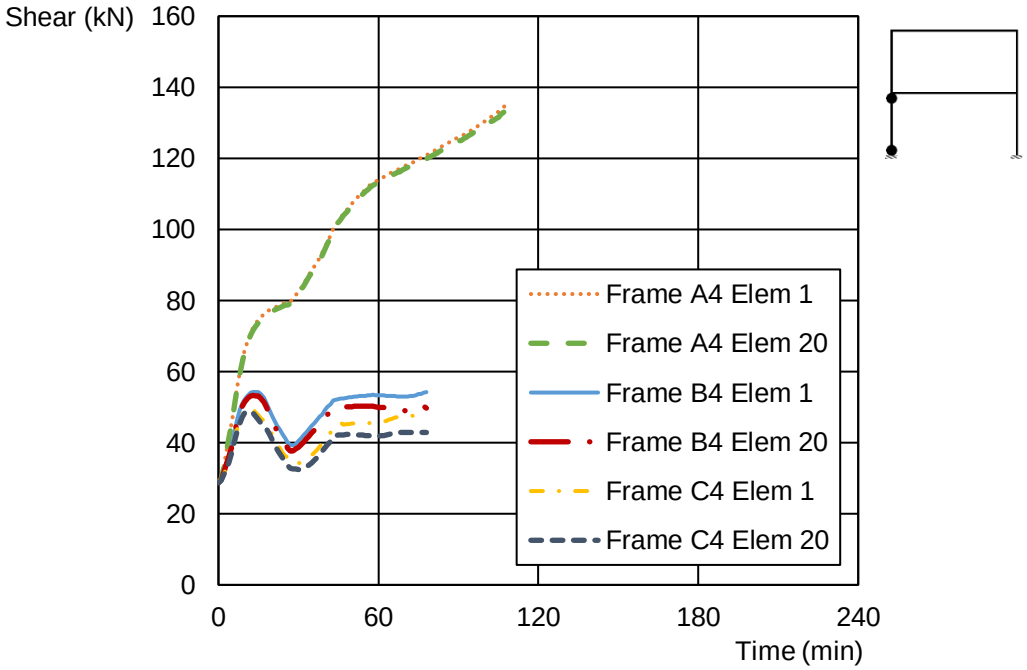

Figure 9.25 – Shear force in elements 1 and 20 in frames A4, B4 and C4.

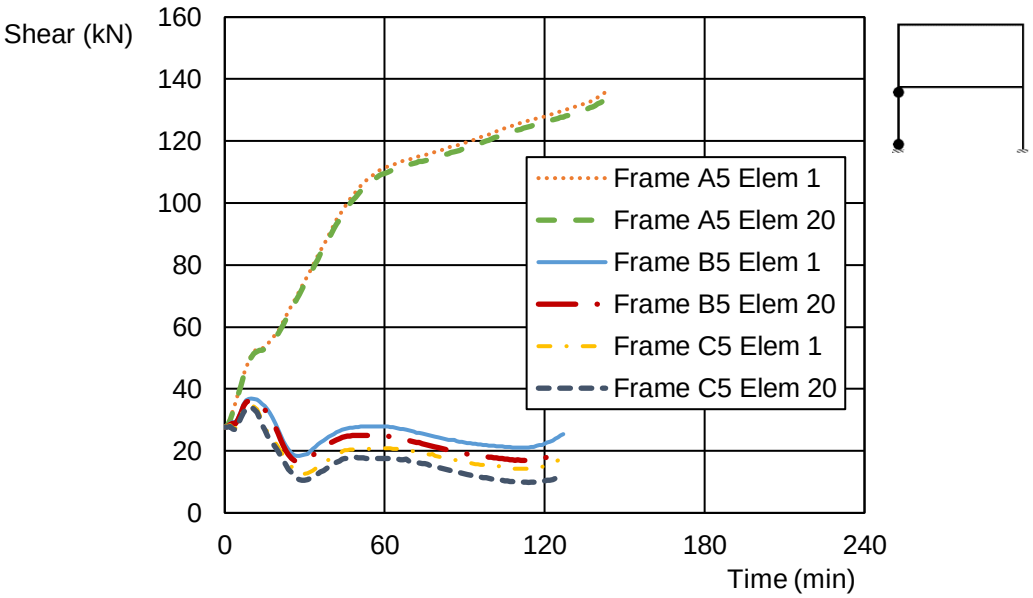

Figure 9.26 – Shear force in elements 1 and 20 in frames A5, B5 and C5.

9.3.7. Displacement at storey level

The displacement analysed in the column of the different frames is the horizontal displacement in node 40. The results are presented in two different ways to be easier to compare the displacements between different frames. First, Figures 9.27 to 9.29 are the horizontal displacements in node 40 for the frames with the same number of fire frontiers in the columns. Figure 9.27 for frames A, Figure 9.28 for frames B and Figure 9.29 for frames C. In these Figures is possible to compare the horizontal displacement according to different typologies of damage in the frames. The second way is presented from Figure 9.30 to 9.34. In each of those Figures the typology of damage is the same, the difference lies in the different number of fire frontiers in the columns. In the appendices are the schematics of the deformed shapes of the frames.

In the Figure 9.27 the displacement in frame A2 is very similar with the displacement in frame A5 and the displacement in frame A3 is very similar with the displacement in frame A4. Frame A2 and A5 have damage D2 in the beam and

frames A3 and A4 have damage D3 in the beam. Even though the damage in the column is different between frames A2 and A5, the horizontal displacement is very similar. The same can be seen in frames A3 and A4. This happens because the horizontal displacement in node 40 is related with the stiffness of the beam. The damage in the beam reduces the stiffness of the beam. The beams with the same damage have the same stiffness and that leads to very similar horizontal displacements in node 40. In the Figure 9.28 and 9.29 the displacements are higher when compared with the displacements in Figure 9.27. This shows that the number of fire frontiers in the columns also affect the horizontal displacement in node 40. In the Figure 9.28 the displacements in frames B2 and B5 are similar but not as similar as the displacements in frames A2 and A5 in the Figure 9.27. The similarity of the results is even less visible in frames B3 and B4. The conclusions obtained in Figure 9.28 are the same conclusions that can be obtained in Figure 9.29. The higher horizontal displacement observed in node 40 is 3 cm and the lower is almost 2,5 cm. The higher horizontal displacement is achieved when there are three or four fire frontiers in the columns and less than damage D3 in the beam. The lower values of horizontal displacement achieve in the end of the calculation procedures are in frames with one fire frontier in the columns and in the frames with damage D3 in the beam. It is important to mention that the horizontal displacement in node 40 increases more rapidly according to the global damage in the frame. More damage in the structure leads to a more rapid increase of the horizontal displacement. This situation can be easily observed in Figures 9.28 and 9.29. Frames with damage D3 in all zones reach a certain displacement sooner than frames with damage D2 in zone 2 and damage D3 in zones 1 and 3 and these reaches sooner that frames with damage D2 in zone 3 and damage D3 in zones 1 and 2. The following frames are the one with damage D2 in all zones and finally the frames with damage D0/D1 in all zones. The same hierarchy can also be observed in the times until collapse of the frames and once again it is easily observed in frames with three and four fire frontiers in the columns. The displacements at storey level are significant and can even increase the damage in the structure, but this situation is not considered in the analysis.

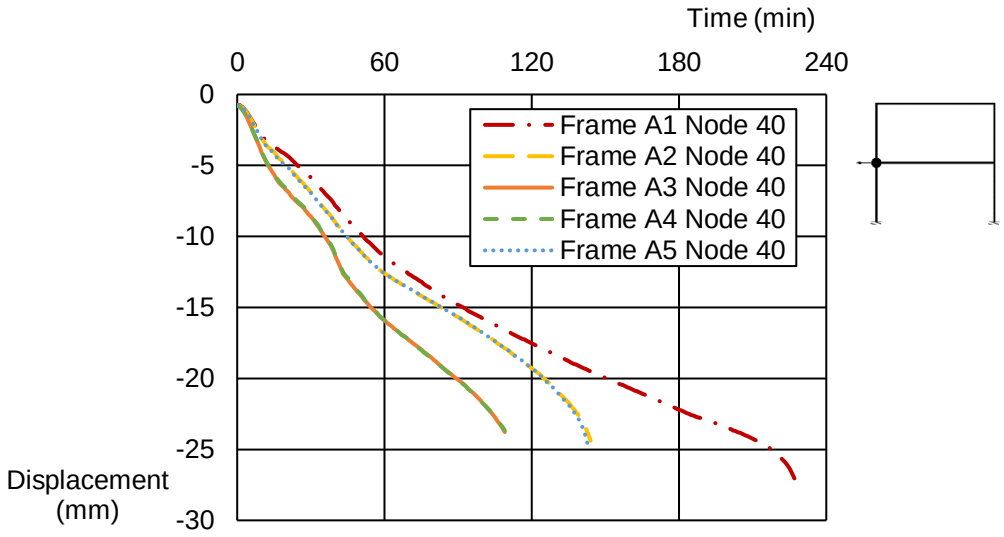

Figure 9.27 – Horizontal displacement in node 40 in frames A1, A2, A3, A4 and A5.

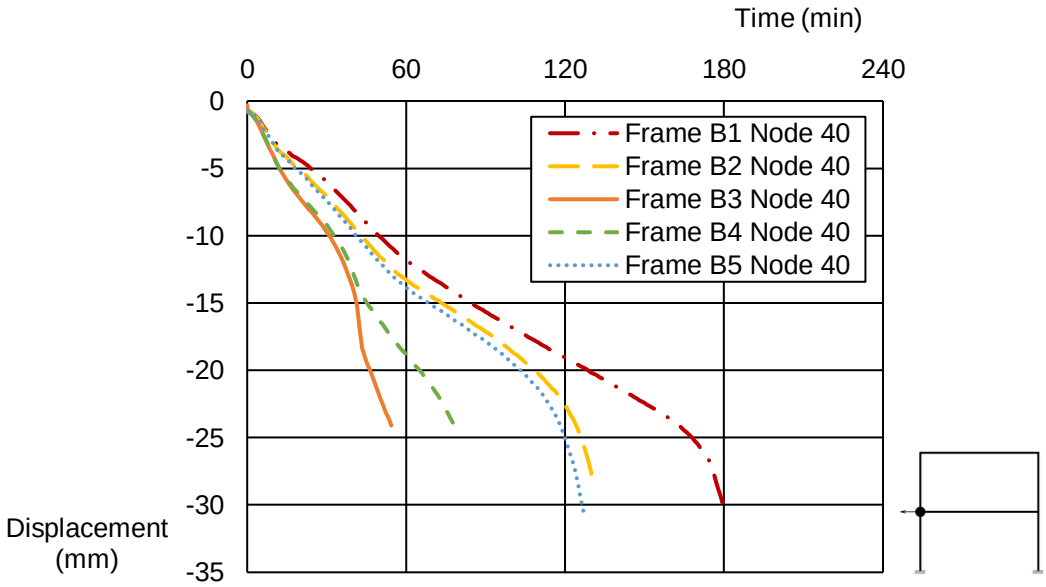

Figure 9.28 – Horizontal displacement in node 40 in frames B1, B2, B3, B4, and B5.

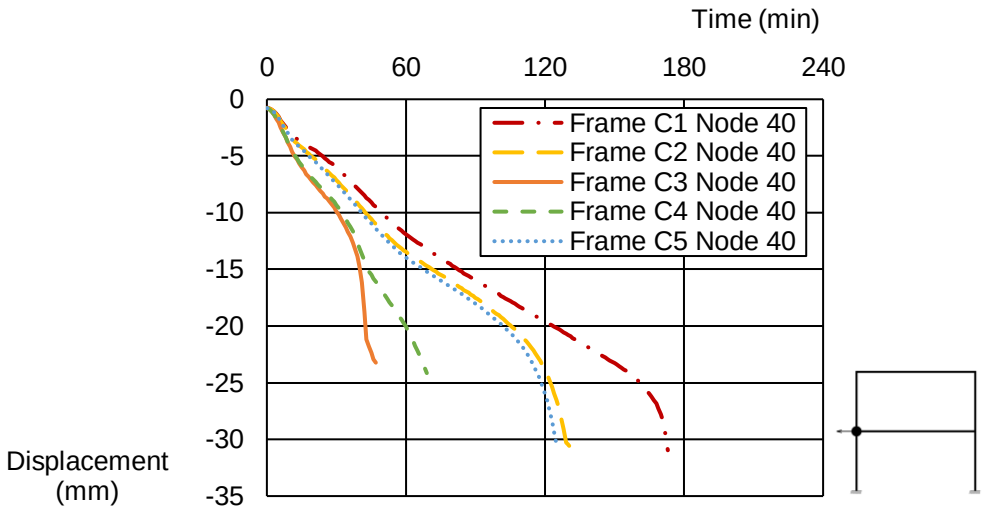

Figure 9.29 – Horizontal displacement in node 40 in frames C1, C2, C3, C4 and C5.

As said before, the following Figures 9.30 to 9.34 allow a comparison between the frames with the same type of damage but with different fire frontiers in the columns. The main conclusion that can be achieved with the analysis of the Figures is that for different typologies of damage having three or four fire frontiers in the columns lead practically to the same results. Before it was observed the similarity between the results of the frames with the same type of damage in the beam and now is possible to see the similarity between frames with three and four fire frontiers in the columns.

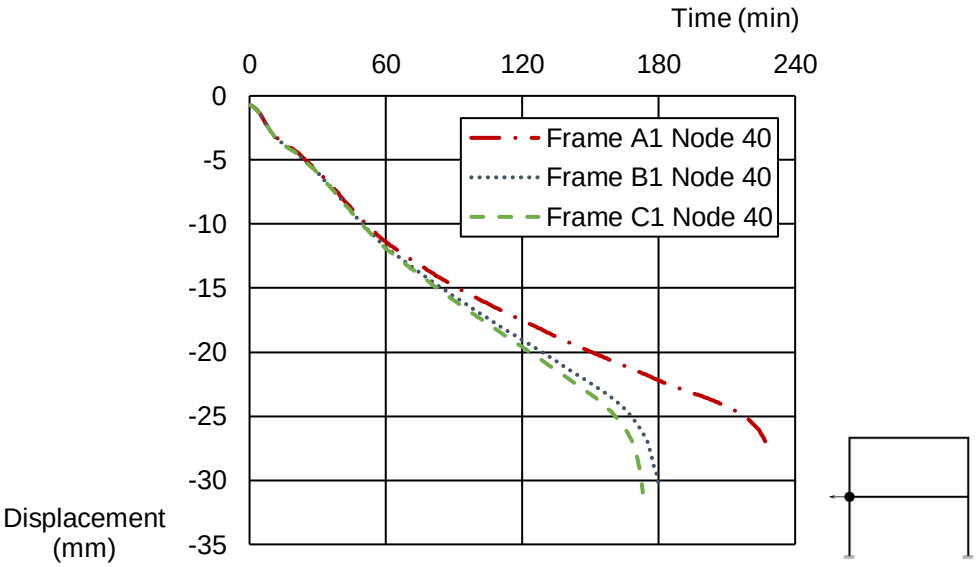

Figure 9.30 – Horizontal displacement in node 40 in frames A1, B1 and C1.

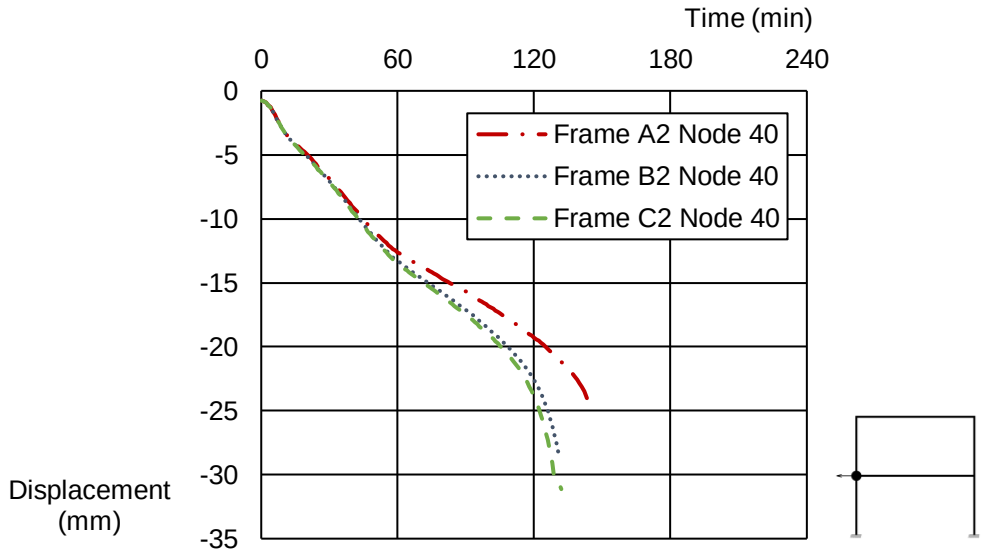

Figure 9.31 – Horizontal displacement in node 40 in frames A2, B2 and C2.

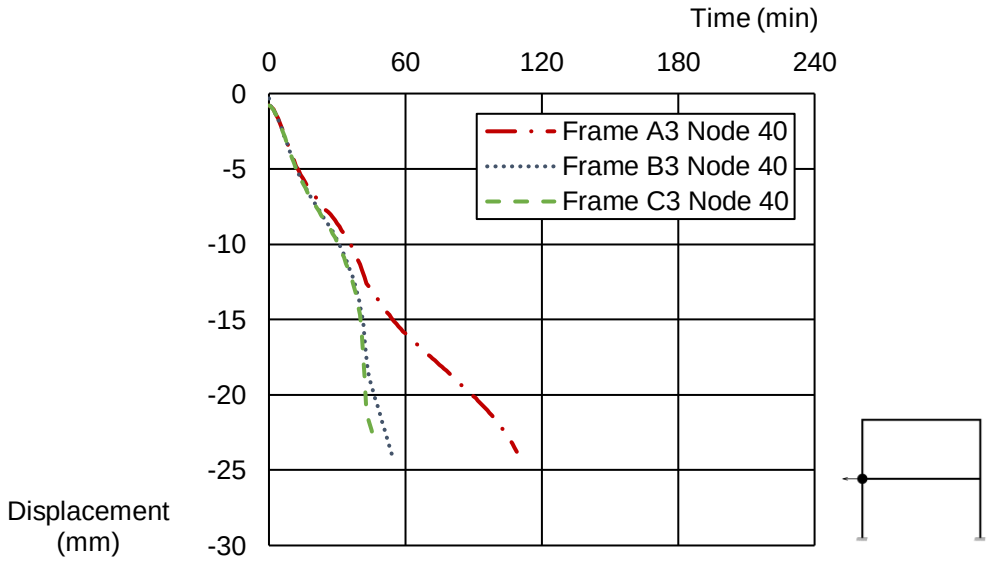

Figure 9.32 – Horizontal displacement in node 40 in frames A3, B3 and C3.

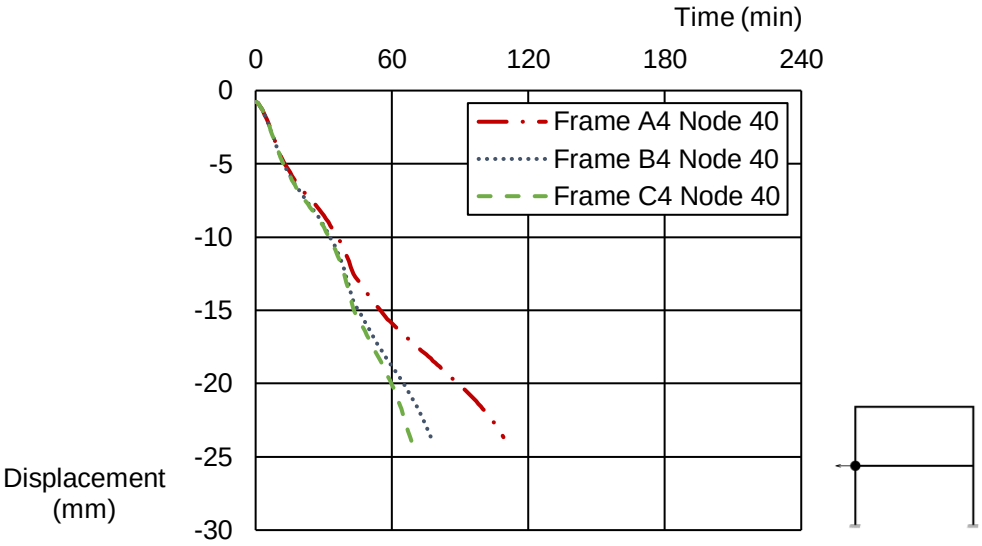

Figure 9.33 – Horizontal displacement in node 40 in frames A4, B4 and C4.

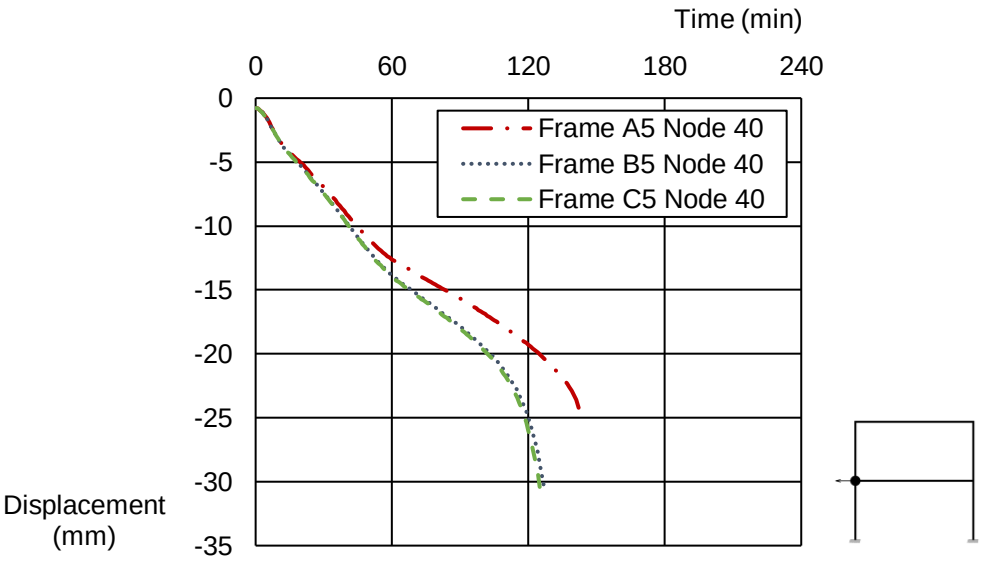

Figure 9.34 – Horizontal displacement in node 40 in frames A5, B5 and C5.

9.3.8. Vertical displacement in beam mid-span

The displacements in the beam mid span is presented in the same manner as the displacements in the column. Figures 9.35 to 9.37 are the vertical displacements in node 201 for the frames with the same number of fire frontiers in the columns. Figure 9.38 to 9.42 represent the vertical displacements in frames with the same typology of damage but with different fire frontiers in the columns. By analysing Figures 9.35 to 9.37 is possible to obtain similar conclusions to the ones obtained earlier in the horizontal displacements in the column. The vertical displacements in the beam are similar in the same way that the horizontal displacements of the column were similar. The displacements obtained in frames A2, B2 and C2 are similar with the displacements obtained in frames A5, B5 and C5. In the same manner, the displacements obtained in frames A3, B3 and C3 are also similar with the displacements obtained in frames A4, B4 and C4. This shows once again that having three or four fire frontiers in the columns leads to approximately the same vertical displacements in the mid-span of the beam. The frame C2 is the one with higher vertical displacement in the beam, approximately 9,5 cm. The frames with damage D3 in the beam have the lower vertical displacements in the beam, especially the ones with three or four fire frontiers in the columns. In those frames the reinforcement in the beams is not protected by the concrete cover and the collapse happens earlier.

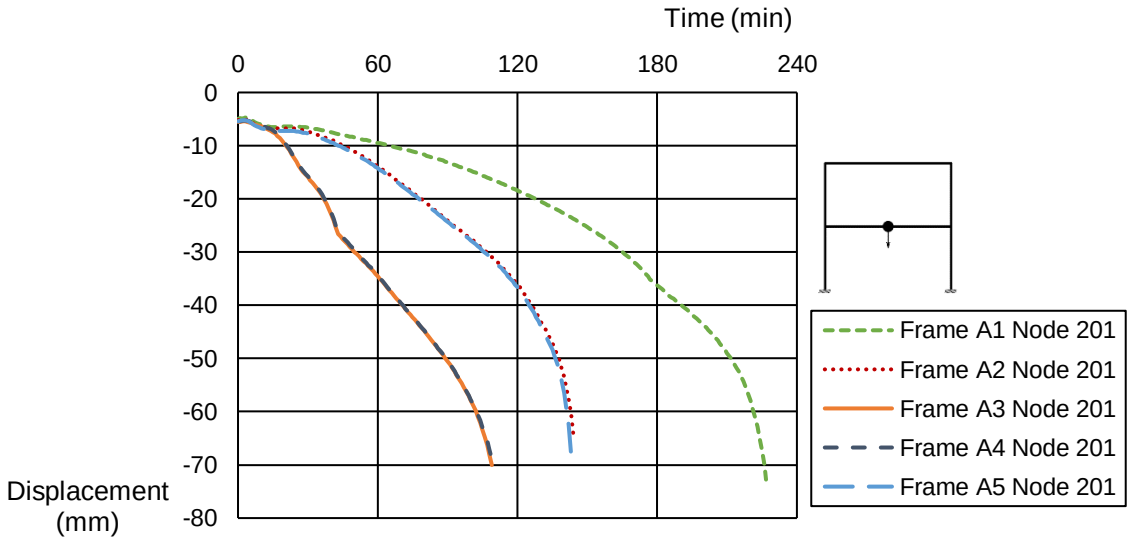

Figure 9.35 – Vertical displacement in node 201 in frames A1, A2, A3, A4 and A5.

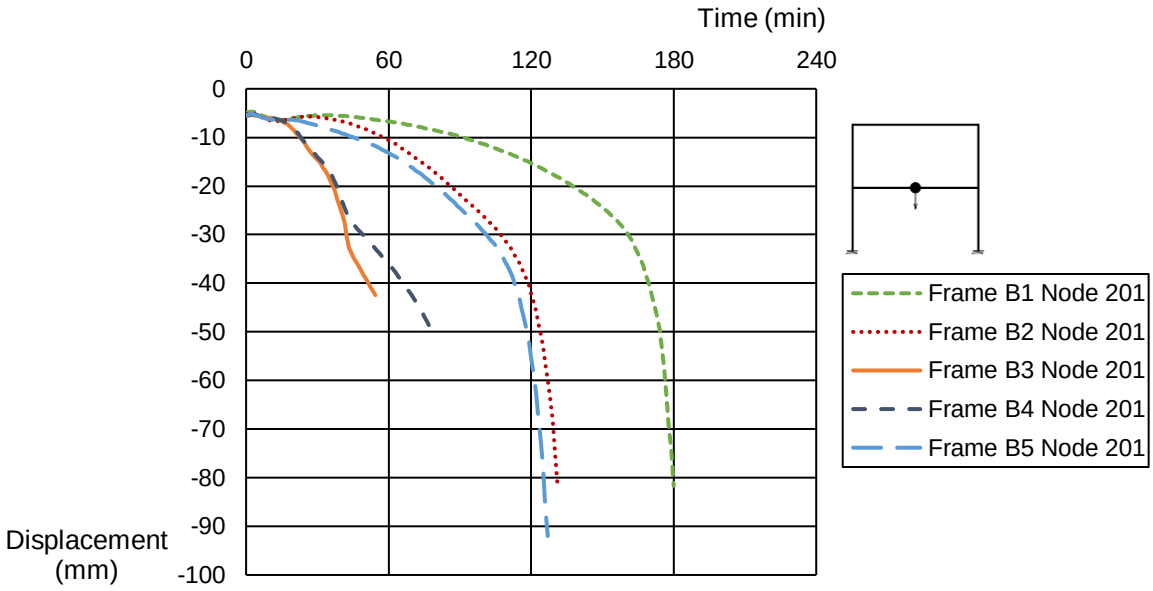

Figure 9.36 – Vertical displacement in node 201 in frames A1, A2, A3, A4 and A5.

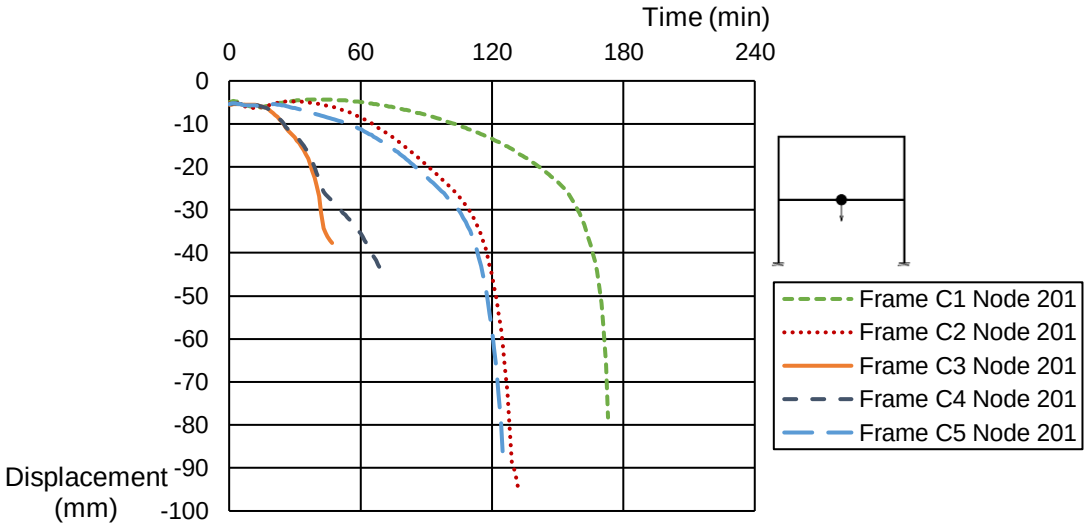

Figure 9.37 – Vertical displacement in node 201 in frames A1, A2, A3, A4 and A5.

As said before, the following Figures 9.38 to 9.42 allow a comparison between the frames with the same type of damage but with different fire frontiers in the columns. The main conclusion that can be achieved with the analysis of the Figures is that for different typologies of damage having three or four fire frontiers in the columns lead practically to the same results. Figures 9.38 and 9.39 show a downward displacement in the early minutes of the fire due to the static loads followed by an upward displacement due to the thermal expansion of the columns. After that, the elevate temperatures deteriorates the material leading to a reduction of the beams stiffness and a reduction of the thermal elongation of the columns that changes the displacements to downward again. The number of fire frontiers in the columns affects the upward displacement. The higher the number of fire frontiers the higher upward displacement. The upward displacement in Figures 9.40, 9.41 and 9.42 is not easy to identify, especially in Figures 9.40 and 9.41. The frames in Figures 9.40 and 9.41 have damage D3 in the beam and that may be the reason why the vertical displacements go downward without a noticeable upward displacement.

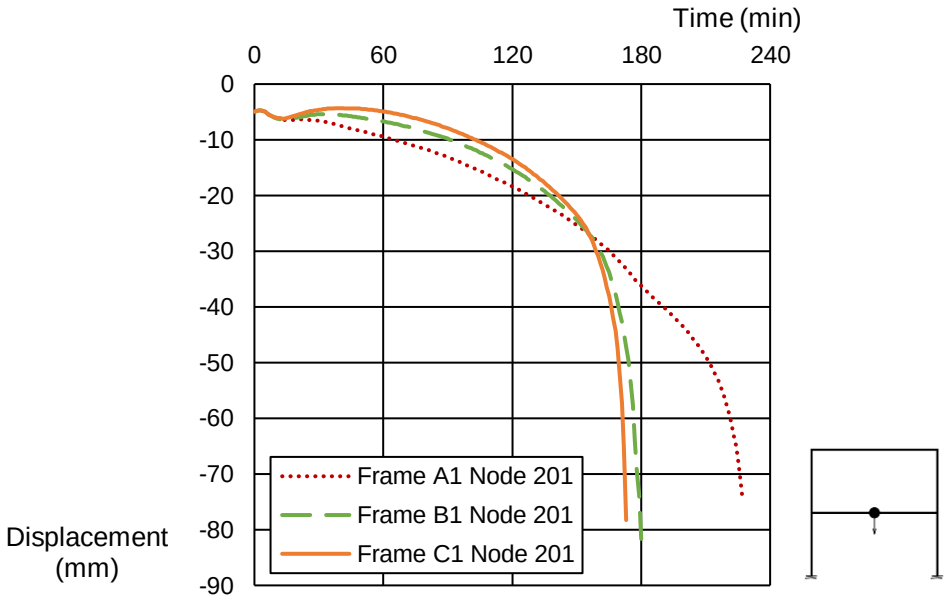

Figure 9.38 – Vertical displacement in node 201 in frames A1, B1 and C1.

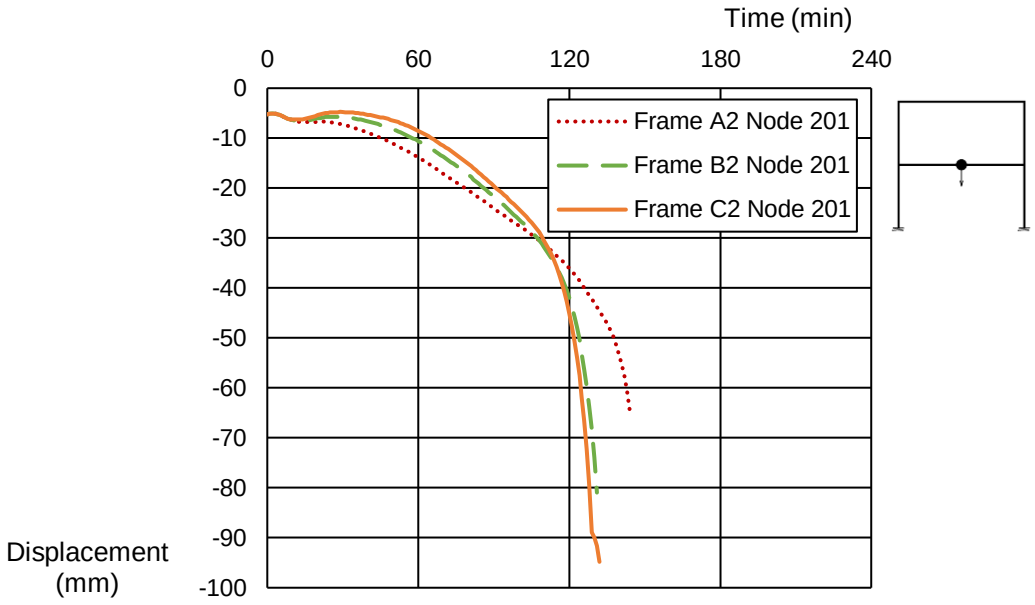

Figure 9.39 – Vertical displacement in node 201 in frames A2, B2 and C2.

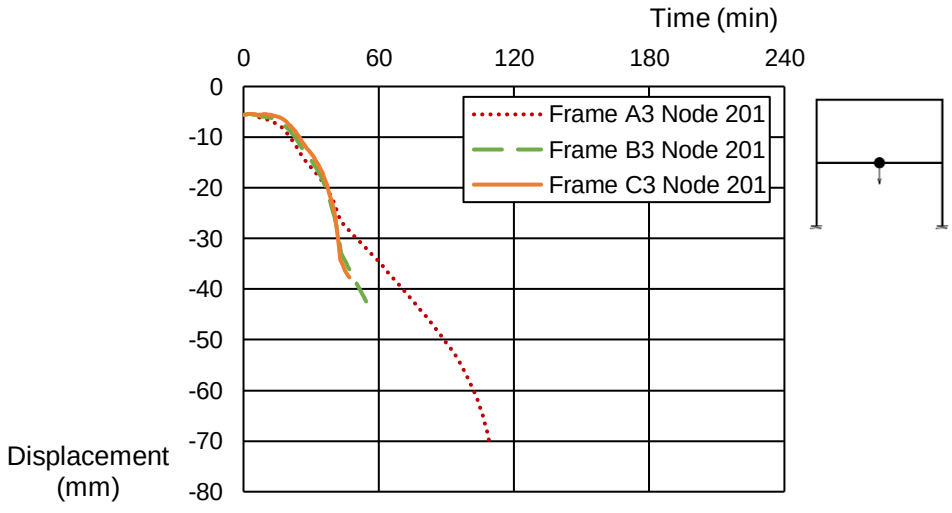

Figure 9.40 – Vertical displacement in node 201 in frames A3, B3 and C3.

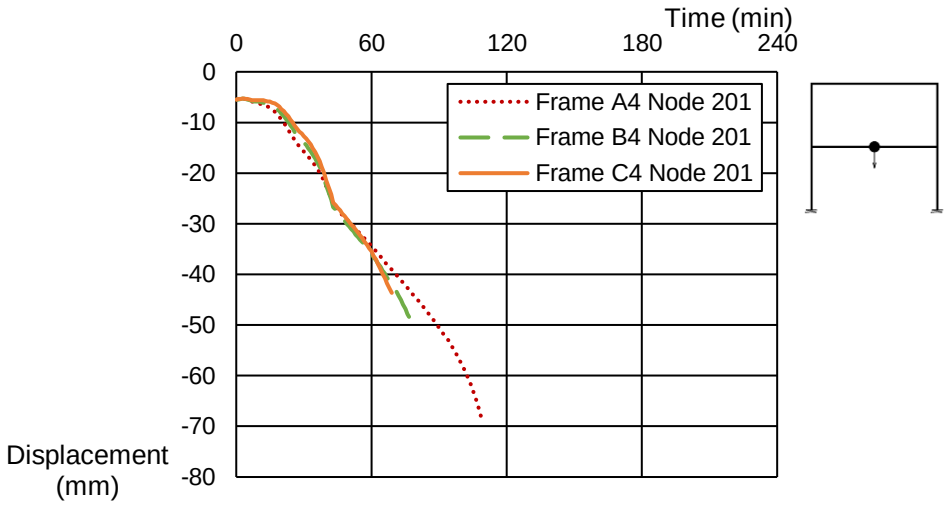

Figure 9.41 – Vertical displacement in node 201 in frames A4, B4 and C4.

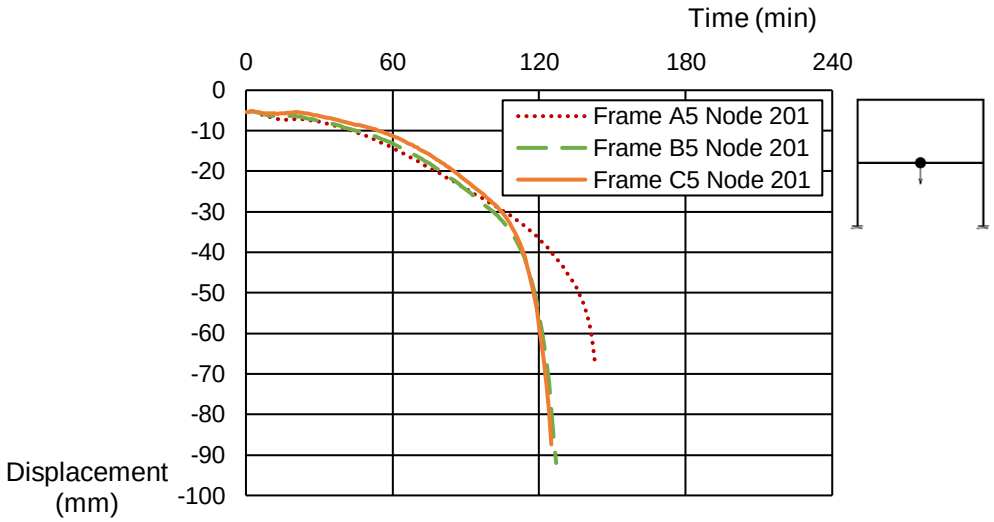

Figure 9.42 – Vertical displacement in node 201 in frames A5, B5 and C5.

10. Conclusions and further works

10.1. Final considerations

In this chapter there will be summarize the main conclusions obtained during the development of this dissertation. The analysis of post-earthquake fire in RC buildings is a complex phenomenon. The fire resistance of the RC structures after an earthquake can be difficult to determine due to the difficulty in predict the damage caused by the earthquake and the origin and developing of the fire. There were developed several numerical models in RC elements, such as columns, beams and frames to better understand the fire resistance of the RC structures after an earthquake.

In Chapter 7 it was analysed the fire resistance of RC columns under different axial loads and fire frontiers. For all the types of damage and relative axial force considered in the columns with one fire frontier it was observed that the time until conventional collapse was more than 240 minutes. As for the columns with three and four fire frontiers the situation is very different. The time until conventional collapse decreases with the increase of the relative axial force, damage and fire frontiers. The difference in time until collapse between columns with damage D0/D1 and D3 can be more than two hours, which show the huge impact of the damage caused by the earthquake on the fire resistance of the column. There is a significative difference between in time until collapse of the columns with three and four fire frontiers, in some cases it can be higher than one hour, which shows that considering three or four fire frontiers can lead to very different results.

In Chapter 8 it was analysed the fire resistance of RC beams with different damage. Once again, the damage hugely influences the time until collapse. The difference in time until collapse between the beam with damage D0/D1 and D3 is more than three hours. The beams considered have fixed supports that do not allow horizontal displacements in the beam. This situation leads to high axial forces created by the thermal elongation of the beam, which shows the impact that the

temperature can have on the forces in the structure. Different types of damage in the beam can also change the evolution of the axial forces, bending moments and displacements. As expected, the beams with damage D3 reach a higher displacement in the mid-span sooner than the beams with damage D2 and D0/D1. The final displacements in the mid-span of the beam do not follow the same trend because the damage have a huge impact on the type until collapse of the beams.

In Chapter 9 it was analysed the fire resistance of RC frames with different typologies of damage and fire frontiers. The results show that considering three or four fire frontiers in the columns do not create considerable changes in the forces, displacements and times until collapse of the frames. The results also show that when the beam has the same type of damage the results are similar even when the damage in the columns is different, this situation shows the importance of the damage in the beams. The frame with damage D3 in all zones and four fire frontiers in the columns is the frame with lower time until collapse. The difference in time until collapse in the frame with four fire frontiers in the columns, between frames with damage D0/D1 and damage D3 is more than two hours. In other words, the frame with damage D3 collapse more than two hours earlier than the frames with damage D0/D1. This shows the huge impact that the damage has on the fire resistance of the frames.

The lower fire resistance of the RC elements combined with higher response times of the rescue teams can lead to terrible consequences, such as losses of lives and infrastructures.

The reinforced concrete structures that suffer less damage after a major earthquake will have higher post-earthquake fire resistance. The first procedure to having a structure with good post-earthquake fire resistance is by designing the structure to have a good behavior to the earthquake action.

10.2. Further works

There are several works that can be developed to better understand the post-earthquake fire effects on reinforced concrete buildings. Following the same ideas analysed in this dissertation it is possible to develop similar numerical analysis on columns, beams and frames with different characteristics and properties. There are several elements than can changed from the ones studied here. It could be considered reinforced concrete elements with other support conditions, other sections, types of concrete and steel, loads, location of the damage and location of the fire frontiers. It can also be developed frames with several compartments where it would be analysed the impact of different fire and damage configurations.

It is also possible to follow a different approach. The temperature of the reinforced concrete elements in a given compartment is not uniform along its longitudinal axis. This situation can also be analysed to see the impact that these different temperatures have on the damaged reinforced concrete structure.

The masonry walls can protect the columns and beams from the fire. Other situation that can be studied is the degree of protection that the walls have on the columns and beams. Different wall configurations can be considered, with different materials and properties.

Experimental investigations can also be developed to validate the numerical models. The experimental investigations are very helpful because can lead to situations not considered in the numerical analysis and that can be a big help to develop numerical models that are more accurate.

References

[1] Lopes, M., 2008. Sismos e edifícios. 1st ed. Alfragide. Edições Orion

[2] Rodrigues, H. (2005). "Desenvolvimento e calibração de modelos numéricos para analises sísmica de edifícios." Master Thesis, University of Porto.

[3] Varum, H. (2003). "Seismic assessment, strengthening and repair of existing buildings". Doct. Thesis, Dept. Civil Engineering, University of Aveiro.

[4] Ates, S., et al. (2013). "*Damages on reinforced concrete buildings due to consecutive earthquakes in Van*". Soil Dynamics and Earthquake Enginnering, 53, 109-118.

[5] Arslan, M. H., Korkmaz, H. H. (2007), "What is to be learned from damage and failure of reinforced concrete structures during recent earthquakes in Turkey?" Engineering Failure Analysis 14, 1-22.

[6] Damci, E. et al. (2015). "Damages and causes on the structures during the October 23, 2011 Van earthquake in Turkey." Case Studies in Construction Materials 3, 112-131.

[7] Coelho, A. L., 2010. Incêndios em edifícios. 1st ed. Amadora. Edições Orion

[8] Buchanan, A. H., 2017. Abu, A. K., Structural design for fire safety. 2nd ed. Chichester. Wiley.

[9] EN 1991-1-2, (November 2002), "*Eurocode 1: Actions on structures – Part 1-2: General Actions – Actions on structures exposed to fire*", European Committee for Standardization, English version, Brussels, Belgium.

[10] Botting, R., (1998), "*The impact of Post-Earthquake Fire on the urban Environment*", Fire Engineering Research Report 98/1.

[11] Gonçalves, M. J. C. R. (2007), "Comportamento ao fogo de elementos estruturais de betão – Análise numérica e metodologia", PhD thesis, Faculdade de Engenharia da Universidade do Porto

[12] Jansson, R. (2013). "Fire Spalling of Concrete, Theoretical and Experimental Studies". Doct. Thesis in Concretes Structures, KTH Architecture and the Built Environment.

[13] Georgali, B., Consolazio, G. R., (2005), "Microstructure of Fire-Damaged Concrete. A Case Study", Cement and Concrete Composites, 27, pp.255-259.

[14] Scawthorn, C. R., (2008). "Fire Following Earthquake". The ShakeOut Scenario – Supplemental Study. Berkeley CA.

[15] Firefighter Gas Safety Products 2013, accessed 22 August 2018, <http://www.littlefirefighter.com/valve-operation.htm>

[16] Koseki, Hiroshi *et al*., (2012), "*Cause and countermeasure way of rubble fires occurred after 2011 Great earthquake of Japan*", Procedia Engineering 45, 617-627.

[17] Murasawa, N., et al., (2014), "*Great East Japan Earthquake disaster waste and the occurrence of fires*", Procedia Engineering 84, 472-484.

[18] Corte, G., Landolfo, R., Mazzolani, F.M., (2003). "Post-earthquake fire resistance of moment resisting steel frames". Fire Safety Journal 38, 593-612.

[19] Zografopoulou, K., Pantousa, D., Mistakidis, E., (2018). "Fire-After-Earthquake behavior of industrial facilities with fire protected steel structural system", 16th European Conference On, Earthquake Thessaloniki Engineering.

[20] Arablouei, A., Kodur, V., (2016). "Effect of fire insulation delamination on structural performance of steel structure during fire following an earthquake or an explosion". Fire Safety Journal 84, 40-49.

[21] Song, Q., Heidarpour, A., Zhao, X., Han, L., (2016). "Post-earthquake fire behavior of welded steel I-beam to hollow column connections: An experimental investigation". Thin-Walled Structures 98, 143-153.

[22] Pucinotti, R., Bursi, O.S., Demonceau, J.F., (2011). "Post-earthquake fire and seismic performance of welded steel-concrete composite beam-to-column joints". Journal of Constructional Steel Research 67, 1358-1375.

[23] Shah, A. H., Sharma, U. K., Bhargava, P., (2017), "Outcomes of a major research on full scale testing of RC frames in post-earthquake fire", Construction and Building Materials 155, 1224-1241.

[24] Kamath, P., et al., (2015), "Full-scale fire test on an earthquake-damaged reinforced concrete frame", Fire Safety Journal 73, 1-19.

[25] Behnam, B., Ronagh H. R., Lim, P. J., (2015), "Numerical evaluation of the post-earthquake fire resistance of CFRP-strengthened reinforced concrete joints based on experimental observations", European Journal of Environmental and Civil Engineering, 20:2, 142-160.

[26] Behnam, B., Ronagh H. R., (August 2014), "Post-earthquake fire resistance of CFRP strengthened reinforced concrete structures", The Structural Design of tall and Special Buildings.

[27] Behnam, B., Lim, P. J., Ronagh H. R., (2015), "Plastic Hinge Relocation in Reinforced Concrete Frames as a Method of Improving Post-Earthquake Resistance", Structures 2, 21-31.

[28] Behnam, B., Ronagh H. R., Baji, H., (2013), “Methodology for investigating the behaviour of reinforced concrete structures subjected to post earthquake fire”, Advances in Concrete Construction, Vol. 1, No.1, 29-44.

[29] Ronagh H. R., Behnam, B., (2012), “Investigating the effect of Prior Damage on the Post-Earthquake Fire Resistance of Reinforced Concrete Portal Frames”, International Journal of Concrete Structures and Materials, Vol.6, No.4, 209-220.

[30] EN 1992-1-2, (December 2004), “*Eurocode 2: Design of concrete structures – Part 1-1: General rules – Structural fire design*”, European Committee for Standardization, English version, Brussels, Belgium.

[31] EN 1993-1-2, (April 2005), “*Eurocode 3: Design of steel structures – Part 1-2: General rules – Structural fire design*”, European Committee for Standardization, English version, Brussels, Belgium.

[32] Franssen, J. M., (2011), “*User’s Manual for SAFIR 2011: A computer program for analysis of structures subjected to fire*”, University of Liège, Department ArGEnCO, Service Structural Engineering, Belgium.

[33] Ervine, A., Gillie, M., Stratford, T. J., Pankaj, P., (May 2012), “*Thermal Propagation through Tensile Cracks in Reinforced Concrete*”, Journal of materials in civil engineering, 516-522.

[34] Gernay, T., Franssen, J. M., (2016), “*SAFIR Manual: Material properties*”, University of Liège, Department ArGEnCO, Service Structural Engineering, Belgium.

[35] Portugal. Leis, decretos, etc. Regulamento técnico de segurança contra incêndio em edifícios. Portaria nº 1532/2008, de 29 de dezembro.

[36] Portugal. Leis, decretos, etc. Regime Jurídico de segurança contra incêndio em edifícios. Decreto-Lei nº 220/2008, de 12 de novembro.

[37] ANPC. 2013. Notas técnicas, Segurança contra incêndios em edifícios.

[38] Ervine, A., Gillie, M., Stratford, T. J., Pankaj, P., (April 2011), “Thermal diffusivity on tensile cracked concrete”, Application of Structural Fire Engineering.

This page was intetionally left blank

Appendix A

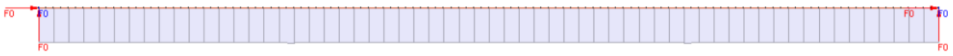

a)

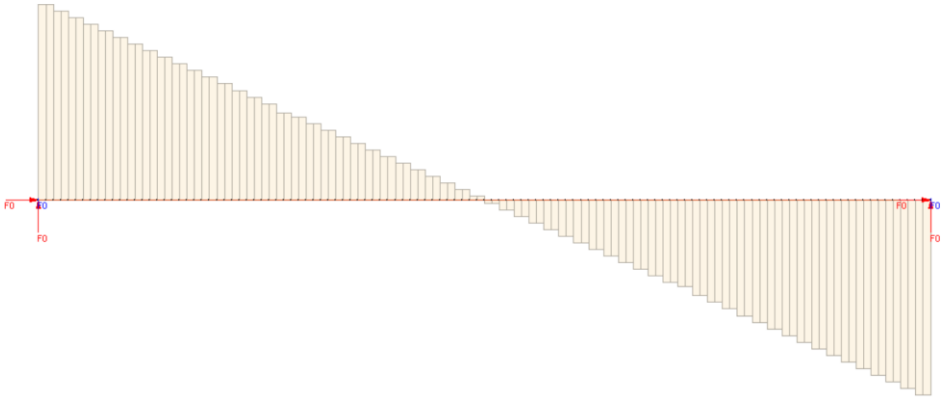

b)

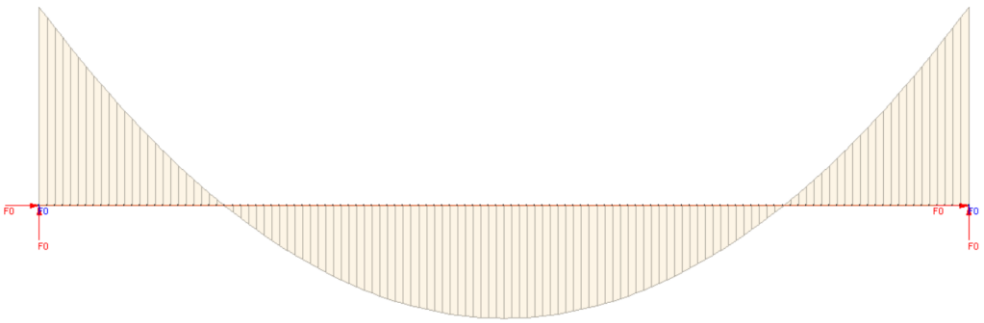

c)

d)

Figure A1 – a) Axial force diagram of beam A1 at 0 minutes. b) Shear force diagram of beam A1 at 0 minutes. c) Bending moment diagram of beam A1 at 0 minutes. d) Deformed shape (scaled 10 times) of beam A1 at 0 minutes.

a)

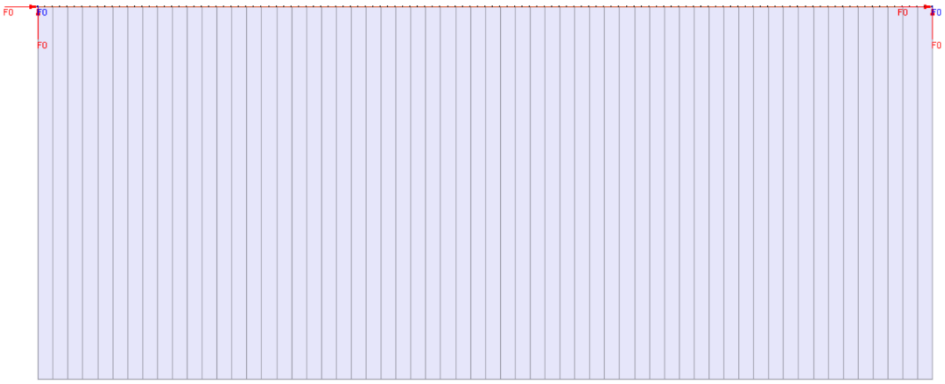

b)

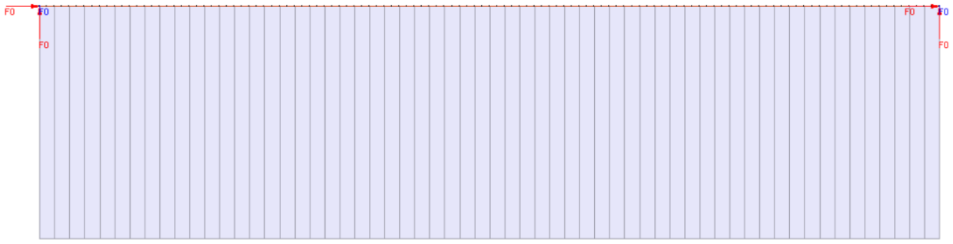

c)

Figure A2 – Axial force diagram of beam A1. a) At 0 minutes. B) At 120 minutes. c) At 240 minutes.

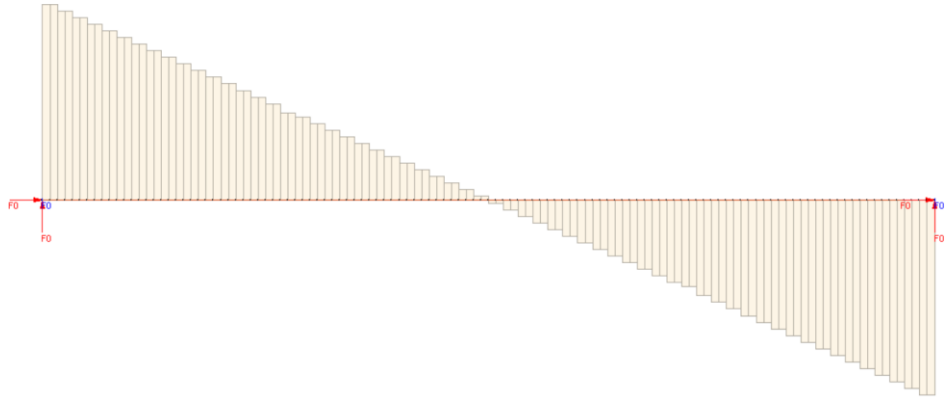

a)

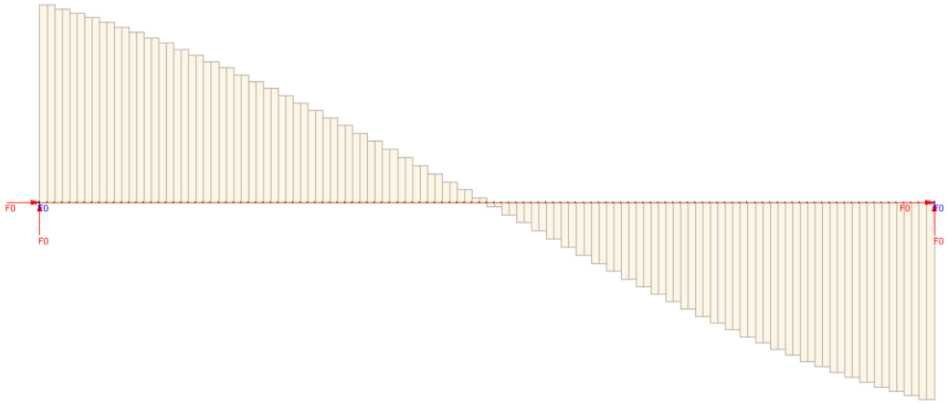

b)

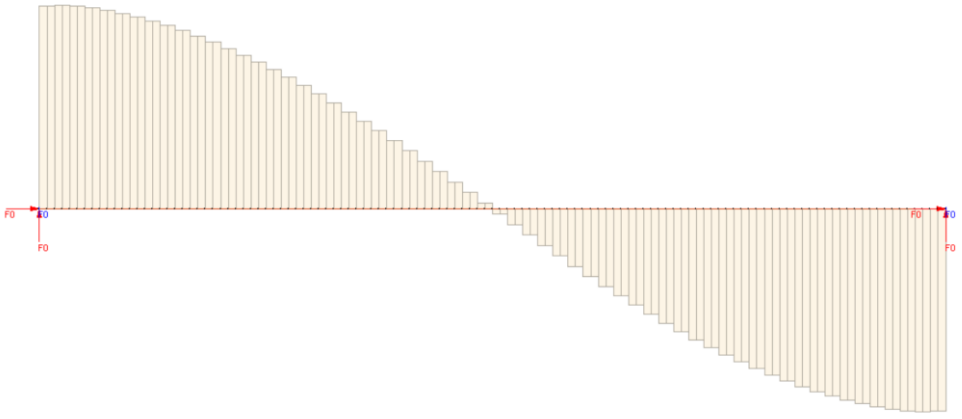

c)

Figure A3 – Shear force diagram of beam A1. a) At 0 minutes. B) At 120 minutes. c) At 240 minutes.

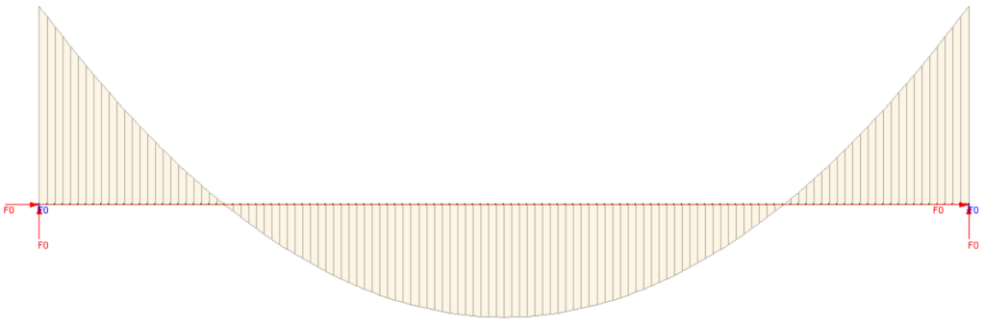

a)

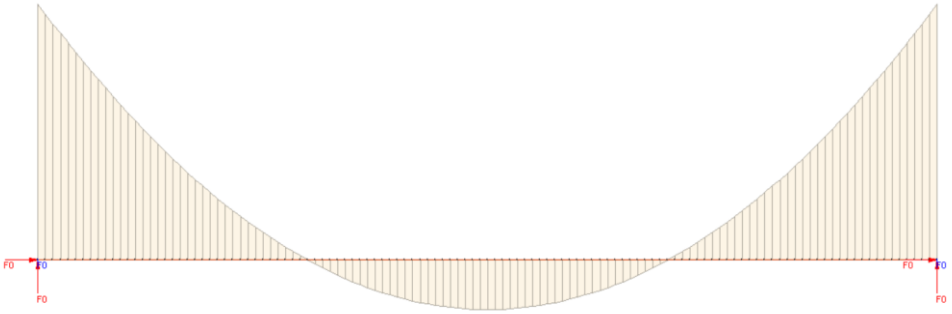

b)

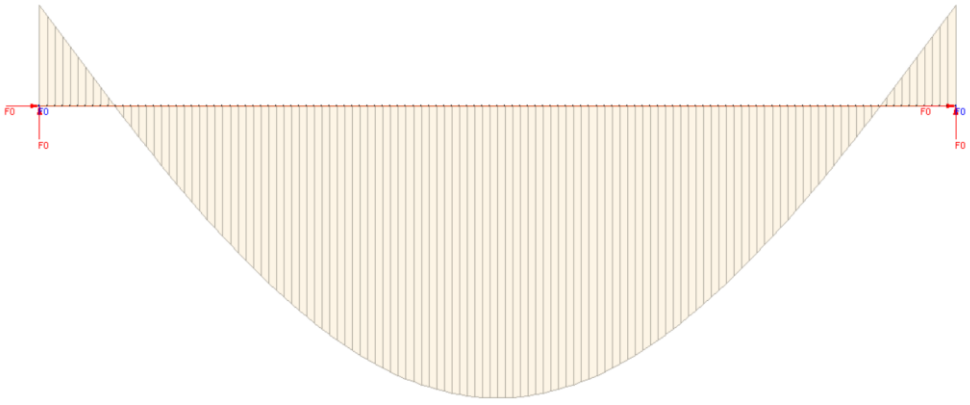

c)

Figure A4 – Bending moment diagram of beam A1. a) At 0 minutes. B) At 120 minutes. c) At 240 minutes.

a)

b)

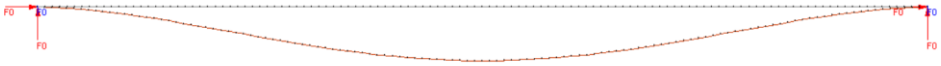

c)

Figure A5 – Deformed shape (scaled 10 times) of beam A1. a) At 0 minutes. B) At 120 minutes. c) At 240 minutes.

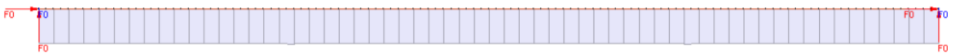

a)

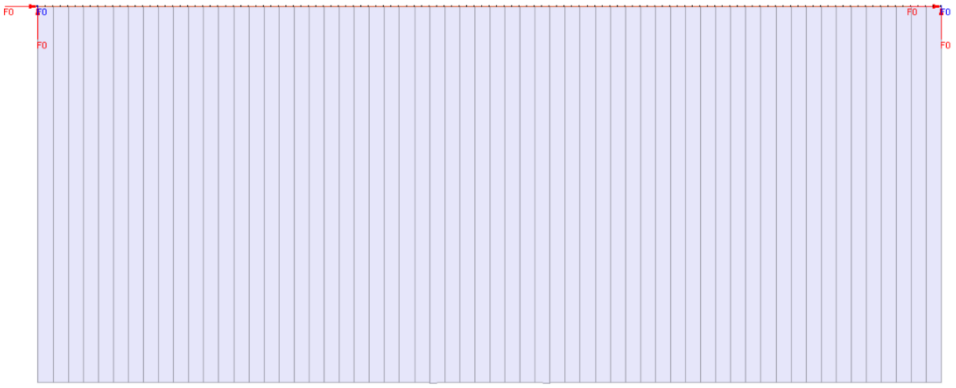

b)

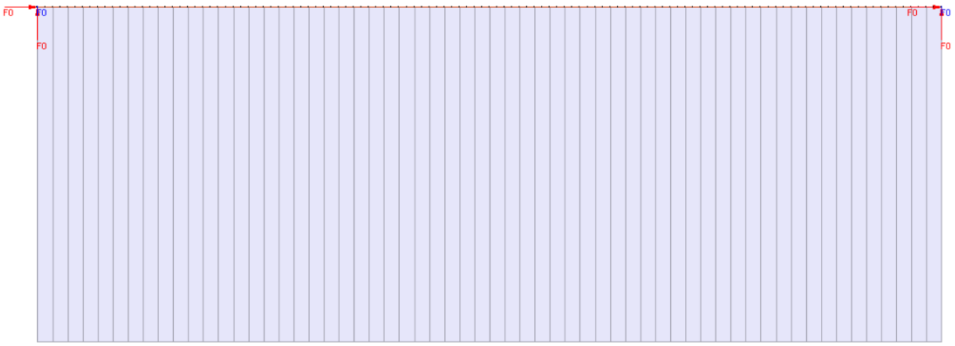

c)

Figure A6 – Axial force diagram of beam A2. a) At 0 minutes. B) At 60 minutes. c) At 106 minutes.

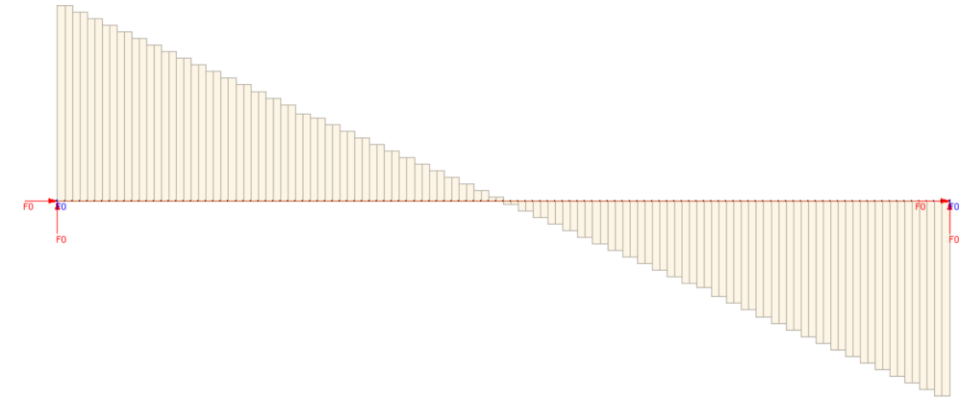

a)

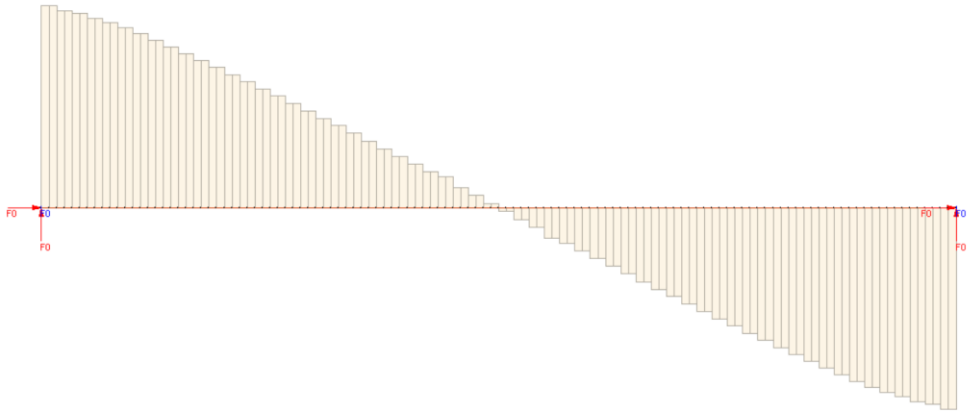

b)

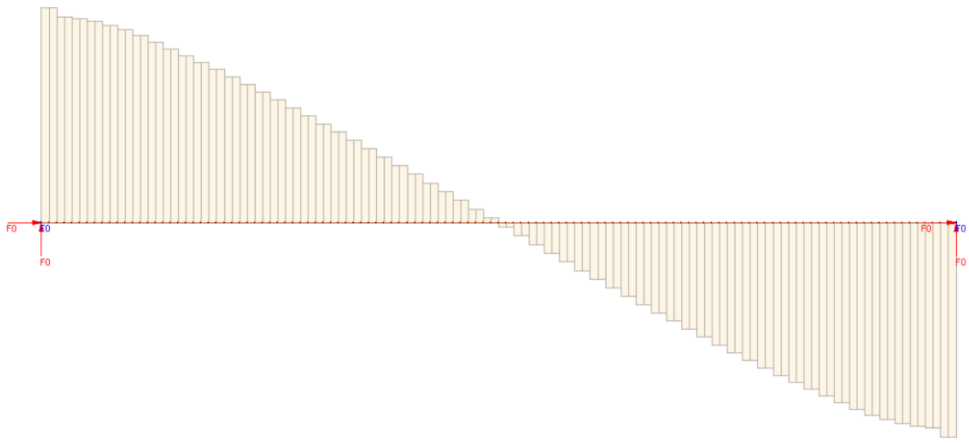

c)

Figure A7 – Shear force diagram of beam A2. a) At 0 minutes. B) At 60 minutes. c) At 106 minutes.

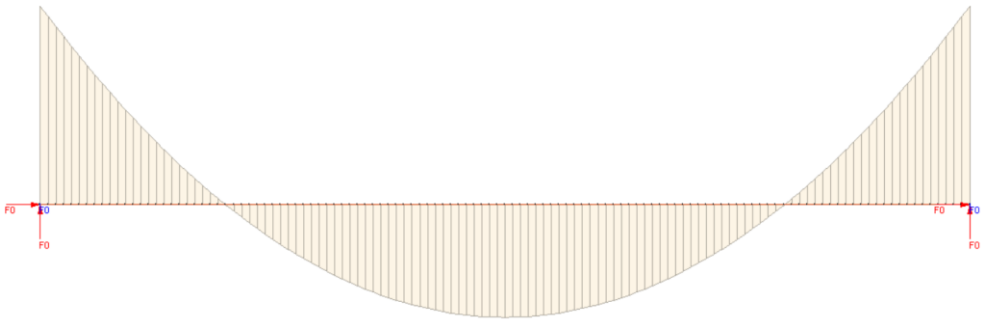

a)

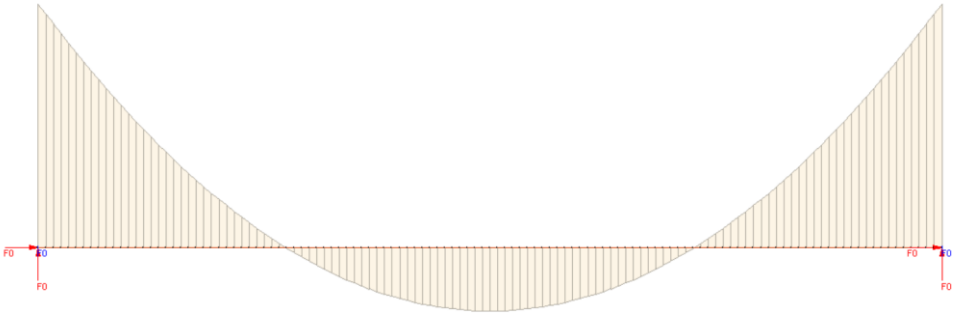

b)

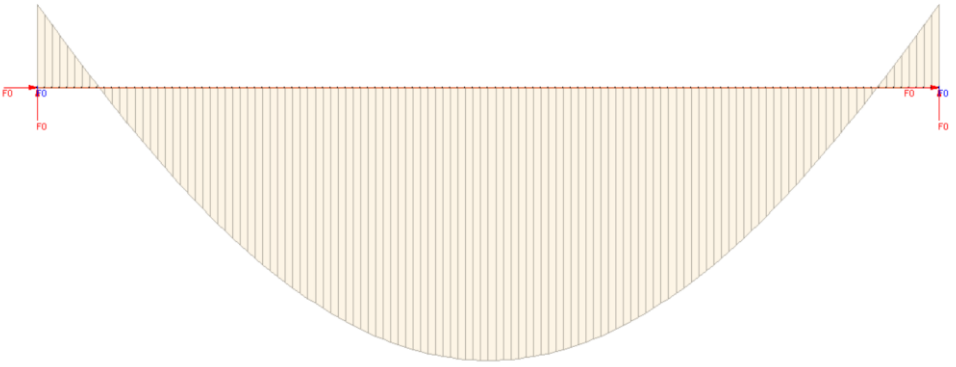

c)

Figure A8 – Bending moment diagram of beam A2. a) At 0 minutes. B) At 60 minutes. c) At 106 minutes.

a)

b)

c)

Figure A9 – Deformed shape (scaled 10 times) of beam A2. a) At 0 minutes. B) At 60 minutes. c) At 106 minutes.

a)

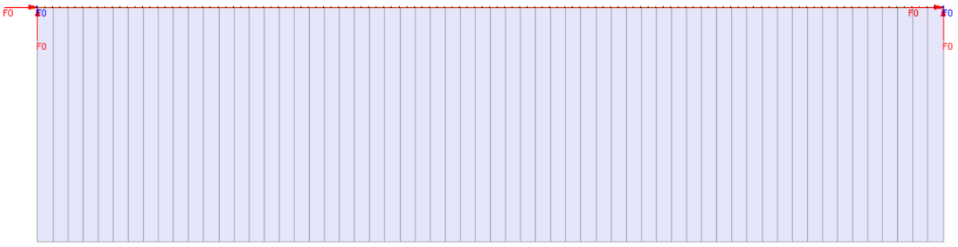

b)

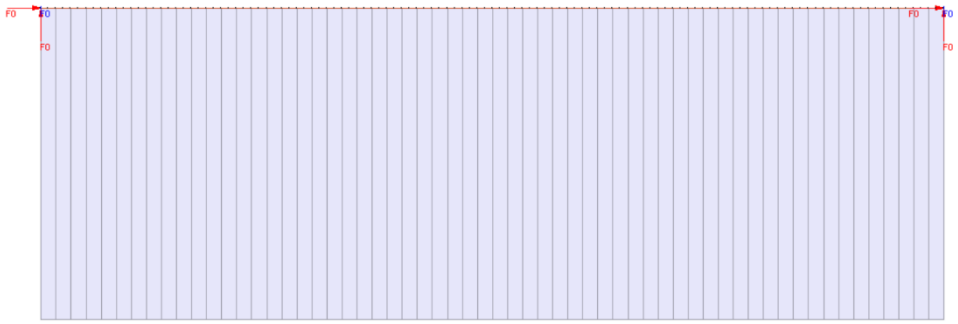

c)

Figure A10 – Axial force diagram of beam A3. a) At 0 minutes. B) At 20 minutes. c) At 49 minutes.

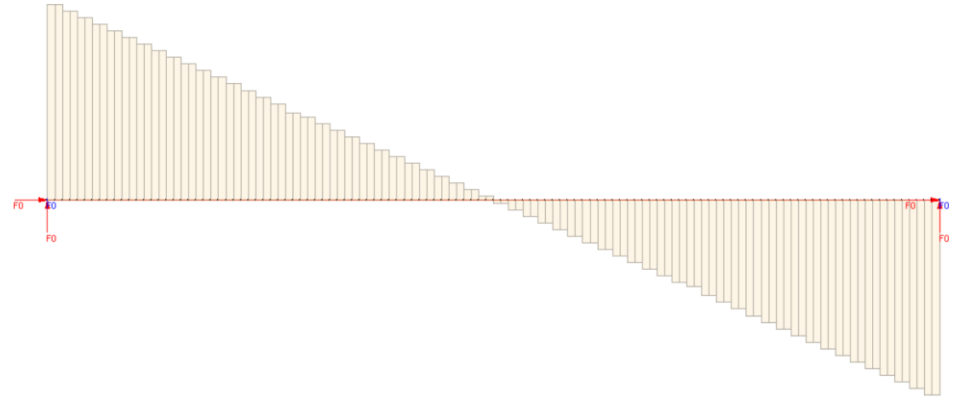

a)

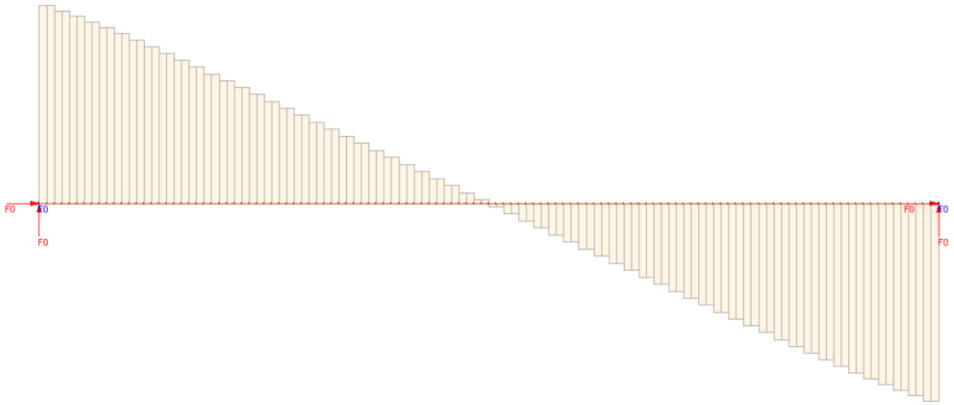

b)

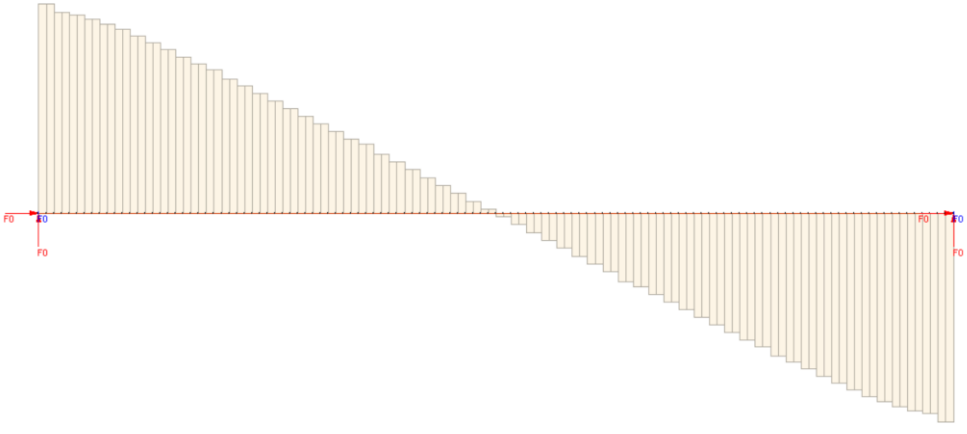

c)

Figure A11 – Shear force diagram of beam A3. a) At 0 minutes. B) At 20 minutes. c) At 49 minutes.

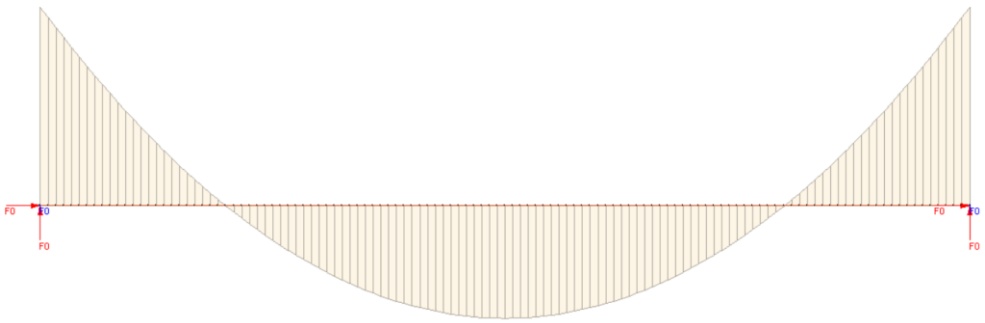

a)

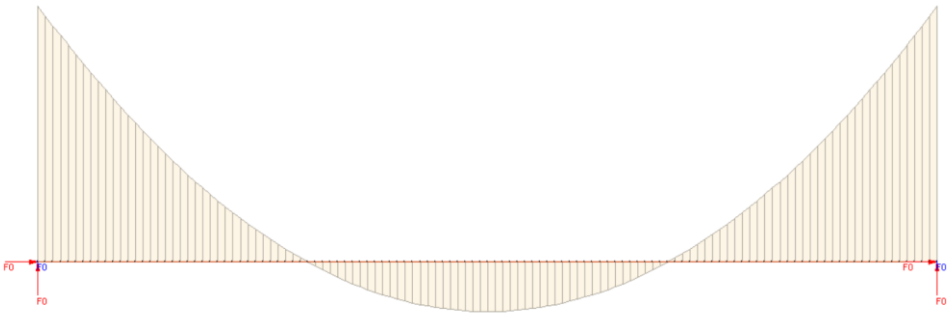

b)

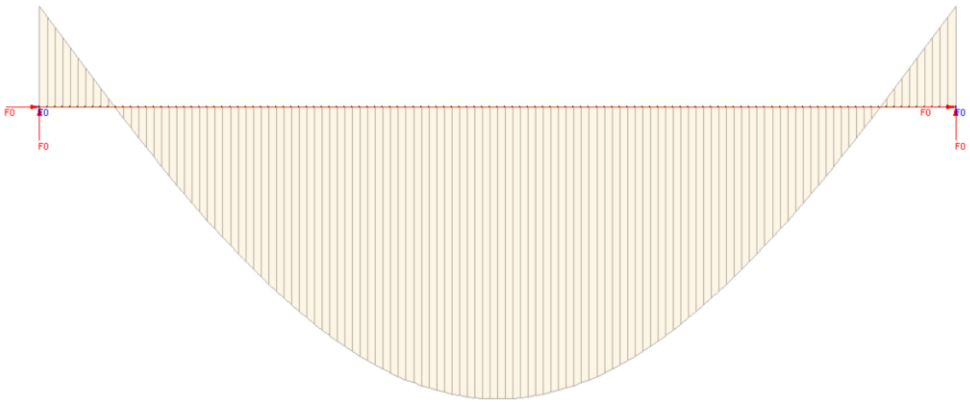

c)

Figure A12 – Bending moment diagram of beam A3. a) At 0 minutes. B) At 20 minutes. c) At 49 minutes.

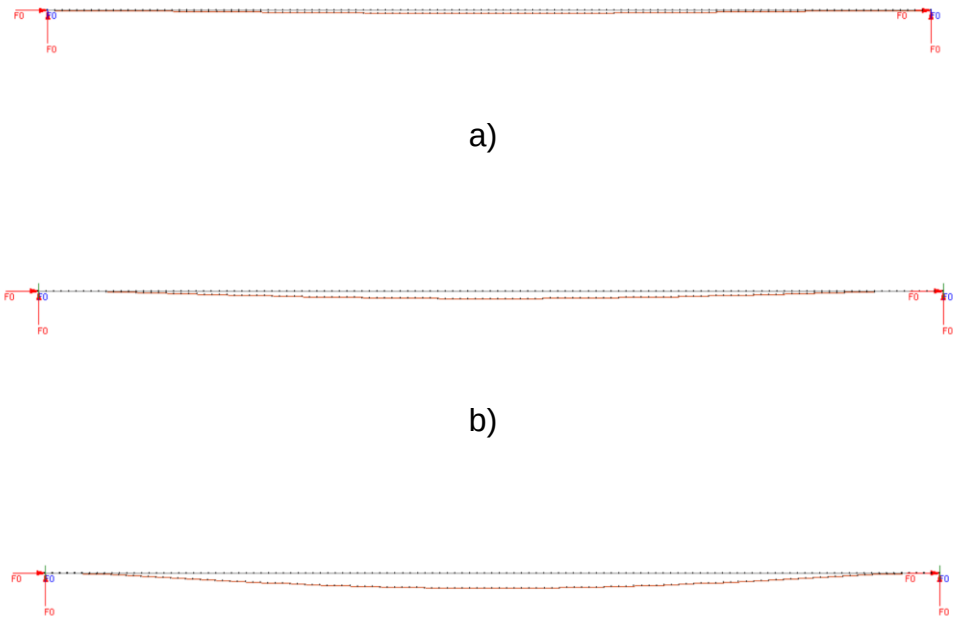

Figure A13 – Deformed shape (scaled 10 times) of beam A3. a) At 0 minutes. B) At 20 minutes. c) At 49 minutes.

Appendix B

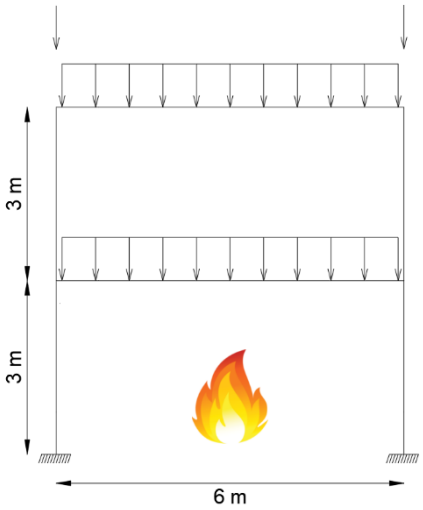

Figure B1 – Frame model.

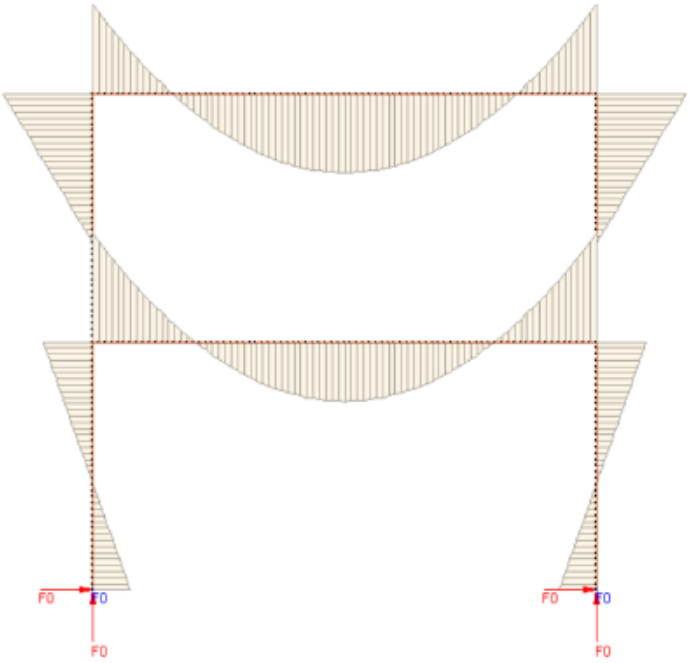

a)

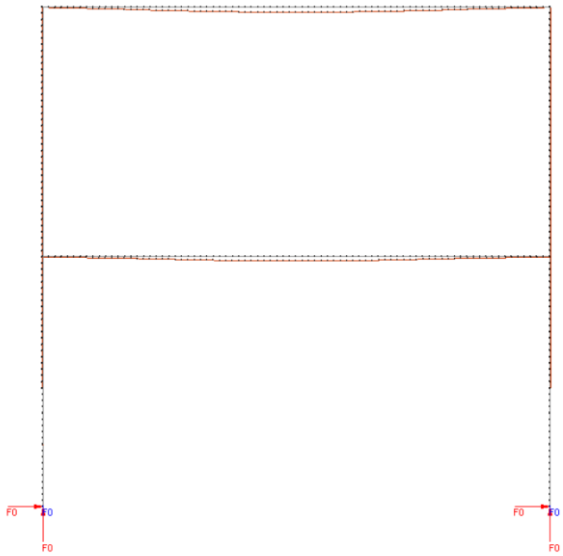

b)

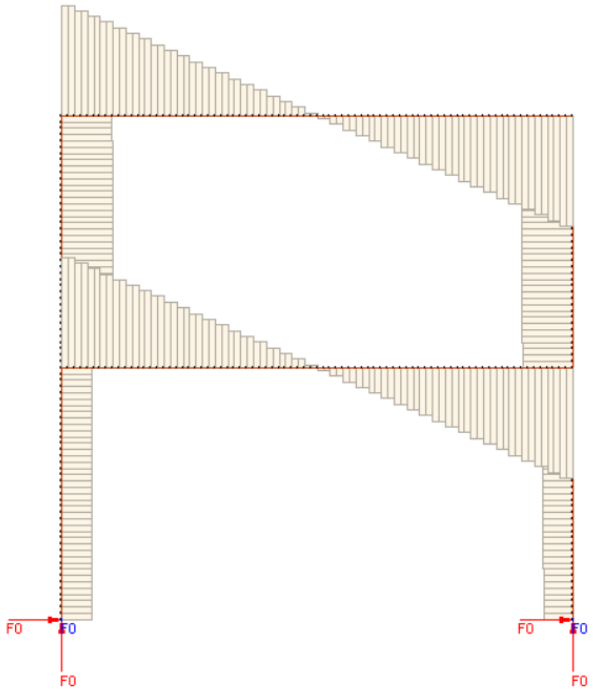

c)

Figure B2 – a) Schematic bending moment diagram of frame A1 at 0 minutes, b) Deformed shape (scaled 10 times) of frame A1 at 0 minutes, c) Schematic shear force diagram of frame A1 at 0 minutes.

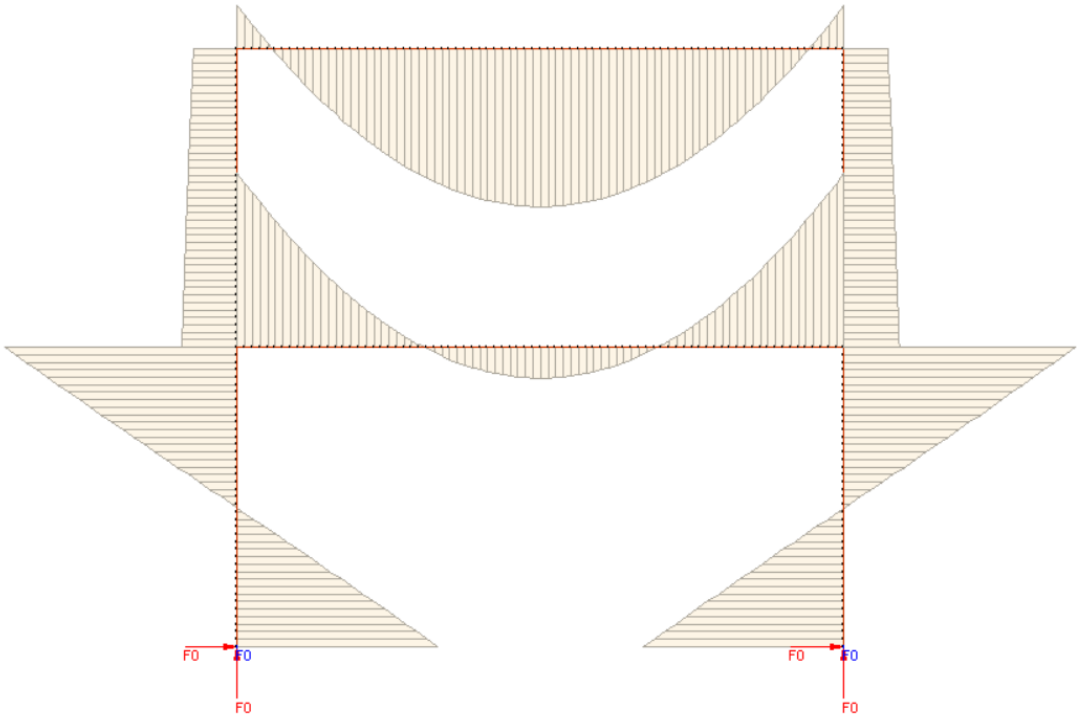

a)

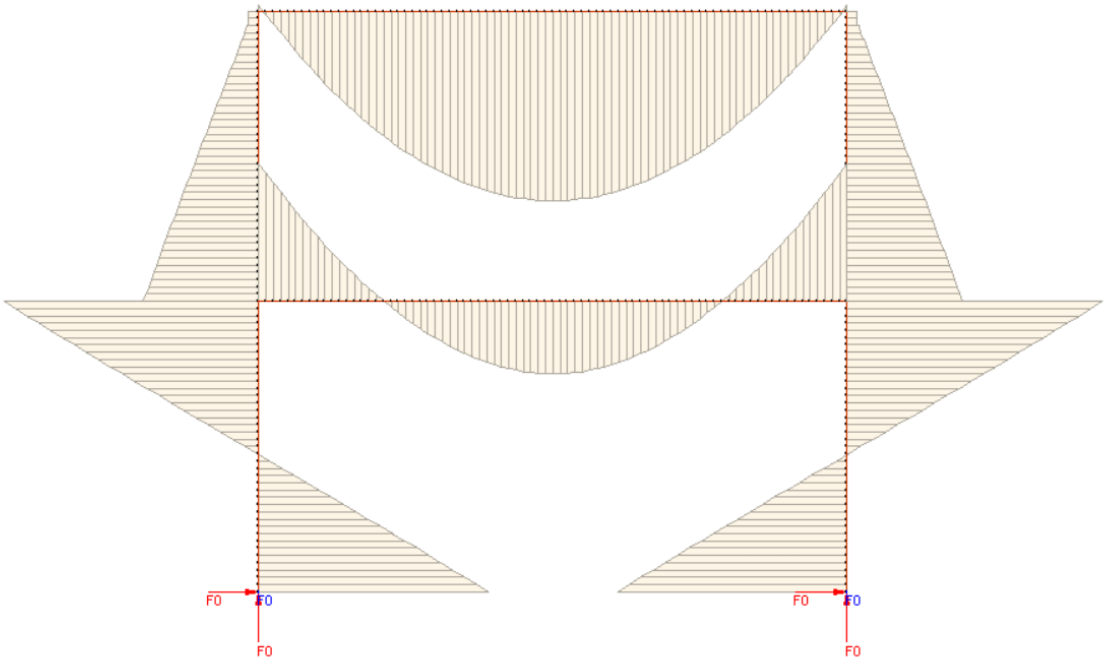

b)

Figure B3 – Schematic bending moment diagram of frame A1: a) 120 minutes, b) 227 minutes.

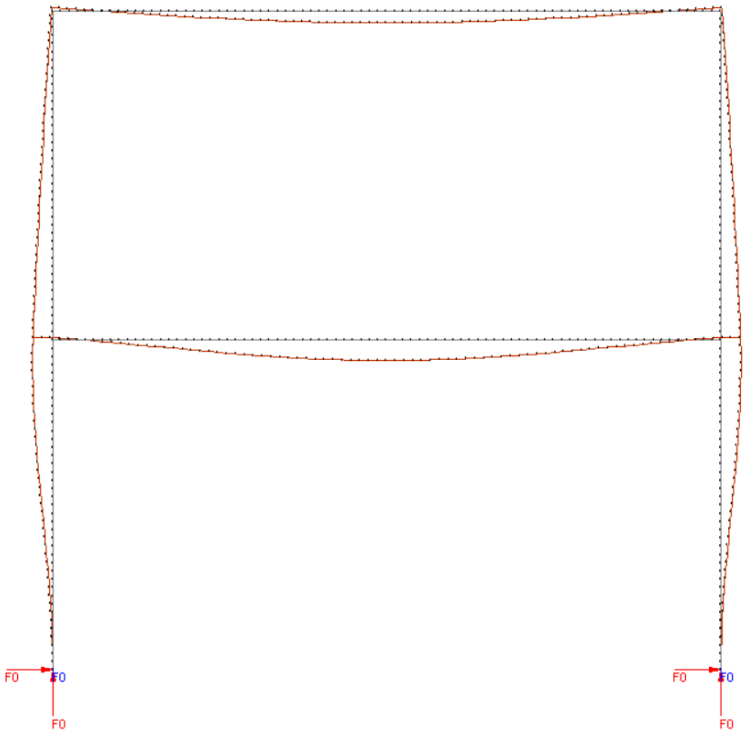

a)

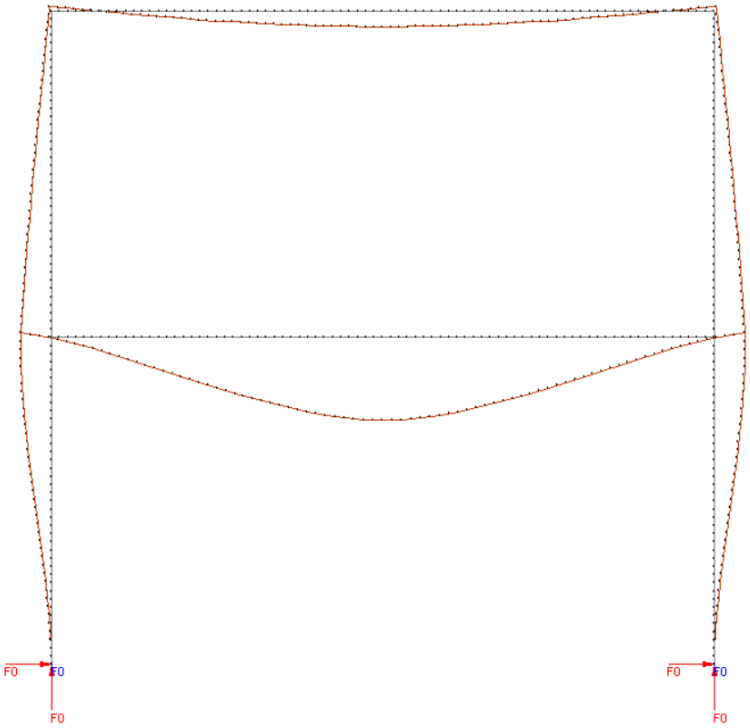

b)

Figure B4 – Deformed shape (scaled 10 times) of frame A1: a) 120 minutes, b) 227 minutes.

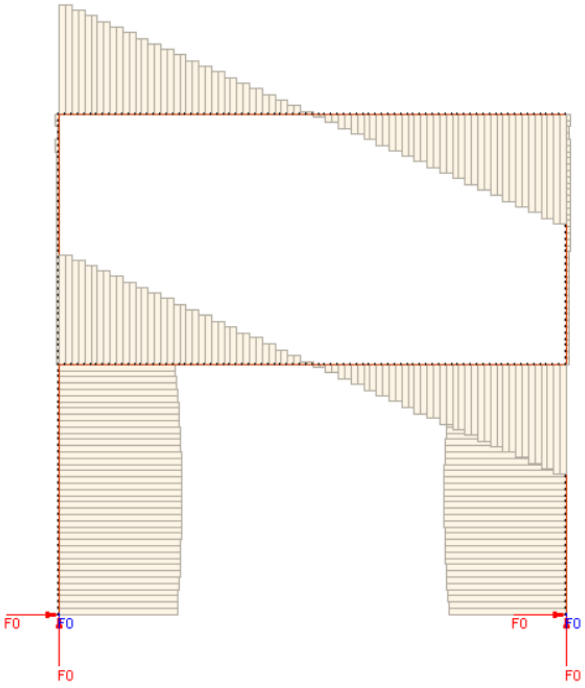

a)

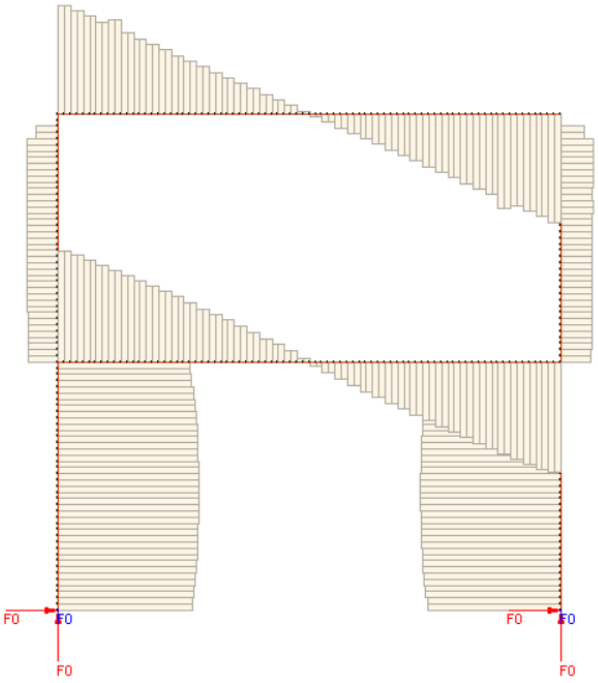

b)

Figure B5 – Schematic shear force diagram of frame A1: a) 120 minutes, b) 227 minutes.

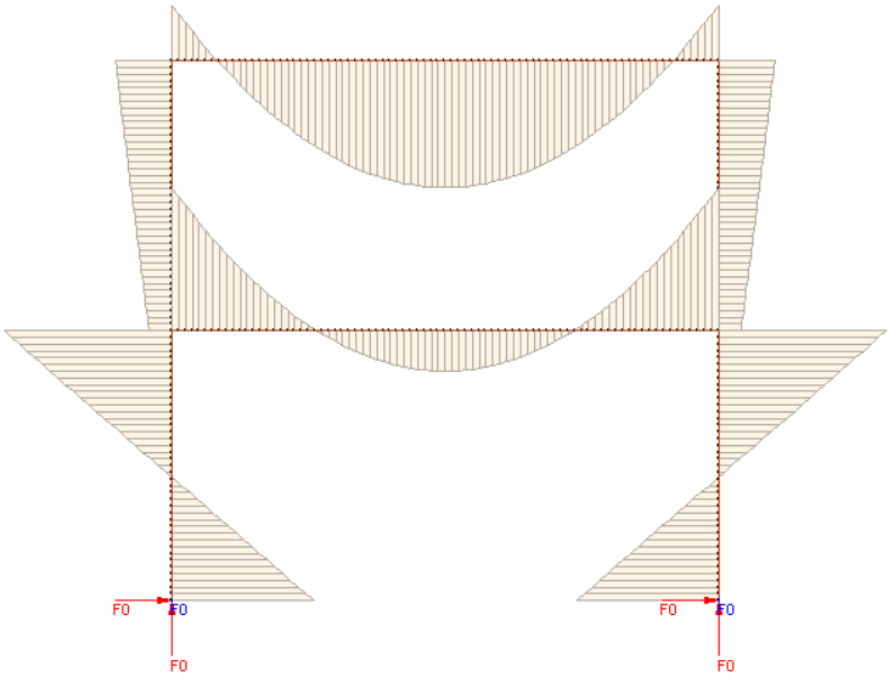

a)

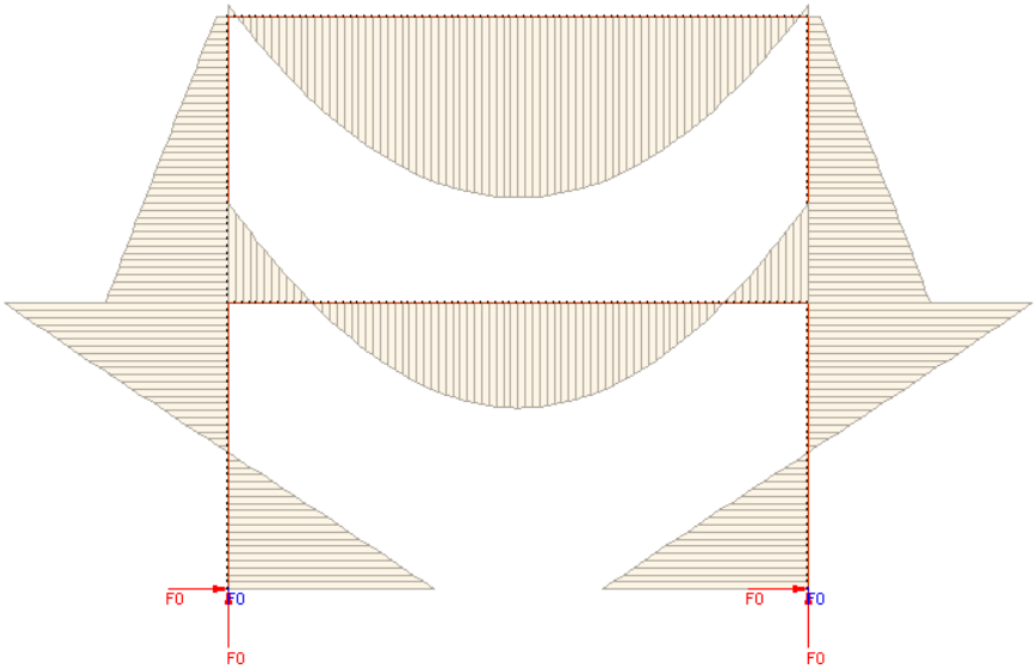

b)

Figure B6 – Schematic bending moment diagram of frame A2: a) 60 minutes, b) 144 minutes.

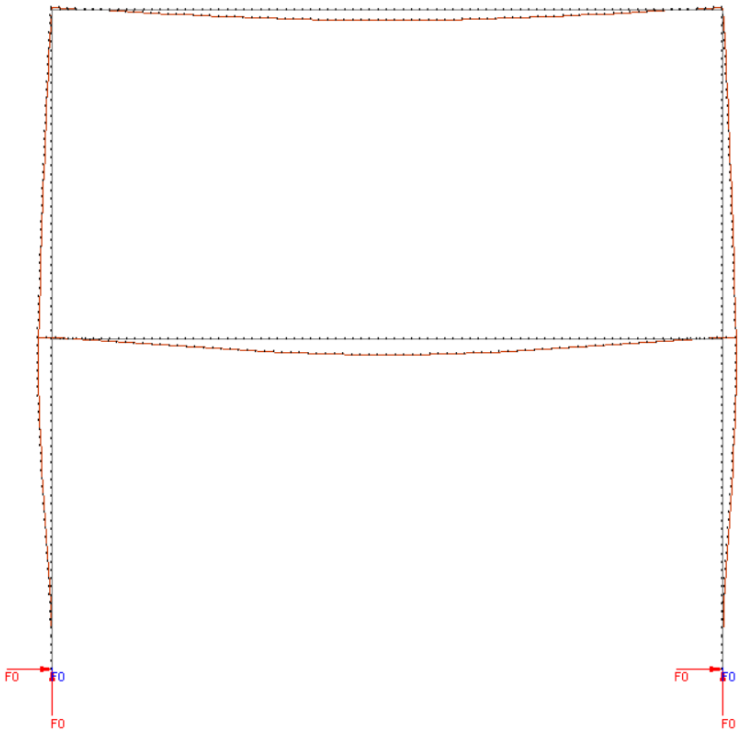

a)

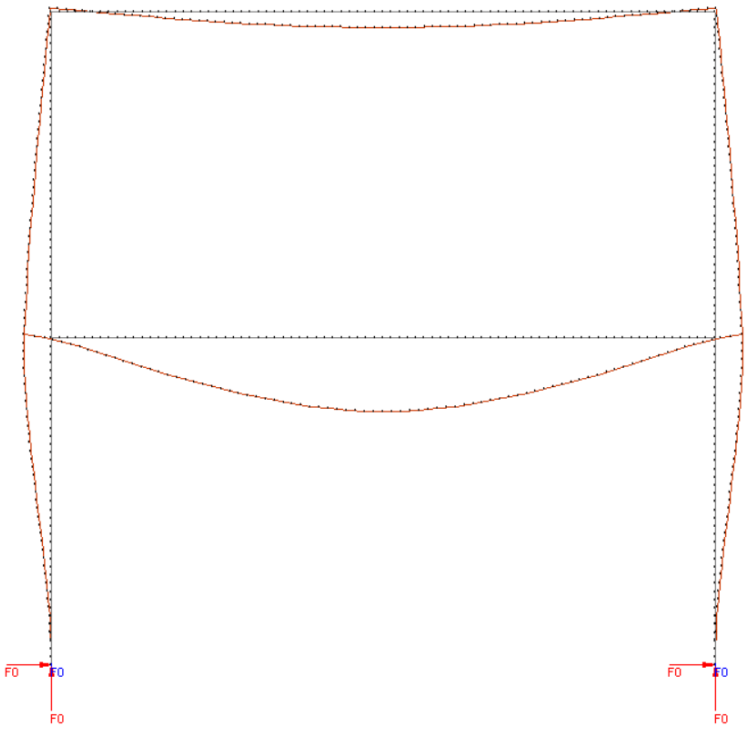

b)

Figure B7 – Deformed shape (scaled 10 times) of frame A2: a) 60 minutes, b) 144 minutes.

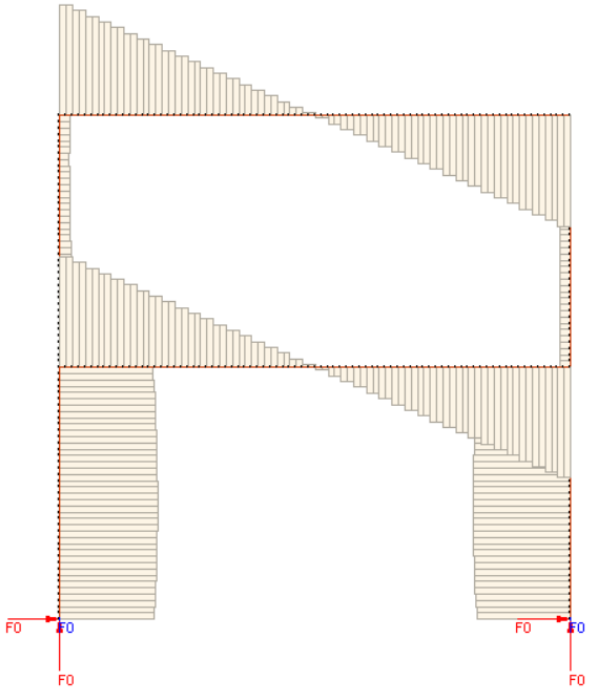

a)

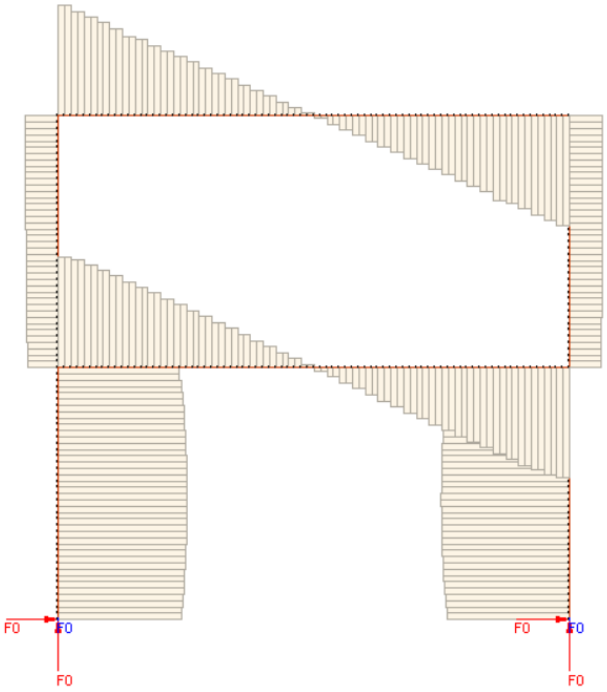

b)

Figure B8 – Schematic shear force diagram of frame A2: a) 60 minutes, b) 144 minutes.

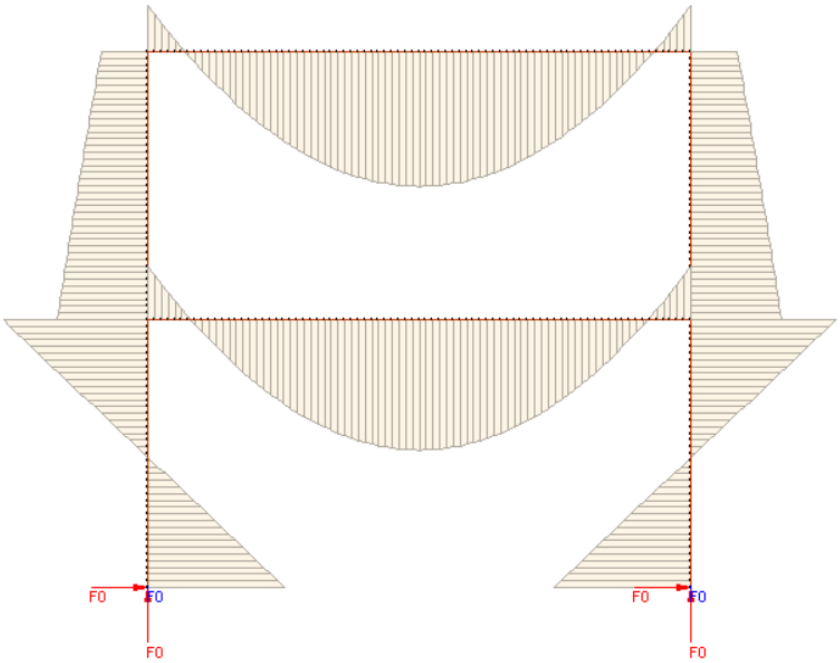

a)

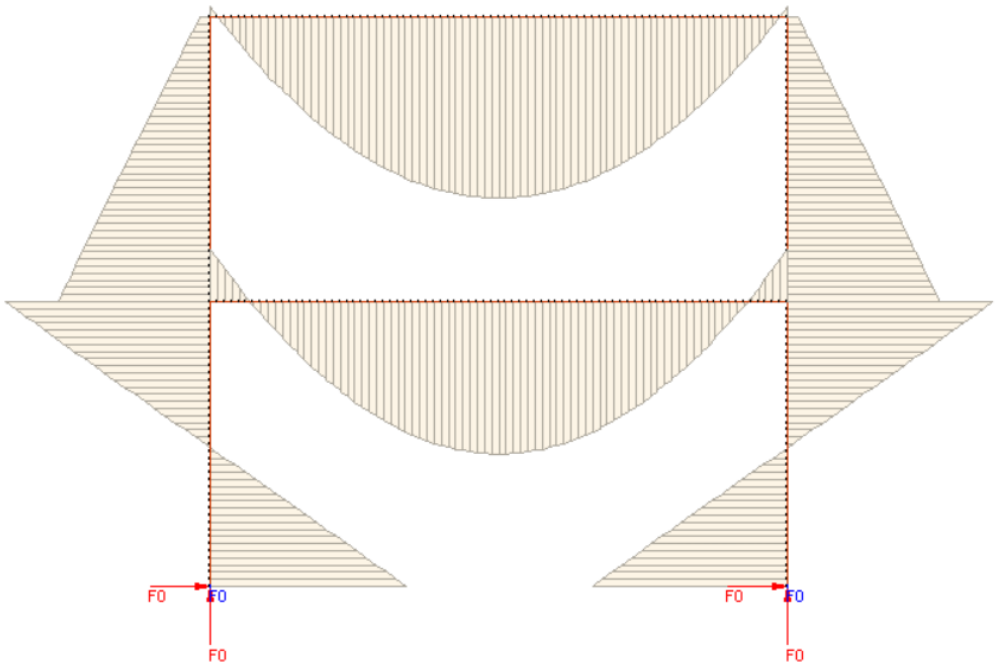

b)

Figure B9 – Schematic bending moment diagram of frame A3: a) 45 minutes, b) 109 minutes.

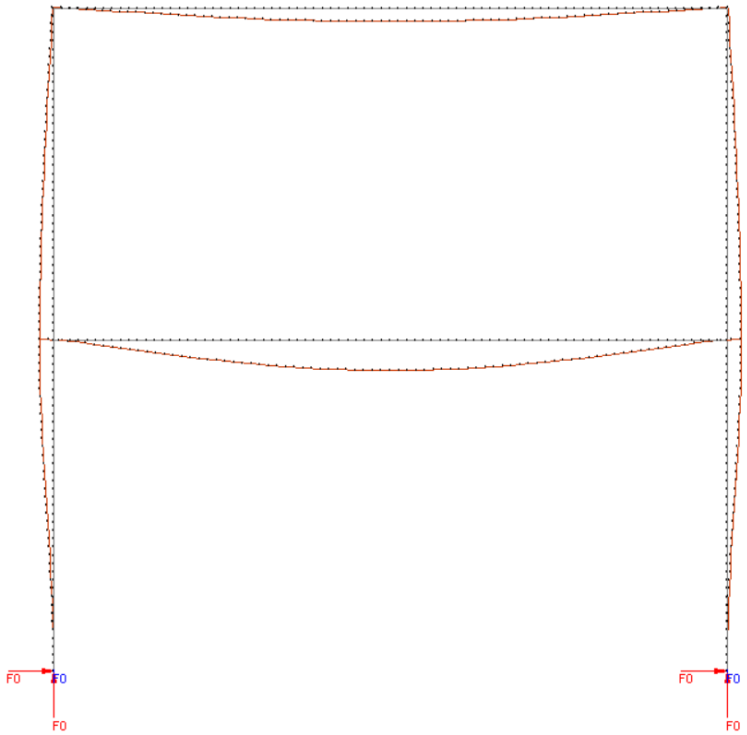

a)

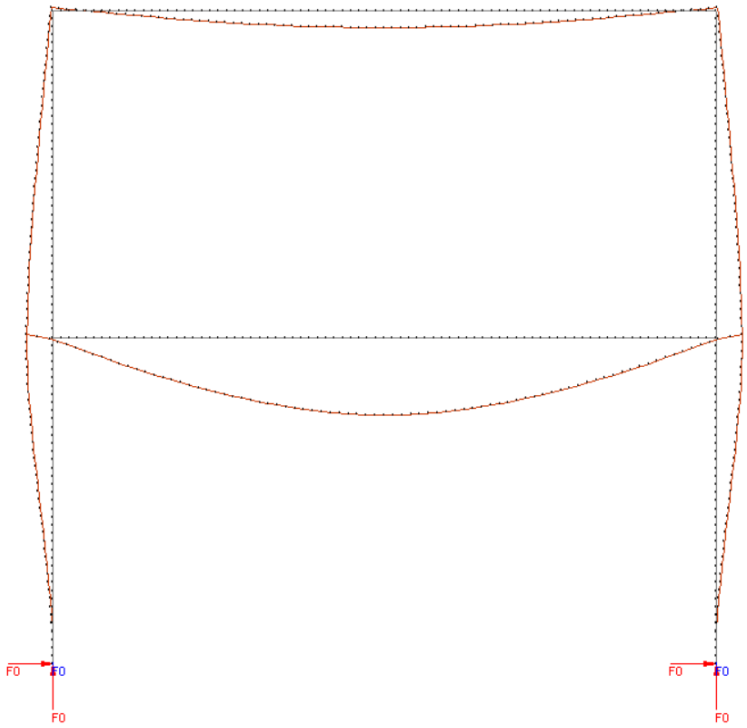

b)

Figure B10 – Deformed shape (scaled 10 times) of frame A3: a) 45 minutes, b) 109 minutes.

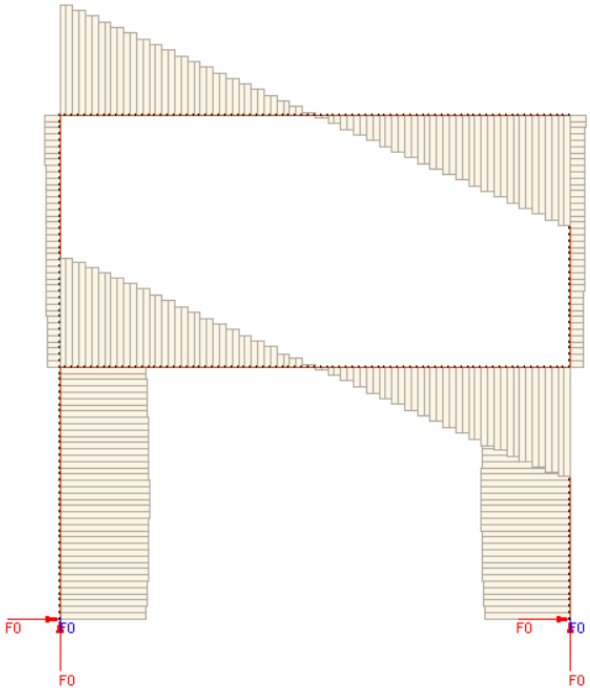

a)

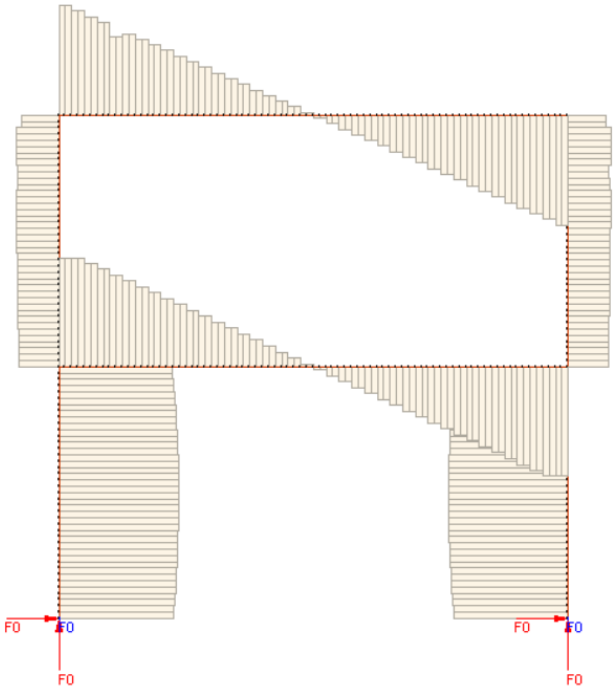

b)

Figure B11 – Schematic shear force diagram of frame A3: a) 45 minutes, b) 109 minutes.

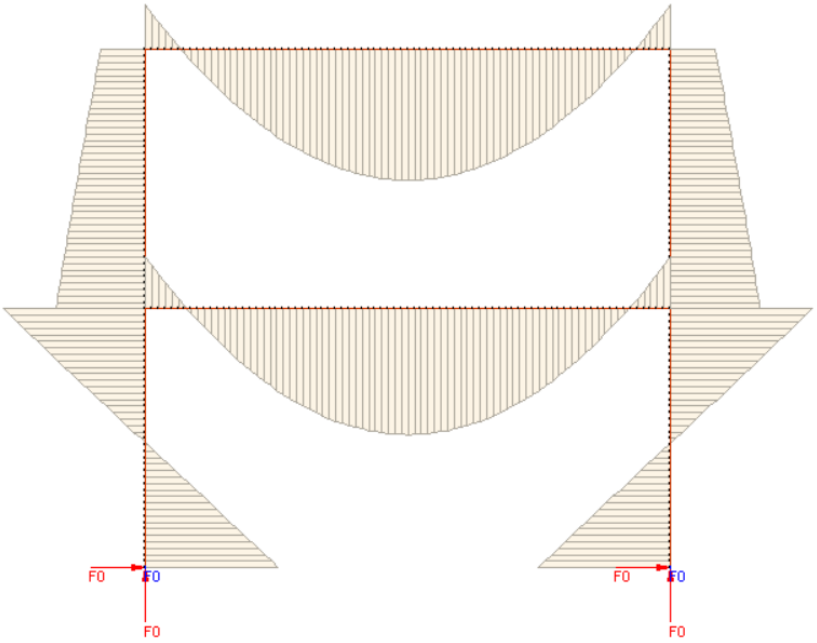

a)

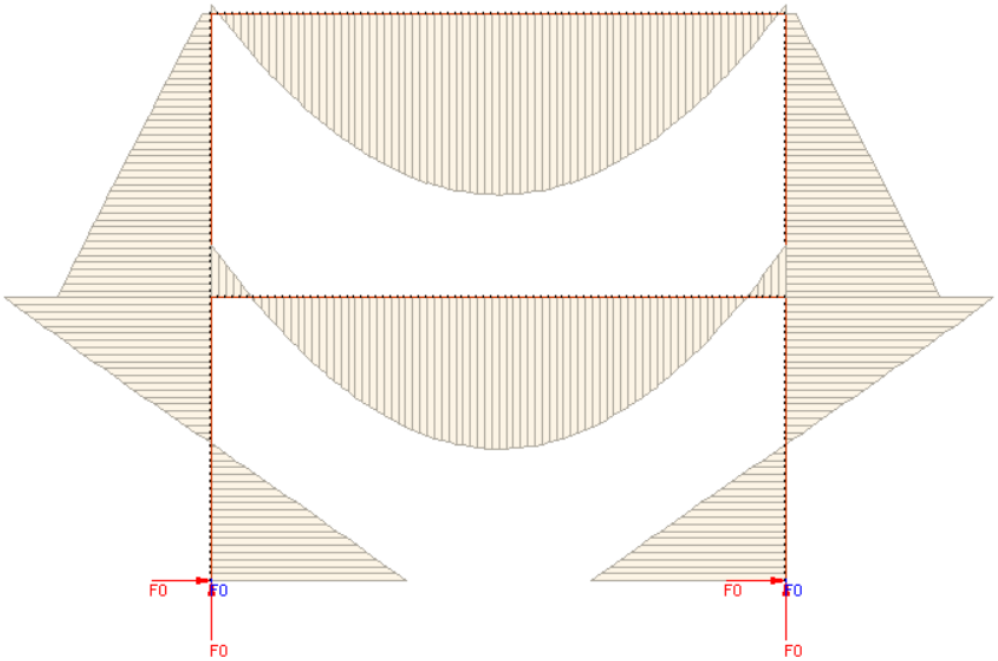

b)

Figure B12 – Schematic bending moment diagram of frame A4: a) 45 minutes, b) 109 minutes.

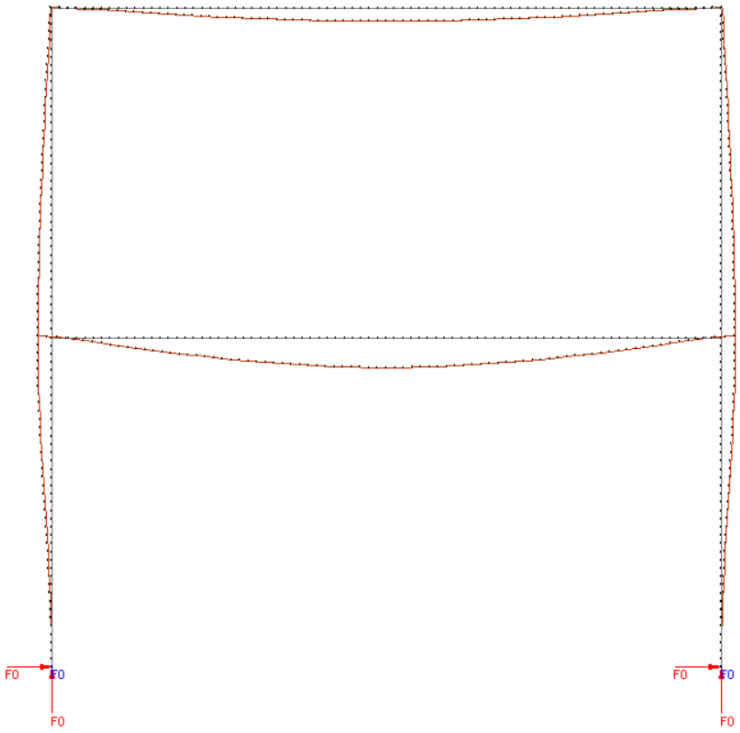

a)

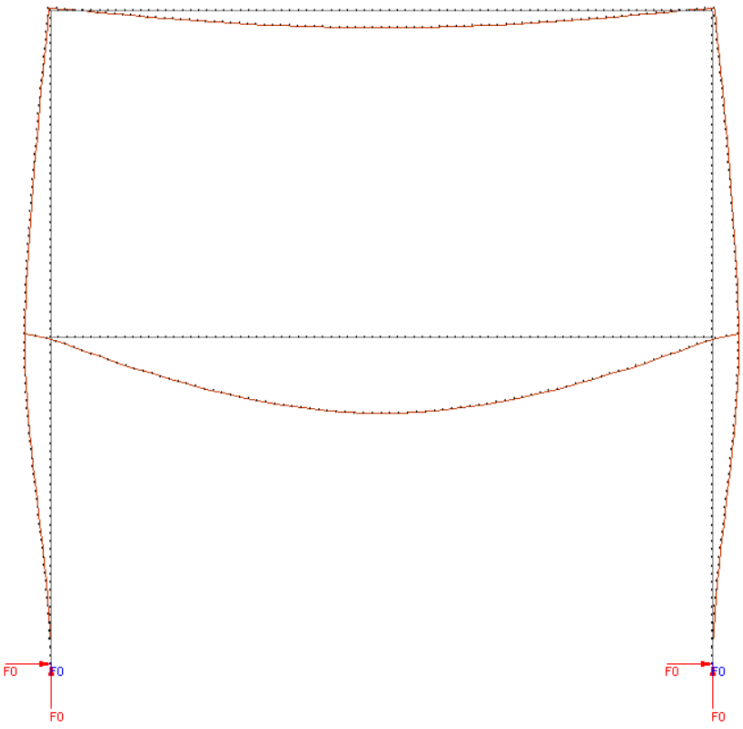

b)

Figure B13 – Deformed shape (scaled 10 times) of frame A4: a) 45 minutes, b) 109 minutes.

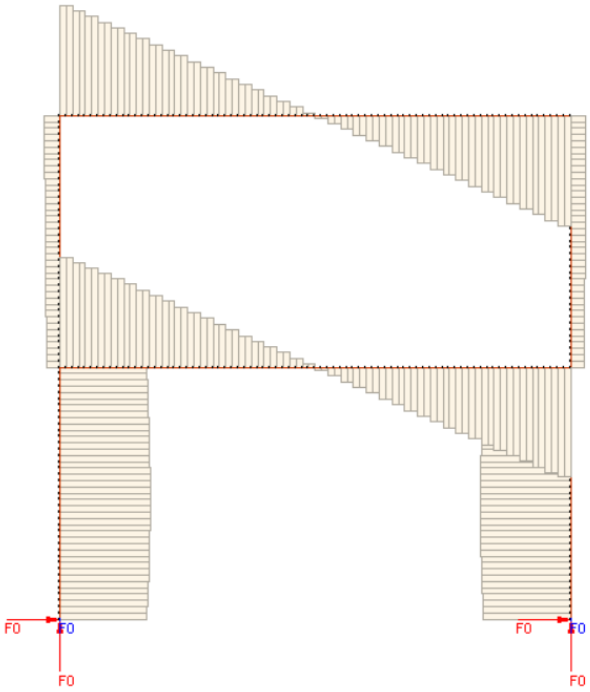

a)

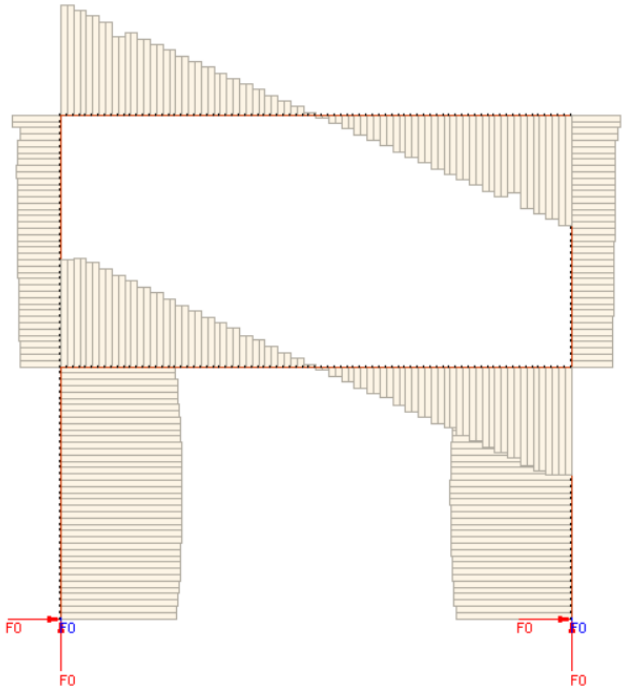

b)

Figure B14 – Schematic shear force diagram of frame A4: a) 45 minutes, b) 109 minutes.

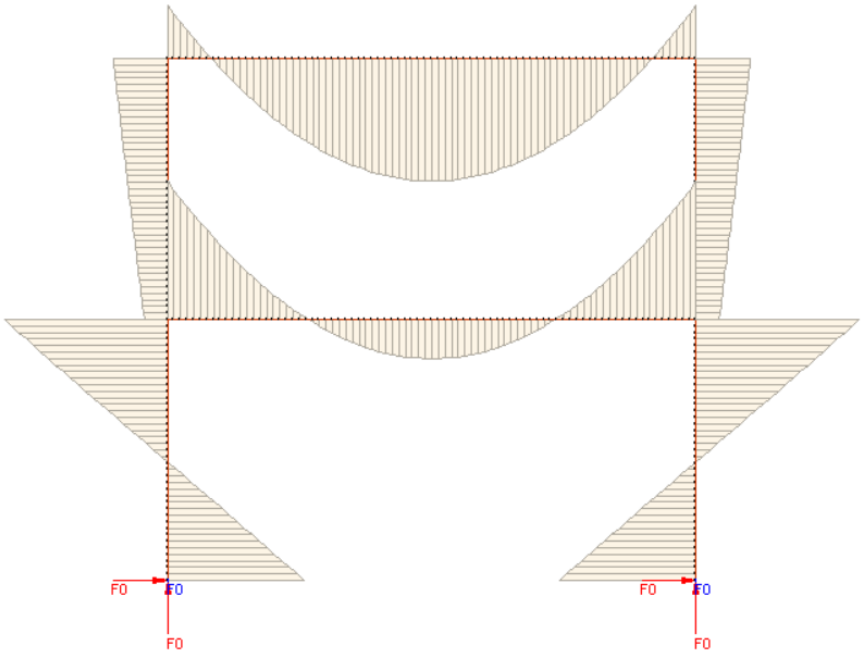

a)

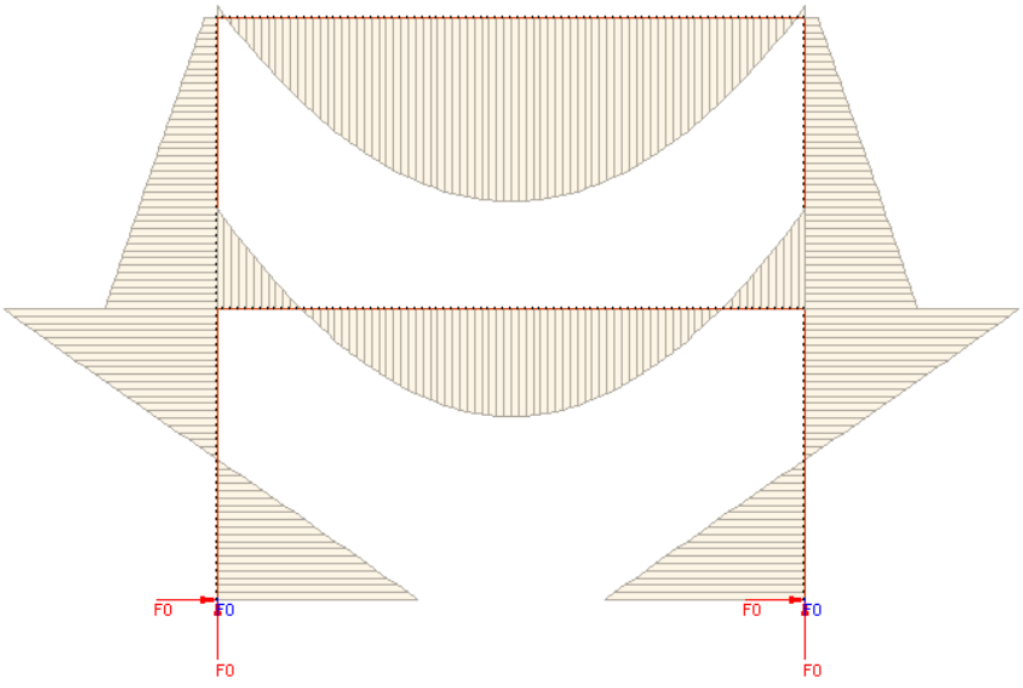

b)

Figure B15 – Schematic bending moment diagram of frame A5: a) 60 minutes, b) 143 minutes.

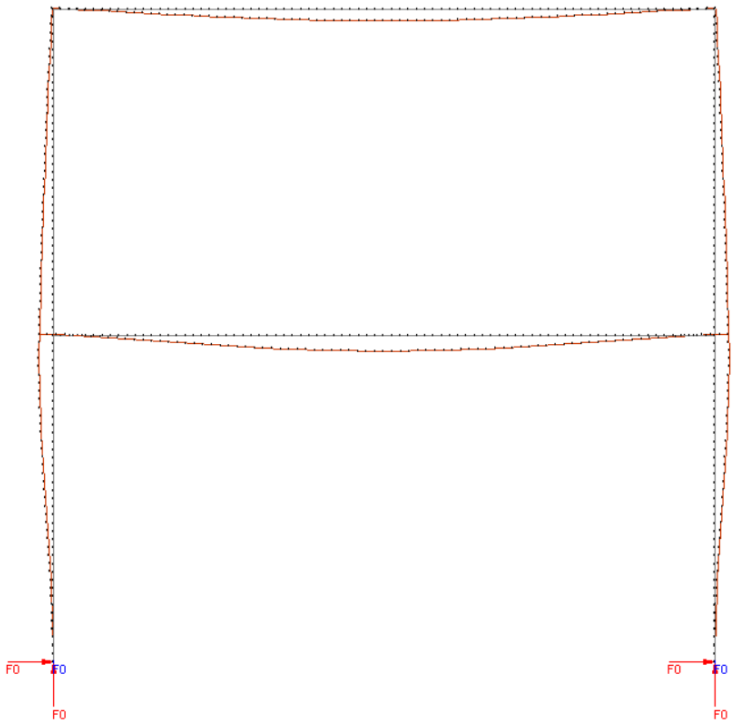

a)

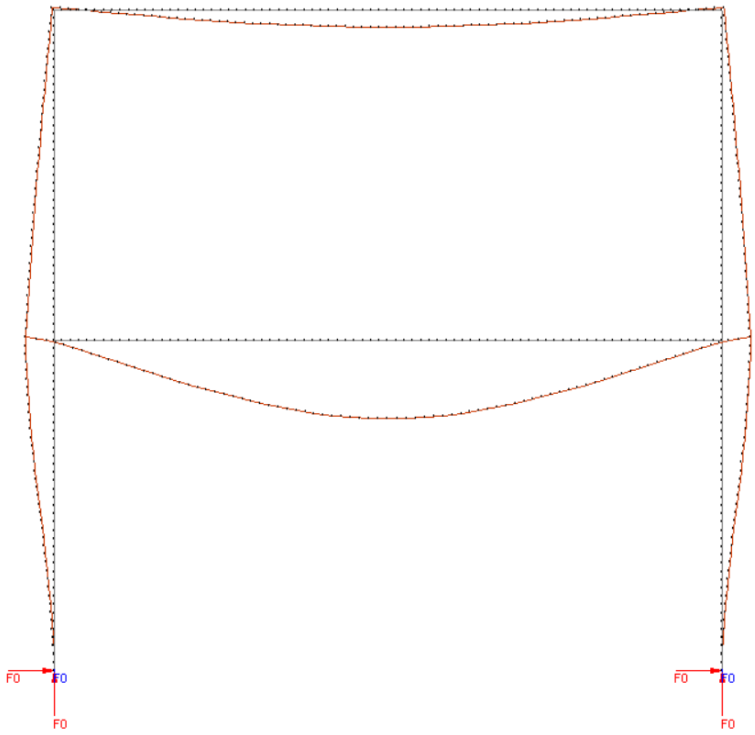

b)

Figure B16 – Deformed shape (scaled 10 times) of frame A5: a) 60 minutes, b) 143 minutes.

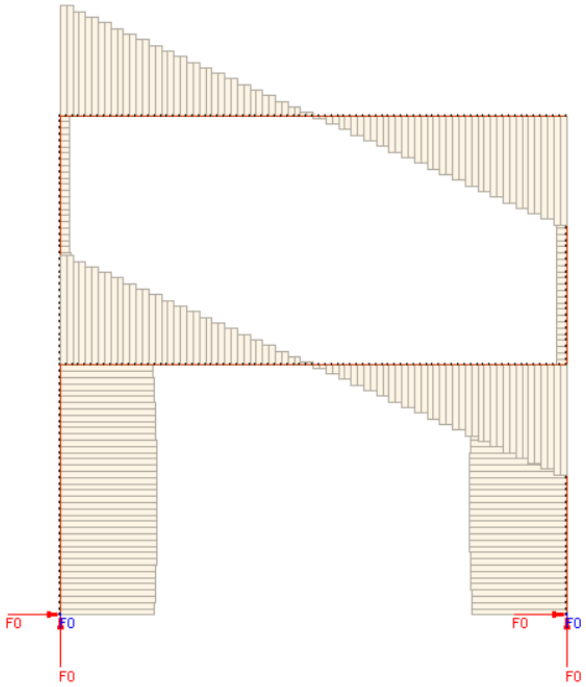

a)

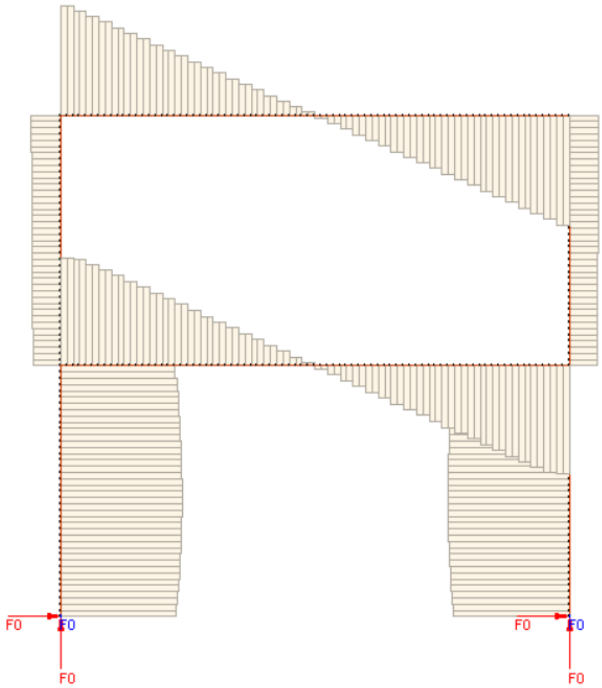

b)

Figure B17 – Schematic shear force diagram of frame A5: a) 60 minutes, b) 143 minutes.

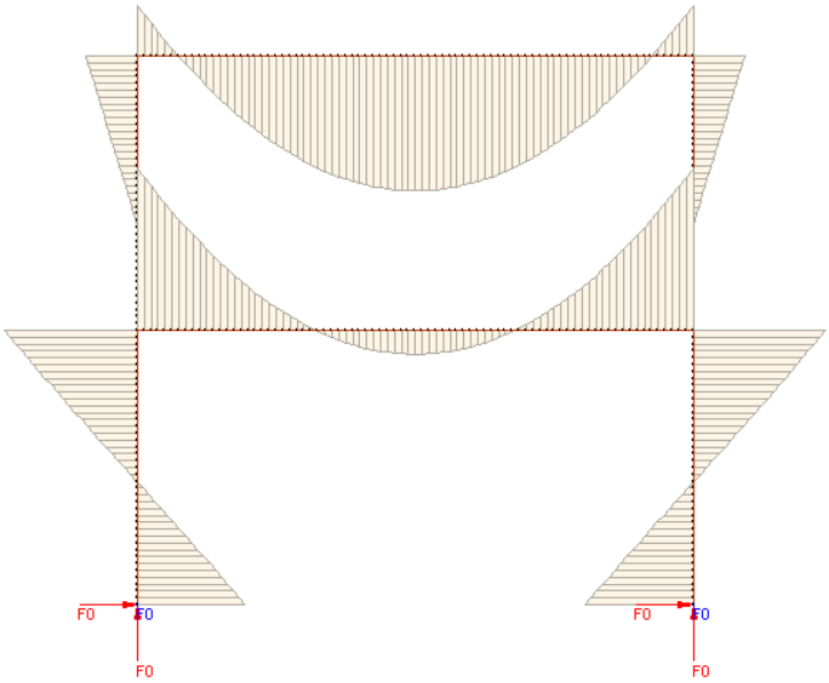

a)

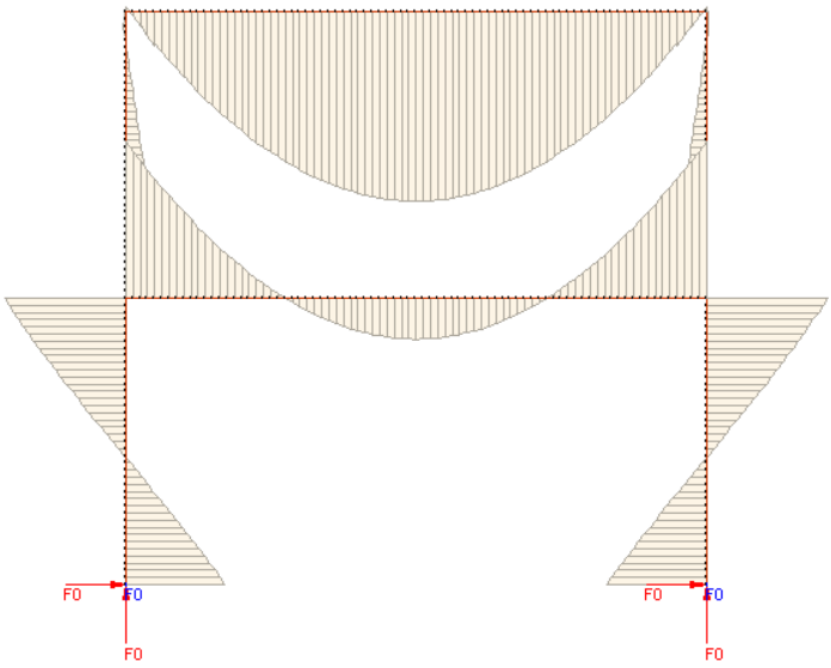

b)

Figure B18 – Schematic bending moment diagram of frame B1: a) 90 minutes, b) 180 minutes.

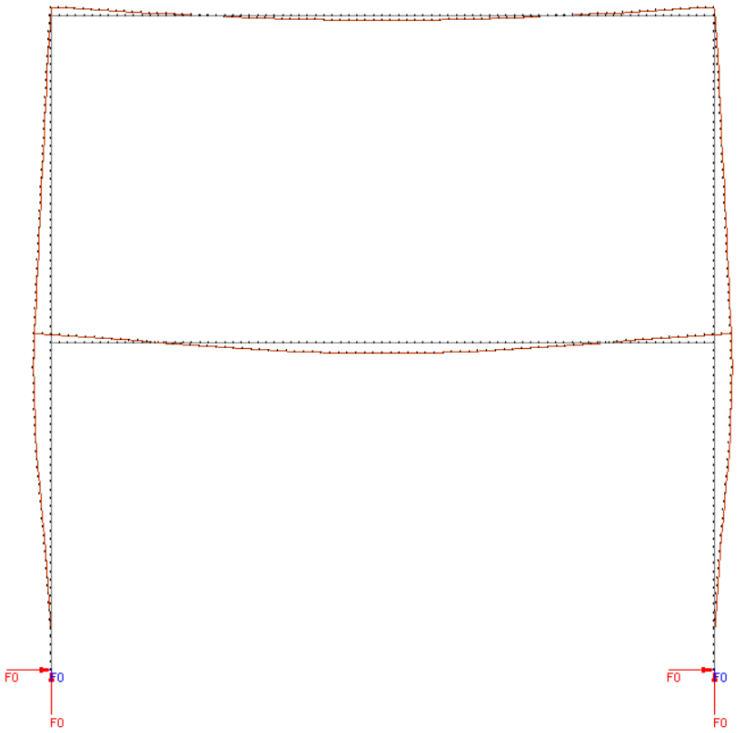

a)

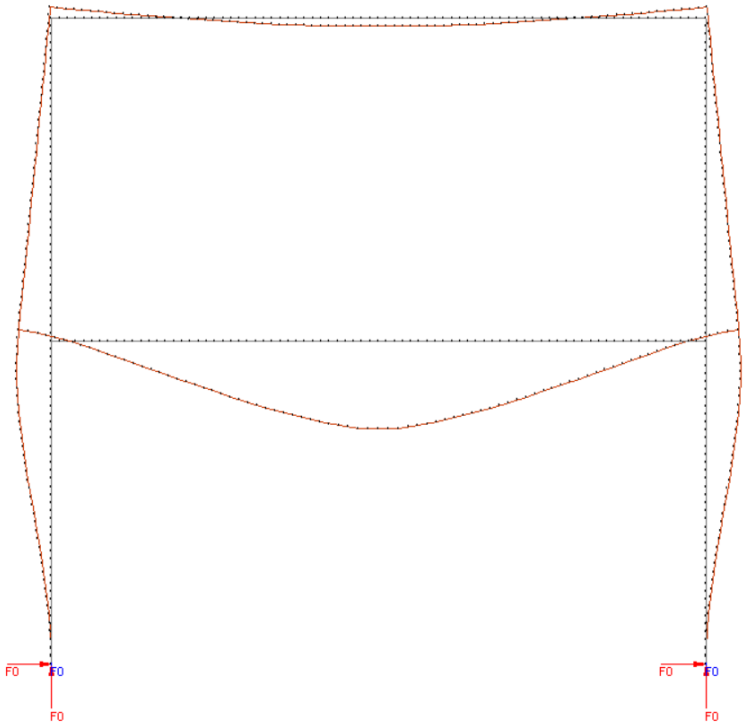

b)

Figure B19 – Deformed shape (scaled 10 times) of frame B1: a) 90 minutes, b) 180 minutes.

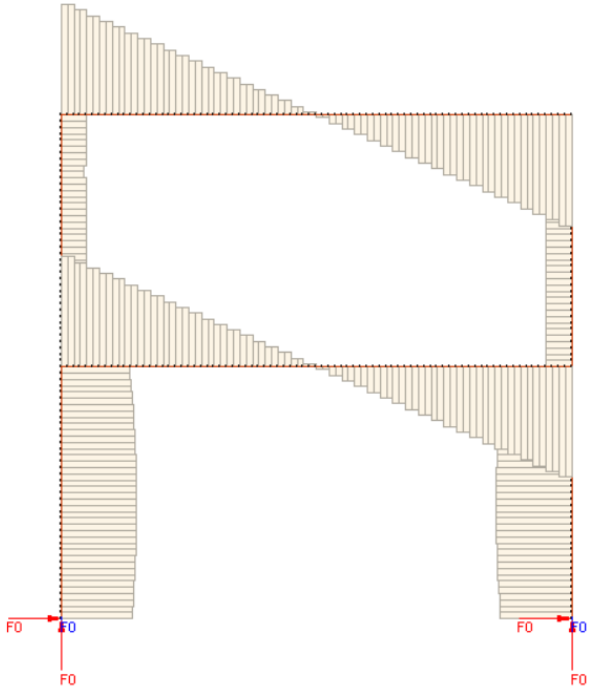

a)

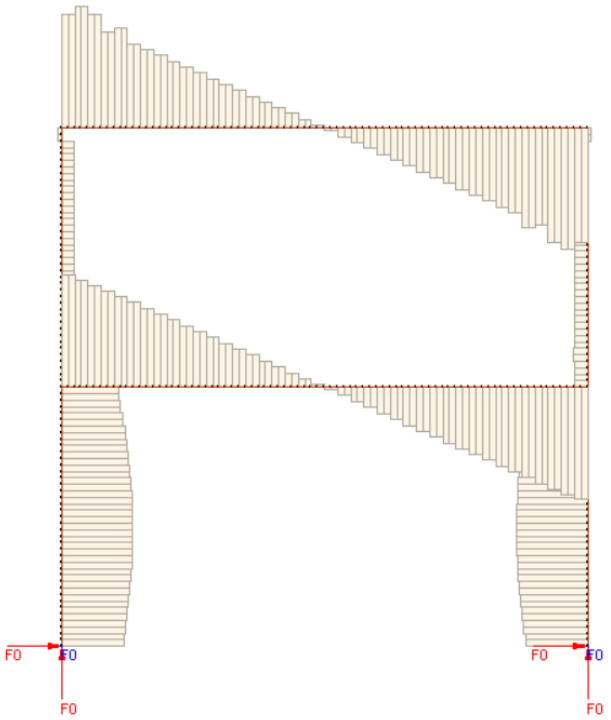

b)

Figure B20 – Schematic shear force diagram of frame B1: a) 90 minutes, b) 180 minutes.

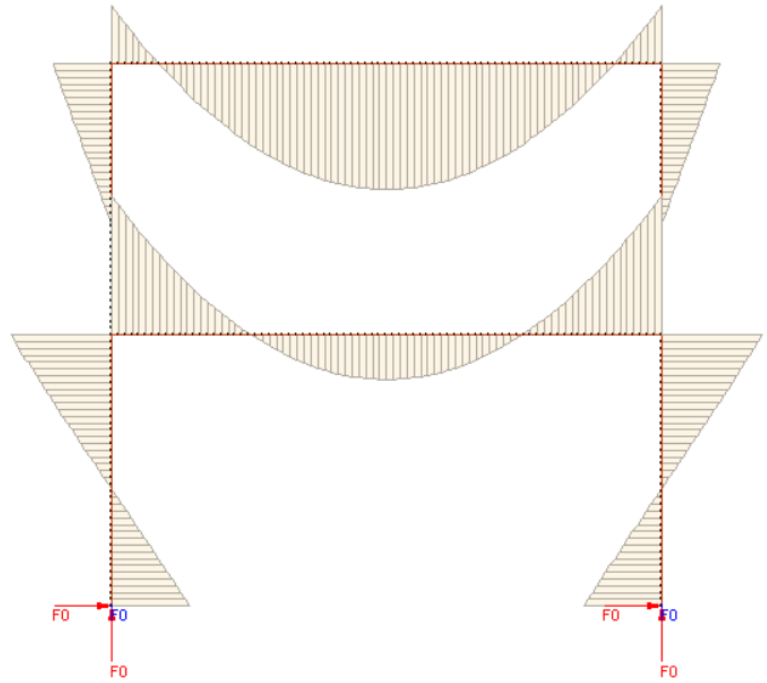

a)

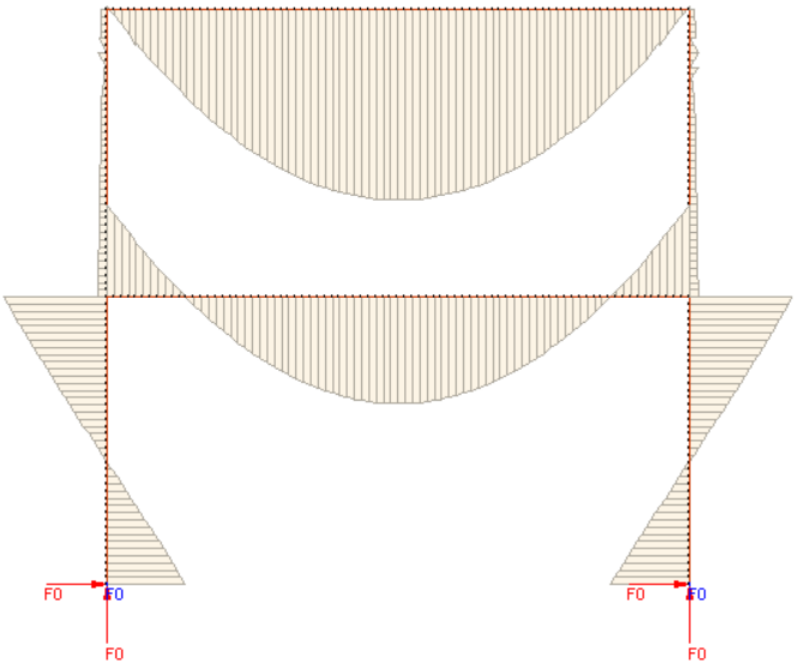

b)

Figure B21 – Schematic bending moment diagram of frame B2: a) 60 minutes, b) 171 minutes.

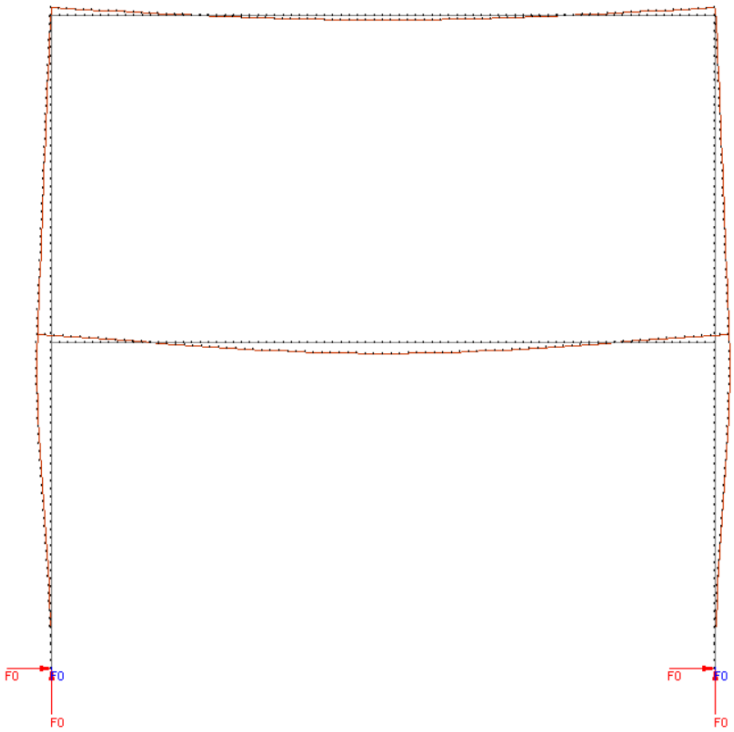

a)

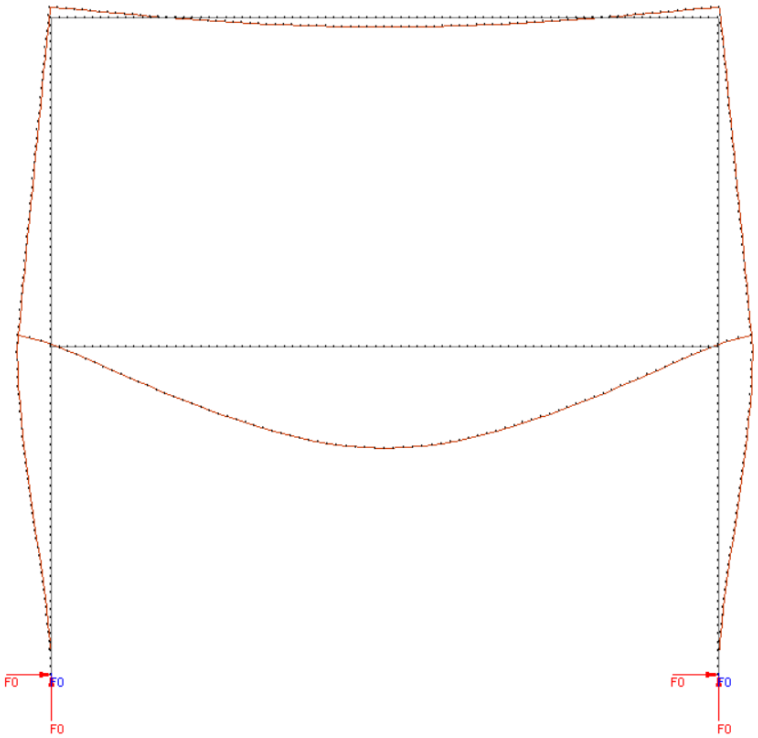

b)

Figure B22 – Deformed shape (scaled 10 times) of frame B2: a) 60 minutes, b) 131 minutes.

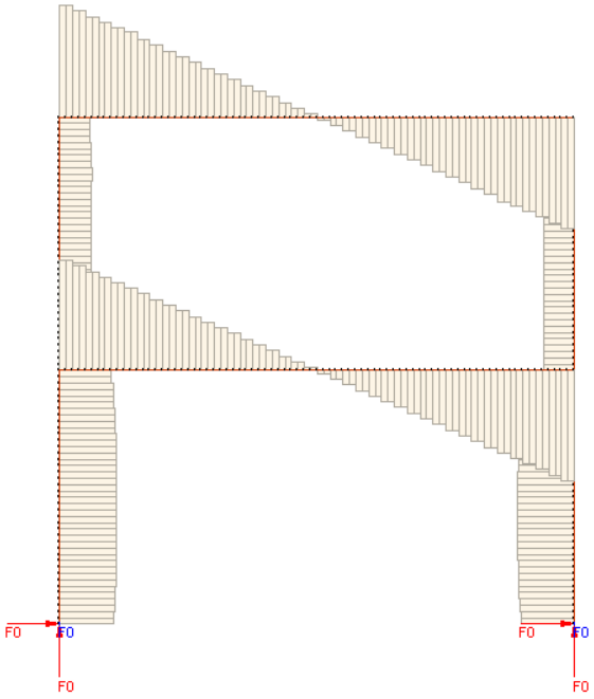

a)

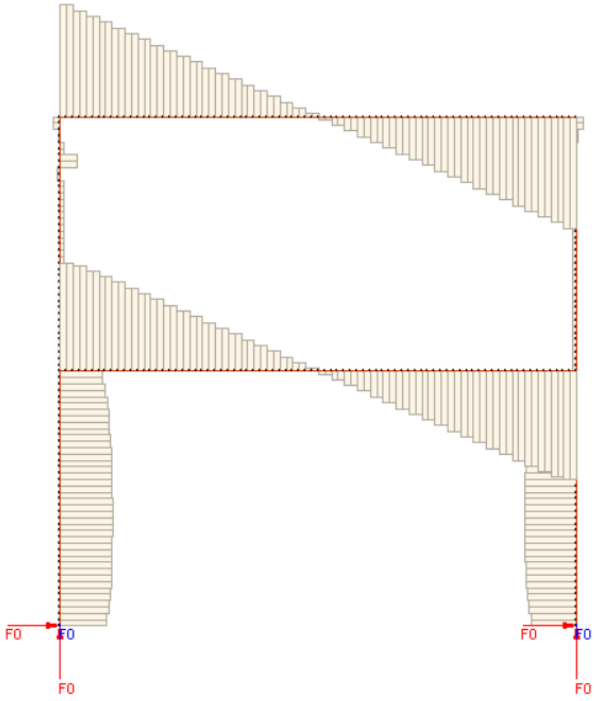

b)

Figure B23 – Schematic shear force diagram of frame B2: a) 60 minutes, b) 130 minutes.

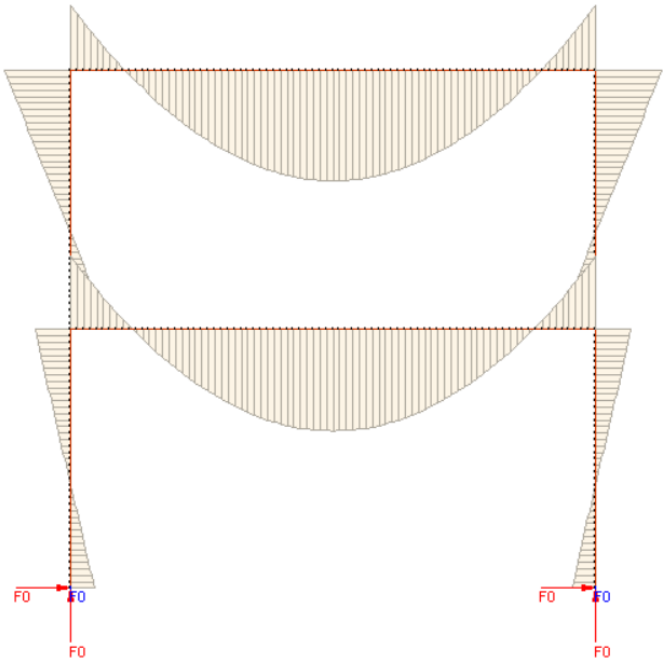

a)

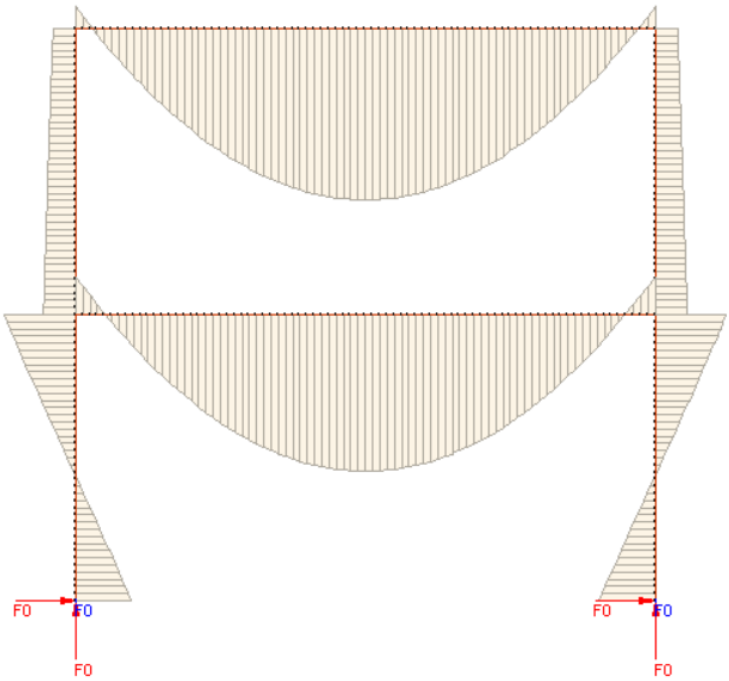

b)

Figure B24 – Schematic bending moment diagram of frame B3: a) 30 minutes, b) 54 minutes.

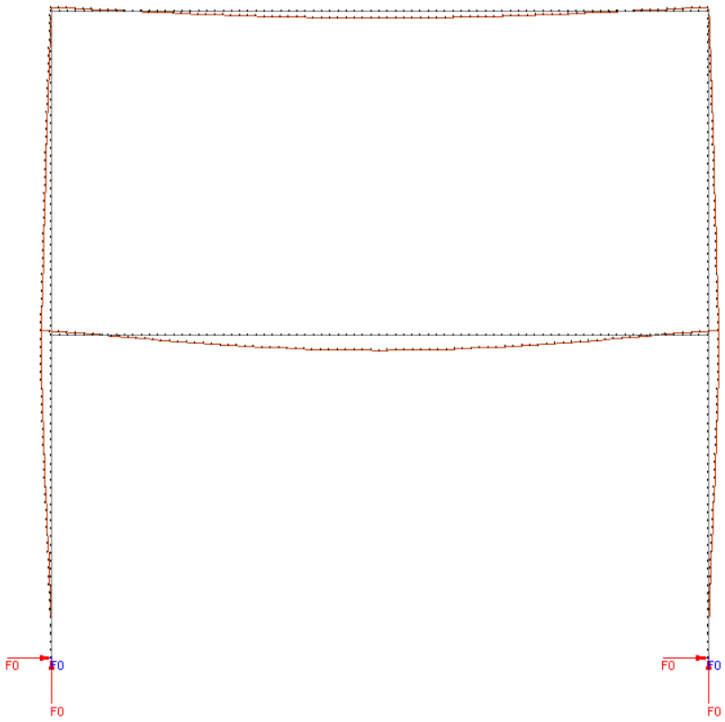

a)

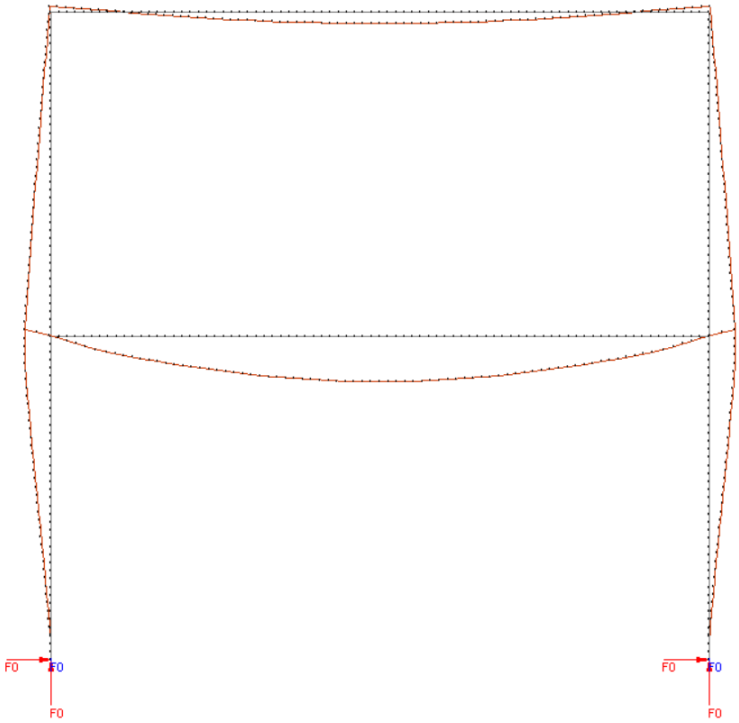

b)

Figure B25 – Deformed shape (scaled 10 times) of frame B3: a) 30 minutes, b) 54 minutes.

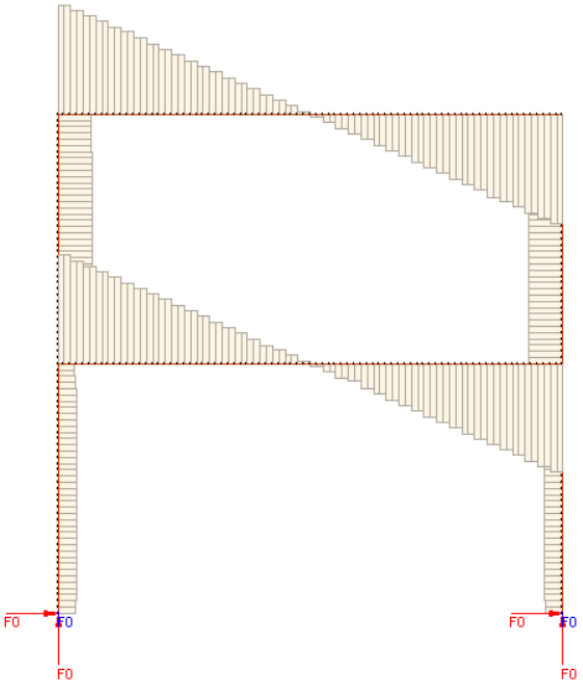

a)

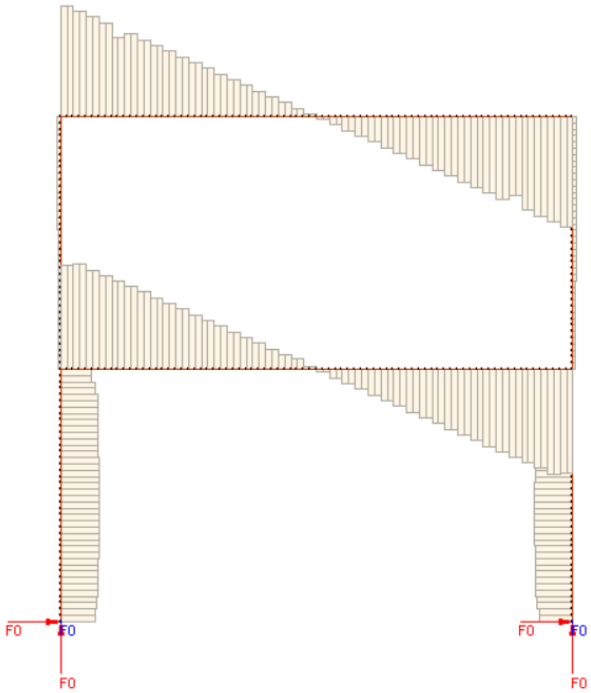

b)

Figure B26 – Schematic shear force diagram of frame B3: a) 30 minutes, b) 54 minutes.

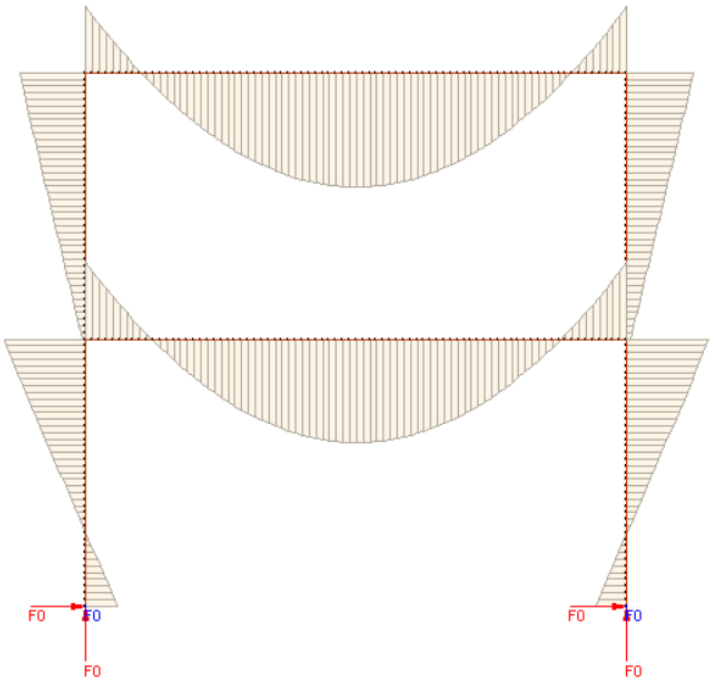

a)

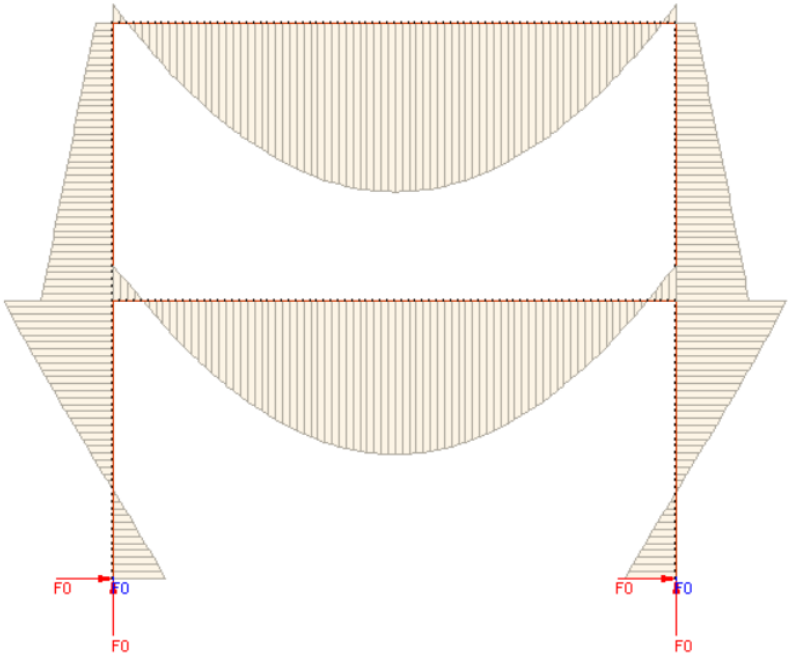

b)

Figure B27 – Schematic bending moment diagram of frame B4: a) 30 minutes, b) 78 minutes.

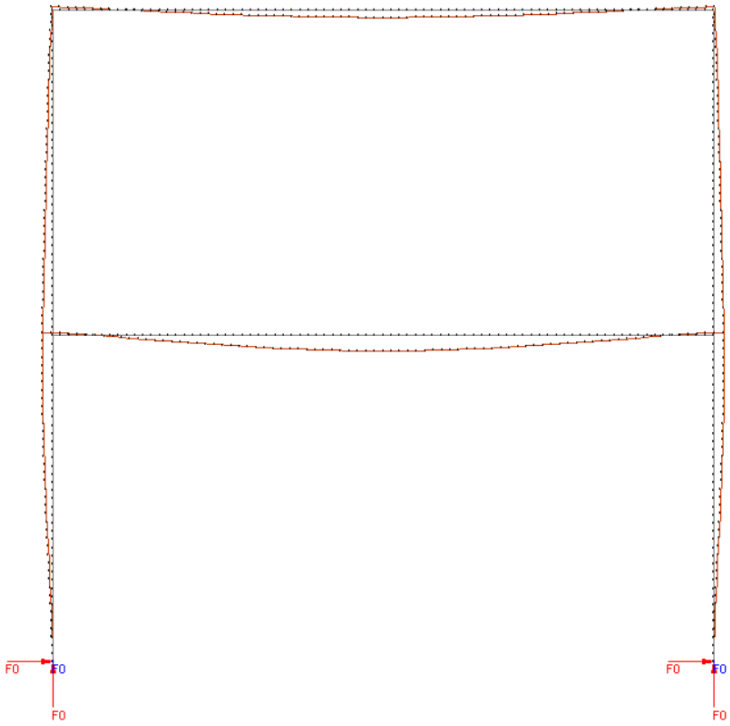

a)

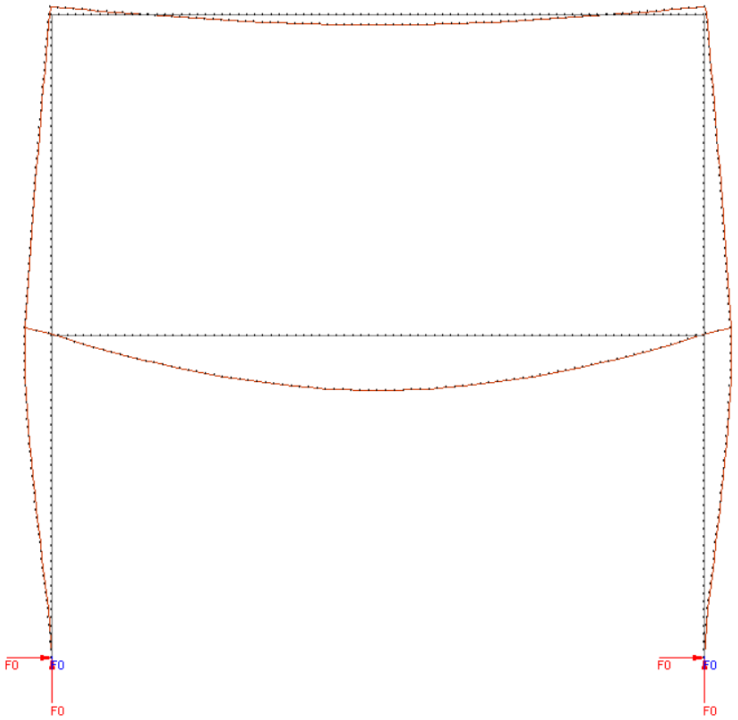

b)

Figure B28 – Deformed shape (scaled 10 times) of frame B4: a) 30 minutes, b) 78 minutes.

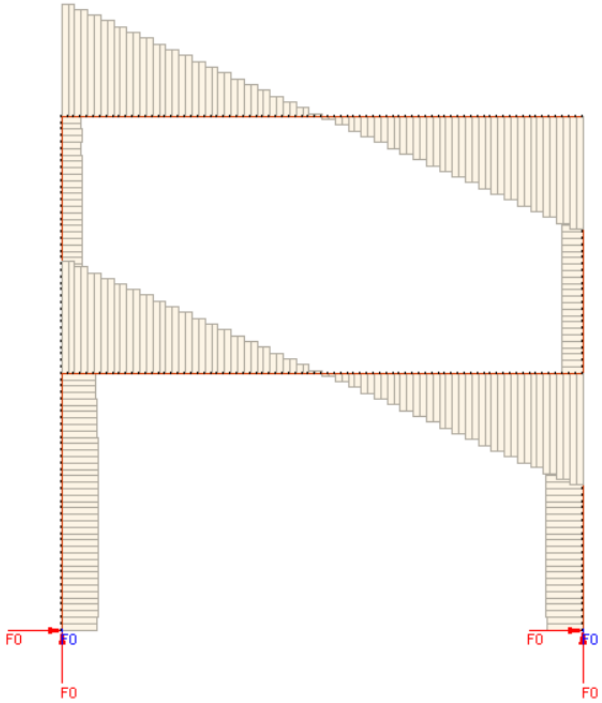

a)

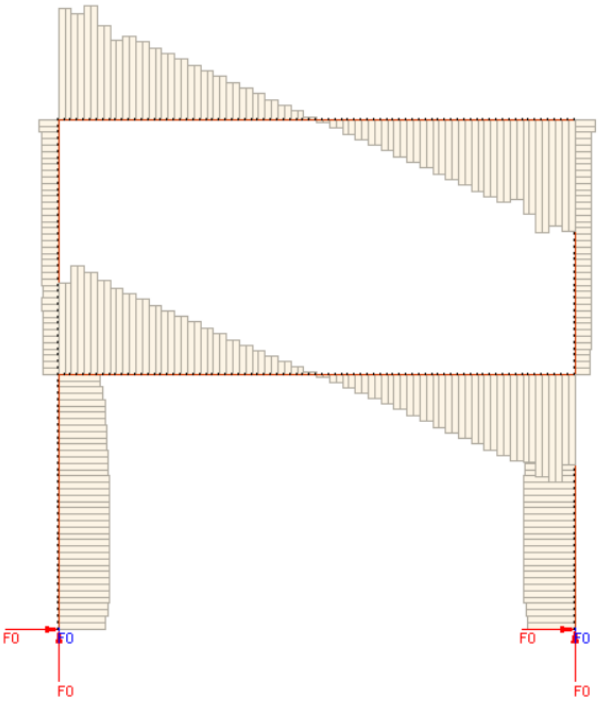

b)

Figure B29 – Schematic shear force diagram of frame B4: a) 30 minutes, b) 78 minutes.

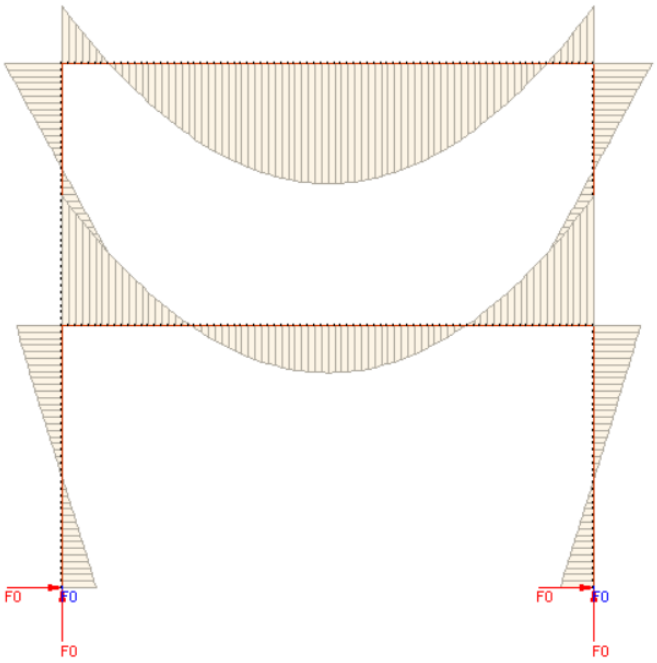

a)

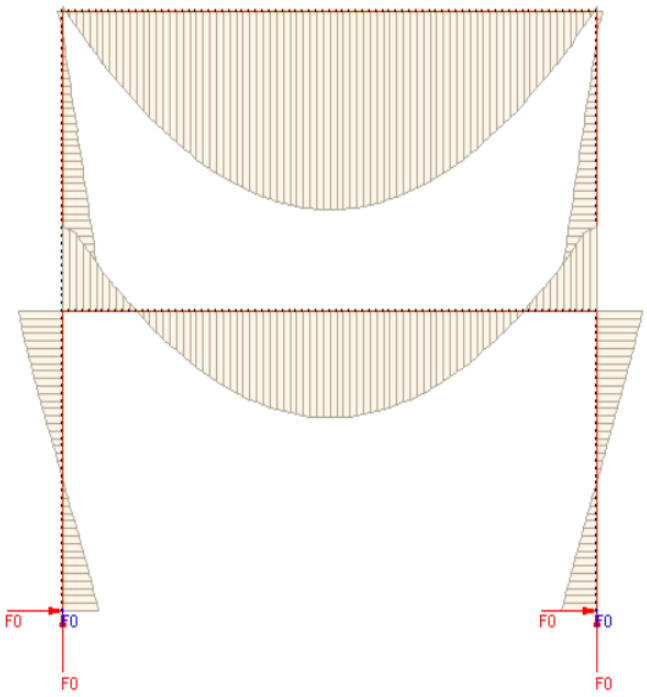

b)

Figure B30 – Schematic bending moment diagram of frame B5: a) 60 minutes, b) 127 minutes.

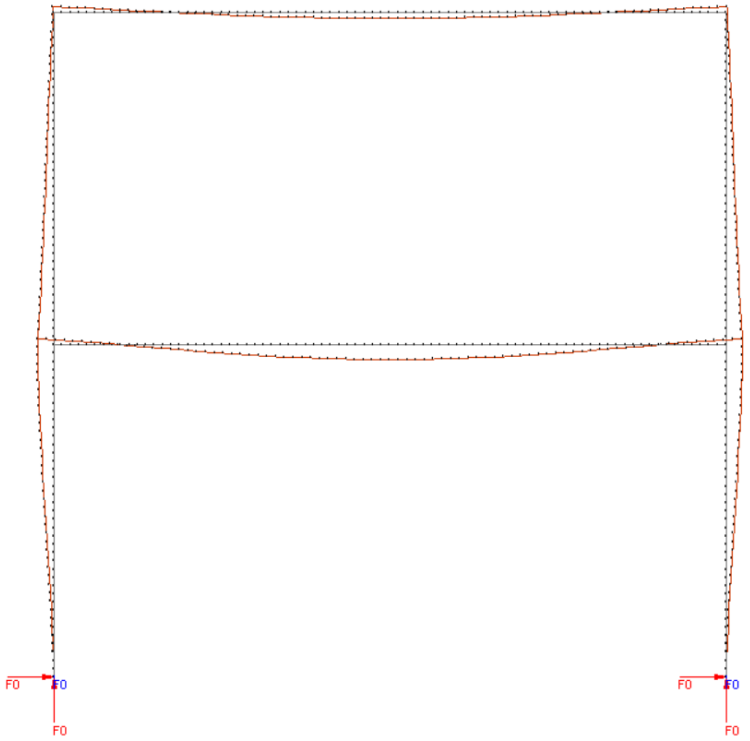

a)

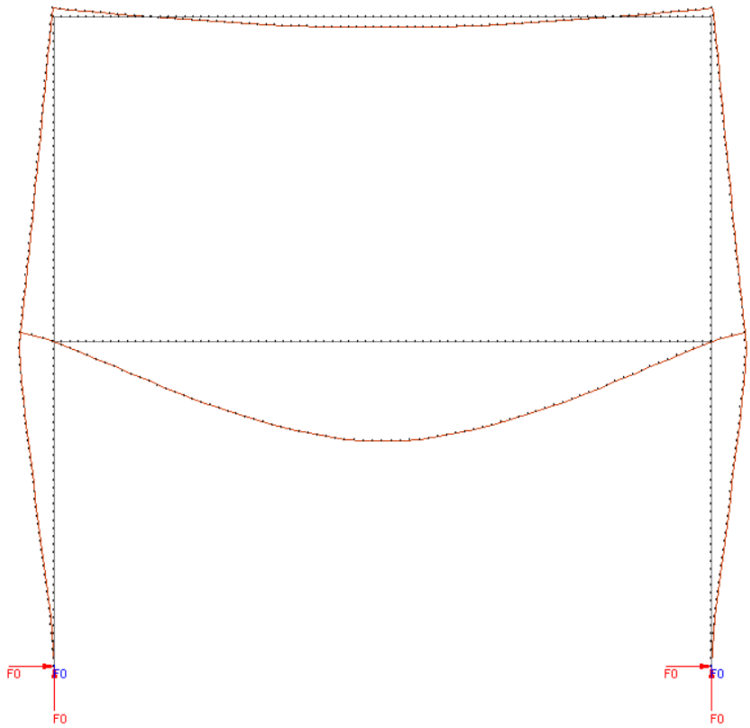

b)

Figure B31 – Deformed shape (scaled 10 times) of frame B5: a) 60 minutes, b) 127 minutes.

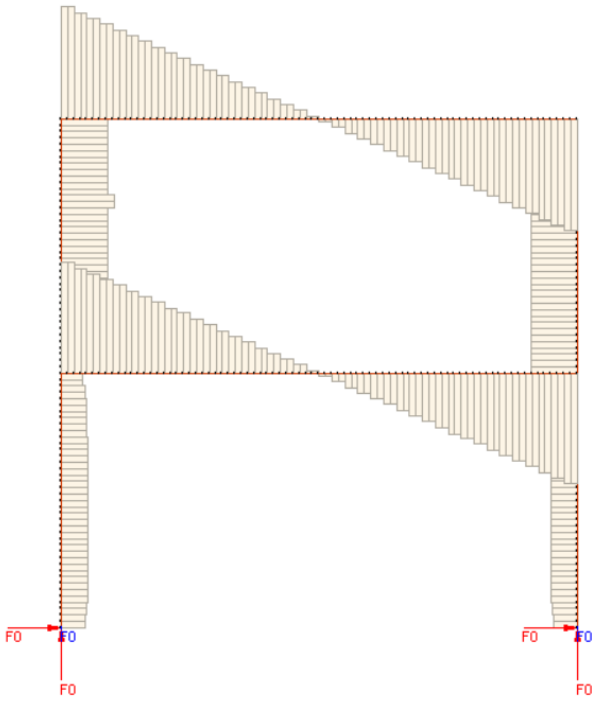

a)

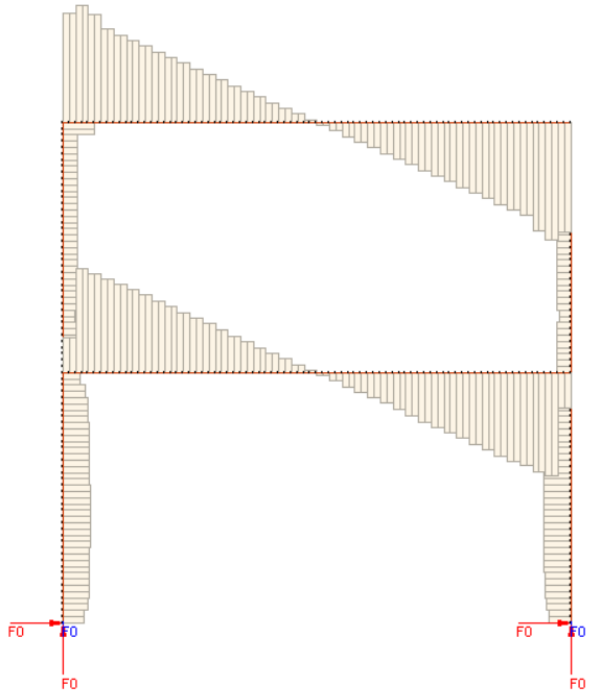

b)

Figure B32 – Schematic shear force diagram of frame B5: a) 60 minutes, b) 127 minutes.

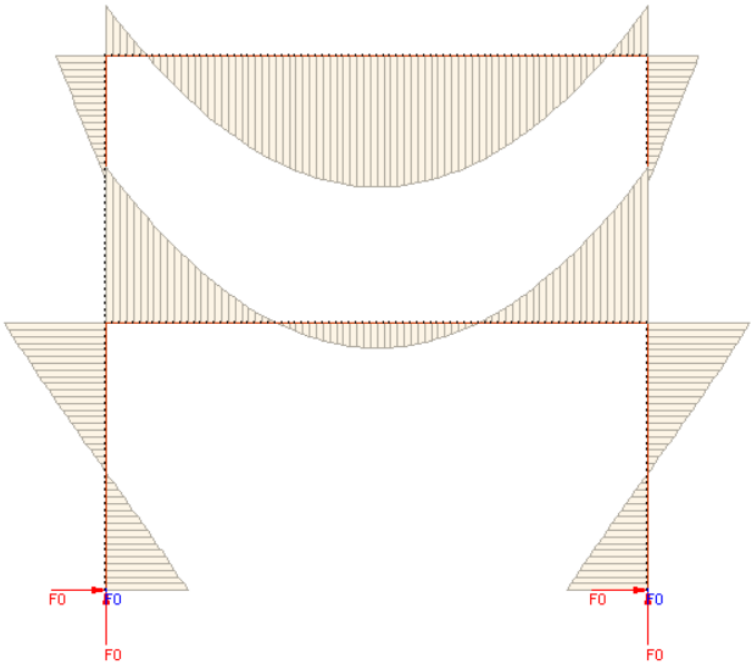

a)

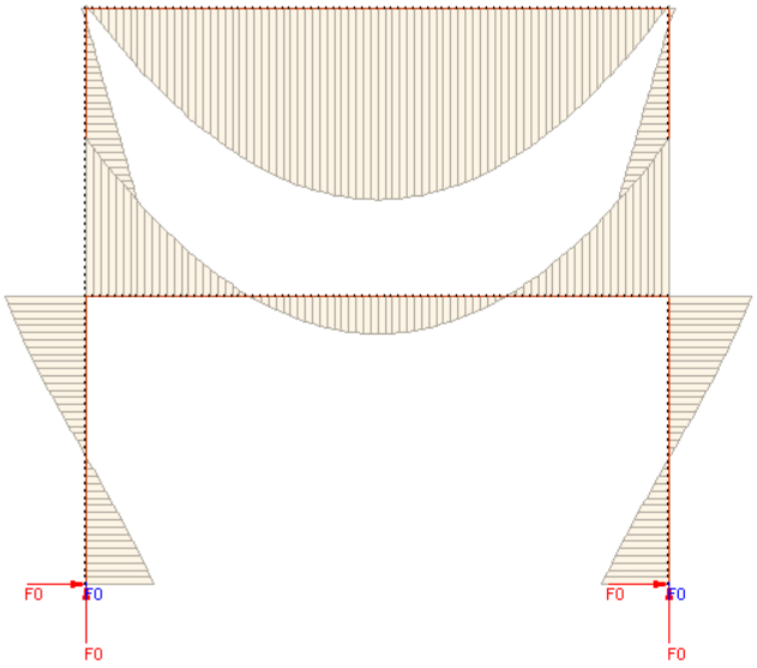

b)

Figure B33 – Schematic bending moment diagram of frame C1: a) 90 minutes, b) 173 minutes.

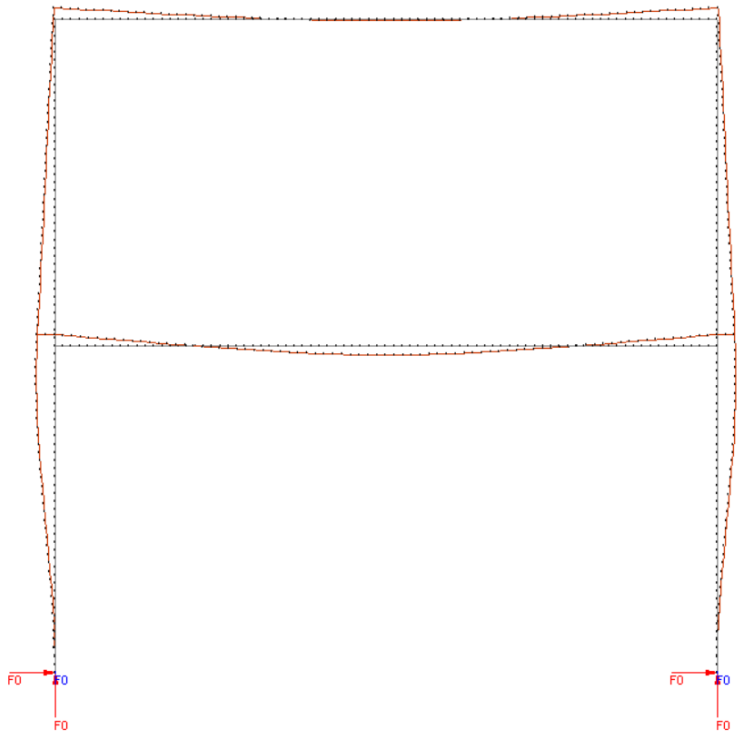

a)

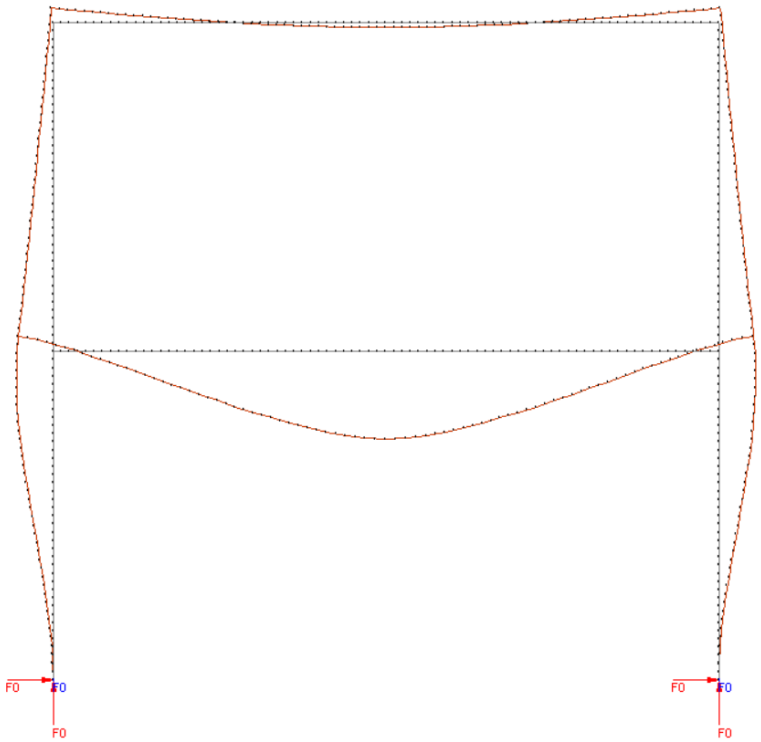

b)

Figure B34 – Deformed shape (scaled 10 times) of frame C1: a) 90 minutes, b) 173 minutes.

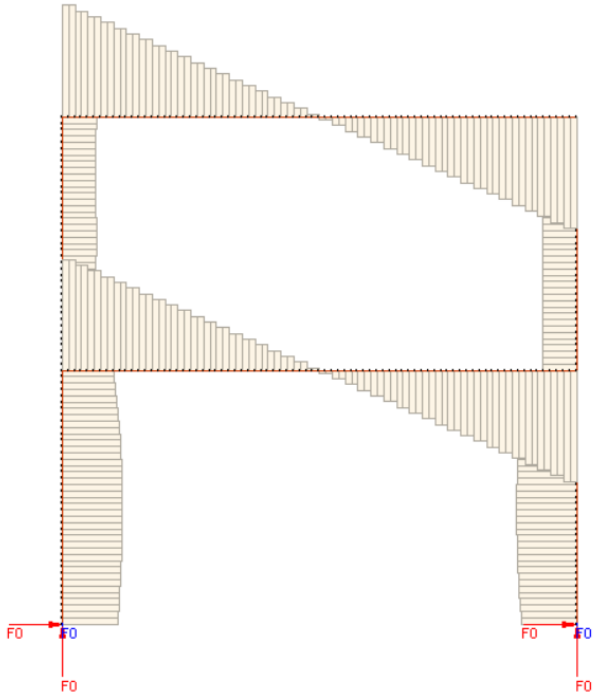

a)

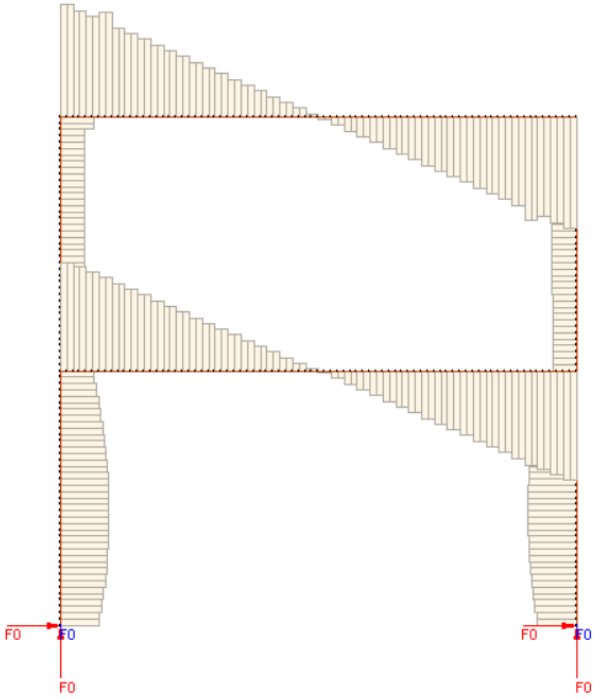

b)

Figure B35 – Schematic shear force diagram of frame C1: a) 90 minutes, b) 173 minutes.

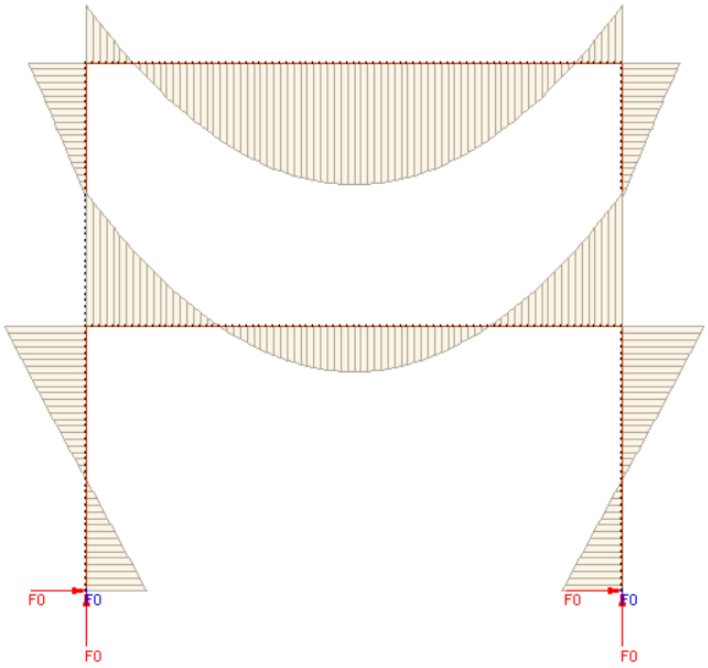

a)

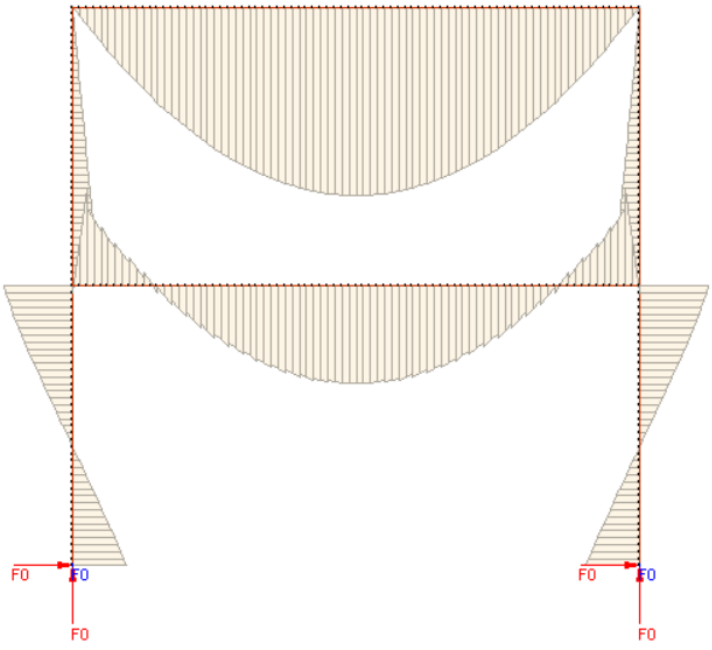

b)

Figure B36 – Schematic bending moment diagram of frame C2: a) 60 minutes, b) 132 minutes.

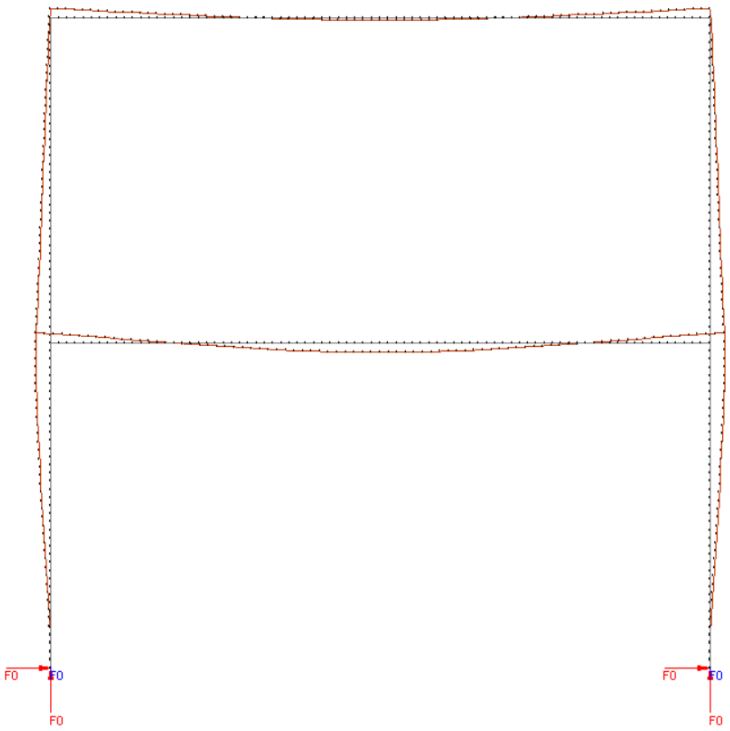

a)

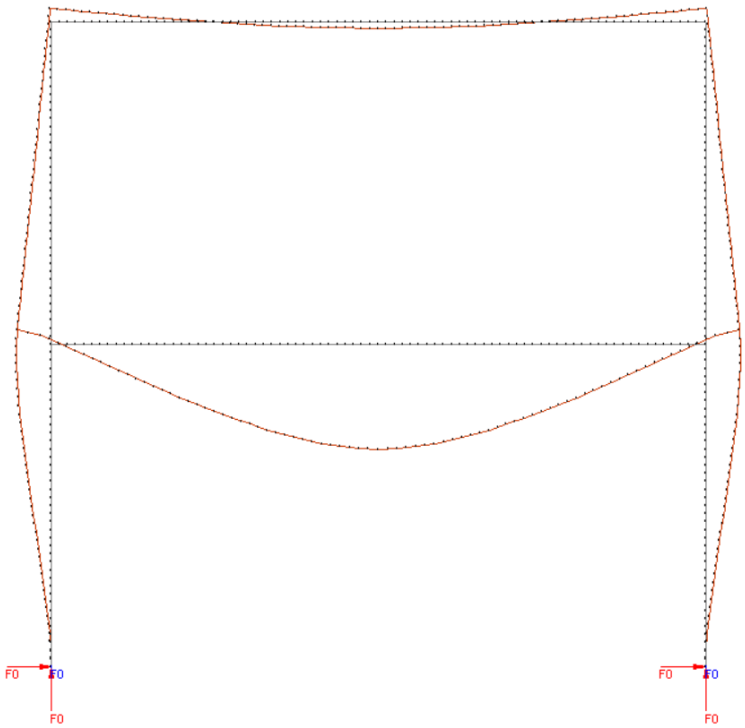

b)

Figure B37 – Deformed shape (scaled 10 times) of frame C2: a) 60 minutes, b) 132 minutes.

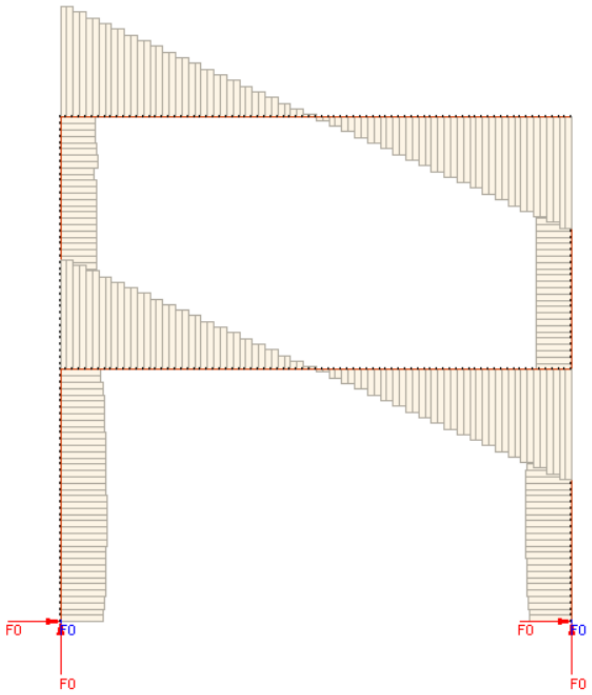

a)

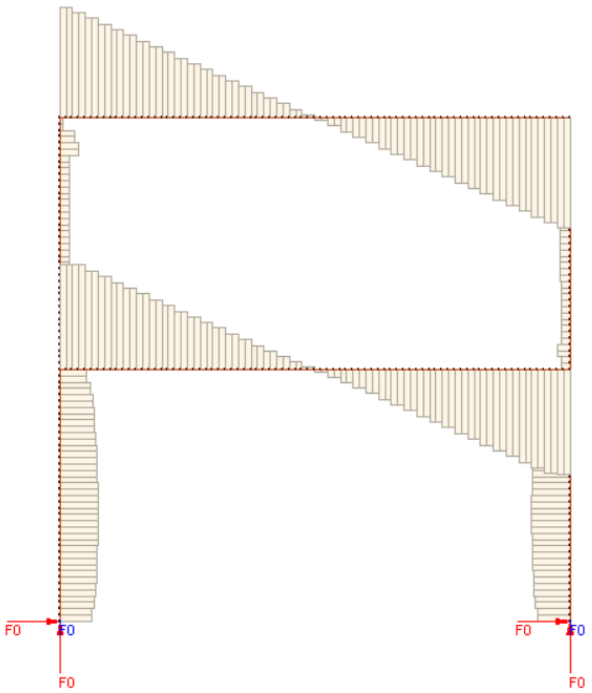

b)

Figure B38 – Schematic shear force diagram of frame C2: a) 60 minutes, b) 128 minutes.

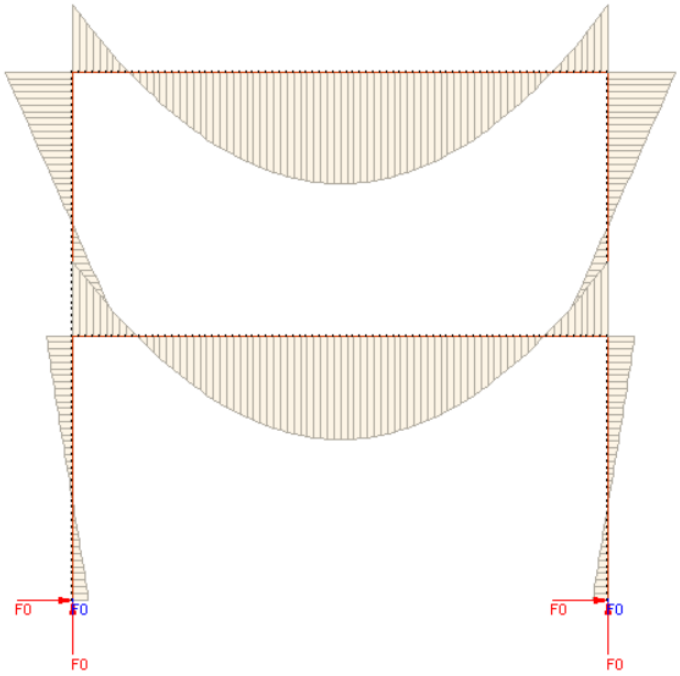

a)

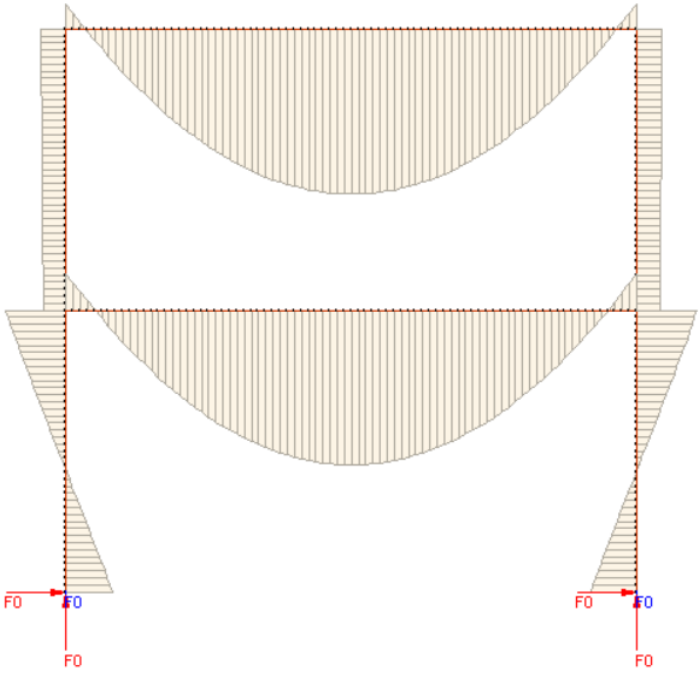

b)

Figure B39 – Schematic bending moment diagram of frame C3: a) 30 minutes, b) 47 minutes.

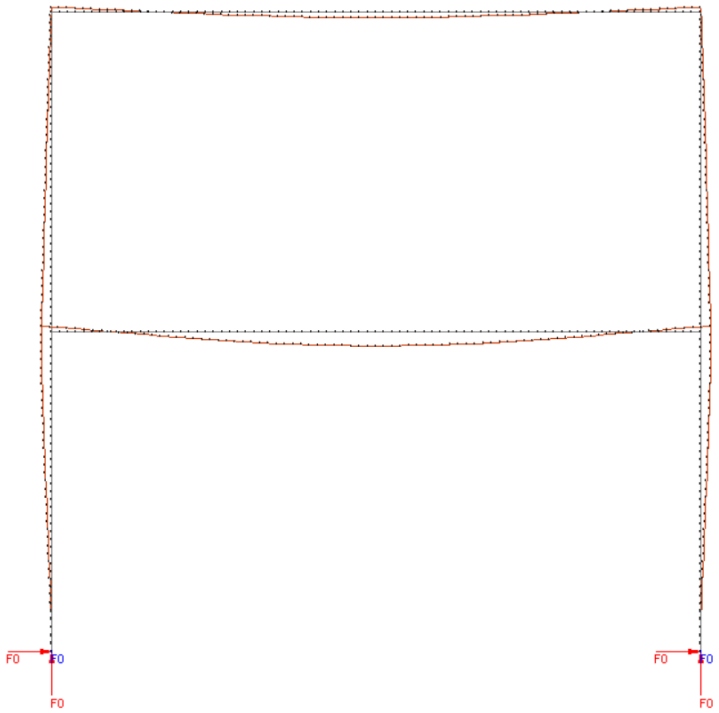

a)

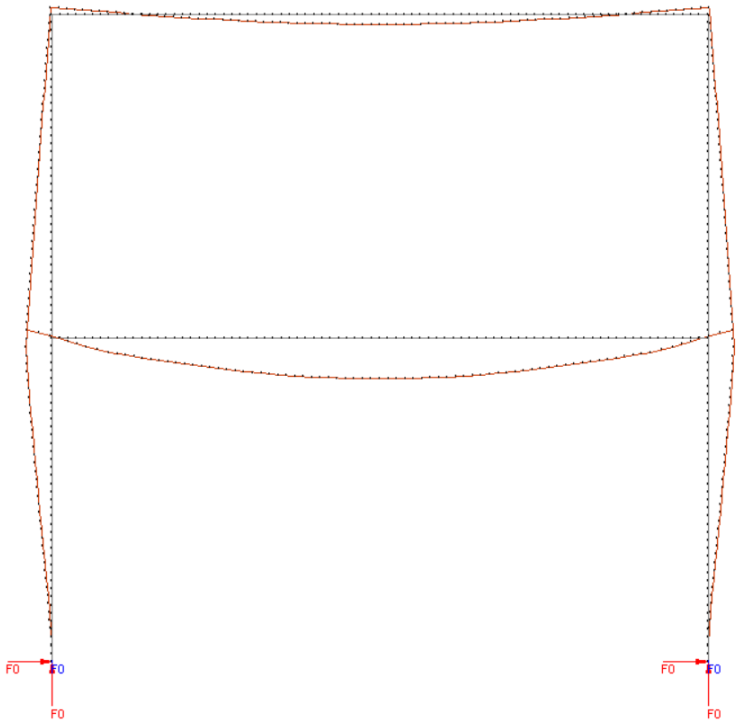

b)

Figure B40 – Deformed shape (scaled 10 times) of frame C3: a) 30 minutes, b) 47 minutes.

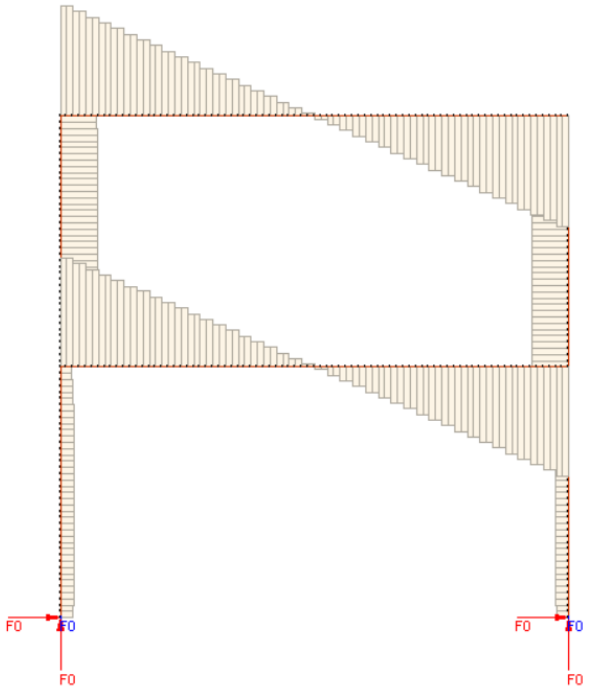

a)

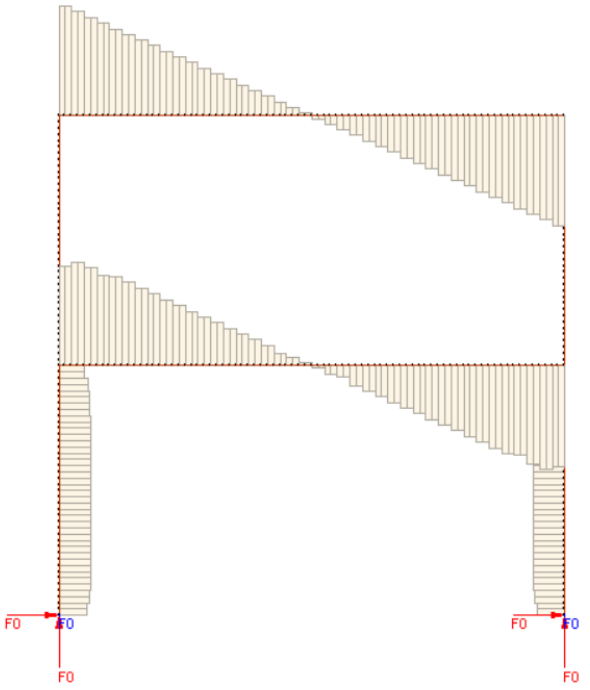

b)

Figure B41 – Schematic shear force diagram of frame C3: a) 30 minutes, b) 47 minutes.

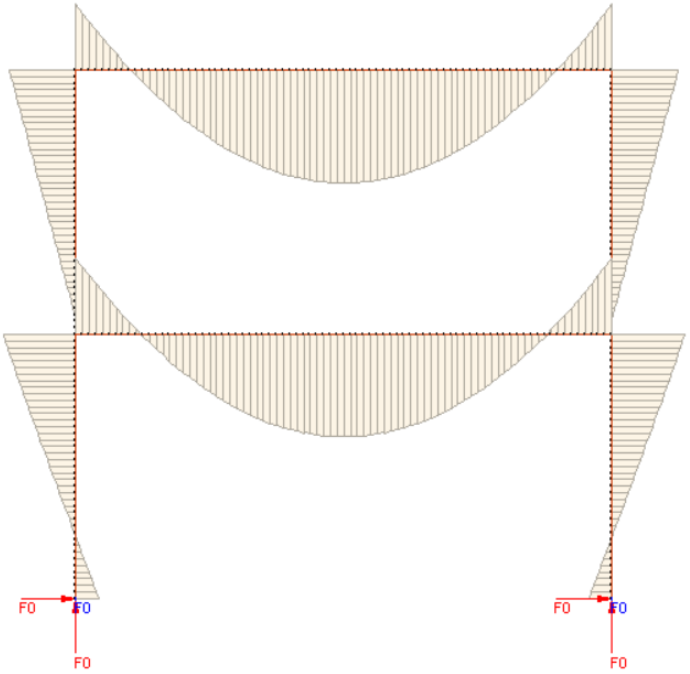

a)

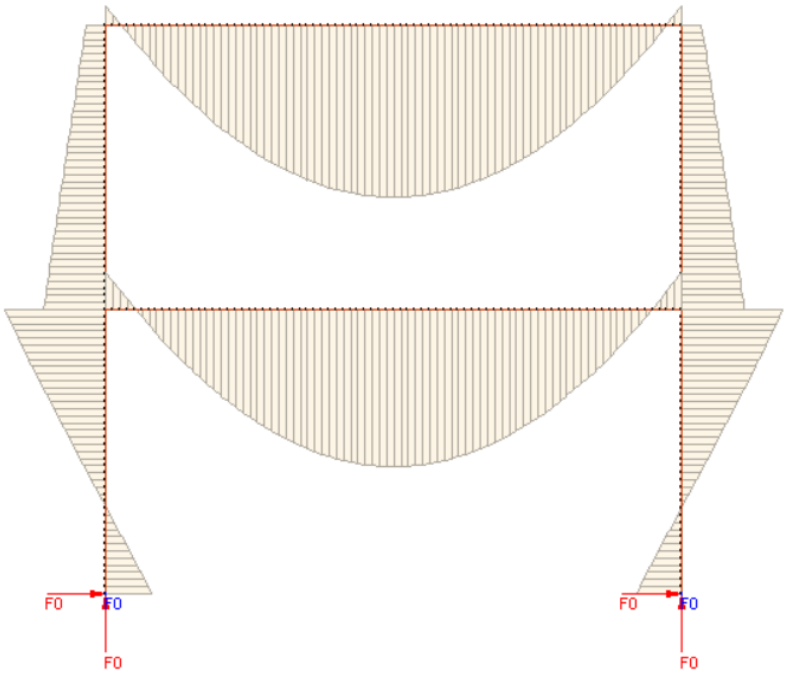

b)

Figure B42 – Schematic bending moment diagram of frame C4: a) 30 minutes, b) 69 minutes.

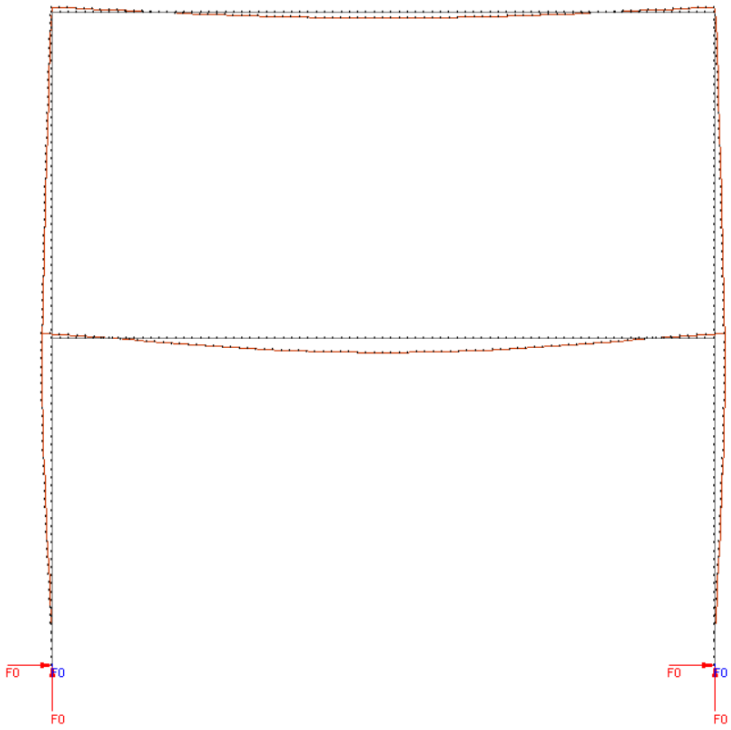

a)

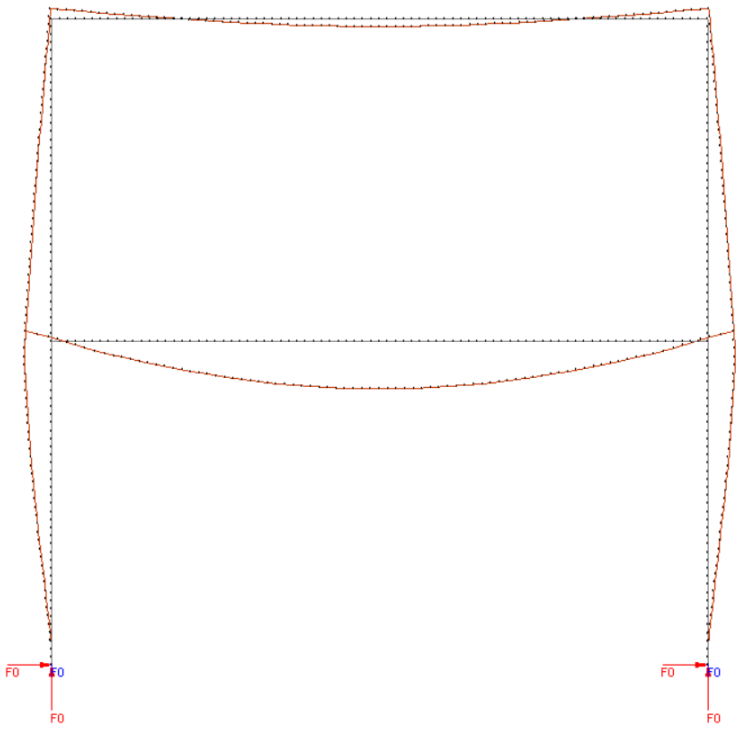

b)

Figure B43 – Deformed shape (scaled 10 times) of frame C4: a) 30 minutes, b) 69 minutes.

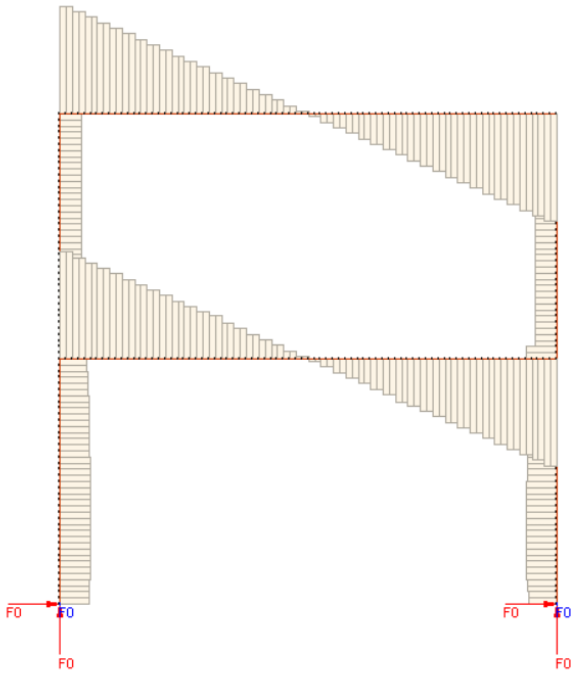

a)

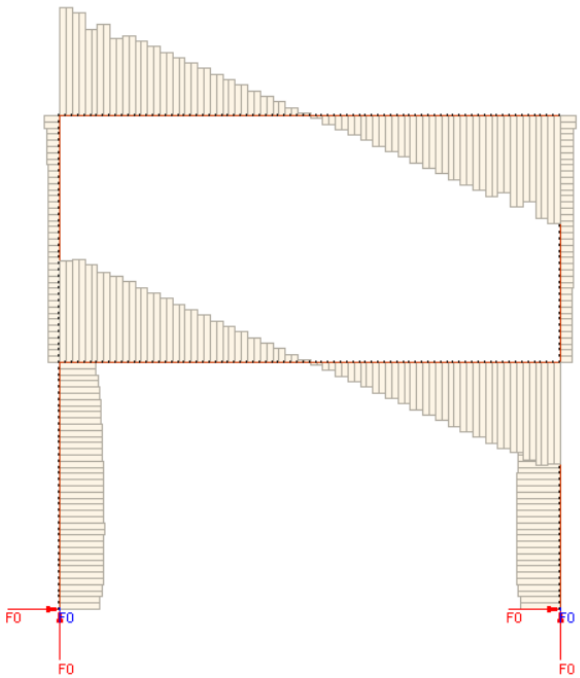

b)

Figure B44 – Schematic shear force diagram of frame C4: a) 30 minutes, b) 69 minutes.

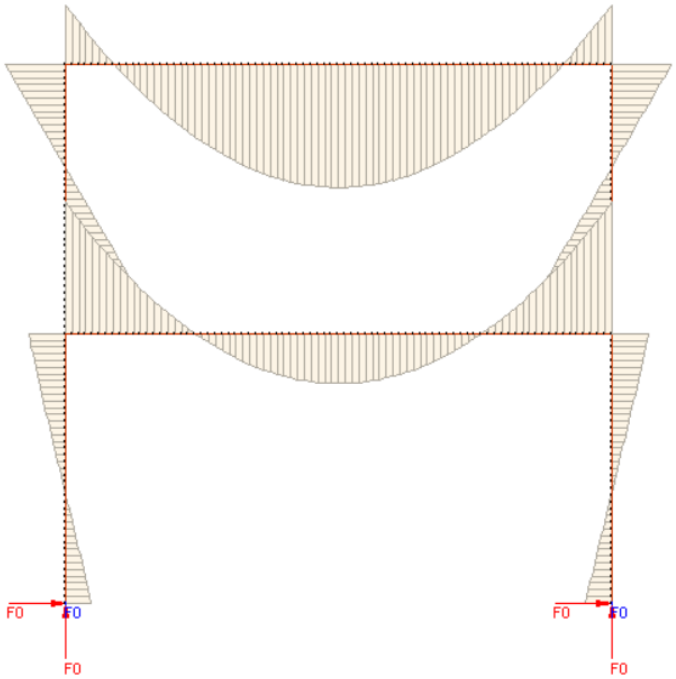

a)

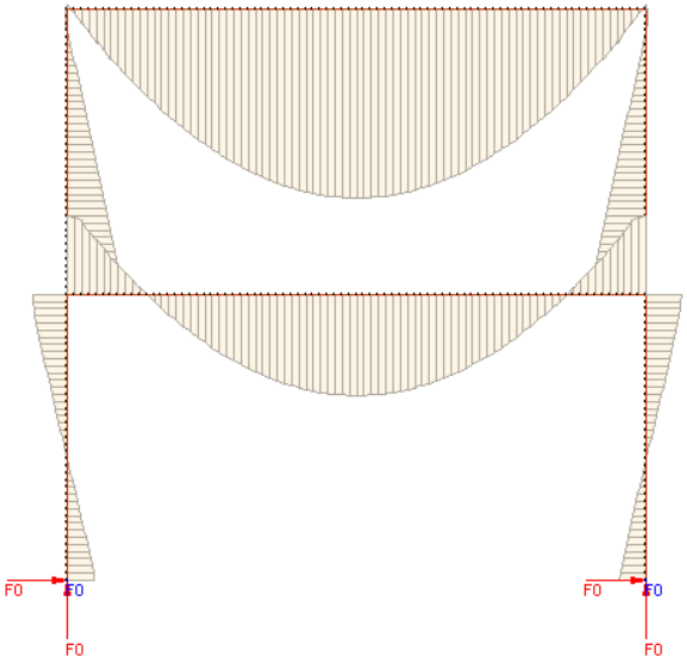

b)

Figure B45 – Schematic bending moment diagram of frame C5: a) 60 minutes, b) 125 minutes.

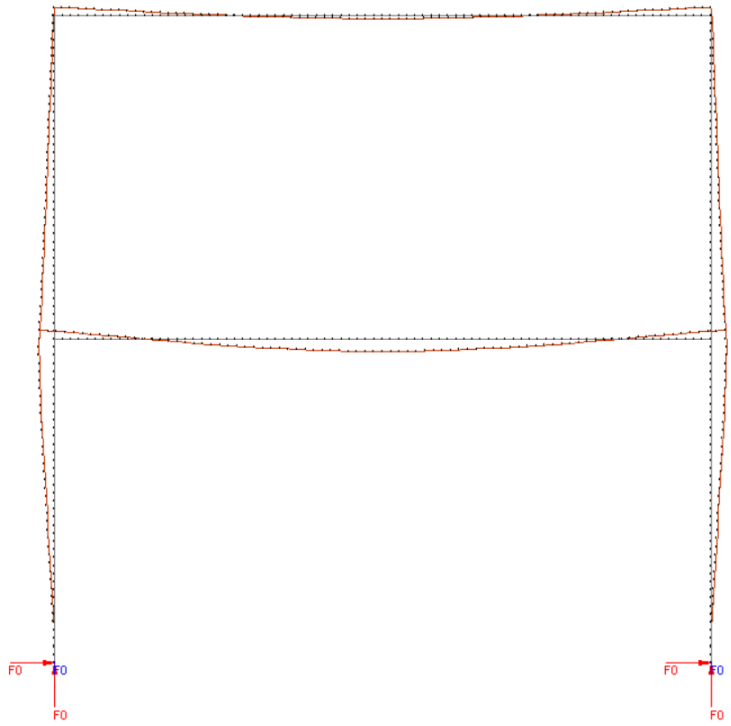

a)

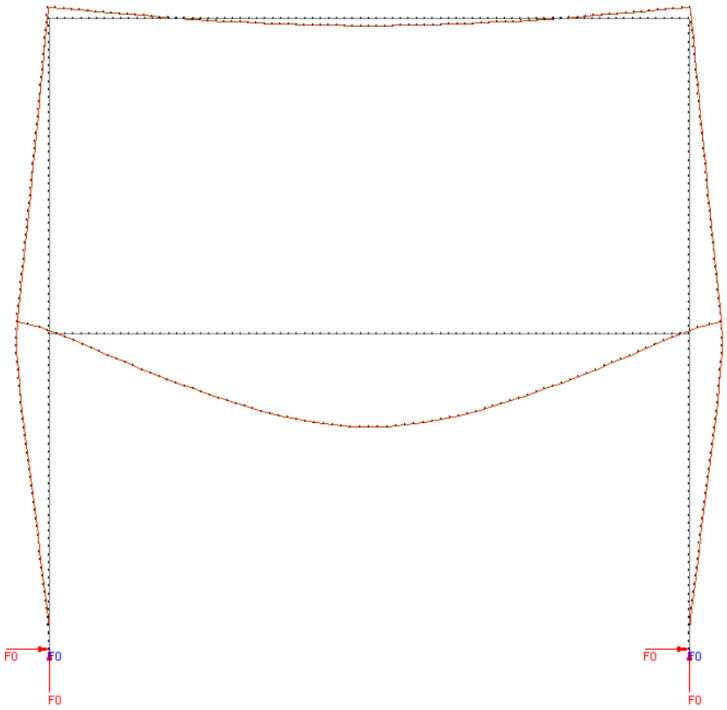

b)

Figure B46 – Deformed shape (scaled 10 times) of frame C5: a) 60 minutes, b) 125 minutes.

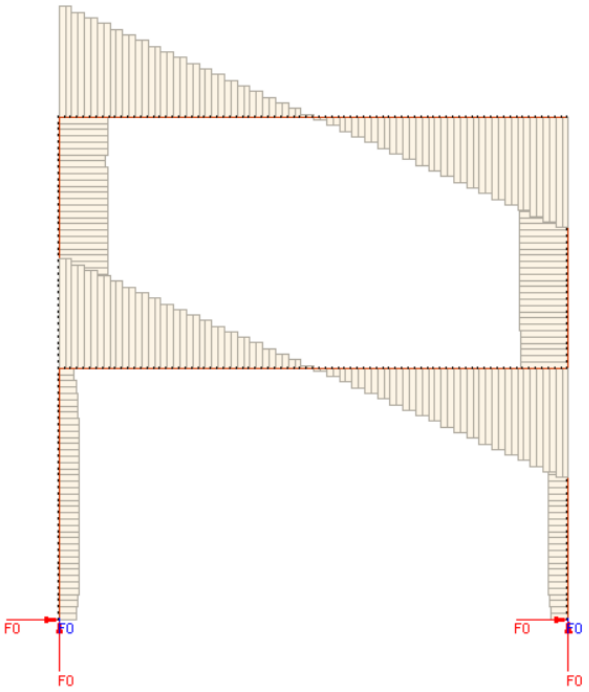

a)

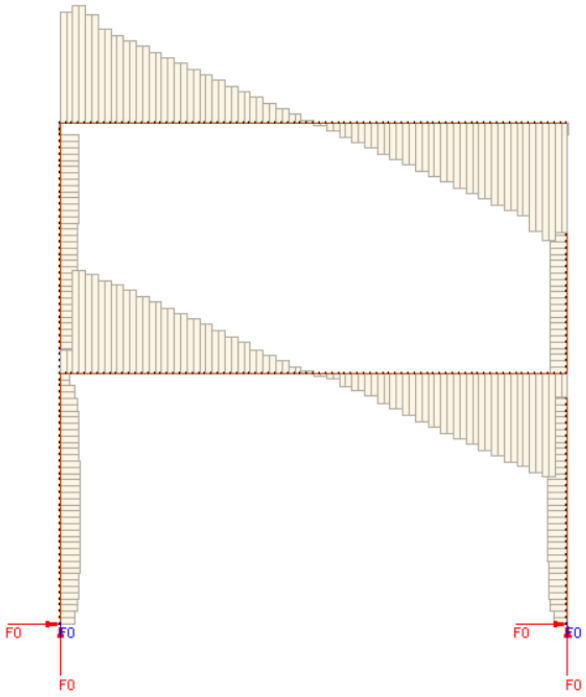

b)

Figure B47 – Schematic shear force diagram of frame C5: a) 60 minutes, b) 125 minutes.

This page was intetionally left blank